N-ANNULATED RYLENE BASED CHROMOPHORES AND THEIR APPLICATION

QI QINGBIAO

(B.S. University of Science and Technology of China)

A THESIS SUBMITTED

FOR THE DEGREE OF PHILOSOPHY

DEPARTMENT OF CHEMISTRY

NATIONAL UNIVERSITY OF SINGAPORE

2016

Declaration

I hereby declare that this thesis is my original work and it has been written by me in its entirety. I have duly acknowledged all the sources of information which have been used in the thesis.

This thesis has also not been submitted for any degree in any university previously.

The content of the thesis has been partly published in:

1) Qi, Q.; Wang, X.; Fan, L.; Zheng, B.; Zeng, W.; Luo, J.; Huang, K.-W.;Wang, Q.; Wu, J.; "*N*-annulated Perylene Based Push-Pull Type Sensitizers". *Org. Lett.* **2015**, *17*, 724.

Name	Signature	Date

ACKNOWLEDGEMENTS

My four-year PhD study has come to the end. During this long journey in my life, I was encouraged by many people. Now I would like to take this opportunity to express my gratitude to those persons for their invaluable help and inspiration.

First of all, I would like to give my sincerest thanks to my supervisor, Prof. Wu Jishan for his unreserved guidance and patience over these years. Without his insightful comments and consistent, illuminating instruction, my thesis could not have reached here. It is my luck to have such an outstanding supervisor at the beginning of my career in chemistry. His enthusiasm for research and excellent personality will be kept in my mind and encourage me to carry on throughout my life.

Second, I would like to thank Professor Chi Chunyan for her enlightening guidance and encouragements during the past few years. I am also very grateful to all past/present group members of both Wu and Chi's groups, especially Hu Pan and Zeng Wangdong for kindly sharing, discussion and help. I am really enjoying and appreciating the friendship with them.

Special thanks are given to our collaborators, Professor Wang Peng and Professor Wang Qing and their students for nice DSC device measurements, Professor Huang Kuo-Wei for the DFT calculations. Professor Dongho Kim for relaible two-photon absorption and transient absorption measurements, Professor Juan Casado for conducting Raman experiments. I am also thankful to the staff in the Department of Chemistry in the National University of Singapore (NUS) for their selfless support.

In addition, my deepest gratitude goes to NUS for admitting me as a PhD student

so that I can pursue my dream in chemistry research.

Last but certainly not least, I would like to thank my beloved family, my parents Mr. Qi Fuliang and Mrs. Li Xiaoxia, my elder sister Ms Qi Qingqing for their unconditional love, strongly support, constant encourage and considerations all the time.

TABLE OF CONTENTS

SUMMARY

Current developments in the field of functional materials have boosted interest in the development of next-generation dyes. Apart from many commercialized dyes (eg. cyanines, polyenes), polycyclic aromatics,e. g., polycyclic aromatic hydrocarbons (PAHs), porphyrins, and 4,4-difluoro-4-bora-3*a*,4*a*-diaza-*s*-indacene (BODIPY), have drawn intensive interest in recently decades. Among them, rylenes have been extensively studied primarily due to their versatile optical and electrochemical properties, ease of functionalization and excellent chemical and thermal stabilities. These advantageous factors make them attractive materials in electronics, optoelectronics, and photonics. In this dissertation, rylenes have been utilized and three different strategies ("push-pull", core extension, quinoidization) have been adopted to synthesize a series of functional rylene molecules with varied physical and optical properties, which include: (1) two series of *N*-annulated perylene (NP)-based push−pull-type sensitizers for high-performance dye-sensitized solar cells (DSCs) (chapter 2 and chapter 3); (2) methylthio-capped rylenes up to hexarylene and their stable radical cations and dications (chapter 4). In this chapter, synthesis and electrochemical, structural properties of those new functional rylenes have been studied in details. We found that these stable chmophores including neutral and charged species show unique optical, electronic and magnetic properties and have potential applications for charge and spin transporting materials; and (3) *N*-annulated rylenequinone (chapter 5) and we found that after quinoidization, the ground state was tunable with different chain length, showing very different physical and chemical properties. Functional rylenequinone dyes with open-shell singlet diradicaldiradical

ground state could be obtained. Throughout the research work, solubility and stability problems have been resolved for these conjugated systems after careful design and modifications. The fundamental structure-property relationships were systematically. Our systematical research may pave the way for a broad range of applications for these rylene based functional dyes in future, such as organic solar cells, organic field effect transitors, organic conductors, organic spintronics, non-linear optics, and so on.

Key Words: dye, push-pull, perylene, rylene, solar cell, diradical

LIST OF TABLES

LIST OF FIGURES

LIST OF SCHEMES

LIST OF ABBREVIATIONS

t-Bu	tertiary butyl
CV	cyclic voltammetry
D-A	donor-acceptor
DCM	dicloromethane
DDQ	2,3-dichloro-5,6-dicyano-1,4-benzoquinone
DMF	*N*, *N*-dimethylformamide
DPV	differential pulse voltammetry
EA	ethyl acetate
EI	electron ionization
HOMO	highest occupied molecular orbital
LUMO	lowest unoccupied molecular orbital
MALDI-TOF	matrix-assisted laser desorption/ionization-time-of-flight
NBS	*N*-bromosuccinimide
NIR	near-infrared
NMR	nuclear magnetic resonce
NP	*N*-annulated perylene
PAH	polycyclic aromatic hydrocarbon
TD-DFT	time-dependent density function theory
TFA	trifluoro acetic acid
THF	tetrahydrofuran
TLC	thin layer chromotography
TPA	two photon absorption
UV	ultraviolet
Vis	visable
BODIPY	4,4-difluoro-4-bora-3a,4a-diaza-*s*-indacene
BT	benzothiadiazole
CDPT	cyclopentadithiophene
ε	molecular extinction coefficient
DSC	dye-sensitized solar cell
PCE	power conversion efficiency
FF	fill factor

HPLC	high performance liquid chromatography
IPCE	Incident photon-to-current conversion efficiency
J_{sc}	short circuit current density
V_{oc}	open circuit voltage

LIST OF PUBLICATIONS

Publications during PhD studies

(1) **Qi, Q.**; Wang, X.; Fan, L.; Zheng, B.; Zeng, W.; Luo, J.; Huang, K.-W.; Wang, Q.; Wu, J. "*N*-annulated perylene based push-pull type sensitizers". *Org. Lett.* **2015**, *17*, 724.

(2) **Qi, Q.**; Li, R.; Luo, J.; Zheng, B.; Huang, K.-W.; Wang, P.; Wu, J. "Push-pull type porphyrin based sensitizers: the effect of donor structure on the light-harvesting ability and photovoltaic performance". *Dyes and Pigments* **2015**, *122*, 199.

(3) Luo, J.; Xu, M.; Li, R.; Huang, K.-W.; Jiang, C.; **Qi, Q.**; Zeng, W.; Zhang, J.; Chi, C.; Wang, P.; Wu, J. "*N*-Annulated perylene as an efficient electron donor for porphyrin-based dyes: enhanced light-harvesting ability and high-efficiency Co(II/III)-based dye-sensitized solar cells". *J. Am. Chem. Soc.* **2014**, *136*, 265.

(4) Luo, J.; Wang, X.; Fan, L.; Li, G.; **Qi, Q.**; Huang, K.-W.; Tam, T. L. D.; Zhang, J.; Wang, Q.; Wu, J. "*N*-Annulated perylene as a donor in cyclopentadithiophene based sensitizers: the effect of linking mode". *J. Mater. Chem. C* **2016**, *4*, 3709.

(5) Luo, J.; Zhang, J.; Huang, K.-W.; **Qi, Q.**; Dong, S.; Zhang, J.; Wang, P.; Wu, J. "*N*-Annulated perylene substituted zinc–porphyrins with different linking modes and electron acceptors for dye sensitized solar cells". *J. Mater. Chem. A* **2016**, *4*, 8428.

(6) Zeng, W.; **Qi, Q.**; Wu, J. "Cyclopenta-fused perylene: a new soluble, stable and functionalizable rylene building block". *Sci. Bull.* **2015**, *60*, 1266.

(7) Luo, J.; Lee, S.; Son, M.; Zheng, B.; Huang, K.-W.; **Qi, Q.**; Zeng, W.; Li, G.; Kim, D.; Wu, J. "*N*-Annulated perylene-substituted and fused porphyrin dimers with intense near-infrared one-photon and two-photon absorption". *Chem. Eur. J.* **2015**, *21*, 3708.

(8) Zeng, Z.; Lee, S.; Son, M.; Fukuda, K.; Burrezo, P. M.; Zhu, X.; **Qi, Q.**; Li, R.-W.; Lopez Navarrete, J. T.; Ding, J.; Casado, J.; Nakano, M.; Kim, D.; Wu, J. "Push−pull type

oligo(*N*-annulated perylene)quinodimethanes: chain length and solvent-dependent ground states and physical properties". *J. Am. Chem. Soc.* **2015**, *137*, 8572.

(9) Hu, P.; Lee, S.; Herng, T.; Aratani, N.; Gonçalves, T. P.; **Qi, Q.**; Shi, X.; Yamada, H.; Huang, K.-W.; Ding, J.; Kim, D.; Wu, J. "Towards tetraradicaloid: the effect of fusion mode on radical character and chemical reactivity". *J. Am. Chem. Soc.* **2016**, *138*, 1065.

Chapter 1 An Introduction to the Low Band Gap Rylene Based Molecules and Materials

1.1 Introduction

Dye chemistry is believed to be one of the most attractive areas in organic chemistry. Nowadays, polycyclic aromatics, e. g., polycyclic aromatic hydrocarbons (PAHs), porphyrins, BODIPY, are of great interest due to their particular physical and chemical properties, excellent stability and photostability and ease of functionalization.[1] Among them, rylene and its derivatives have been extensively studied over recent decades.[2] Their versatile optical and electrochemical properties, processibility, and chemical and thermal stabilities make them attractive materials in electronics, optoelectronics, and photonics. Moreover, low band gap π-extended rylene arrayshave been demonstrated more promising due to their attributes，such as red-shifted NIR absorption bands, large nonlinear optical response, exceptionally large electron delocalization and possible open-shell character. Numerous π-extended functional rylene derivatves with varied physical and optical properties have been achieved by extension of the π-conjugation or by construction of push-pull motif or by quinoidization. All the three methods will definitely lower the HOMO-LUMO band gaps of the molecules and lead to bathochromic shift of their absorption and emission bands. The key troublesome issues for rylenes are their poor solubility and serious aggregation and these problems become more and more serious upon an increase of the π-conjugation and the molecular size. In most cases, in order to resolve the solubility problem as well as reduce the aggregation, the attachment of long alkyl chains, bulky moieties and/or induced distortion from planarity of the aromatic core is

highly desirable. Recently, our group has demonstrated that certain type of polycyclic aromatic hydrocarbons could show an open-shell diradicalsingle ground state. This type of molecule is of interest due to their unique electronic, optical and magnetic properties and potential applications in organic electronics, non-linear optics, spintronics, and energy storage devices. Considering this fact, quinoidal rylene based ddiradicaloids with chain-length dependent optical, electrochemical and magnetic findings were successfully synthesized and characterized. This studies will lead to new opportunities to develop new rylene based NIR chromophores and semiconductors for photonics, electronics and spintronics. In this chapter, recent synthetic chemistry and physical characterization of functional rylenes achieved by extension of the π-conjugation or by construction of push-pull motif or by quinoidization would be introduced.

1.2 Literature review

1.2.1 Rylene derivatives

Rylene is a series of polycyclic aromatic hydrocarbons based on naphthalene units that are linked by single bonds at the *peri*-positions. Only one aromatic sextet benzenoid ring can be drawn for each naphthalene units and two zig-zag edges exist at the terminal naphthalene units (Figure 1.1). In pursuit of stable dyes with high extinction coefficients, long-wavelength absorption/emission and facile functionalization, rylenes have drawn a great deal of attention.

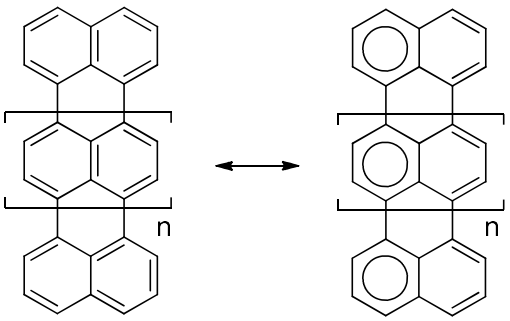

1-1a n = 0, Perylene
1-1b n = 1, Terrylene
1-1c n = 2, Quaterrylene
1-1d n = 3, Pentarylene
1-1e n = 4, Hexarylene
1-1f n = 5, Heptarylene
1-1g n = 6, Octarylene

Figure **1.1** General structures of rylene molecules.

As the simplest example of rylene molecules, perylene **1-1a** (n = 0) has been intensively studied owing to its owing to its outstanding chemical, thermal, and photochemical stability, excellent photophysical properties, facile functionalization and low cost.[3] The most important representatives of perylene are the perylene-3,4:9,10-tetracarboxydimide (PDI). They are widely used as dyes and pigments in a variety of applications such as paints, lacquers, organic photovoltaics, sensors, bio-imaging labels, supramolecular assemblies and so on.[4] In order to obtain π-extended functional rylene dyes with long-wavelength absorption, extension of the conjugation length in a longitudinal manner of perylene by incorporation of additional naphthylene units has proven to be an effective method. For example, terrylene **1-1b**,[5] quaterrylene **1-1c**,[6] hexarylene **1-1d**[7] absorb in the visible region with absorption maxima at 560 nm, 662 nm and 853 nm, respectively. A variety of synthetic methods such as base-induced ring formation including molten KOH in ethanolamine, *t*-BuOK–DBN in diglyme, $FeCl_3$–CH_3NO_2 in CH_2Cl_2, DDQ/$Sc(OTf)_3$, a combination of $CuCl_2$-$AlCl_3$ and so on have been developed to deal with the challenging synthesis. Sometimes, combination of different methods was necessary. One good example is

the synthesis of terrylene, quaterrylene and pentarylene by Müllen and coworkers (Scheme 1.1).[8] Naphthylperylene **1-3a** or biperylene derivative **1-3b** or peryleneylterrylene **1-3c** was obtained by potassium metal-mediated reaction. Then further treatment with a mixture of $CuCl_2$ and $AlCl_3$ afforded soluble terrylene **1-4a**, quaterrylene **1-4b** and pentarylene **1-4c**. Four *tert*-butyl groups were used to resolve the solubility problem resulting from the strong π-π stacking. However, relative low solubility of **1-4c** indicated that more sufficient solubilizing groups are needed for higher order rylene.

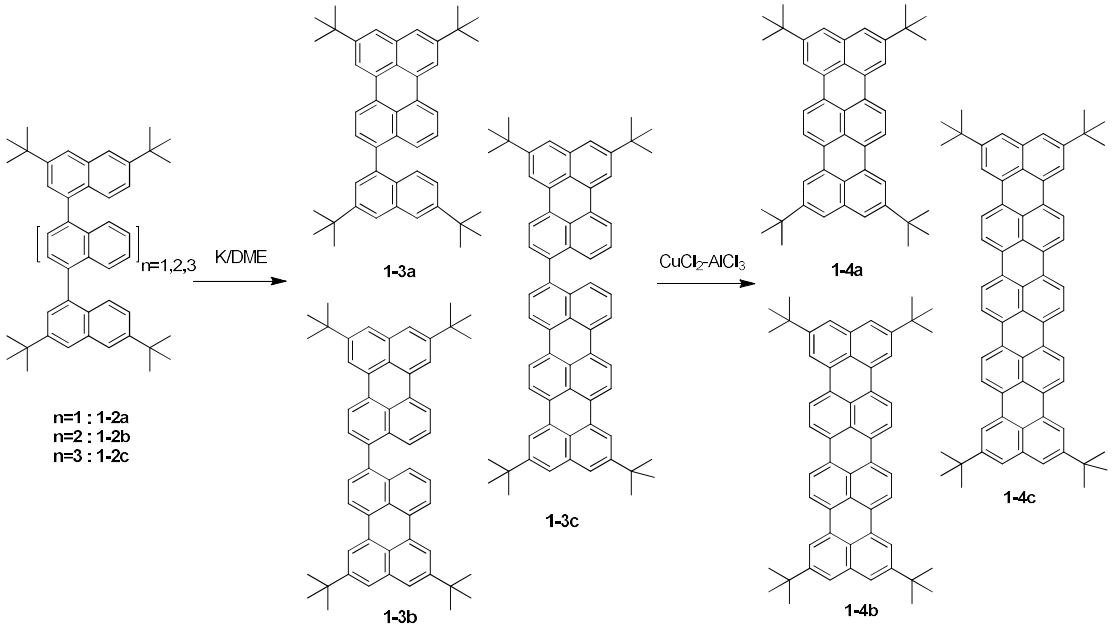

Scheme 1.1 Synthesis of terrylene derivative **1-4a**, quarterrrylene derivative **1-4b** and pentarylene **1-4c**.

Due to electron-rich character and low band-gap, higher order rylenes are relatively unstable upon exposure to air. Dicarboxylic imide are then introduced to the reactive *peri*-positions to improve their chemical stability and photostability. The rylene bis(dicarboximde)s **1-5a-g** (Figure **1.2**)[9] were found to be more stable than the parent

rylenes. Flexible alkyl chains or bulky groups can be readily introduced to the imide sites to significantly improve the solubility and reduce aggregation. Moreover, the donor-acceptor interaction resulted in bathochromic shift in absorption. Furthermore, substitution with bulky phenoxy groups at the bay position can further enhance solubility and promote bathochromic shift due to the electron donating effect of the phenoxy group. Taking these advantages, preparation of higher rylene bisimides are accessible. Same to the parent rylenes, extension of the conjugation length along the long molecular axis not only promotes their absorption into NIR region but also significantly enhances their molar extinction coefficients. Most recently, synthesis of octarylene diimide (ODI) **1-9** (Figure **1.2**) was achieved with a length of approximately 4 nm.[10] It is noteworthy that ring cyclization reactions sometimes suffer from the dealkylation of the phenoxy group under strong basic conditions. In this case, alternative substitution group at the bay positions of ODI was used to facilitate an easy synthesis.

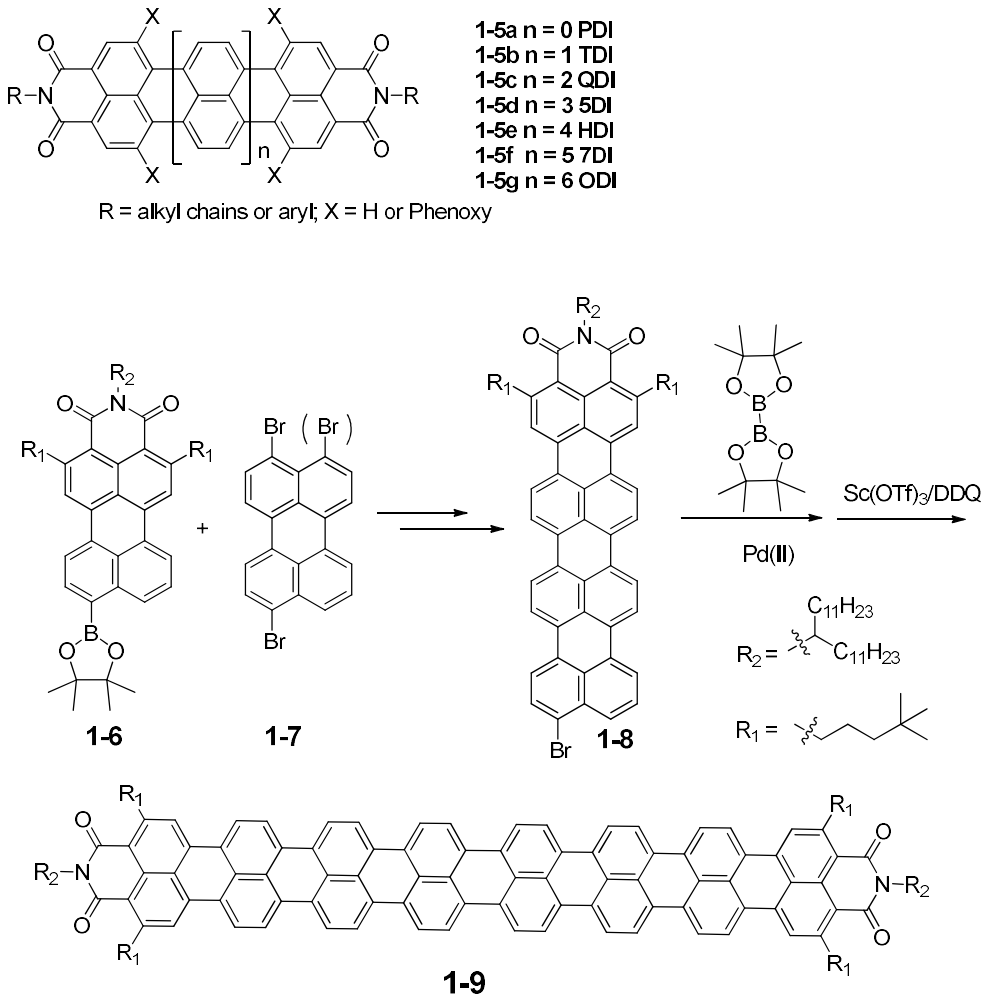

Figure **1.2** Structure of rylene bis(dicarboximide)s and synthetic route towards **ODI.**

Recently, *N*-annulation of perylene in which the nitrogen atom is annulated at the bay position becomes a good way to construct functional rylene dyes because additional flexible alkyl chains or bulky group can be easily introduced by alkylation reaction at the amine site and thus improve the solubility and surpress aggregation. In addition, the electron-donating character of amines can increase the electron density of the entire π-system and lead to new opto-electronic properties which is beneficial to practical applications in organic photovoltaics.[11] Wang and coworkers has reported

several *N*-annulated perylenes.[12] Interestingly, processable bis-*N*-annulated quaterrylene **1-10** was also successfully synthesized by DDQ/$Sc(OTf)_3$ nediated oxidative ring fusion.[13] In parallel to this studies, our group also reported a facile synthesis of a new bis-*N*-annulated quaterrylenebis(dicarboximide).[14] Interestingly, compound **1-11** exhibited absorption at near-infrared (NIR) region and emitted strong fluorescence with high quantum yield up to 55% in dichloromethane (DCM). Compound **1-11** showed relatively high photostability due to the attachment of electron-withdrawing dicarboximide groups in comparison with the electron-rich analog **1-12**. The opto-electronic properties of all these *N*-annulated rylene derivatives were quite appealing to many potential applications such as organic field-effect transistors (OFETs), light emitting diodes (LEDs), photovoltaic devices, and other organic optoelectronic devices.

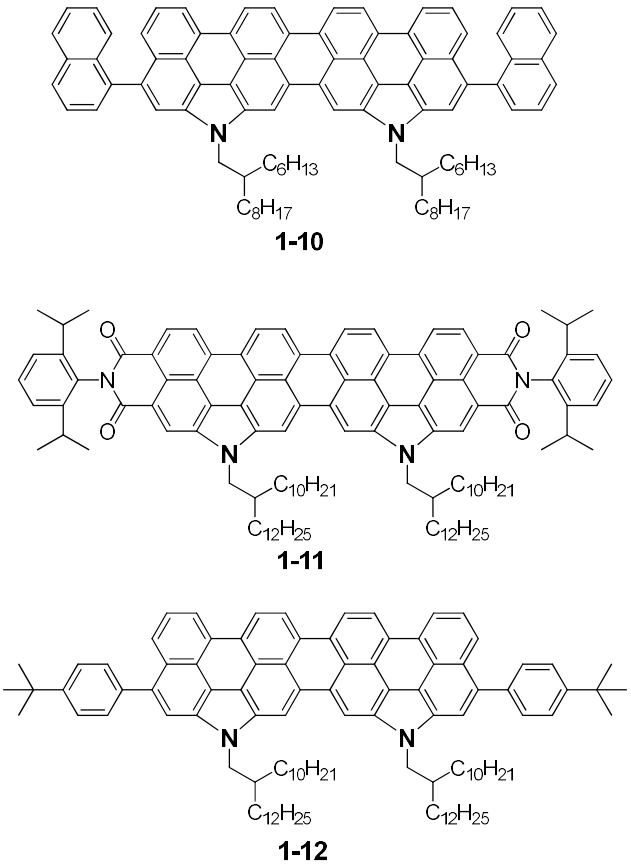

Figure 1.3 Molecular structures of bis-*N*-annulated quaterrylene **1-10, 1-12** and quaterrylenebis(dicarboximide) **1-11**.

Later, several tris-*N*-annulated hexarylenes (**1-14a**, **1-14b** and **1-14c**) were synthesized in Wang's group (Scheme 1.2),[7] which can be regarded as model compounds for the narrowest armchair graphene nanoribbons with large dipoles. These hexarylene dyes display remarkably large dipole moments associated with the formation of H aggregation, favoring the formation of highly ordered supramolecular structures, which can enhance charge carrier mobilities.

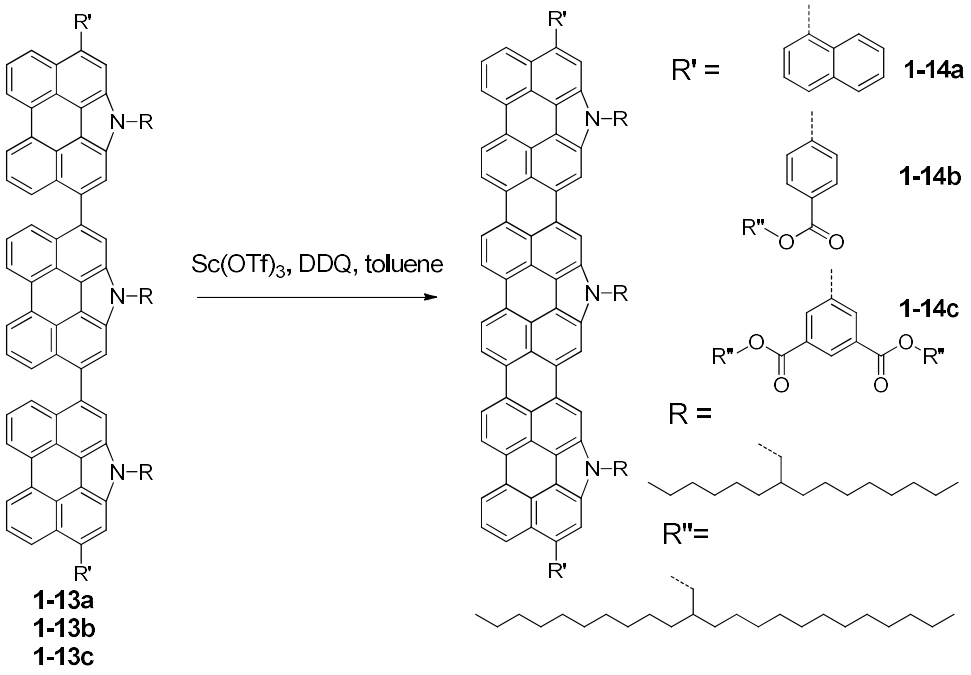

Scheme 1.2 Synthesis of *N*-annulated hexarylenes **1-14a**, **1-14b** and **1-14c**.

According to the calculations by Nagao *et al.*[15] and Sun *et al.*,[16] the extension of π-conjugation along the long molecular axis of rylene will result in largely bathochromic shift of the main absorption band into the NIR region by narrowing of the HOMO-LUMO energy gap, and molar extinction coefficient will also significantly increase. It is worth to note that the obtained experimental results discussed above agreed well with their prediction until now. For example, as shown in Figure 1.2, from **1-5a** PDI to **1-5d** HDI, the exhibited absorption maxima was observed at 580, 677, 762, 877 and 953 nm, respectively, and showed almost linear increase of the extinction coefficient.

The expansion along the molecular short axis of rylene is another good way to explore higher rylene analogues. However, this manner is challenging because of the difficulties in methodology. Typical core-expansion includes annulation of benzene

rings and heterocycles in the bay-region of the perylene core (Figure 1.4).

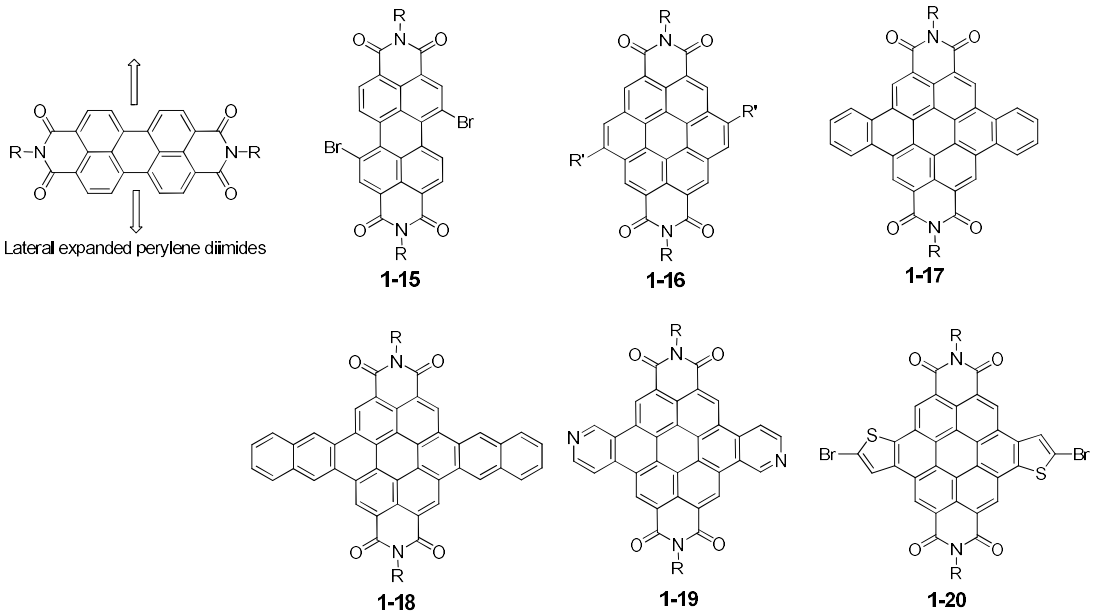

Figure 1.4 Synthesis of lateral extension perylene derivatives.

Coronene diimides (CDI) **1-16**,[17] dibenzocoronene diimides **1-17**,[18] and dinaphthocoronene diimides **1-18**[19] can be prepared from the 1,7-dibromo-PDI **1-15**. The absorption bands of **1-16** displayed red-shift (ca. 89 nm) when compared to the parent coronene (428 nm). CDI **1-16** could form discotic mesophases by incorporating appropriate alkyl substitution, which can provide possibility for practical applications. Further expansion of a perylene core from coronene to dibenzocoronene dyes **1-17** was abtained *via* Suzuki coupling followed by palladium-catalyzed dehydrohalogenation reactions. Furthermore, by refluxing **1-15** with 3-(trimethylsilyl)naphthyl- trifluoromethane sulfonate in a mixture of toluene and acetonitrile, dinaphthocoronene diimide **1-18** was afforded. It is noteworthy that **1-18** exhibits a broad absorption from 450 to 600 nm. Recently, Wang and coworkers reported synthesis of **1-19**[20] by choosing a more stable 4-pyridine boronic acid as the precursor. In addition to the heterocycle annulation, Facchetti *et al*. reported a

thiophene-fused CDI **1-20**[21] with two bromo groups, which opened the way to synthesize of a series of functional low band gap donor–acceptor π-conjugated polymers.

Besides the aforementioned annulation of ethylene, benzene, pyridine, and thiophene units, Wang *et al*. reported a series of ribbon-like PDI oligomers fused at the bay-positions (Figure 1.5), which were of high potential for application in *n*-type semiconductors.[22]

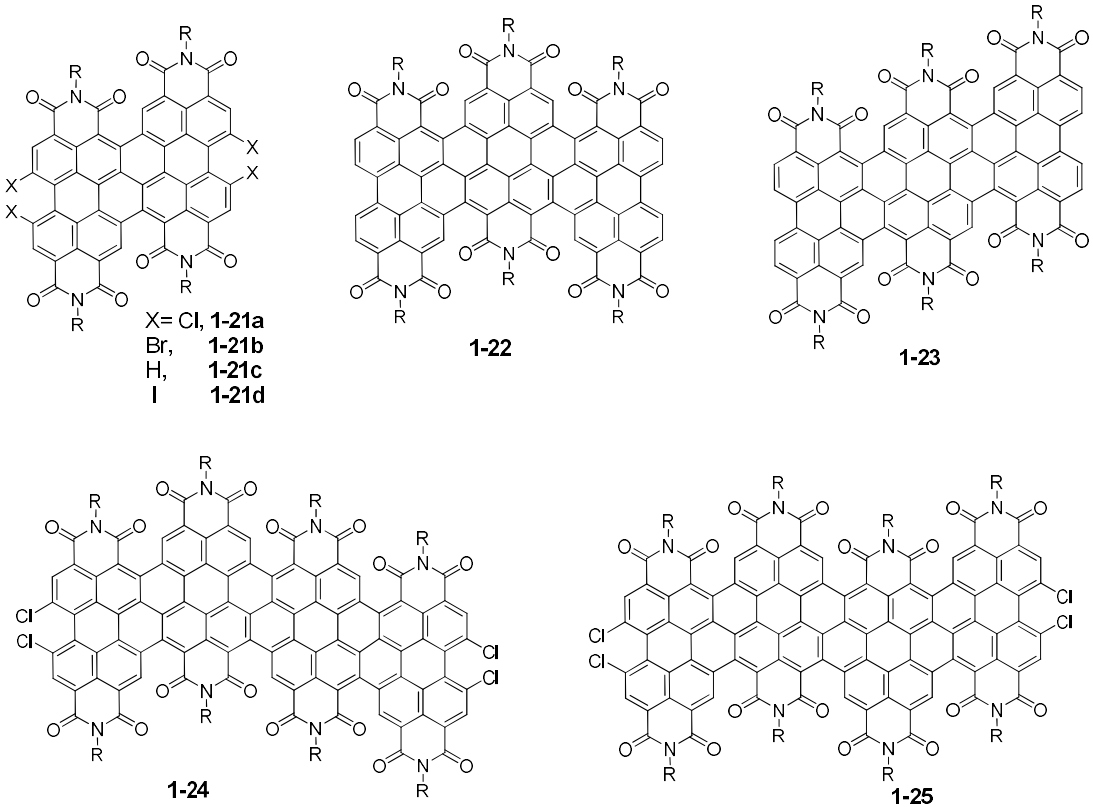

Figure 1.5 Synthesis of ribbon-like perylene diimide derivatives.

Another example of laterally expanded system is the bisanthracene bis(dicarboxylic imide)s (Scheme 1.3).[23] In 1995, Désilets *et al*. treated **1-26a-d** with molten KOH followed by an air oxidation and fused compounds **1-27a-d** were obtained in low yields, which exhibited absorption maxima as long as 701-704 nm with extinction

coefficients around 35300 M^{-1} cm^{-1}. However, the fully fused bisanthracene diimide cannot be directly synthesized by this method. A multiple-step synthesis starting from anthracene was taken into consideration. In our group, we firstly described the successful step-by-step synthesis of a fully laterally expanded rylene molecule, bisanthene bis(dicarboxylic imide) **1-34** (Scheme **1.3**). Compared with perylene bis(dicarboximide), dye **1-34** showed absorption maximum at 830 nm (ε =15000 M^{-1} cm^{-1}), which is remarkably red-shifted by 300 nm.**1-34** also displayed good solubility and stability under ambient air and light condition over parent bisanthene[24] due to the attachment of two bulky electron-withdrawing dicarboxylic imide groups at the active zig-zag edges.

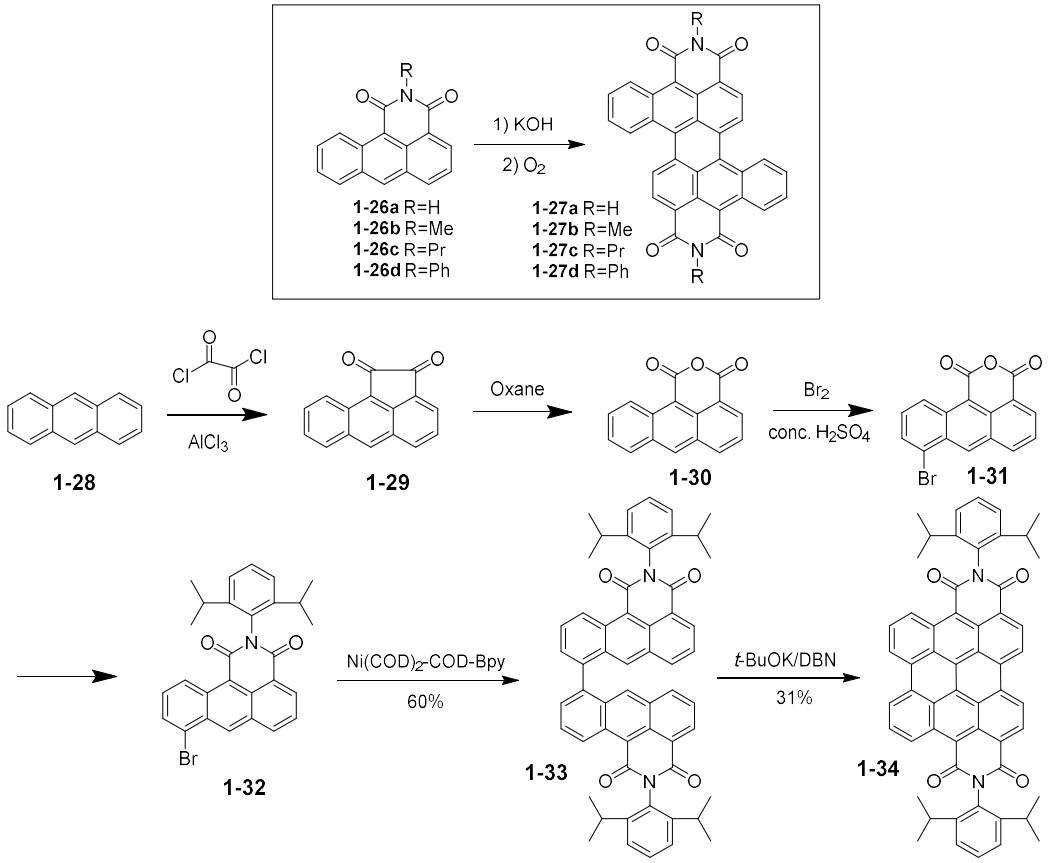

Scheme **1.3** Synthesis of fully fused bisanthene bis(dicarboximide).

Three *meso*-substituted bisanthenes **1-35a** to **1-35c** (Figure **1.6**)[25] were also synthesized by our group. The active *meso*- positions of the bisanthene were protected by either aryl or alkyne group. The absorption maxima of **1-35a** to **1-35c** in toluene were observed at 687, 683, and 727 nm, respectively, all of which are more or less red-shifted due to π-extension through the aryl and triisopropylsilylethynyl substitution. In addition, better stability over parent bisanthene was observed. The solutions of **1-35a** to **1-35c** are of no change under ambient conditions for one week. Moreover the excellent photoluminescence quantum yields of **1-35a** to **1-35c** (0.81, 0.80 and 0.38) make them good candidates for fluorescent dyes.

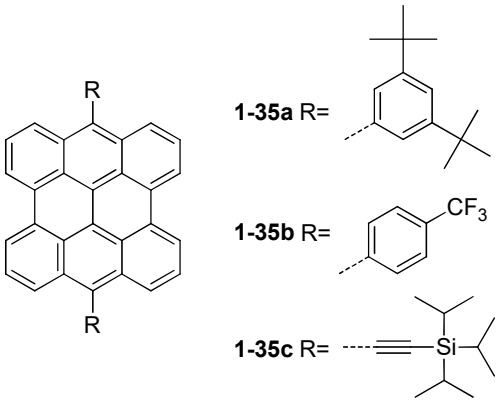

Figure **1.6** *Meso*-substituted bisanthenes **1-35a-c**.

Combination of extension along either the long and short molecular axis also can afford new kind of functional dyes. For examples, extension of π-conjugation in both molecular axes of rylene diimide (eg. TDI, QDI, 5DI) were successfully achieved. Recently, synthesis of large disc-shaped diimide **1-36**[26] *via* intramolecular oxidative cyclodehydrogenation by ferric chloride was reported by Ba *et al*. Furthermore, Wang and coworkers introduced a tetrathiophene annulated TDI **1-37**.[27] Müllen's group reported benzene rings annulated TDI **1-38**.[28] For **1-38**, the large steric encumbrance effect, existing between the four neighboring benzene rings at the bay-positions,

resulted in two diastereomers. The two atropoenantiomers of the isomer with an "up-down" conformation were further isolated by chiral HPLC. High thermodynamic stabilities were achieved for the two atropo-enantiomers of **1-38** owing to the high racemization barrier, which can be applied in chiral molecular switches. Furthermore, extended QDI **1-39**,[27] **1-40**[18] and 5DI **1-41**[29]in lateral manner were also successfully realized by Scholl conditions using $FeCl_3$–CH_3NO_2 or a second base-promoted reaction with K_2CO_3–ethanolamine and $FeCl_3$.

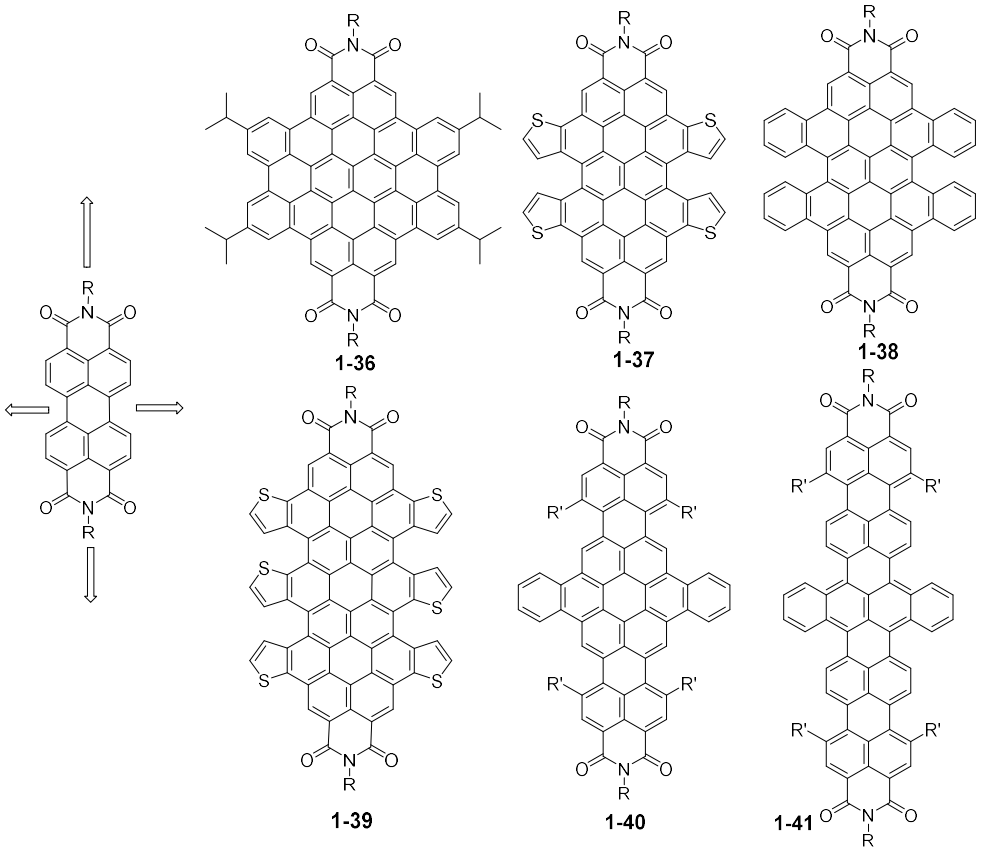

Figure 1.7 Representatives of both laterally and longitudinally expanded rylenes.

Another way to make functional rylene dyes besides extension of π-conjugation by a multi-step synthesis is to incorporate donor and acceptor substituents into the sturctures. As already briefly discussed above, the introduction of substituents such as

phenoxy, or alkylamino groups to the bay positions or the amine site of *N*-anulation of rylene have been widely applied in rylene chemistry. These substituents not only improve solubility and processability but also enhance tunability over the energy levels. A more pronounced push–pull effect can be introduced by incorporating donor and acceptor moieties to the opposite peri-positions of the perylene core.

In 2009, Müllen and coworkers reported a series of donor-acceptor functionalized perylenes (**1-42** – **1-46**) by using the carboxylic diimide group as the electron acceptor and functionalizing 9-positions with different donors (Figure 1.8).[30] In addition, the 1, 6-positions were also modified selectively with different functional groups. Both *peri*-substituents and bay substituents allow tuning of the spectroscopic and electrochemical properties of **1-42** - **1-46**. Thus a rainbow of colors was achieved by carefully tuning the donor and acceptor as well as the substituents at the bay positions. Moreover, functionalization with a donor and an acceptor in the opposite *peri*-positions of perylene allowed strong intramolecular charge tansfer. Based on these facts, a highly efficient perylene sensitizer **1-47**[31] was designed and applied in dye sensitized solar cells (DSCs). The dicarboxylic acid groups served not only acceptor but also anchoring group on TiO_2 surface. An overall power conversion efficiency up to 6.8% for **1-47** under the 100 mW cm^{-2}, standard AM1.5G sunlight was obtained with a monochromatic incident photon-to-electron conversion efficiency (IPCE) of 87%. This example paved a way to generate new "push-pull" type perylene sensitizers with proper HOMO and LUMO energy levels for efficient DSCs.

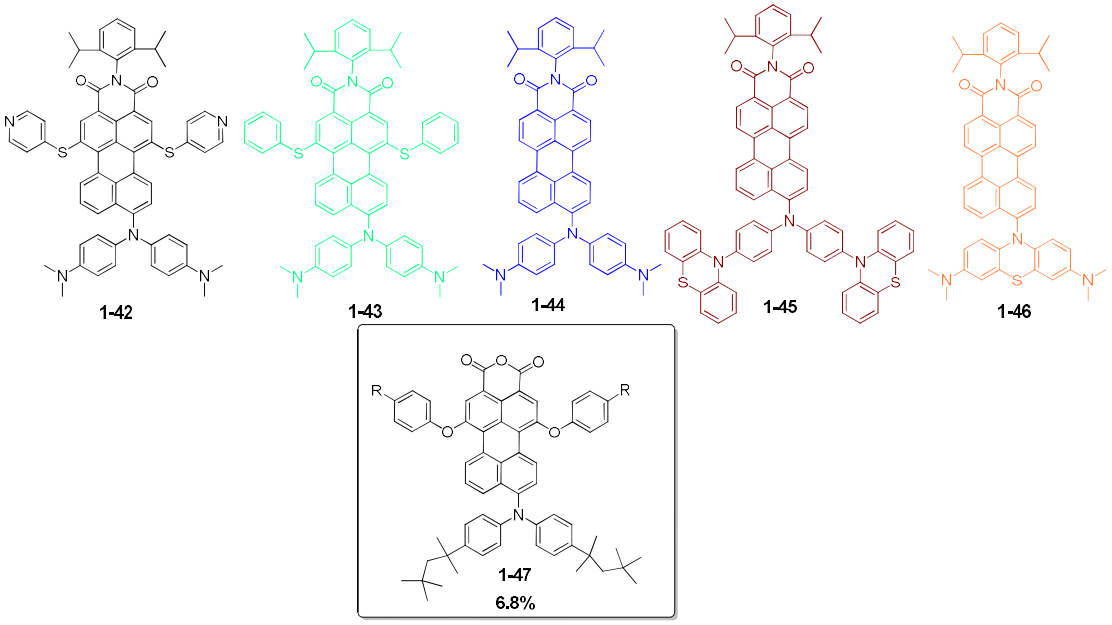

Figure 1.8 Representatives of structures of "push–pull" functionalized perylene dyes and a related sensitizer for DSCs.

N-annulated perylene (NP) was recently used as a very good building block for the design of sensitizers of DSSs. Compared with the parent perylene, the two *peri*-positions near the amino- site are more reactive than other positions, so regio-selective functionalization (e.g., bromination) can be conducted at the *peri*-positions, which opens the opportunities to generate push-pull type coplanar NP based sensitizers (Figure 1.9). In addition, flexible alkyl chains or bulky groups can be readily introduced to the amine site to significantly improve the solubility and suppress dye aggregation. Moreover, NP itself has good light-harvesting ability and can also serve as an electron donor. Our group first reported several NP-substituted porphyrins sensitizers (**1-48** and **1-49**) with improved light harvesting capability in the near-infrared region and power conversion efficiency (η) up to 10.5% was achieved in Co(II)/(III) based DSCs.[32] Moreover, NP functionalized CPDT dye (**1-50**) with efficiency as high as 7.8% was also reported by our group.[33] It is noteworthy that

peri-NP linked sensitizers **1-50** and **1-51** showed better performance than *bay*-NP linked sensitizers **1-52** and **1-53** owing to better intramolecular charge transfer (ICT) and light harvesting properties.

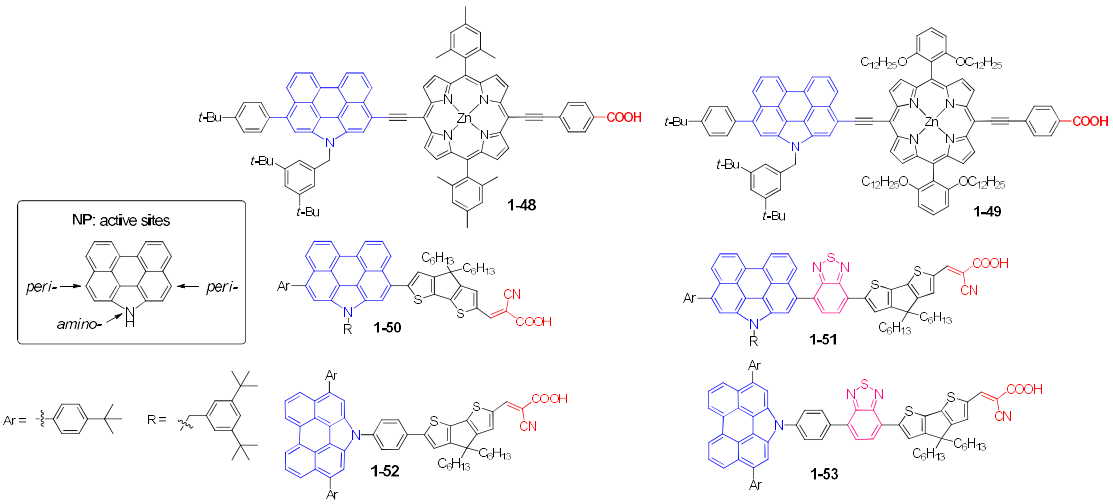

Figure 1.9 Representatives of NP-based sensitizers reported by our group.

Following our report, P. Wang and coworkers reported a series of functional perylene sensitizers by using NP as a coplanar π-linker with different acceptor segments: cyanoacrylic acid (**1-54a**), benzothiadiazole–benzoic acid (**1-54b**), and pyridothiadiazole–benzoic acid (**1-54c**) (Figure 1.10).[34] Power conversion efficiencies of 5.0–8.8% were achieved under the 100 mW cm^{-2}, simulated AM1.5G sunlight. By introducing an alkoxyphenyl group in the donor part of the dye together with ethynylbenzothiadiazole- benzoic acid as acceptor part, **1-55b** resulted in a PCE of 10.4%. Very recently, even higher values (12%, 12.5%) were reported in P. Wang's group for the modified NP sensitizers (**1-56** and **1-57**) (*N*-Annulated thienocyclopentaperylene dye and **N**-annulated indenoperylene sensitizers).[35] Z. Wang and coworkers also reported push-pull triphenyl amine functionalized NP molecules together with different number of thiophenes as π-linkers for DSCs

application (Figure 1.10).[36] A range of 4.9-8.3% efficiency was obtained for **1-58a-c.**

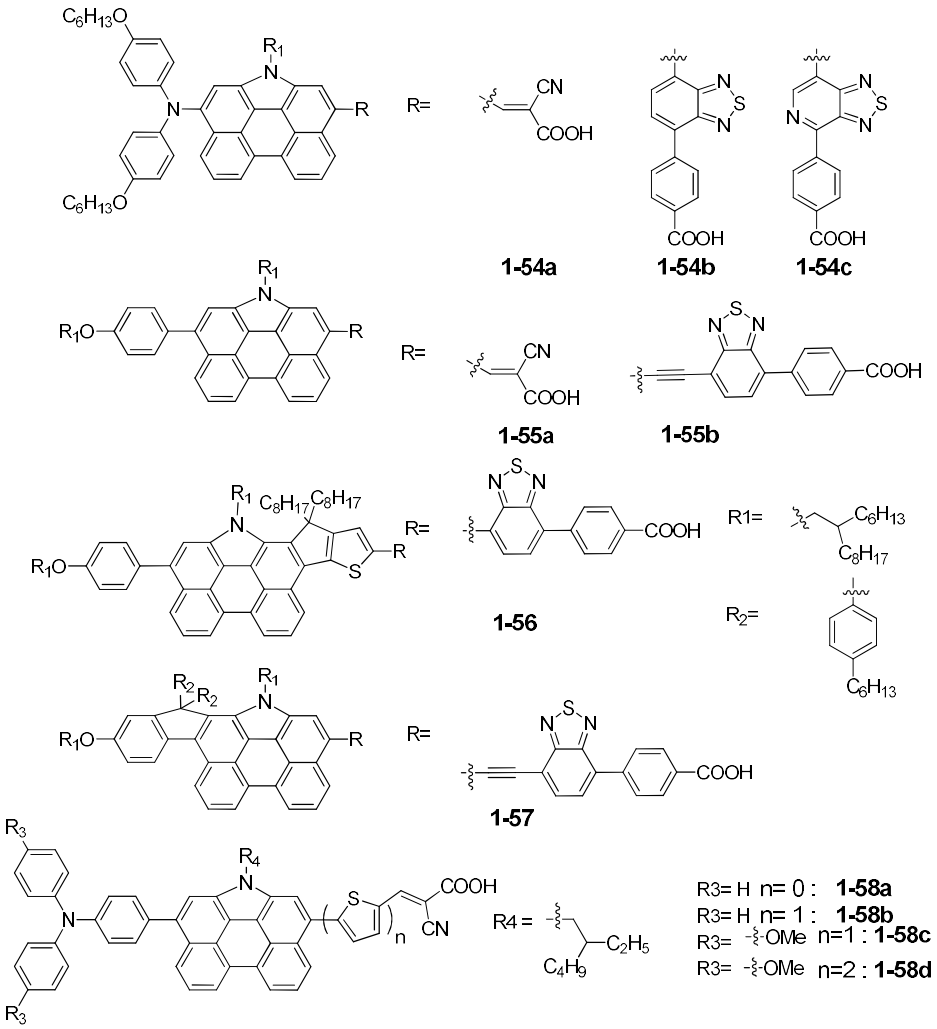

Figure 1.10 Representatives of NP-based sensitizers reported by other groups.

The combination of core-extension strategy with a push-pull effect also can afford new functional rylene dyes. For example, as shown in Scheme 1.4, two NIR rylene dyes **1-61a** and **1-61b** were successfully synthesized from **1-59a** and **1-59b**, respectively (Scheme **1.4**).[37] According to the UV spectra, two very broad ICT absorption bands were observed at 778 nm (ε = 15900 M^{-1} cm^{-1}) for **1-61a** and 1106 nm (ε = 37500 M^{-1} cm^{-1}) for **1-61b**, and at the low wavelength range, typical fine absorption structures of rylenedicarboximides were found. More interestingly, The

dyes **1-61a** and **1-61b** exhibited high thermal stability > 400 °C and photostability. Under UV irradiation, the solutions in 1,2,4-trichlorobenzene were of no obvious change after a week.

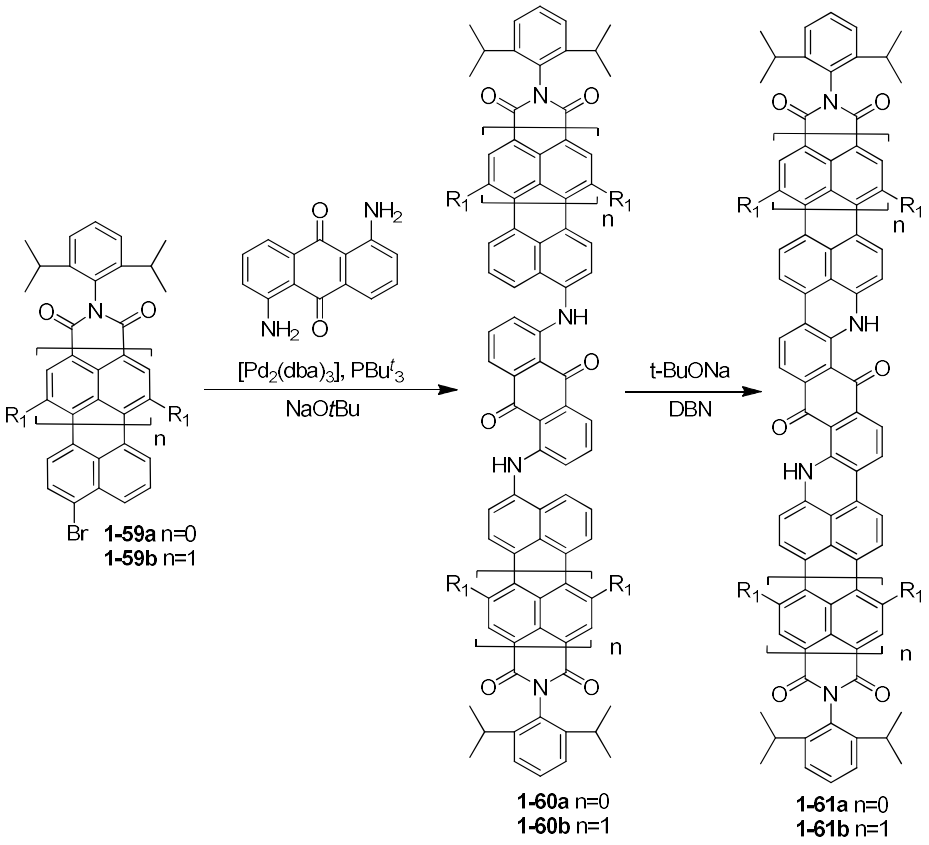

Scheme **1.4** Representatives of "Push-pull" and core extension rylene dyes.

Generally speaking, the band gap of quinoidal π-conjugated systems is lower than that of their parent aromatic analogues. From this point of view, quinoidization thus may be a feasible way for obtaining functional rylene dyes with unique physical, chemical properties and NIR absorption. Recent research in our group has demonstrated that certain type of polycyclic hydrocarbons PAHs could show an open-shell singlet diradicaldiradical ground state. Their unique optical, electronic and magnetic properties made them potential candidates for organic electronics,

spintronics and photonics. Quinodial rylenes are one type of the most interesting diradicaldiradicaloids.

Aseries of quinoidal rylene chromophores based on *N*-annulated perylene were reported by our group (Figure 1.11). As shown in the structures, CN-goup and *N*-alkylated goup were used to ensure sufficient stability and solubility, respectively. Molecules **1-62a-f**[38] represented the quinoidal NP oligomers with chain-length dependent ground states. The monomer **1-62a** showed typical closed-shell quinoidal charater, while dimer **1-62b**, trimer **1-62c** and tetramer **1-62d** possessed singlet diradicaldiradical ground state. With longer chain length, pentamer **1-62e** and hexamer **1-62e** showed weakly coupled diradical charater. Two proposed driving forces were accounted for this transformation. One is the aromatization stability obtained upon recovery of aromatic naphthalene rings in the diradicaldiradical form; another is the strain releasing upon transformation from quinoidal form to diradicaldiradical form. More interestingly, dimer **1-62b** with a moderate diradicaldiradical character gave the higher two-photon absorption (TPA) cross sections (Table 1.1), which paved the way for further rational design of functional dyes in TPA application.

Fully fused quinoidal π-extented rylene, **1-63a** QR-CN and **1-63b** HR-CN[39] were synthesized by Takahashi coupling from corresponding dibromo-quterrylene and dibromo-hexarylene, which were obtained by DDQ/$Sc(OTf)_3$ oxidative coupling of dibromo-oligomers. In this case, the effect of strain releasing is minimized and aromatization stability dominated the transformation. In contrast to **1-62b**, fused **1-63a** displayed closed-shell quinoidal character owing to efficient intramolecular

antiferromagnetic coupling between the two spins. With extended π-conjugation, **1-63b** displayed singlet diradicaldiradical ground state with a small diradicaldiradical character, which is also distinctively different from diradicalthe diradicaloid **1-62c**. Interestingly, as showing in Table 1.1, **1-63a** and **1-63b** showed quite stronger one-photon absorption and large two-photon cross sections in the NIR region than the unfused oligomers, indicating their superior non-linear optical properties. It is noteworthy that by careful controlling of aromaticity and steric hindrance, molecules with tunable diradical character and tunable propertes can be rational designed. Based on these facts, recently, **1-64a-b** were designed and successfully synthesized. As shown in Figure 1.11, two thiophene rings were incorporated into the quinoidal rylene structures.[40] The resulting compounds **1-64a** and **1-64b** exhibited distinct diradical characters owing to recovery of two additional aromatic thiophene rings in the diradical resonance forms as well as the conformational flexibility around the thiophene– rylene connections. Similar to **1-63a-b** above, the π-extension molecule **1-64b** showed higher TPA cross sections than **1-64a**.

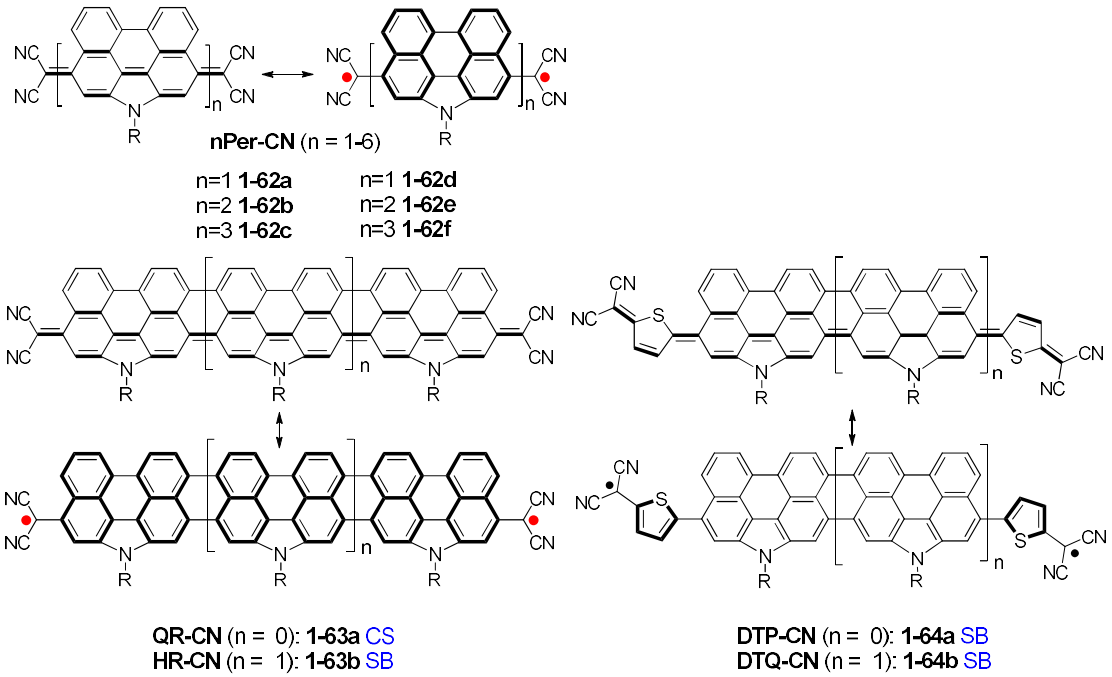

Figure 1.11 Representives of quinoidal tetracyano- *N*-annulated rylene.

By combining the push-pull motif and quinoidization, very recently, push-pull type quinoidal compounds have been successfully synthesized and characterized in our group.[41]

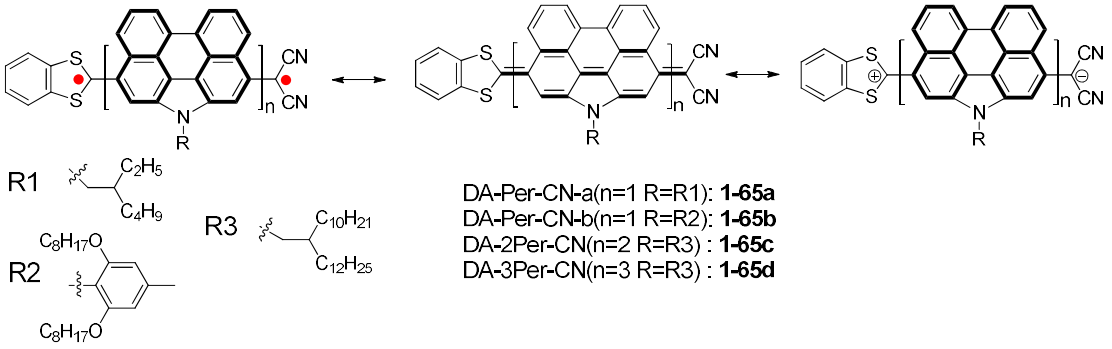

Figure 1.12 Representives of quinoidal push-pull type rylene.

1-65a and **1-65b** represented the simplest donor – acceptor perylene monomers. The only difference is that for **1-65b** bulky ortho-alkoxy substituted phenyl group rather

than flexible alkyl chain was chosen to suppress dye aggregation in **1-65a**. As shown in Figure 1.12, three resonance structures (closed-shell quinoidal form, open-shell diradical form, and closed-shell zwitterionic form) contribute to the ground state and physicochemical properties. Interestingly, unique chain length and solvent dependent ground states and properties were found for these molecules. With increasing chain length, the diradical character greatly increased, while the contribution of the zwitterionic form diminished. For monomer **1-65b**, an obvious red shift of the absorption band and change of band shape were found unpon the increase of solvent polarity, indicating more contribution of aromatic zwitterionic resonance form to the ground state with increased solvent polarity. For dimer **1-65c** and trimer **1-65d**, no obvious phenomena were found with different polar solvents. In addition, as shown in Table 1.1, D−π−A type chromophores exhibited TPA activities compared to A-π-A type chromophores (**1-62a-f**). This newly push-pull quinioidal system will provide guidance for further design of TPA chromophores.

Table 1.1 Ground states, TPA cross-sections, electrochemical energy gap and singlet-triplet gap data for quinoidal rylene arraies.

Compds.	Ground State	$\sigma^{(2)}{}_{max}$ (GM)	E_g^{EC} (eV)	$\Delta E_{S\text{-}T}$ (kcal/mol)
1-62a	CS[a]	1300 (1200 nm)	-	-
1-62b	SB[b]	1060 (1700 nm)	0.61	-0.342
1-62c	SB	770 (1700 nm)	0.53	-0.107
1-62d	SB	710 (1700 nm)	0.52	0.064
1-62e	DR[c]	730 (1700 nm)	0.57	0.556
1-62f	DR	710 (1700 nm)	0.53	0.883
1-63a	CS	1400	0.80	-

		(1800 nm)		
1-63b	SB	3300 (2000 nm)	-	-4.21
1-64a	SB	1000 (1700 nm)	0.83	-4.71
1-64b	SB	1700 (2400 nm)	0.37	-0.16
1-65b	CS	1000 (1500nm)	1.21	
1-65c	SB	660 (1800nm)	0.6	-1.46
1-65d	SB	670 (1900nm)	0.5	-0.48

[a] CS: closed-shell. [b] SB: singlet diradical. [c] DR: weakly coupled diradical.

Combination of the three discussed strategies (core-extension, push–pull motif and quinoidization) also proved to be good way to synthesize functional rylene dyes. One typical example was the quinoidal amino-substituted rylene dicarboximides **1-69**, **1-70** and **1-71** (Scheme 1.5).[42] After converting to the quinoidal structures **1-69** to **1-70** from **1-67**, bathochromic shift into NIR region were achieved, showing absorptions at 826 nm (ε = 90400 M^{-1} cm^{-1}) for **1-69**, 1008 nm (ε = 132200 M^{-1} cm^{-1}) for **1-70**, and 1186 nm (ε = 65100 M^{-1} cm^{-1}) for **1-71**. Owing to the strong electron-withdrawing imide group, the negative charge could be delocalized in quinoidal form and thus no nucleophilic attack of the imide group in **1-69b** to **1-71b** could be observed, resulting in persistent stability of these molecules.

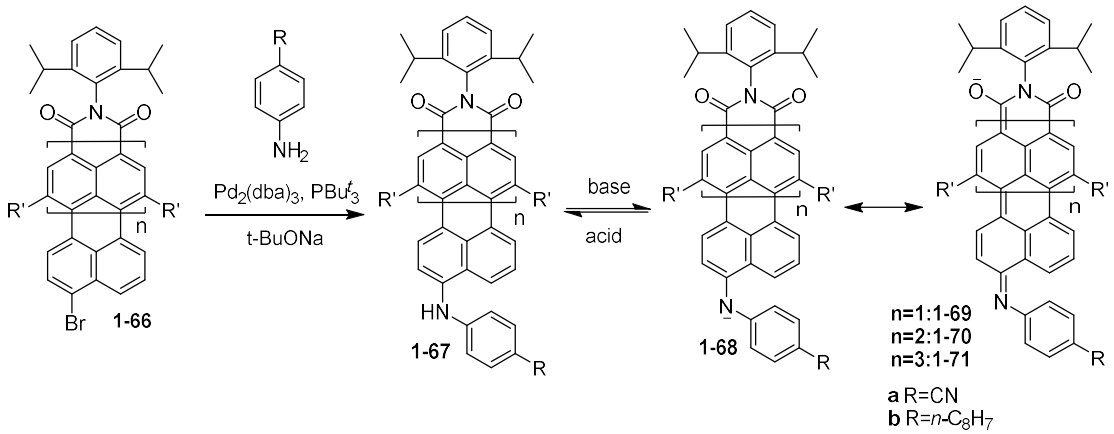

Scheme **1.5** Structures of rylene monoimide and their quinoidal species

1.3 Objectives

As discussed above, rylene dyes are of great interest in dye chemistry. Their versatile optical and electrochemical properties, ease of functionalization, excellent thermal and stablility make them promising candidates in materials such as electronics, photovoltaics and so on. Several concepts including “push-pull” motification, core extension and quinoidization have been developed to construct newly functional chromophores.

In our group, we are particularly intereted in *N*-annulated rylene dyes. The regioselectivity of NP mentioned section 1.1 opens the opportunities for rational design and facile synthesis of newly functional rylene dyes. In this thesis, rylenes have been utilized and three strategies (“push-pull”, core extension, quinoidization) have been adopted to synthesize numerous π-extended molecules with varied physical and optical properties. Apart form flat- and bulk-heterojunction devices, the application of rylene-based dyes for DSCs application were rarely studied . In chapter 3, a series of novel push-pull type dyes were synthesized and applied into DSCs device in order to primariliy examine the design and structure-property relationship.

In chapter 4, further modification was done in order to obtain more rational sensitizers for highly efficient DSCs. Our research will give guidance for the design of new high performance rylene based sensitizers in the future. In chapter 5, a series dimethylthiocapped *N*-annulated rylene dyes were successfully synthesed in longtitudal extension manner. Moreover, with rational design, the reversible oxidation waves and relatively low HOMO allow insight in radical cation and cation species. And this research will pave the way for applying potential rylene dyes in charge transport material as well as organic conductor. Open-shell molecules are of great interest in dye chemistry due to their electronic, optical and magnetic properties. Among them, stable and transient phenoxyl radical species are extensively studied due to the importance in chemical processes, however phenoxyl derivative with large π–system without bulky group are rarely synthesized due to the instablity. Thus making extended pheoxyl derivatives without bulky group is still challenging. In chapter 6, quinoidization as well as π-extension methods were used to synthesize a series of newly functional rylenequinone to carefully study the stucture-properties relationship and primarily examine the potential application.

1.4 References

(1) (a) Randić, M. *Chem. Rev.* **2003**, *103*, 3449. (b) De Proft, F.; Geerlings, P. *Chem. Rev.* **2001**, *101*, 1451. (d) Mitchell, R. H. *Chem. Rev.* **2001**, *101*, 1301. (e) Slayden, S. W.; Liebman, J. F. *Chem. Rev.* **2001**, *101*, 1541. (a) Wu, J.; Pisula, W.; Müllen, K. *Chem. Rev.* **2007**, *107*, 718. (b) Wu, J. *Curr. Org. Chem.* **2007**, *11*, 1220. (c) Jiao, C.; Wu, J. *Curr. Org. Chem*. **2010**, 14, 2145.

(2) (a) Werner, T. C.; Chang, J.; Hercules, D. M. *J. Am. Chem. Soc.* **1969**, *92*, 5560. (b)

Rathore, R.; Kumar, A. S.; Lindeman, S. V.; Kochi, J. K. *J. Org. Chem.* **1998**, *63*, 5847. (c) Shkrob, I. A. *J. Phys. Chem. A*. **1998**, *102*, 4976.

(3) (a) Nagao, Y. *Prog. Org. Coatings* **1997**, *31*, 43-49. (b) Gade, L. H.; Galka, Ch. H.; Hellmann, K. W.; Williams, R. M.; de Cola, L.; Scowen, I. J.; McMartin, M. *Chem. Eur. J.* **2002**, *8*, 3732-3746. (c) Lang, E.; Würthner, F.; Kohler, J. *ChemPhysChem.* **2005**, *6*, 935-941. (d) Cremer, J.; Bäuerle, P. *Eur. J. Org. Chem.* **2005**, 3715-3723.

(4) (a) Herrmann, A.; Müllen, K. *Chem. Lett*. **2006**, 35, 978. (b) Li, C.; Wonneberger, H. *Adv. Mater*. **2012**, *24*, 613. (c) Zhan, X.; Facchetti, A.; Barlow, S.; Marks, T. J.; Ratner, M. A.; Wasielewski, M. R.; Marder, S. R. *Adv. Mater.* **2011**, *23*, 268. (d) Zang, L.; Che, Y.; Moore, J. S. *Acc. Chem. Res*. **2008**, *41*, 1596.

(5) Avlasevich, Y.; Kohl, C.; Müllen, K. *J. Mater. Chem.* **2006**, *16*, 1053.

(6) Bohnen, A.; Koch, K. H.; Lüttke, W.; Müllen, K. *Angew. Chem. Int. Ed.* **1990**, *29*, 525-527.

(7) Li, Y.; Gao, J.; Motta, S. D.; Negri, F.; Wang, Z. *J. Am. Chem. Soc*. **2010**, *132*, 4208.

(8) (a) Bohnen, A.; Koch, K.-H.; Lüttke, W.; Müllen, K. *Angew. Chem., Int. Ed. Engl.* **1990**, *29*, 525.(b) Koch, K.-H. and Müllen, K. *Chem. Ber*. **1991**, *124*, 2091.

(9) (a) Hortrup, F. O.; Müller, G. R. J.; Quante, H.; de Feyter, S.; de Schryver, F. C.; Müllen, K. *Chem. Eur. J.* **1997**, *3*, 219. (b) Nolde, F; Qu, J.; Kohl, C.; Pschirer, N. G.; Reuther, E.; Müllen, K. *Chem. Eur. J.* **2005**, *11*, 3959. (c) Quante, H.; Müllen, K. *Angew. Chem. Int. Ed. Engl.* **1995**, *34*, 1323. (d) Langhals, H.; Schönmann, G.; Feiler, L. *Tetrahedron Letters* **1995**, *36*, 6423. (e) Geerts, Y.; Quante, H.; Platz, H.; Mahrt, R.; Hopmeier, M.; Böhm, A.; Müllen, K. *J. Mater. Chem.* **1998**, *8*, 2357. (f) Tam-Chang,

S. W.; Seo, W.; Iverson, I. K. *J. Org. Chem.* **2004**, *69*, 2719. (g) Tam-Chang, S. W.; Seo, W.; Iverson, I. K.; Casey, S. M. *Angew. Chem. Int. Ed.* **2003**, *42*, 897. (h) Pschirer, N. G.; Kohl, C.; Nolde, F.; Qu, J.; Müllen, K. *Angew. Chem. Int. Ed.* **2006**, *45*, 1401.

(10) Yuan, Z.; Lee, S.-L.; Chen, L.; Li, C.; Mali, K. S.; De Feyter, S.; Müllen, K. *Chem. Eur. J*. **2013**, *19*, 11842.

(11) (a) Looker, J. J. *J. Org. Chem*. **1972**, *37*, 3379. (b) Jiao, C.; Huang, K.-W.; Guan, Z.; Xu, Q.-H.; Wu, J. *Org. Lett.* **2010**, *12*, 4046. (c) Jiao, C.; Huang, K.-W.; Wu, J. *Org. Lett*. **2011**, *13*, 632.

(12) (a) Jiang, W.; Li Y.; Wang, Z. *Chem. Soc. Rev.* **2013**, *42*, 6113. (b) Jiang, W.; Li, Y.; Wang, Z. *Acc. Chem. Res.* **2014**, *47*, 3135

(13) Li, Y.; Wang, Z. *Org. Lett*. **2009**, *11*, 1385.

(14) Jiao, C.; Huang, K.-W.; Luo, J.; Zhang, K.; Chi, C.; Wu, *J. Org. Lett.* **2009**, *11*, 4508.

(15) Adachi, M.; Nagao, Y. *Chem. Mater.* **2001**, *13,* 662.

(16) Zhao, Y.; Ren, A.-M..; Feng, J.-K.; Sun, C.-C. *J. Chem. Phys.* **2008**, *129*, 014301.

(17) Müller, S.; Müllen, K. *Chem. Commun.* **2005**, 4045.

(18) Avlasevich, Y.; Müller, S.; Erk, P.; Müllen, K., *Chem. Eur. J*. **2007**, *13*, 6555.

(19) Lütke Eversloh, C.; Li, C.; Müllen, K. *Org. Lett*. **2011**,*13*, 4148.

(20) Jiang, W.; Li, Y.; Yue, W.; Zhen, Y.; Qu, J.; Wang, Z. *Org. Lett.* **2010**, *12*, 228.

(21) Usta, H.; Newman, C.; Chen, Z.; Facchetti, A. *Adv. Mater*. **2012**, *24*, 3678.

(22) Qian, H.; Wang, Z.; Yue, W.; Zhu, D. *J. Am. Chem. Soc.* **2007**, *129*, 10664. (b) Shi, Y.; Qian, H.; Li, Y.; Yue, W.; Wang, Z. O*rg. Lett.* **2008**, *10*, 2337. (c) Qian, H.; Negri, F.; Wang, C.; Wang, Z. *J. Am. Chem. Soc.* **2008**, *130*, 17970. (d) Zhen, Y.;

Wang, C.; Wang, Z. *Chem. Commun.* **2010**, *46*, 1926.

(23) (a) Désilets, D.; Kazmaier, P. M.; Burt, R. A.; Hamer, G. K. *Can. J. Chem.* **1995**, *73*, 325. (b) Yao, J.; Chi, C.; Wu, J.; Loh, K. *Chem. Eur. J.* **2009**, *15*, 9299.

(24) (a) Arabei, S. M.; Pavich, T. A. *J. Appl. Spectr.* **2000**, *67*, 236. (b) Kuroda, H. *J. Chem. Soc.* **1960**, 1856. (c) Clar, E. *Chem. Ber*. **1948**, *81*, 52.

(25) Li, J.; Zhang, K.; Zhang, X.; Huang, K.; Chi, C.; Wu, J. *J. Org. Chem.* **2010**, *75*, 856.

(26) Bai, Q.; Gao, B.; Ai, Q.; Wu, Y.; Ba, X. *Org. Lett.* **2011**, *13*, 6484.

(27)Li, Y.; Xu, W.; Motta, S. D.; Negri, F.; Zhu, D.; Wang, Z. *Chem. Commun*. **2012**, *48*, 8204.

(28) Lütke Eversloh, C; Liu, Z.; Müller, B.; Stangl, M.; Li, C.; Müllen, K. *Org. Lett*. **2011**, *13*, 5528.

(29) Avlasevich, Y.; Müllen, K. *Chem. Commun*. **2006**, 4440.

(30) Li, C.; Schöneboom, J.; Liu, Z.; Pschirer, N.G.; Erk, P.; Hermann, A.; Müllen, K. *Chem. Eur. J.* **2009**, *15*, 878.

(31) Li, C.; Yum, J.-H.; Moon, S.-J.; Herrmann, A.; Eickemeyer, F.; Pschirer, N. G.; Erk, P.; Schöneboom, J.; Müllen, K.; Grätzel, M.; Nazeeruddin, M. K. *ChemSusChem* **2008**, *1*, 615.

(32) Luo, J.; Xu, M.; Li, R.; Huang, K.-W.; Jiang, C.; Qi, Q.; Zeng, W.; Zhang, J.; Chi, C.; Wang, P.; Wu, J. *J. Am. Chem. Soc.* **2014**, *136*, 265.

(33) Luo, J.; Wang, X.; Fan, L.; Li, G.; Qi, **Q.;** Huang, K.-W.; Tam, T. L. D.; Zhang, J.; Wang, Q.; Wu, J. *J. Mater. Chem. C* **2016**, *4*, 3709.

(34) (a) Yao, Z.; Yan, C.; Zhang, M.; Li, R.; Cai, Y.; Wang, P. *Adv. Energy Mater.* **2014**,

4, 1400244; (b) Zhang, M.; Yao, Z.; Yan, C.; Cai, Y.; Ren, Y.; Zhang, J.; Wang, P. *ACS Photonics* **2014**, *1*, 710; (c)Yang, L.; Ren, Y.; Yao, Z.; Yan, C.; Ma, W.; Wang, P. *J. Phys. Chem. C* **2015**, *119*, 980.

(35) (a) Yao, Z.; Wu, H.; Ren, Y.; Guo, Y.; Wang, P. *Energy Environ. Sci.* **2015**, *8*, 1438; (b) Yao, Z.; Zhang, M.; Wu, H.; Yang, L.; Li, R.; Wang, P. *J. Am. Chem. Soc.* **2015**, *137*, 3799; (C) Yao, Z.; Zhang, M; Li, R; Yang, L.; Qiao, Y.; Wang, P. *Angew. Chem.* **2015**, *127*, 6092.

(36) Yang, L.; Zheng, Z.; Li, Y.; Wu, W.; Tian, H.; Wang, Z. *Chem. Commun.* **2015**, *51*, 4842.

(37) Kohl, C.; Becker, S.; Müllen, K. *Chem. Commun*. **2002**, 2778.

(38) Zeng, Z.; Ishida, M.; Zafra, J. L.; Zhu, X.; Sung, Y. M.; Bao, N.; Webster, R. D.; Lee, B. S.; Li, R.-W.; Zeng, W.; Li, Y.; Chi, C.; Navarrete, J. T. L.; Ding, J.; Casado, J.; Kim, D.; Wu, J. *J. Am. Chem. Soc.* **2013**, *135*, 6363.

(39) Zeng, Z.; Lee, S.; Zafra, J. L.; Ishida, M.; Zhu, X.; Sun, Z.; Ni, Y.; Webster, R. D.; Li, R.-W.; López Navarrete, J. L.; Chi, C.; Ding, J.; Casado, J.; Kim, D.; Wu, J. *Angew. Chem. Int. Ed.* **2013**, *52*, 8561

(40) Zeng, Z.; Lee, S.; Zafra, J. L.; Ishida, M.; Bao, N.; Webster, R. D.; López Navarrete, J. T.; Ding, J.; Casado, J.; Kim, D.; Wu, J. *Chem. Sci.* **2014**, *5*, 3072.

(41) Zeng, Z.; Lee, S.; Son, M.; Fukuda, K.; Burrezo, P. M.; Zhu, X.; Qi, Q**.;** Li, R.-W.; Lopez Navarrete, J. T.; Ding, J.; Casado, J.; Nakano, M.; Kim, D.; Wu, J. *J. Am. Chem. Soc.* **2015**, *137*, 8572.

(42) Liu, Z.; Li, C.; Wagner, M.; Avlasevich, Y.; Herrmann, A.; Müllen, K. *Chem. Commun.* **2008**, 5028.

Chapter 2 *N*-Annulated Perylene-Based Push−Pull-Type Sensitizers

2.1 Introduction

Design and synthesis of stable organic dyes with appropriate energy level alignment, appropriate push-pull structure and large light-harvesting capability were proven to be key to achieving high-performance dye-sensitized solar cells (DSCs).[1] In recent years, various types of organic dyes with donor-π-acceptor structure have been investigated.[2] Among them, porphyrin based push-pull type sensitizers have demonstrated superior performance in comparison to other metal-free organic dyes.[3] However, the tedious synthesis makes it very hard to apply this kind of dyes in practical applications.

Therefore, we started to look for a good replacement of porphyrin. Perylene could be a suitable candidate as it has an intense absorption band around 410 nm which is close to the Soret band of porphyrin. As mentioned in chapter 1, perylene based dyes have shown excellent photophysical properties such as a high extinction coefficient, a high fluorescence quantum yield, and outstanding chemical, thermal, and photochemical stability.[4] In fact, perylene-based dyes have been successfully used for both organic photovoltaics[5] and DSCs.[6] However, most of them exhibited relatively low overall power conversion efficiencies and were limited to perylene anhydride with modification at bay position to improve solubility and suppress aggregation.

As our group has a solid research background on rylene derivatives, our attention was then shifted to a new perylene derivative, the so-called *N*-annulated perylene (NP) in which a nitrogen atom is annulated at the bay position.[7] Compared with the parent

perylene, regio-selective functionalization (e.g., bromination) can be conducted at the *peri*- positions near the amine side,[8] which opens the opportunities to generate push-pull type sensitizers by using NP as a new rigid and coplanar π-linker (Figure 2.1). In addition, flexible alkyl chains or bulky groups can be readily introduced to the amine site, which can significantly improve the solubility and suppress dye aggregation. Moreover, NP itself has good light-harvesting ability and can also serve as an electron donor. In fact, our group recently demonstrated that NP-substituted porphyrins showed largely improved light harvesting in near-infrared region and power conversion efficiency (η) higher than 10% was achieved in Co(II)/(III) based DSCs.[9] In this context, three NP-based push-pull sensitizers **QB1**-**QB3** (Figure 2.1) were synthesized and tested in DSCs in this work. The design is based on the following considerations: (1) NP shows strong absorption in visible range (λ_{abs}^{max} = 413 nm) with high extinction coefficient and high fluorescence quantum yield,[8] which will be good for light harvesting; (2) bulky *ortho*-alkoxy substituted phenyl group rather than flexible alkyl chain was chosen to suppress the problematic dye aggregation as well as to ensure sufficient solubility;[10] (3) triphenylamine (TPA) was chosen for electron-donating donor while cyanoacetic acid (CAA) was chosen as electron-acceptor/anchoring group because they have been proved to be efficient for many metal-free sensitizers;[2] (4) for **QB2**, a 4,4-dihexyl-4H-cyclopenta[2,1-b:3,4-b′]dithiophene (CPDT) unit was inserted between NP and CAA in QB1 in order to extend π-conjugation; (5) for **QB3**, an electron-deficient benzothiadiazole (BT) moiety was inserted between the NP and the CPDT unit in **QB2** to facilitate intramolecular charge separation and to tailor the

light harvesting property.

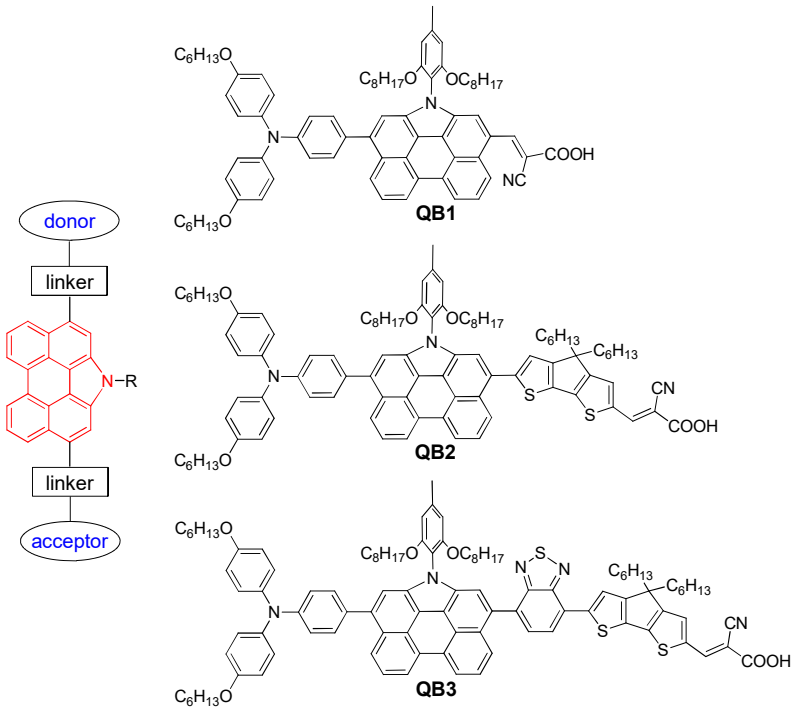

Figure 2.1 Molecular design and structures of NP-based sensitizers **QB1-QB3**.

2.2 Results and discussion

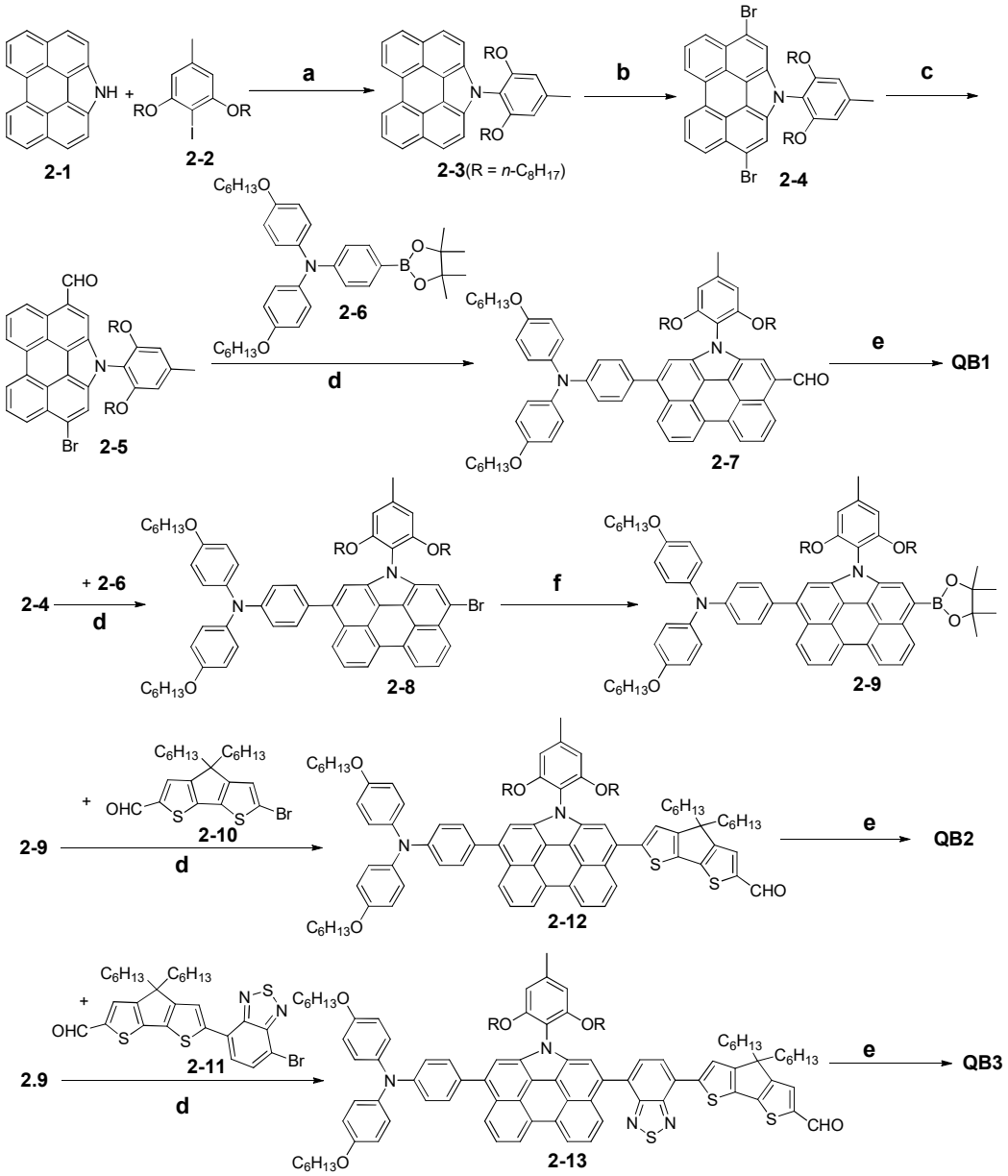

Scheme 2.1 Synthetic routes of **QB1-QB3**: (a) Cu, 18-crown-6, K_2CO_3, DMAc ,170 ^oC,30%; (b) NBS, $CHCl_3$, 90%; (c) n-BuLi, -78 ^oC, then DMF, 25%; (d) $Pd(PPh_3)_4$, aq K_2CO_3 toluene or THF; (e) cyanoacetic acid, piperidine, $CHCl_3$, reflux, 89% for **QB1** 85% for **QB2** and **QB3**;(f) pinacolborane, $Pd(PPh_3)_2Cl_2$, Et_3N/THF, reflux, 86%.

The synthesis commenced with the *N*-arylation of the parent NP **2-1**[7,8] with the 2,6-bisoctyloxy-1-iodobenzene **2-2** in the presence of Cu and K_2CO_3 to give the key compound **3.3** (Scheme 3.1). Regio-selective bromination of **2-3** with **2-2** equiv of *N*-bromosuccinimide (NBS) at room temperature gave the dibrominated NP **2-4** in 90% yield. The NP monoaldehyde **2-5** was then prepared by the mono- lithiation of **2-4** followed by reaction with anhydrous DMF. Suzuki coupling of compound **2-5** with 4,4,5,5-tetramethyl-2-{4-[*N*,*N*-bis(4-hexyloxyphenyl)amino]phenyl}-1,3,2-dioxaborol ane **(2-6)**[11] generated the NP aldehyde **2-7** and subsequent Knoevenagel condensation with cyanoacetic acid in presence of piperidine afforded the target compound **QB1** in 89% yield over two steps. Suzuki coupling between **2-4** and **2-6** gave the monobromo- NP **2-8** yield and then the NP monoboronic ester **2-9** as another key intermediate was prepared by Miyaura borylation reaction from **2-8**. Suzuki coupling between **2-9** with the monobromo- CPDT **2-10**[11] or CPDT-BT **2-11**[12] gave the aldehydes **2-12** and **2-13**, respectively, and similar Knoevenagel condensation with cyanoacetic acid afforded the corresponding dyes **QB2** and **QB3**.

The absorption spectra of **QB1-QB3** in chloroform all exhibit a broad band at 400–700 nm region with large molecular extinction coefficient (ε), which can be attributed to the intramolecular donor-acceptor interaction (Figure 2.2a). Time-dependent DFT (TD-DFT) calculations have been performed at the B3LYP/6-31G* level of theory,[13] as implemented in the Gaussian 09 program package.[14] The geometries of **QB1**-**QB3** were fully optimized in gas phase using the default convergence criteria without any constraints and confirmed by frequency calculations. UV-vis-NIR absorption spectra were generated assuming an average UV-vis width of 4000 cm^{-1} at half-height using

the SWizard program.[15] TD-DFT calculations suggest that the band around 400–700 nm region is a combination of several electronic transitions dominated by HOMO→LUMO, HOMO-1→LUMO, HOMO→LUMO+1 and HOMO-1→LUMO+1 (Figure 2.5, Table 2.2, 2.3, 2.4). The absorption maximum was observed at 531 nm (ε = 3.27×104 $M^{-1}cm^{-1}$) for **QB1**, 550 nm (ε = 4.45×104 M^{-1} cm^{-1}) for **QB2**, and 502 nm (ε = 4.96×104 M^{-1} cm^{-1}) for **QB3**. In comparison with **QB1**, the absorption maximum and absorption edge of **QB2** shift to red by 19 nm and 58 nm, respectively, and the spectra become more broad and intense, which can be explained by the extended π-conjugation after inserting of a CPDT unit. **QB3** shows similar spectral broadening and intensity enhancement, with the absorption edge shifted to the red by 60 nm. However, its absorption maximum exhibits a 29 nm blue shift, which can be explained by a larger dihedral angle (59.4°) between the NP and BT units in **QB3** than that (42.2°) between NP and CDPT units in **QB2** based on the DFT calculations (Figure. 2.4). The absorption spectra of three sensitizers adsorbed on transparent mesoporous TiO_2 films all show some blue shift presumably due to the deprotonation of –COOH group on TiO_2 surface (Figure 2.2b). The spectra of **QB1** and **QB2** are slightly broadened but there is no significant change on the shape, indicating that there is not much dye aggregation due to the introduction of bulky bisoctyloxyphenyl group to the amine site.[10] However, for **QB3**, the shape of its absorption spectrum is quite different and largely blue-shifted, implying possible formation of H-aggregates after inserting a BT moiety. In fact, the ^{1}H NMR spectra of **QB1** and **QB2** show sharp peaks even in concentrated solutions, but the **QB3** exhibits relatively broadened resonances.

The HOMO and LUMO energy levels of **QB1-QB3** were determined to be 5.03, 4.98, 4.98 eV (HOMO) and 3.44, 3.41, 3.42 eV (LUMO), respectively, by cyclic voltammetry in CH_2Cl_2 solution (Figure 2.3 and Table 2.1). The electrochemical energy gaps were calculated accordingly to be 1.59, 1.57, and 1.56 eV, which are in agreement with the optical energy gaps. DFT (B3LYP/6-31G*) calculations show that for **QB1**, the HOMO is delocalized along both the TPA and the NP core, while the LUMO is delocalized through the NP core and the CAA group (Figure 2.4). **QB2** and **QB3** exhibit even more segregated HOMO and LUMO. Such a spatially well-separated orbital distribution is desirable for efficient intramolecular charge separation and fast injection of photo-excited electron into the conduction band of TiO_2 via the carboxylic group adsorbed on the TiO_2 surface.

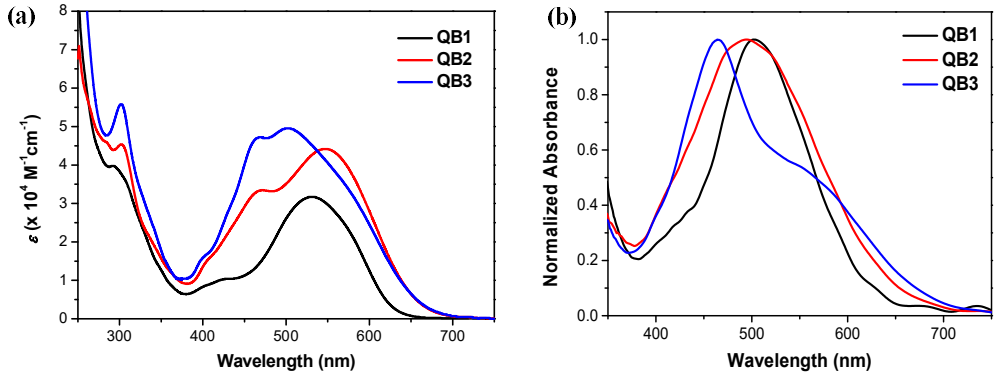

Figure 2.2 (a) UV-Vis absorption spectra of **QB1-QB3** in chloroform; (b) Normalized UV-vis absorption spectra of **QB1-QB3** sensitizers adsorbed on transparent mesoporous TiO_2 films.

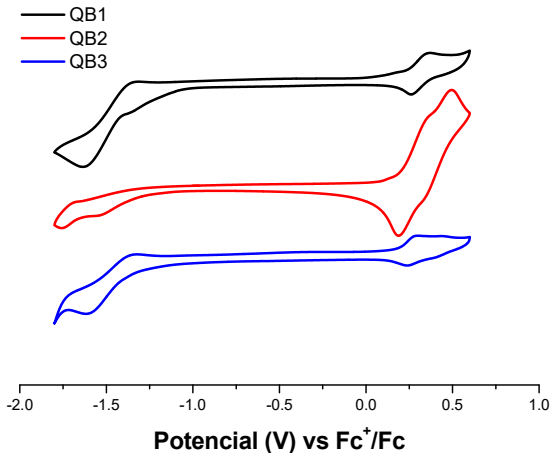

Figure 2.3 Cyclic voltammograms of **QB1** – **QB3** in dry CH_2Cl_2 with $TBAPF_6$ as supporting electrolyte, AgCl/Ag as reference electrode, Au disk as working electrode, Pt wire as counter electrode, and scan rate at 50 mV/s.

Table 2.1 Summary of optical and electrochemical properties of **QB1**, **QB2** and **QB3**.

Dye	λ_{abs} (nm)	ε ($M^{-1}cm^{-1}$)	E_g^{opt} (eV)	$E_{1/2}^{ox}$ (V)	$E_{1/2}^{red}$ (V)	HOMO[a] (eV)	LUMO[a] (eV)	E_g^{EC} (eV)
QB1	531	32700	1.95	0.31	-1.49	-5.03	-3.44	1.59
QB2	550	44500	1.83	0.26	-1.44	-4.98	-3.41	1.57
				0.42	-1.71			
QB3	502	49600	1.80	0.25	-1.48	-4.98	-3.42	1.56
				0.44				

[a]The HOMO and LUMO energy levels were determined from the onset of first oxidation and reduction wave, respectively.

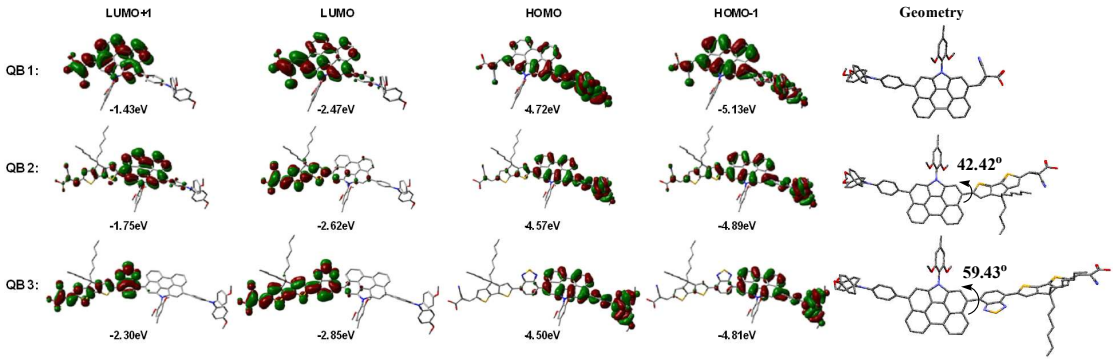

Figure 2.4 Optimized geometry, calculated HOMO and LUMO profiles and energy levels of **QB1** – **QB3** (B3LYP/6-31G*).

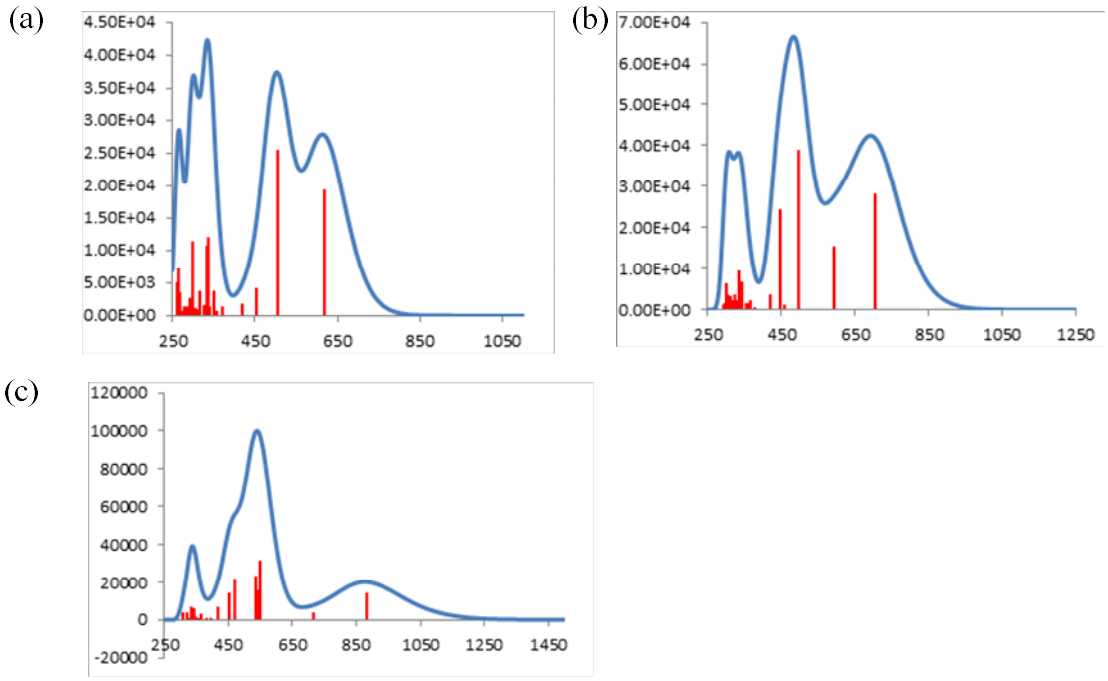

Figure 2.5 Calculated absorption spectrum for (a)**QB1**, (b)**QB2** and (c)**QB3.**

Table 2.2 Selected TD-DFT (B3LYP/6-31G*) calculated energies, oscillator strength and compositions of major electronic transitions of **QB1**

Wavelength (nm)	Osc. Strength (*f*)	Major contributions
616.5	0.3749	H-0->L+0(+98%)
503.7	0.4909	H-1->L+0(+96%)
418.7	0.0331	H-0->L+1(+96%)
338.3	0.2300	H-0->L+2(+42%) H-2->L+1(+34%)
332.6	0.2043	H-0->L+2(+43%) H-2->L+1(+35%)
300.5	0.2187	H-0->L+7(+82%) H-0->L+10(+6%)
263.8	0.1401	H-1->L+5(+25%) H-6->L+1(+22%)

Table 2.3 Selected TD-DFT (B3LYP/6-31G*) calculated energies, oscillator strength and compositions of major electronic transitions of **QB2**

Wavelength (nm)	Osc. Strength (*f*)	Major contributions

703.4	0.5425	H-0->L+0(+99%)
594.5	0.2951	H-1->L+0(+99%)
495.4	0.7505	H-0->L+1(+89%)
		H-2->L+0(10%)
447.3	0.4684	H-2->L+0(+43%) H-1->L+1(+41%)
		H-3->L+0(+9%)
342.6	0.1319	H-0->L+3(+45%)
		H-0->L+5(18%)
		H-0->L+4(+9%) H-1->L+2(+6%)
337.0	0.1813	H-1->L+3(+5%)
		H-0->L+4(+67%) H-0->L+3(+10%)
302.9	0.1223	H-9->L+0(+8%) H-8->L+0(5%)
		H-0->L+9(+32%)
		H-1->L+5(24%) H-0->L+10(+9%)
		H-4->L+1(+6%) H-1->L+4(6%)

Table 2.4 Selected TD-DFT (B3LYP/6-31G*) calculated energies, oscillator strength and compositions of major electronic transitions of **QB3**

Wavelength (nm)	Osc. Strength (*f*)	Major contributions
883.7	0.2703	H-0->L+0(+92%) H-1>L+0(+5%)
549.3	0.5982	H-2->L+0(+52%)
		H-1->L+1(34%) H-0->L+1(+6%)
539.3	0.3076	H-1->L+1(+44%)
		H-3->L+0(33%)
		H-2->L+0(+17%)
534.8	0.4514	H-3->L+0(+60%) H-2->L+0(+20%)
		H-1->L+1(+14%)
470.3	0.4133	H-0->L+2(+89%)
		H-2->L+1(+6%)
452.9	0.2758	H-2->L+1(+80%) H-2->L+0(7%)

415.3	0.1343	H-1->L+2(+92%)
340.5	0.1183	H-0->L+4(+51%)
		H-0->L+6(28%)
		H-1->L+4(+6%)
335.9	0.1239	H-7->L+1(+32%)
		H-6->L+1(31%) H-11->L+0(+10%)
335.6	0.1367	H-0->L+6(+9%)
		H-0->L+6(+50%) H-0->L+4(+22%)
318.8	0.0751	H-6->L+1(+8%) H-0->L+5(+7%)
		H-0->L+8(+28%)
		H-1->L+6(14%)
		H-0->L+10(13%) H-0>L+11(+10%)
		H-1->L+5(7%)

The newly synthesized dyes **QB1**-**QB3** were adsorbed onto a bilayer titania film to serve as a working electrode for photovoltaic characterizations with Co(II)/(III) based electrolyte.[12] Figures 2.6a-b show the photocurrent density–voltage (J-V) characteristics and the corresponding incident photon-to-current efficiency (IPCE) action spectra under illumination of the standard AM 1.5 simulated sunlight (1 sun, 100 mWcm^{-2}). Dyes **QB1-QB3** showed an average power conversion efficiency of 5.79%, 6.10% and 5.46%, respectively (Table 2.5), which is impressive since most reported perylene based sensitizers exhibited low or moderate performance.[6] In particular, DSCs based on **QB**1 showed large open circuit voltage (V_{oc} = 0.825 V), which could be ascribed to its optimal frontier molecular orbital profile and lower HOMO energy level compared with **QB2** and **QB3.** Broad IPCE action spectra covering most of the visible region were observed for all three dyes, which is in

consistence with their absorption spectra. Dyes **QB1** and **QB2** showed IPCE values up to 75%, while dye **QB3** exhibited lower maximum IPCE value (~54%). The onset of IPCE action spectra is red-shifted from 663 nm for **QB1** to 715 nm for **QB2** and to 725 nm for **QB3**. As a result, **QB2** cell showed the highest short circuit current density (Jsc) of 12.31 mA cm^{-2} while **QB1** and **QB3** displayed smaller Jsc values (Table 2.5). After co-adsorption with deoxycholic acid (DCA), the power conversion efficiency dropped for the **QB1** cell (η = 4.76%) while slightly increased for **QB2** cell (η = 6.95%). Significant improvement of performance was observed for **QB3** (η = 6.30%) presumably due to the suppression of dye aggregation.

To further understand the dye structure-device performance relationship, electrochemical impedance measurements were conducted on the **QB1-QB3** cells under illumination and open circuit states. As commonly understood, V_{OC} is intimately correlated to the conduction band (CB) position and the charge recombination rate.[16] Figure 2.6c shows the dependence of chemical capacitance (Q) of the three cells on V_{OC}. At a fixed bias voltage, the difference in chemical capacitance indicates the conduction band (CB) position of TiO_2 varies among the three cells. Apparently, **QB1** cell presented the largest upward shift of the CB, while **QB2** the least,[17] largely interpreting the V_{OC} difference of the cells. Figure 2.6d shows the recombination resistance (R_{ct}) of the cells at different Q. At a fixed electron density, the Rct for **QB1** cell is larger than that for **QB2** and **QB3**, the latter two being fairly similar, which implies charge recombination be more effectively retarded by **QB1** dye. As a result, the above two factors render the highest V_{OC} of **QB1** cell.

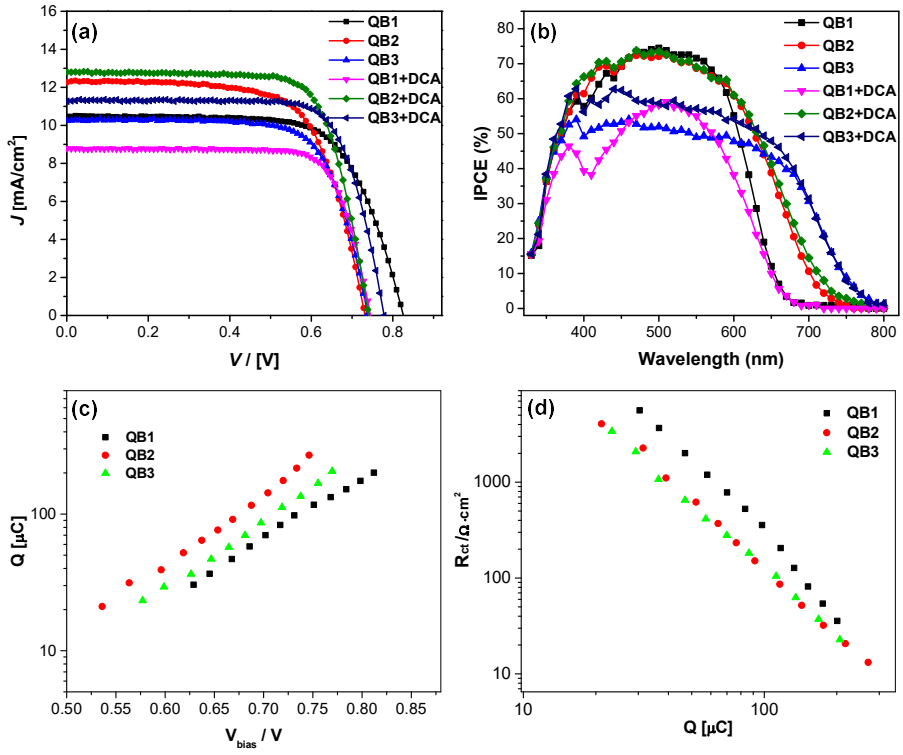

Figure 2.6 (a) Photocurrent-voltage curves and (b) IPCE action spectra of the DSCs based on **QB1-QB3** with and without co-adsorbent DCA; (c) TiO_2 chemical capacitance (Q) versus bias voltage and (d) electron recombination resistance (R_{ct}) versus Q for **QB1-QB3** cells.

Table 2.5 Photovoltaic parameters of DSCs based on **QB1-QB3** with and without co-adsorbent DCA

cell name	V_{OC}/mV	J_{SC}/mA cm^{-2}	*ff* (%)	η (%)
QB1	825	10.48	69.1	5.79[a]
QB2	731	12.31	67.8	6.10[a]
QB3	739	10.27	72.0	5.46[a]
QB1 + DCA	729	8.76	74.4	4.76[b]
QB2 + DCA	740	12.80	73.3	6.95[b]
QB3 + DCA	766	11.32	72.6	6.30[b]

[a]The cell employed 5.3 μm TiO_2 transparent with 4.0 μm light scattering layers. [b]Co-adsorbed with DCA, dye: DCA = 1:10.

2.3 Conclusion

In summary, alkoxy-wrapped *N*-annulated perylene was first used as a rigid and coplanar π-spacer for the design of push-pull type sensitizers. The obtained dyes **QB1**-**QB3** showed good light harvesting ability and superior device performance compared to many known perylene-based sensitizers. Our research suggests that NP could be a good replacement of porphyrin for the design of new high performance sensitizers in the future. Optimization of sensitizer structure by extending π-conjugation and/or by tuning the donor and acceptor structures is underway to further improve the device performance.

2.4 Experimental section

2.4.1 General

All reagents and starting materials were obtained from commercial suppliers and used without further purification unless otherwise noted. Anhydrous toluene and THF were distilled from sodium-benzophenone immediately prior to use. The ^{1}H NMR and ^{13}C NMR spectra were recorded in solution of $CDCl_3$ or THF-d_8 on Bruker DPX 300 or DRX 500 NMR spectrometers with tetramethylsilane (TMS) as the internal standard. The following abbreviations were used to explain the multiplicities: s = singlet, d = doublet, t = triplet, m = multiplet. MALDI-TOF or APCI mass spectrometry was used to confirm the mass of compound. The electrochemical measurements were carried out in anhydrous methylene chloride with 0.1 M $TBAPF_6$ as the supporting electrolyte at room temperature under the protection of nitrogen. A gold stick was used as working electrode, platinum wire was used as counting electrode, and Ag/AgCl (3M KCl solution) was used as reference electrode. The potential was externally calibrated

against the ferrocene/ferrocenium couple. Steady-state UV-vis absorption were recorded on a Shimadzu UV-1700 spectrometer. The solvents used for UV-vis measurements are of HPLC grade (Merck). Infrared (IR) spectra in KBr pellet were recorded by using Bio-Rad Excalibur FTS 3000.

2.4.2 Detailed synthetic procedures and characterization data

Compound 2-2

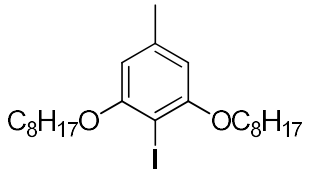

In a dried two-neck round-bottom flask, 3,5-dihydroxytoluene (2.85 g, 23 mmol) was dissolved in cold (0℃) acetonitrile (500 mL). N-iodosuccinimide (5.175g, 23mmol) was added in portion. The reaction was quenched by adding saturated sodium thiosulfate solution. After removal of acetonitrile by rotary evaporator, the residue was extracted with ethyl acetate for three times, followed by washing with saturated thiosulfate solution and sodium chloride solution. The organic solvent was removed under reduced pressure. The crude product was dissolved in DMF (150 mL) and then 1-bromooctane (9.7g, 50 mmol) and K_2CO_3 (12.7 g, 93 mmol) were added. The reaction was heated under flux for 24h. The solvent was removed under reduced pressure and the residue was extracted with dichloromethane (DCM) (3 × 100 mL). The organic phase was washed with water and dried over anhydrous Na_2SO_4. After removal of solvent under reduced pressure, the residue was purified by column chromatography eluting with hexanes to give the final product (6 g, 55%). 1H NMR ($CDCl_3$, 300 MHz): δ ppm = 6.28(s, 2H), 4.00 (t, J = 6.3 Hz, 4H), 2.31 (s, 3H),

1.77-1.86 (m, 4H), 1.46-1.53 (m, 4H), 1.28-1.37 (m, 16H), 0.88 (t, J = 6.6 Hz, 6H). 13C NMR ($CDCl_3$, 75 MHz): δ ppm = 158.80, 139.89, 106.17, 75.11, 69.31, 31.81, 29.27, 29.23, 29.17, 26.09, 22.66, 21.84, 14.10. HR MS (EI): m/z = 474.2011; calcd. for $C_{23}H_{39}IO_2$: 474.1995 (error: +3.47 ppm).

Compound 2-3

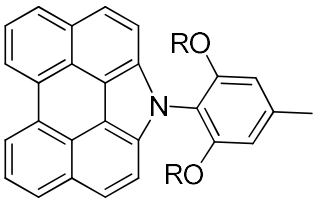

(R = *n*-C_8H_{17})

A mixture of compound **2-2** (474.4 mg, 1 mmol), K_2CO_3 (220 mg, 1.6 mmol) and 18-crown-6 (5.3 mg, 0.02 mmol) was loaded into a two-necked round bottom flask, which was degassed and refilled with argon. Then CuI (15.2 mg, 0.08 mmol), *N*-annulated perylene (1, 53 mg, 0. 2 mmol) and DMF (3 ml) were added under argon. The reaction was refluxed for two days. The mixture was extracted with ethyl acetate for three times, followed by washing with water and saturated sodium chloride solution. After removal of solvent under reduced pressure, the residue was purified by column chromatography eluting with hexane/DCM (5:1) to give final product (36.4 mg, 30%). 1H NMR ($CDCl_3$, 300 MHz): δ ppm = 8.66 (d, J = 7.5 Hz, 2H), 8.12 (d, J = 7.8 Hz, 2H), 7.80-7.86 (m, 4H), 7.58 (d, J = 8.7 Hz, 2H), 6.66 (s, 2H), 3.89 (t, J = 6.6 Hz, 4H), 2.52 (s, 3H), 1.32-1.36 (m, 4H), 1.01-1.06 (m, 4H), 0.86-0.91 (m, 16H), (t, J = 7.2 Hz, 6H). 13C NMR ($CDCl_3$,75MHz): δ ppm = 155.93, 139.31, 133.15, 130.60, 129.08, 124.93, 124.90, 124.31, 122.94, 120.29, 117.84,115.40, 114.41, 106.99, 69.06, 31.50, 28.90, 25.64, 22.46, 22.35, 13.95. HR-MS (APCI, m/z): calcd.

for $C_{43}H_{50}NO_2$ ([M+1]), 612.3836; found, 612.3837 (error: +0.2 ppm).

Compound 2-4

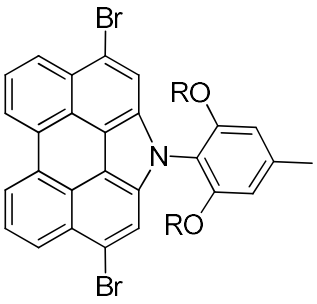

(R = *n*-C_8H_{17})

To the solution of compound **2-3** (892 mg, 1.46 mmol) in DCM (200 mL) was slowly added NBS (520 mg, 2.92 mmol) in portion over half an hour. The mixture was stirred at room temperature for 30 min. The reaction mixture was quenched with water (50 mL). The organic layer was washed with water, and then washed with saturated brine and dried over anhydrous Na_2SO_4. The solvent was removed under reduced pressure and the crude product was purified by column chromatography (silica gel, hexane : DCM = 6 : 1) to give compound as a yellow solid (1.01 g, 90%). ^{1}H NMR ($CDCl_3$, 300 MHz): δ ppm = 8.69 (d, J = 7.5 Hz, 2H), 8.36 (d, J = 8.1 Hz, 2H), 7.86-7.91 (m, 4H), 6.63 (s, 2H), 3.95 (t, J = 6.3 Hz, 4H), 2.51 (s, 3H), 1.34-1.40 (m, 4H), 0.96-1.03 (m, 4H), 0.82-0.91 (m, 16H), 0.70 (t, J = 6.9 Hz, 6H). ^{13}C NMR ($CDCl_3$, 75 MHz): δ ppm = 155.48, 139.96, 132.75, 130.10, 128.13, 125.37, 125.05, 124.23, 121.48, 119.27, 117.56, 116.78, 112.89, 106.38, 68.90, 31.43, 29.63, 28.96, 28.87, 28.82, 25.74, 22.38, 13.87. HR-MS (APCI, m/z): calcd. for $C_{43}H_{48}Br_2NO_2$ ([M+1]), 768.2046; found, 768.2054 (error: +0.9 ppm).

Compound 2-5

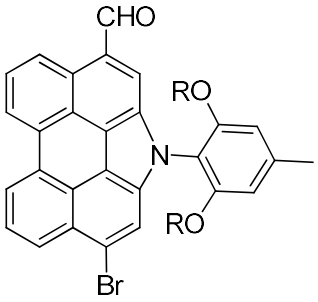

(R = *n*-C_8H_{17})

To a solution of **2-4** (769 mg, 1.0 mmol) in dry THF (25 mL) was added dropwise 1.6 M n-BuLi in hexane solution (0.56 mL, 0.9 mmol) at -78 ^{o}C under argon atmosphere. After the mixture was stirred at -78 ^{o}C for 1 h, anhydrous DMF (0.36 g, 5 mmol) was added into the mixture. After slowly warming up to room temperature overnight, the mixture was poured into aqueous NH_4Cl solution. The aqueous layer was extracted with ethyl acetate, and the combined organic phase was washed with saturated brine and dried over anhydrous Na_2SO_4. The solvent was removed under reduced vacuum and the residue was purified by column chromatography (silica gel, DCM: hexane = 1:3) to afford **2-5** as an orange waxy solid (180 mg, 25%). ^{1}H NMR ($CDCl_3$, 500 MHz): δ ppm = 10.45 (s, 1H), 9.39 (d, J = 8.0 Hz, 1H), 8.81 (d, J = 7.5 Hz, 2H), 8.40 (d, J = 8.0 Hz, 1H), 8.10 (s, 1H), 8.04 (t, J = 8.0 Hz, 1H), 7.98 (t, J = 8.0 Hz, 1H), 7.92 (s, 1H), 6.66 (s, 2H), 3.94 (t, J = 6.5 Hz, 4H), 2.52 (s, 3H), 1.32-1.38 (m, 4H), 0.94-0.99 (m, 4H), 0.79-0.88 (m, 16H), 0.77 (t, J = 7.5 Hz, 6H). ^{13}C NMR ($CDCl_3$,125 MHz): δ ppm = 193.11, 155.60, 140.47, 135.87, 131.93, 130.31, 130.08, 129.29, 128.18, 127.46, 127.25, 127.09, 125.84, 125.56, 124.72, 124.26, 122.55, 122.02, 121.74, 121.02, 119.29, 116.56, 112.55, 106.54, 69.02, 31.44, 28.94, 28.89, 28.85, 25.79, 22.46, 22.39, 13.88. HR-MS (APCI, m/z): calcd. for $C_{44}H_{49}BrNO_3$ ([M+1]), 718.2890; found, 718.2907 (error: +2.3 ppm).

Compound 2-8

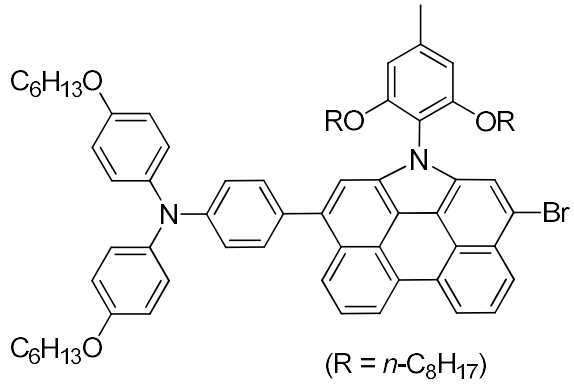

To a suspended solution of 2-4 (76 mg, 0.1 mmol), 4,4,5,5-tetramethyl-2-{4-[N,N-bis(4-hexyloxyphenyl)amino]phenyl}-1,3,2-dioxaborolane (**2-6**, 54 mg, 0.08 mmol), and tetrakis(triphenylphosphine)palladium (11 mg, 0.01 mmol) in THF (5 mL) was added potassium carbonate aqueous solution (2 M, 0.4 mL) under argon. The reaction mixture was refluxed for 24 h and then water (5 mL) was added. The crude compound was extracted into ethyl acetate, washed with brine and water, and dried over anhydrous sodium sulfate. After removing solvent under reduced pressure, the residue was purified by column chromatography (silica gel, ethyl acetate : hexanes = 1 : 50) to yield a viscous orange oil (67 mg, 60% yield). ^{1}H NMR ($CDCl_3$, 500 MHz): δ ppm = 8.70 (m, 2H), 8.33 (d, J = 8.5 Hz, 1H), 8.24 (d, J = 8.0 Hz, 1H), 7.90 (m, 2H), 7.79 (t, J = 8.0 Hz, 1H), 7.49 (s, 1H), 7.46 (d, J = 8.5 Hz, 2H), 7.14 (d, J = 9.0 Hz, 4H), 7.06 (d, J = 8.5 Hz, 2H), 6.87 (d, J = 9.0 Hz, 4H), 6.61 (s, 2H), 3.96 (t, J = 6.5 Hz, 4H), 3.89 (t, J = 6.5 Hz, 4H), 2.48 (s, 3H), 1.75-1.81 (m, 4H), 1.45-1.49 (m, 4H), 1.33-1.36 (m, 8H), 0.87-0.96 (m, 30H), 0.86 (t, J = 6.5 Hz, 6H). ^{13}C NMR ($CDCl_3$,125 MHz): δ ppm = 155.81, 155.43, 147.77, 140.96, 139.68, 139.28, 137.55, 134.04, 133.53, 132.61, 130.94, 130.90, 130.70, 130.27, 128.84,

128.22, 126.58, 125.26, 124.87, 124.72, 124.63, 124.60, 124.44, 121.02, 120.92, 120.29, 119.20, 117.40, 116.72, 116.59, 115.80, 115.32, 114.06, 113.67, 106.72, 69.04, 68.31, 31.62, 31.49, 29.70, 29.36, 28.99, 28.98, 28.84, 25.78, 25.73, 22.62, 22.42, 14.04, 13.92. HR-MS (APCI, m/z): calcd. for $C_{73}H_{86}BrN_2O_4$ ([M+1]), 1133.5765; found, 1133.5799 (error: +3 ppm).

Compound 2-9

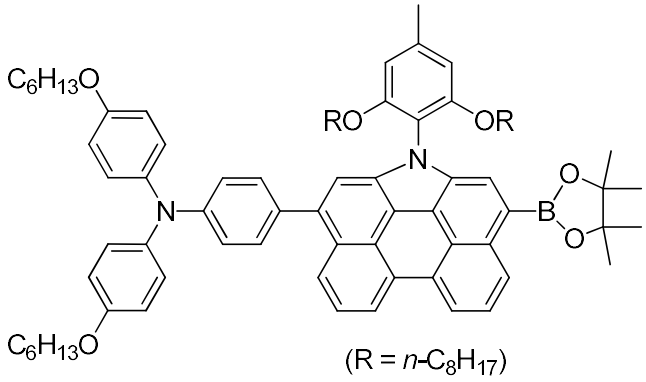

A 100 mL Schlenk flask was charged with 2-8 (113 mg, 0.1 mmol), pinacolborane (63 mg, 0.5 mmol), triethylamine (102 mg, 1.0 mmol), $PdCl_2(PPh_3)_2$ (4 mg, 0.005 mmol) and 1,2-dichloroethane (10 mL) under argon. The reaction mixture was stirred at 90 °C overnight. After removal of the solvent, the crude product was purified by column chromatography (silica gel, hexane : DCM = 5 : 1) to give compound **2-9** as a yellow oil (64 mg, 86%). ^{1}H NMR ($CDCl_3$, 500 MHz): δ ppm = 9.04 (d, J = 8.0 Hz, 1H), 8.71 (m, 2H), 8.26 (s, 1H), 8.23 (d, J = 8.0 Hz, 1H), 7.89 (t, J = 8.0 Hz, 1H), 7.80 (t, J = 8.0 Hz, 1H), 7.53 (s, 1H), 7.51 (d, J = 8.5 Hz, 2H), 7.17 (d, J = 9.0 Hz, 4H), 7.10 (d, J = 8.5 Hz, 2H), 6.89 (d, J = 9.0 Hz, 4H), 6.64 (s, 2H), 3.98 (t, J = 6.5 Hz, 4H), 3.90 (t, J = 6.5Hz, 4H), 2.51 (s, 3H), 1.79-1.82 (m, 4H), 1.48 (br, 16H), 1.36-1.39 (m, 8H), 0.85-1.00 (m, 30H), 0.70 (t, J = 6.5 Hz, 6H). ^{13}C NMR ($CDCl_3$, 125 MHz): δ

ppm = 155.99, 155.37, 147.69, 140.99, 139.21, 137.87, 134.28, 134.13, 132.90, 132.72, 130.71, 130.07, 128.07, 126.68, 126.52, 124.96, 124.86, 124.70, 124.24, 120.63, 120.54, 120.33, 119.98, 116.88, 115.72, 115.29, 114.29, 114.05, 106.83, 83.25, 69.02, 68.27, 31.60, 31.47, 29.68, 29.34, 28.98, 28.94, 28.82, 25.76, 25.66, 25.02, 22.60, 22.38, 14.01, 13.89. HR-MS (APCI, m/z): calcd. for $C_{79}H_{98}BN_2O_6$ ([M+1]), 1181.7525; found, 1181.7551 (error: +2.2 ppm).

Compound 2-12

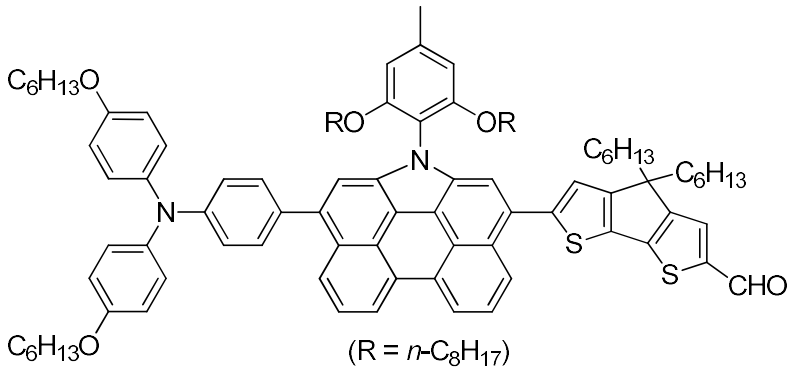

To a suspension of **2-9** (118 mg, 0.1 mmol), **2-10** (58 mg, 0.12 mmol), and tetrakis(triphenylphosphine)palladium (11.6 mg, 0.01 mmol) in toluene (5 mL) was added potassium carbonate aqueous solution (2 M, 0.4 mL) under argon. The reaction mixture was refluxed for 24 h and then water (5 mL) added. The crude compound was extracted with ethyl acetate three times, followed by washing with brine and water, and dried over anhydrous sodium sulfate. After removing solvent under reduced pressure, the residue was purified by column chromatography (silica gel, ethyl acetate : hexanes' = 1 : 50) to yield a viscous red oil (64 mg, 45% yield). ^{1}H NMR ($CDCl_3$, 300 MHz): δ ppm = 9.85 (s, 1H), 8.73 (m, 2H), 8.46 (d, J = 8.1 Hz, 1H), 8.26 (d, J = 8.1 Hz, 1H), 7.74-7.87 (m, 3H), 7.61 (s, 1H), 7.46-7.52 (m, 3H), 7.33 (s, 1H),

7.15 (dd, 3J = 6.9 Hz, 4J = 2.1 Hz, 4H), 7.08 (d, J = 8.4 Hz, 2H), 6.88 (dd, 3J = 6.9 Hz, 4J = 2.1 Hz, 4H), 6.62 (s, 1H), 3.97 (m, 8H), 2.46 (s, 3H), 1.94-1.99 (m, 4H), 1.74-1.81 (m, 4H), 1.45-1.50 (m, 4H), 1.33-1.39 (m, 14H), 1.21-1.28 (m, 14H), 1.08-1.12 (m, 4H), 0.77-0.95 (m, 36H), 0.65 (t, J = 6.9 Hz, 6H). ^{13}C NMR ($CDCl_3$, 125 MHz): δ ppm = 182.43, 163.03, 157.32, 155.82, 155.42, 149.77, 148.50, 147.78, 142.72, 140.93, 139.62, 137.74, 134.37, 134.07, 134.00, 132.50, 131.23, 130.88, 128.81, 128.21, 127.97, 127.78, 126.58, 125.01, 124.98, 124.89, 124.77, 124.45, 123.45, 121.53, 120.87, 120.80, 120.26, 118.37, 117.09, 116.80, 115.76, 115.30, 113.76, 106.73, 69.02, 54.18, 37.74, 31.61, 31.45, 30.19, 29.68, 29.64, 29.35, 29.02, 28.99, 28.80, 25.77, 25.72,24.69, 22.61, 22.56, 22.39, 22.34, 14.02, 13.89. HR-MS (APCI, m/z): calcd. for $C_{95}H_{114}N_2O_5S_2$ ([M+1]), 1427.8242; found, 1427.8257 (error: +1.1 ppm).

QB1

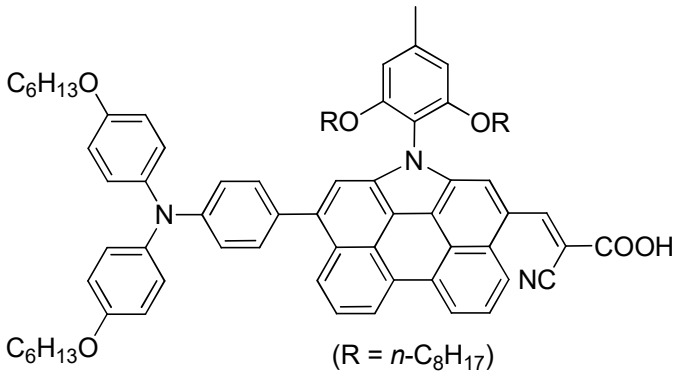

To a suspended solution of **2-5** (72 mg, 0.1 mmol), 4,4,5,5-tetramethyl-2-{4-[N,N-bis(4-hexyloxyphenyl)amino]phenyl}-1,3,2-dioxaborol ane (**2-6**, 68 mg, 0.12 mmol), and tetrakis(triphenylphosphine)palladium (11.6 mg, 0.01 mmol) in toluene (5 mL) was added potassium carbonate aqueous solution (2 M,

0.4 mL) under argon. The reaction mixture was refluxed for 24 h and then water (5 mL) added. The crude compound was extracted into ethyl acetate, washed with brine and water, and dried over anhydrous sodium sulfate. The separation of pure compound **2-7** was difficult so it was used directly for the next step. After removing solvent under reduced pressure, the residue (**2-7**) was loaded into a two-necked round bottom flask. To a stirred solution of the residue containing **2-7** and cyanoacetic acid (10 mg, 0.12 mmol) in chloroform (5mL) was added piperidine (23 mg, 0.28 mmol). The reaction mixture was refluxed under argon for 18 h and then acidified with 2 M hydrochloric acid aqueous solution (3 mL). The crude product was extracted by chloroform, washed with water, and dried over anhydrous sodium sulfate. After removing solvent under reduced pressure, the residue was purified by flash chromatography with chloroform and methanol/chloroform (1/10, v/v) in turn as the eluent to yield a dark red powder (51 mg, 89%). Mp: 88-90 oC. IR (KBr): 3443.18, 2955.35, 2919.15, 2851.37, 2365.65, 2339.92, 2215.23, 1735.92, 1603.34, 1505.97, 1421.38, 1382.57, 1353.14, 1301.34, 1239.75, 1176.97, 1031.08, 801.87, 757.03, 656.15, 531.87 cm-1. ^{1}H NMR (THF-d_8, 500 MHz): δ ppm = 9.09(s, 1H), 8.94 (m, 2H), 8.65 (s, 1H), 8.39 (d, J = 8.5 Hz, 1H), 8.20 (d, J = 9.0 Hz, 1H), 8.03 (t, J = 7.5Hz, 1H), 7.89 (t, J = 7.5 Hz, 1H), 7.47 (d, J = 8.5 Hz, 2H), 7.38 (s, 1H), 7.10 (d, J = 9.0 Hz, 4H), 6.93 (m, 6H), 6.81 (s, 2H), 3.98 (m, 8H), 2.46 (s, 3H), 1.66-1.70 (m, 4H), 1.39-1.42 (m, 4H), 1.25-1.30 (m, 12H), 0.55-0.87 (m, 26H), 0.52 (t, J = 7.5 Hz, 6H). ^{13}C NMR (THF-d_8, 125 MHz): δ ppm = 172.86, 156.62, 156.49, 149.28, 141.52, 140.70, 140.59, 136.64, 135.59, 134.18, 133.11, 131.92, 131.22, 131.12, 130.18, 128.89, 127.33, 126.38, 125.73, 125.63, 125.48, 125.29, 125.23, 122.29, 122.01,

121.78, 121.52, 120.64, 117.67, 116.31, 115.87, 114.44, 107.05, 69.43, 66.59, 32.83, 32.64, 32.37, 32.19, 30.40, 30.26, 30.31, 29.77, 29.63, 27.13, 26.53, 26.48, 23.31, 23.05, 14.17, 14.07. HR-MS (APCI, m/z): calcd. for $C_{77}H_{88}N_3O_6$ ([M+1]), 1150.6668; found, 1150.6636 (error: -2.7 ppm).

QB2

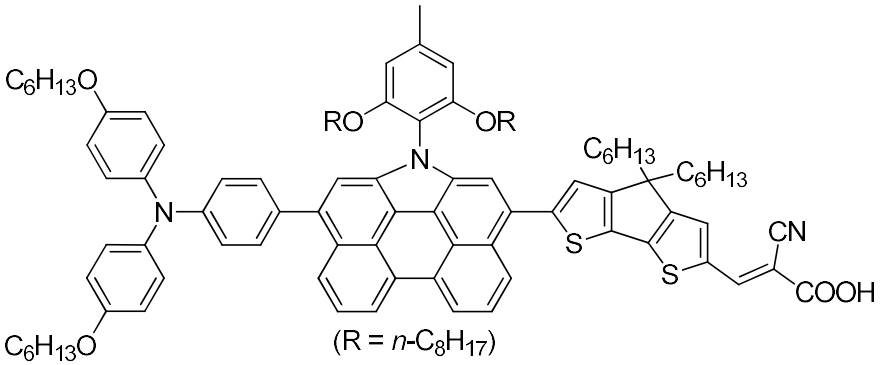

To a stirred solution of **2-12** (47 mg, 0.03 mmol) and cyanoacetic acid (10 mg, 0.12 mmol) in chloroform (5mL) was added piperidine (23 mg, 0.28 mmol). The reaction mixture was refluxed under argon for 18 h and then acidified with 2 M hydrochloric acid aqueous solution (3mL). The crude product was extracted by chloroform, washed with water, and dried over anhydrous sodium sulfate. After removing solvent under reduced pressure, the residue was purified by flash column chromatography with chloroform and methanol/chloroform (1/10, v/v) in turn as the eluent to yield a dark red powder (40 mg, 85%). Mp: 83-85 ^{o}C. IR (KBr): 3463.09, 2956.27, 2927.77, 2855.73, 2362.57, 2339.27, 1654.92, 1632.64, 1508.55, 1104.26, 976.64, 800.27, 470.77 cm-1. ^{1}H NMR (THF-d_8, 500 MHz): δ ppm = 8.79 (m, 2H), 8.50 (d, J = 8.0 Hz, 1H), 8.36 (s, 1H), 8.21 (d, J = 8.5 Hz, 1H), 7.85 (t, J = 8.0 Hz, 1H), 7.81 (s, 1H), 7.78 (t, J = 8.0 Hz, 1H), 7.74 (s, 1H), 7.48 (m, 4H), 7.11(d, J = 8.5 Hz, 4H), 7.05 (d, J = 8.5 Hz, 2H), 6.87 (d, J = 8.5 Hz, 4H), 6.76 (s, 2H), 3.97 (m, 8H), 2.48 (s, 3H), 2.03-2.06

(m, 4H), 1.75-1.80 (m, 4H), 1.46-1.52 (m, 4H), 1.35-1.39 (m, 14H), 1.22 (m, 14H), 1.10-1.15 (m, 4H), 0.76-0.93 (m, 36H), 0.62 (t, J = 7.0 Hz, 6H). ^{13}C NMR (THF-d_8, 75 MHz): δ ppm= 179.14, 163.26, 156.12, 156.05, 150.19, 148.44, 141.03, 139.99, 138.12, 134.34, 134.01, 133.87, 132.77, 132.57, 130.6, 128.47, 128.38, 126.72, 125.19, 125.16, 125.12, 124.72, 124.67, 124.63, 121.99, 121.11, 117.13, 116.80, 115.75, 115.33, 106.74, 68.94, 68.07, 54.40, 37.81, 31.83, 31.80, 31.66, 29.86, 29.58, 29.23, 29.04, 25.99, 22.77, 22.72, 22.52, 13.62, 13.53. HR-MS (APCI, m/z): calcd. for $C_{98}H_{116}N_3O_6S_2$ ([M+1]), 1494.8300; found, 1494.8284 (error: -1.1 ppm).

QB3

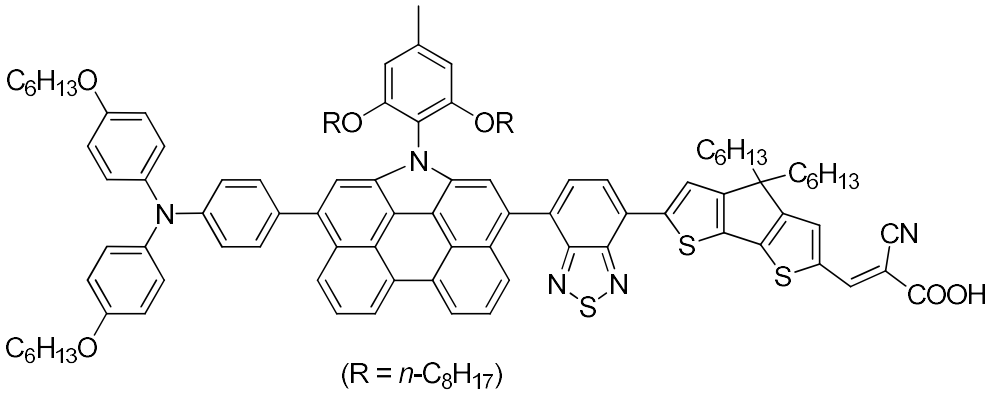

Similar procedure to that of synthesis of QB1 gave QB3 as a purple solid (40 mg, 85%). Mp: 126-128 °C. IR (KBr): 3464.87, 2953.39, 2927.21, 2855.72, 1655.23, 1603.76, 1505.52, 1369.48, 1318.93, 1289.58, 1239.55, 1163.51, 1124.68, 827.75, 803.61, 758.17, 542.21 cm-1.^{1}H NMR (THF-d_8, 300 MHz): δ ppm = 8.66 (m, 2H), 8.47 (br, 1H), 8.34 (s, 1H) 8.20 (d, J = 8.4 Hz, 2H), 7.92 (d, J = 6.9 Hz, 1H), 7.69-7.85 (m, 4H), 7.62 (br, 1H), 7.48-7.51 (m, 3H), 7.12 (d, J = 8.7 Hz, 4H), 7.06 (d, J = 8.4 Hz, 2H), 6.88 (d, 8.7 Hz, 4H), 6.71 (s, 2H), 3.97 (m, 8H), 2.42 (s, 3H), 2.09 (m, 4H), 1.77-1.79 (m, 4H), 1.47-1.52 (m, 4H), 1.36-1.38 (m, 14H), 1.21 (br, 18H), 0.79-0.94

(m, 36H), 0.64 (t, J = 6.9 Hz, 6H). Clear ^{13}C NMR spectrum was not obtained even after overnight collection of data due to the poor solubility of the compound. HR-MS (APCI, m/z): calcd. for C104H118N5O6S3 ([M+1]), 1628.8239; found, 1628.8232 (error: -0.4 ppm).

2.4.3 Device fabrication and characterization

Solar cell fabrications: Fluorine-doped tinoxide (FTO, Pilkington TEC-15, 15Ωsq−1) glass plate was cleaned by 5% Decon 90 solution, deionized water, and ethanol sequentially in an ultrasonic bath sequentially. A compact TiO_2 layer was synthesized onto that cleaned FTO glass by spray pyrolysis at 500 °C. A transparent mesoporous TiO_2 layer (90 T, Dyesol, ~5.3μm) and scattering layer (~4 μm, no scattering layer for TA) were prepared onto the substrate by screen-printing method. Thereafter, the electrode was gradually heated at 125 °C for 5 min, at 325 °C for 5 min, at 375 °C for 5 min, at 450 °C for 15 min and at 500 °C for 15 min. Finally, the TiO_2 electrode was treated by 40 mM $TiCl_4$ aqueous solution at 70 °C for 30 min and then sintered at 500 °C for 30 min. DSCs were assembled by separating the sensitized TiO_2 film and the platinized FTO glass with a hot-melt spacer (25 μm, Surlyn, DuPont) and followed by heating at 110 °C for 1 min. The platinized FTO counter electrode was prepared by thermal decomposition of hexachloroplatinic acid at 400 °C for 15 min. The dye loading was performed by immersing the photoanodes in 0.15 mM in a mixture solutions (DCM:EtOH = 4:1) of the individual dyes and kept for 18 h in dark at room temperature. The co-sensitized photo-anodes were prepared by dyeing them into appropriate (0.15 mM) of the individual dyes and in a mixture solutions (DCM:EtOH=4:1) containing DCA (1.5 mM). The redox electrolyte (0.2 M

$Co(bpy)_3(PF_6)_2$, 0.02 M $Co(bpy)_3(PF6)_3$, 0.5M $LiClO_4$, and 0.5M 4-tert-butylpyridine in acetonitrile) was injected through a hole at the platinized FTO a partial vacuum. Finally, the hole was sealed with a small piece of hot-melt polymer and a cover glass.

Characterizations: Electrochemical impedance spectroscopy (EIS) were measured under 627 nm illumination from a high-power LED using a potentiostat equipped with a frequency response analyzer (Ecochemie, AUTOLAB PGSTAT302N/FRA2) and the Nova 1.6 software package. Different light intensities were achieved by using neutral density filters mounted in an automated filter wheel system (Newport). The frequency range of the EIS measurement was 105 to 0.1Hz with a perturbation of 10 mV. Photocurrent–voltage characteristics were measured with a Keithley 2400 Source Meter under AM 1.5G illumination at 100 mW cm-2 from a solar simulator (450 W, Newport class A) calibrated with a silicon reference cell. The active area of the cells was 0.12 cm2 defined by a mask. The incident photon-to current conversion efficiency (IPCE) spectra were attained under a 300W Xenon lamp and a grating monochromator with a spectral resolution of ~5 nm (Newport/Oriel) controlled by TRACQ basic software (Newport).

2.5 References

(1) (a) Oregan, B.; Grätzel, M. *Nature* **1991**, 353, 737. (b) Imahori, H.; Umeyama, T.; Ito, S. *Acc. Chem. Res.* **2009**, 42, 1809. (c) Hagfeldt, A.; Boschloo, G.; Sun, L.; Kloo, L.; Pettersson, H. *Chem. Rev.* **2010**, 110, 6595. (d) Hardin, B. E.; Snaith, H. J.; McGehee, M. D. *Nat. Photonics* **2012**, 6, 162. (e) Zhang, S.; Yang, X.; Numata, Y.; Han, L. *Energy Environ. Sci.* **2013**, 6, 1443. (f) Ying, W.; Yang, J.; Wielopolski, M.; Moehl, T.; Moser, J.–E.; Comte, P.; Hua, J.; Zakeeruddin, S. M.; Tian, H.; Grätzel, M.

Chem. Sci. **2014**, 5, 206. (g) Huang, Z.; Feng, H.; Zang, X.; Iqbal, Z.; Zeng, H.; Kuang, D.; Wang, L.; Meierd, H.; Cao, D. *J. Mater. Chem. A* **2014**, 2, 15365.

(2) See recent reviews: (a) Mishra, A.; Fischer, M. K. R.; Bäuerle, P. *Angew. Chem. Int. Ed* **2009**, 48, 2474. (b) Clifford, J. N.; Martínez-Ferrero, E.; Viterisi, A.; Palomares, E. *Chem. Soc. Rev.* **2011**, 40, 1635. (c) Liang, M.; Chen, J. *Chem. Soc. Rev.* **2013**, 42, 3453.

(3) (a) Li, L.-L.; Diau, E. W.-G. *Chem. Soc. Rev.* **2013**, 42, 291. (b) Yella, A.; Lee, H.-W.; Tsao, H. N.; Yi, C.; Chandiran, A. K.; Nazeeruddin, M. K.; Diau, E.W.-G.; Yeh, C.-Y.; Zakeeruddin, S. M.; Grätzel, M. *Science* **2011**, 334, 629. (c) Mathew, S.; Yella, A.; Gao, P.; Humphry-Baker, R.; Curchod, B. F. E.; Ashari-Astani, N.; Tavernelli, I.; Rothlisberger, U.; Nazeeruddin, M. K.; Grätzel, M. *Nat. Chem.* **2014**, 6, 242. (d) Yella, A.; Mai, C.-L.; Zakeeruddin, S. M.; Chang, S.-N.; Hsieh, C.-H.; Yeh, C.-Y.; Grätzel, M. *Angew. Chem. Int. Ed.* **2014**, 53, 2973. (e) Higashino, T.; Imahori, H. *Dalton Trans.* **2015**, 44,448.

(4) See recent review: Chen, L.; Li, C.; Müllen, K. *J. Mater. Chem. C* **2014**, 2, 1938.

(5) (a) Schmidt-Mende, L.; Fechtenköter, A.; Müllen, K.; Moons, E.; Friend, R. H.; MacKenzie, J. D. *Science* **2001**, 293, 1119. (b) Cremer, J.; Mena-Osteritz, E. M.; Pschierer, N. G.; Müllen, K.; Bauerle, P. *Org. Biomol. Chem*. **2005**, 3, 985. (c) Zhan, X. W.; Tan, Z. A.; Domercq, B.; An, Z. S.; Zhang, X.; Barlow, S.; Li, Y. F.; Zhu, D. B.; Kippelen, B.; Marder, S. R. *J. Am. Chem. Soc.* **2007**, 129, 7246. (d) Sharma, G. D.; Suresh, P.; Mikroyannidis, J. A.; Stylianakis, M. M. *J. Mater. Chem.* **2010**, 20, 561.

(6) (a) Ferrere, S.; Zaban, A.; Gregg, B. A. *J. Phys. Chem. B* **1997**, 101, 4490. (b) Edvinsson, T.; Li, C.; Pschirer, N.; Schoneboom, J.; Eickemeyer, F.; Sens, R.;

Boschloo, G.; Herrmann, A.; Müllen, K.; Hagfeldt, A. *J. Phys. Chem. C* **2007**, 111, 15137. (c) Shibano, Y.; Umeyama, T.; Matano, Y.; Imahori, H. *Org. Lett.* **2007**, 9, 1971. (d) Li, C.; Yum, J.-H.; Moon, S.-J.; Herrmann, A.; Eickemeyer, F.; Pschirer, N. G.; Erk, P.; Schöneboom, J.; Müllen, K.; Grätzel, M.; Nazeeruddin, M. K. *ChemSusChem* **2008**, 1, 615. (e) Li, C.; Liu, Z. H.; Schoneboom, J.; Eickemeyer, F.; Pschirer, N. G.; Erk, P.; Herrmann, A.; Müllen, K. *J. Mater. Chem.* **2009**, 19, 5405. (f) Imahori, H.; Mathew, S. *J. Mater. Chem.* **2011**, 21, 7166. (g) Jiao, C.; Zu, N.; Huang, K.-W.; Wang, P.; Wu, J. *Org. Lett.* **2011**, 13, 3652. (h) Li, C.; Wonneberger, H. *Adv. Mater.* **2012**, 24, 613. (i) Yao, Z.; Yan, C.; Zhang, M.; Li, R.; Cai, Y.; Wang, P. *Adv. Energy Mater.* **2014**, 4, 1400244.

(7) Looker, J. J. *J. Org. Chem*. **1972**, 37, 3379.

(8) (a) Li, Y.; Wang, Z. *Org. Lett.* **2009**, 11, 1385. (b) Jiao, C.; Huang, K.-W.; Luo, J.; Zhang, K.; Chi, C.; Wu, J. *Org. Lett*. **2009**, 11, 4508. (c) Li, Y.; Gao, J.; Motta, S. D.; Negri, F.; Wang, Z. *J. Am. Chem. Soc.* **2010**, 132, 4208. (d) Jiao, C.; Huang, K.-W.; Guan, Z.; Xu, Q.-H.; Wu, J. *Org. Lett.* **2010**, 12, 4046. (e) Jiao, C.; Huang, K.-W.; Wu, J. *Org. Lett*. **2011**, 13, 632. (f) Zeng, Z.; Ishida, M.; Zafra, J. L.; Zhu, X.; Sung, Y. M.; Bao, N.; Webster, R. D.; Lee, B. S.; Li, R.-W.; Zeng, W.; Li, Y.; Chi, C.; Navarrete, J. T. L.; Ding, J.; Casado, J.; Kim, D.; Wu, J. *J. Am. Chem. Soc.* **2013**, 135, 6363. (g) Zeng, Z.; Lee, S.; Zafra, J. L.; Ishida, M.; Zhu, X.; Sun, Z.; Ni, Y.; Webster, R. D.; Li, R.-W.; López Navarrete, J. L.; Chi, C.; Ding, J.; Casado, J.; Kim, D.; Wu, J. *Angew. Chem. Int. Ed.* **2013**, 52, 8561.

(9) Luo, J.; Xu, M.; Li, R.; Huang, K.-W.; Jiang, C.; Qi, Q.; Zeng, W.; Zhang, J.; Chi, C.; Wang, P.; Wu, J. *J. Am. Chem. Soc*. **2014**, 136, 265.

(10) (a) Lee, C. Y.; She, C. X.; Jeong, N. C.; Hupp, J. T. Chem. Commun. 2010, 46, 6090. (b) Chang, Y. C.; Wang, C. L.; Pan, T. Y.; Hong, S. H.; Lan, C. M.; Kuo, H. H.; Lo, C. F.; Hsu, H. Y.; Lin, C. Y.; Diau, E. W.-G. *Chem. Commun.* **2011**, 47, 8910. (c) Wang, C.-L., Lan, C.-M., Hong, S.-H., Wang, Y.-F., Pan, T.-Y., Chang, C.-W.; Kuo, H.-H.; Kuo, M.-Y.; Diau, E. W.-G.; Lin, C.-Y. *Energy Environ. Sci.* **2012**, 5, 6933. (d) Ripolles-Sanchis, T.; Guo, B. C.; Wu, H. P.; Pan, T. Y.; Lee, H. W.; Raga, S. R.; Fabregat-Santiago, F.; Bisquert, J.; Yeh, C. Y.; Diau, E. W.-G. *Chem. Commun*. **2012**, 48, 4368.

(11) Li, R. Z.; Liu, J. Y.; Cai, N.; Zhang, M.; Wang, P. *J. Phys. Chem. B* **2010**, 114, 4461.

(12) Wang, X. Z.; Yang, J.; Yu, H.; Li, F.; Fan, L.; Sun, W.; Liu, Y.; Koh, Z. Y.; Pan, J. H.; Yim, W.-L.; Yan, L.; Wang, Q. *Chem. Commun.* **2014**, 50, 3965.

(13) (a) O'Regan, B. C.; Bakker, K.; Kroeze, J.; Smit, H.; Sommeling P.; Durrant, J. R. *J. Phys. Chem. B* **2006**, 110, 17155. (b) Duffy, N. W.; Peter, L. M.; Rajapakse, R. M. G.; Wijayant, K. G. U. *Electrochem. Commun* **2000**, 2, 658.

(14) (a) Ditchfie, R. W.; Hehre, J.; Pople, J. A. J. Chem. Phys 1971, 54, 724. (b) Hehre, W. J.; Ditchfie R.; Pople, J. *J. Chem. Phys* **1972**, 56, 2257. (c) Becke, A. D. *J. Chem. Phys* **1993**, 98, 1372. (d) *Gaussian 09;* Revision A.2; Frisch, M. J.; Trucks, G. W.; Schlegel, H. B.; Scuseria, G. E.; Robb, M. A.; Cheeseman, J. R.; Scalmani, G.; Barone, V.; Mennucci, B.; Petersson, G. A.; Nakatsuji, H.; Caricato, M.; Li, X.; Hratchian, H. P.; Izmaylov, A. F.; Bloino, J.; Zheng, G.; Sonnenberg, J. L.; Hada, M.; Ehara, M.; Toyota, K.; Fukuda, R.; Hasegawa, J.; Ishida, M.; Nakajima, T.; Honda, Y.; Kitao, O.; Nakai, H.; Vreven, T.; Montgomery, J., J. A.; Peralta, J. E.; Ogliaro, F.;

Bearpark, M.; Heyd, J. J.; Brothers, E.; Kudin, K. N.; Staroverov, V. N.; Kobayashi, R.; Normand, J.; Raghavachari, K.; Rendell, A.; Burant, J. C.; Iyengar, S. S.; Tomasi, J.; Cossi, M.; Rega, N.; Millam, N. J.; Klene, M.; Knox, J. E.; Cross, J. B.; Bakken, V.; Adamo, C.; Jaramillo, J.; Gomperts, R.; Stratmann, R. E.; Yazyev, O.; Austin, A. J.; Cammi, R.; Pomelli, C.; Ochterski, J. W.; Martin, R. L.; Morokuma, K.; Zakrzewski, V. G.; Voth, G. A.; Salvador, P.; Dannenberg, J. J.; Dapprich, S.; Daniels, A. D.; Farkas, Ö.; Foresman, J. B.; Ortiz, J. V.; Cioslowski, J.; Fox, D. J.; Gaussian, Inc., Wallingford CT, 2009.

(15) Gorelsky, S. I., *SWizard program*, http://www.sg-chem.net/, University of Ottawa, Ottawa,Canada, 2010.

(16) (a) Marinado, T.; Nonomura, K.; Nissfolk, J.; Karlsson, M. K.; Hagberg, D. P.; Sun, L.; Mori, S.; Hagfeldt, A. *Langmuir* **2010**, 26, 2592. (b) Ronca, E.; Pastore, M.; Belpassi, L.; Tarantelli, F.; De Angelis, F. *Energy Environ. Sci.* **2013**, 6, 183.

(17) Kopidakis, N.; Neale, N. R.; Frank, A. J. *J. Phys. Chem. B* **2006,** 110, 12485.

Chapter 3 Push-pull Type *N*-annulated Perylene Based Sensitizers: the Effect of Acceptor Structure on the Light-Harvesting Ability and Photovoltaic Performance

3.1 Introduction

As discussed in Chapter 2, the alkoxy-wrapped *N*-annulated perylene (NP), in which a nitrogen atom is annulated at the bay position was successfully ultilized in constructing push-pull type sensitizers for DSCs. Due to their outstanding photophysical properties, regio-selective functionalization at the peri-positions, the higher electron density of NP, the obtained dyes **QB1**-**QB3** showed good light harvesting ability and superior device performance compared to many known perylene-based sensitizers. For further improvement of the device, it is highly desirable to develop new dyes with even enhanced light harvesting ability both in the visible (ca. 400-700) and the near infrared (NIR) region (ca. 700-1400 nm) since a significant portion of solar energy falls within this range and develop stable push-pull type organic dyes with appropriate energy level alignment and good light-harvesting capability.[1-6] In addition, the choice of donor is critical to achieve good light-harvesting ability and efficient intramolecular charge separation upon photo-irradiation. Recently, our group demonstrated several modificatied NP sensitizers with high device performance.[7] Meanwhile, P. Wang and Z. Wang's groups also showed very good results by employing NP as a basic building block for the organic sensitizers with careful design and modification.[8]

In this work, we designed and synthesized three new alkoxyl-chain wrapped NP

sensitizers (**QB4-QB6** shown in Figure 3.1) to further explore the fundamental structure-physical property-device performance relationship. The design is based on the following considerations: (1) NP with bulky *o*-alkoxy-substituted phenyl group rather than flexible alkyl chain on amine site was chosen to suppress the problematic dye aggregation, to eliminate charge recombination at the TiO_2 interface, and to improve the dye solubility;[9] (2) triphenylamine with long alkoxyl chain was chosen as the donor because of its excellent electron donating character as well as good solubility;[2] (3) carbon-carbon triple bond was inserted as a π bridge between the triphenylamine and NP (**QB4** and **QB5**) or between the NP and the acceptor moieties (**QB5**) in order to extend the π-conjugation and to form a rigid structure;[10] (4) benzoic acid was chosen as acceptor for **QB4**[4] while for **QB5**, an electron-deficient benzothiadiazole (BT) moiety was inserted to facilitate intramolecular charge separation as well as to tailor the light-harvesting property;[11] (5) for **QB6**, cyclopentadithiophene (CPDT) together with cynoacetic acid was used as electron acceptor part because CPDT has been proved to be an efficient building block for many metal-free sensitizers,[12] and it also allows us to compare with **QB4** and **QB5** in this work and another dye (**QB2**) in our previous work.[9]

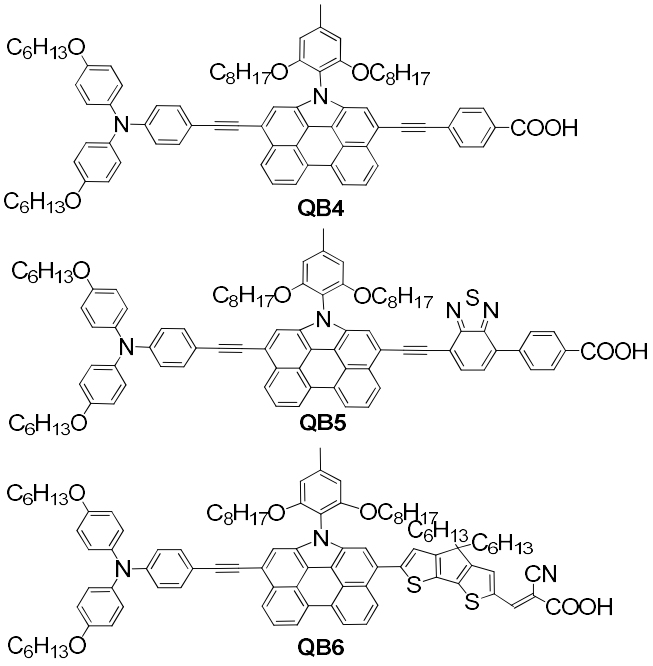

Figure 3.1 Structures of **QB4**, **QB5** and **QB6**.

3.2 Results and discussion

The synthetic route for the dyes **QB4**, **QB5** and **QB6** is outlined in Scheme 3.1. The NP building blocks **3-1** and **3-4** were synthesized according to our previous report.[9] Sonogashira coupling between **3-1** and terminal alkynes **3-2** and **3-3** in one step gave the **QB4** in 30% yield. Compound **3-5** was synthesized in 70% yield by selective bromination of **3-4** with one equivalent of *N*-bromosuccinimide (NBS). Then iodination of **3-5** with *N*-iodosuccinimide (NIS) resulted in compound **3-6** in 60% yields. The key intermediate compound **3-7** was synthesized by Sonogashira coupling reaction between **3-2** and **3-6** in 45% yield. Another Sonogashira coupling reaction between **3-7** and compound **3-8**[13] gave the target compound **QB5** in 35% yield. Pd-catalysed borylation of **3-7** with pinacolborane followed by Suzuki coupling with compound **3-9**[11] afforded the aldehyde **3-10** in 50% yields for two steps. **QB6** was then prepared by Knoevenagel condensation of compound **3-10** with cyanoacetic acid

in 87% yield. All the dyes **QB4**, **QB5** and **QB6** are black powder and soluble in normal organic solvents such as dichloromethane (DCM), chloroform and tetrahydrofuran (THF). They were thoroughly characterized by ^{1}H NMR, ^{13}C NMR, and high resolution mass spectrometry (HR MS).

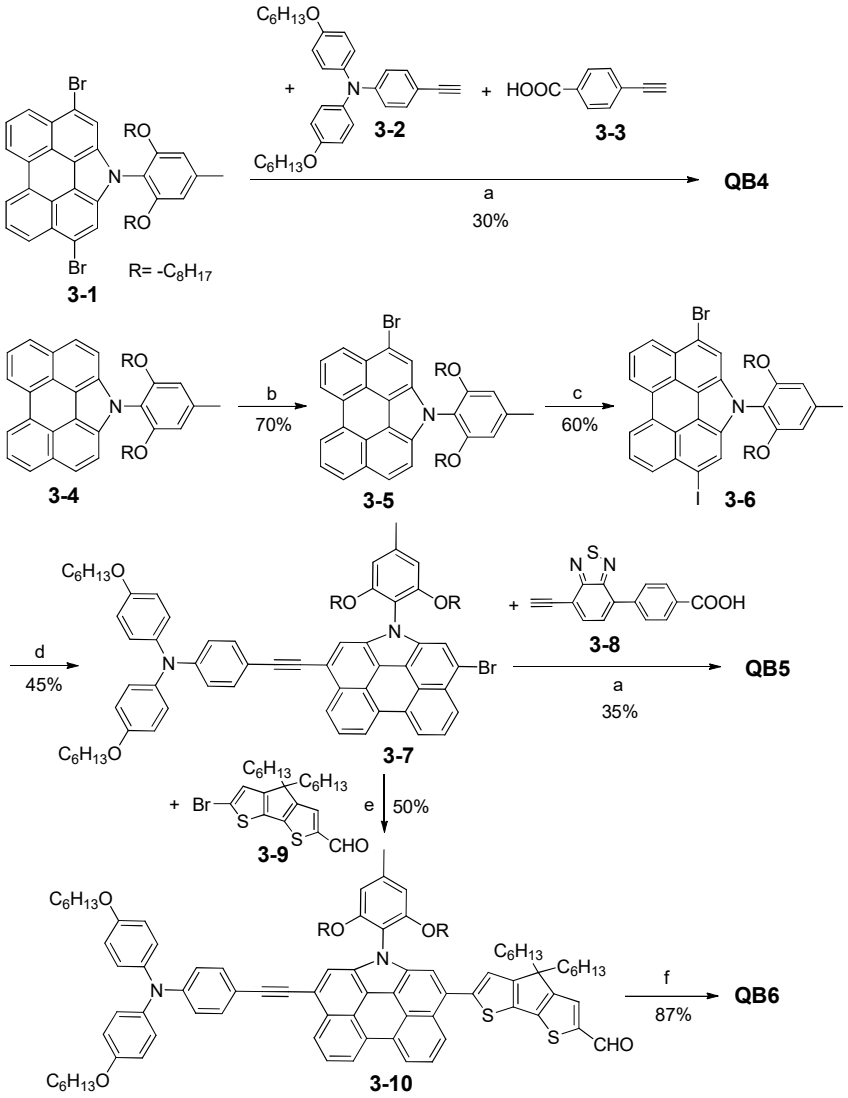

Scheme 3.1 Synthetic route of sensitizers **QB4**-**QB6**. Conditions: (a)$Pa_2(dba)_3/AsPh_3$, THF/Et_3N, 75°C; (b) NBS, $CHCl_3$, 0 °C; (c) NIS/TFA (one drop), CH_2Cl_2; (d) $Pd(PPh_3)_2Cl_2$/CuI, THF/Et_3N,75°C; (e) i) pinacolborane, $Pd(PPh_3)_2Cl_2/Et_3N$/1,2-dichloroethane, 90 °C; ii) $Pd(PPh_3)_4/K_2CO_3$, toluene, reflux; (f) cyanoacetic acid, $CHCl_3$/piperidine, reflux.

The absorption spectra of **QB4**, **QB5** and **QB6** in DCM are shown in Figure 3.2 and the corresponding data are collected in Table 3.1. **QB4** exhibits an intense and broad absorption band with peak at 507 nm (ε = 4.11×10^4 M^{-1}cm^{-1}). Compared to **QB4**, when BT unit was inserted between the NP and benzoic acid moieties, the absorption spectrum of **QB5** becomes even broader, and the absorption maximum is bathochromically shifted by 25 nm from 507 to 532 nm (ε = 4.47× 10^4 M^{-1}cm^{-1}), while the absorption onset is remarkably red-shifted by about 100 nm. This suggests the presence of the electron-withdrawing BT unit can further increase the intramolecular donor-acceptor interaction and enhance the light-harvesting capability. **QB6** shows an intense band covering the major part of visible region with absorption maximum at 525 nm (ε = 4.86× 10^4 M^{-1}cm^{-1}). The absorption band shape of **QB6** is quite different from that of **QB4** and **QB5** due to a different acceptor part. Interestingly, when **QB6** was compared with its analogue **QB2** in which the carbon-carbon triple bond is missed,[9] the absorption is blue shifted by 25 nm. Such a change may be due to the increase of the distance between the donor and acceptor unit in **QB6**. UV-vis absorption spectra of three organic dyes on TiO_2 transparent film are also shown in Figure 3.2. The absorption maximum of the dyes **QB4**, **QB5** and **QB6** is hypsochromically shifted by 23, 48 and 6 nm on TiO_2 film in comparison to that in solution, which could be attributed to either the formation of H-aggregates[14] or deprotonation of carboxylic acid.[15]

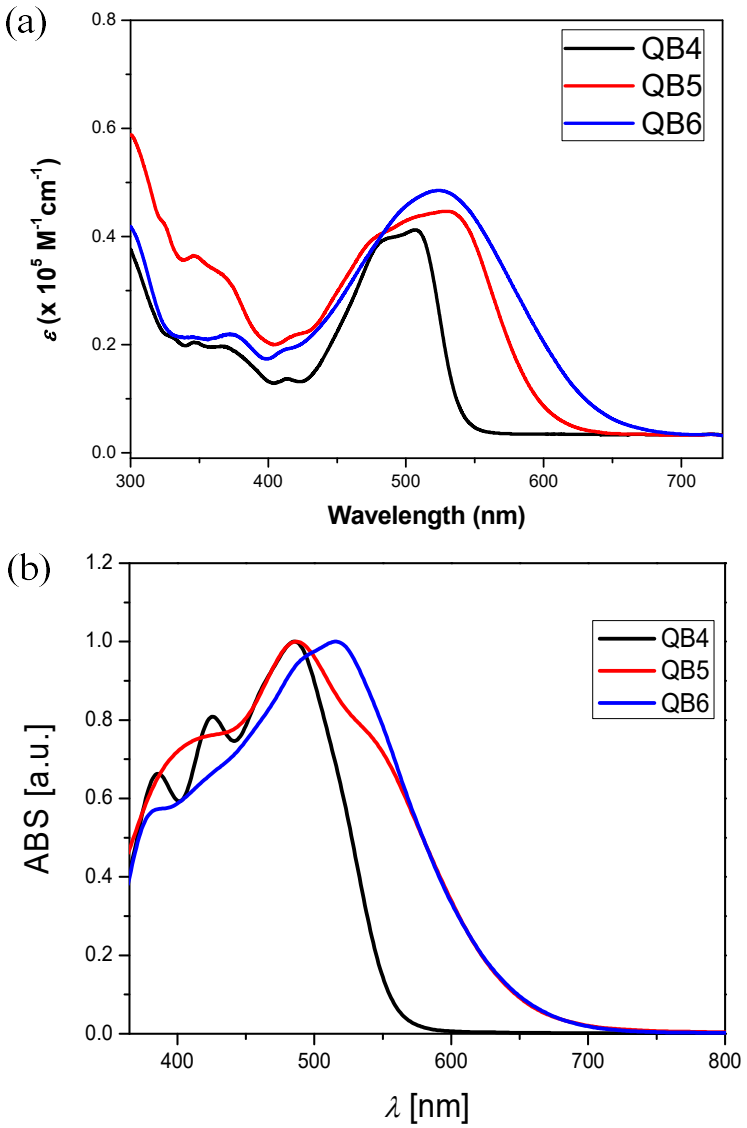

Figure 3.2 The UV-Vis absorption spectra of **QB4** (black), **QB5** (red) and **QB6** (blue) (a) in dichloromethane and (b) on TiO_2.

The electrochemical properties of **QB4**, **QB5** and **QB6** were investigated by cyclic voltammetry (CV) and differential pulse voltammetry (DPV) in deoxygenated DCM solution containing 0.1 M tetra-*n*-butylammonium hexafluorophosphate ($TBAPF_6$) as supporting electrolyte (Figure 3.3). Multiple quasi-reversible or irreversible redox waves were observed for all three compounds (see the list of half-wave potentials

$E_{1/2}^{ox}$ (anodic scan) and $E_{1/2}^{red}$ (cathodic scan) in Table 3.1). The HOMO and LUMO energy levels were estimated according to equations: HOMO = -[4.8 + E_{ox}^{onset}] eV, and LUMO = -[4.8 + E_{red}^{onset}] eV, where E_{ox}^{onset} and E_{red}^{onset} are the onset of the first oxidation and reduction wave respectively (*vs*. Fc^{+}/Fc).[16] The HOMO and LUMO energy levels of **QB4**−**QB6** were determined to be -5.10, -5.12, -5.09 eV (HOMO) and -3.46, -3.52, -3.51 eV (LUMO), respectively (Table 3.1). The electrochemical energy gaps were calculated accordingly to be 1.64, 1.60, and 1.58 eV for **QB4-QB6**. The trend is in agreement with the optical energy gaps.

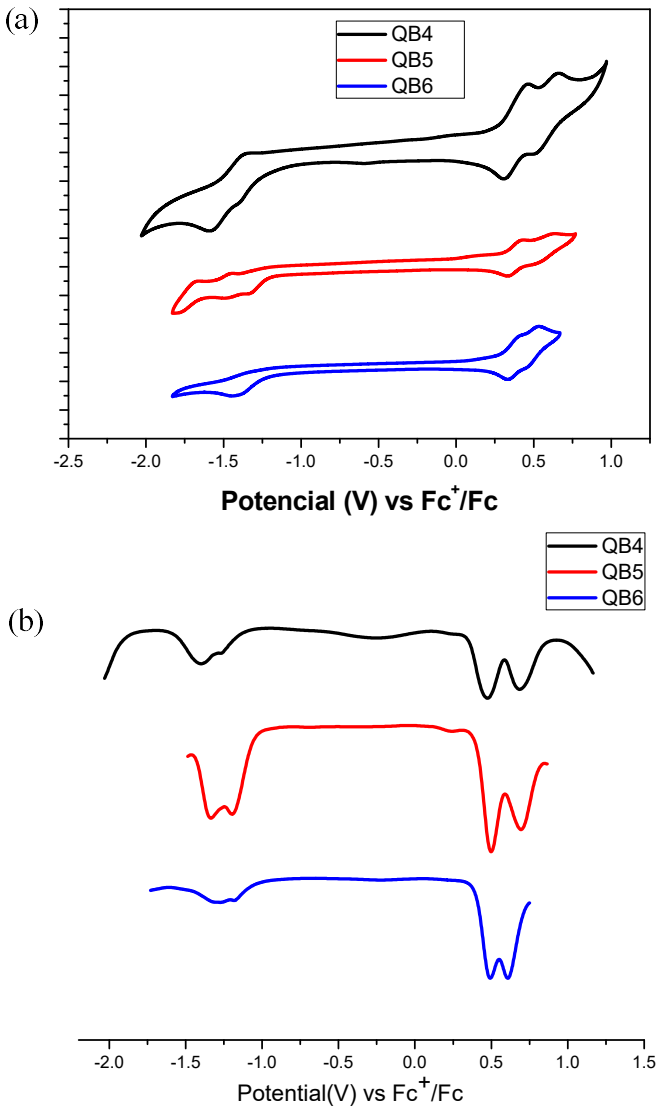

Figure 3.3 Cyclic voltammograms of **QB4** – **QB6** in dry DCM.

To gain better understanding of the molecular structure and electron distribution, density functional theory (DFT) calculations were conducted at the B3LYP/6-31G* level. Figure 3.4 shows their optimized molecular structures and frontier molecular orbital profiles together with the calculated energy levels of HOMOs and LUMOs (Figure 3.4 and Table 3.2-3.4). For **QB4**, the HOMO is delocalized along both the donor group and the NP core, while the LUMO is delocalized through the NP core

and the acceptor group. Compared to **QB4**, **QB5** and **QB6** exhibit even more segregated HOMO and LUMO with a proper overlap. Such a spatially well-separated orbital distribution is desirable for efficient intramolecular charge separation and fast injection of photo-excited electron into the conduction band of TiO_2 *via* the carboxylic group adsorbed on the TiO_2 surface. Time-dependent DFT calculations also predicted that **QB5** and **QB6** showed more red-shifted spectra than that of **QB4** (Table 3.2-3.4 and Figure3.5), and this trend is well in agreement with the experimental data.

Table 3.1 Summary of optical and electrochemical properties of **QB4**, **QB5** and **QB6**.

Dye	λ_{abs} (nm)	ε ($M^{-1}cm^{-1}$)	E_g^{opt} (eV)	$E_{1/2}^{ox}$ (V)	$E_{1/2}^{red}$ (V)	HOMO[a] (eV)	LUMO[a] (eV)	E_g^{EC} (eV)
QB4	501	41100	2.21	0.34 0.58	-1.47	-5.10	-3.46	1.64
QB5	532	44700	1.95	0.36 0.57	-1.27 -1.48 -1.72	-5.12	-3.52	1.60
QB6	525	48600	1.88	0.37 0.50	-1.34	-5.09	-3.51	1.58

[a]The HOMO and LUMO energy levels were determined from the onset of first oxidation and reduction wave *vs* Fc^+/Fc, respectivel

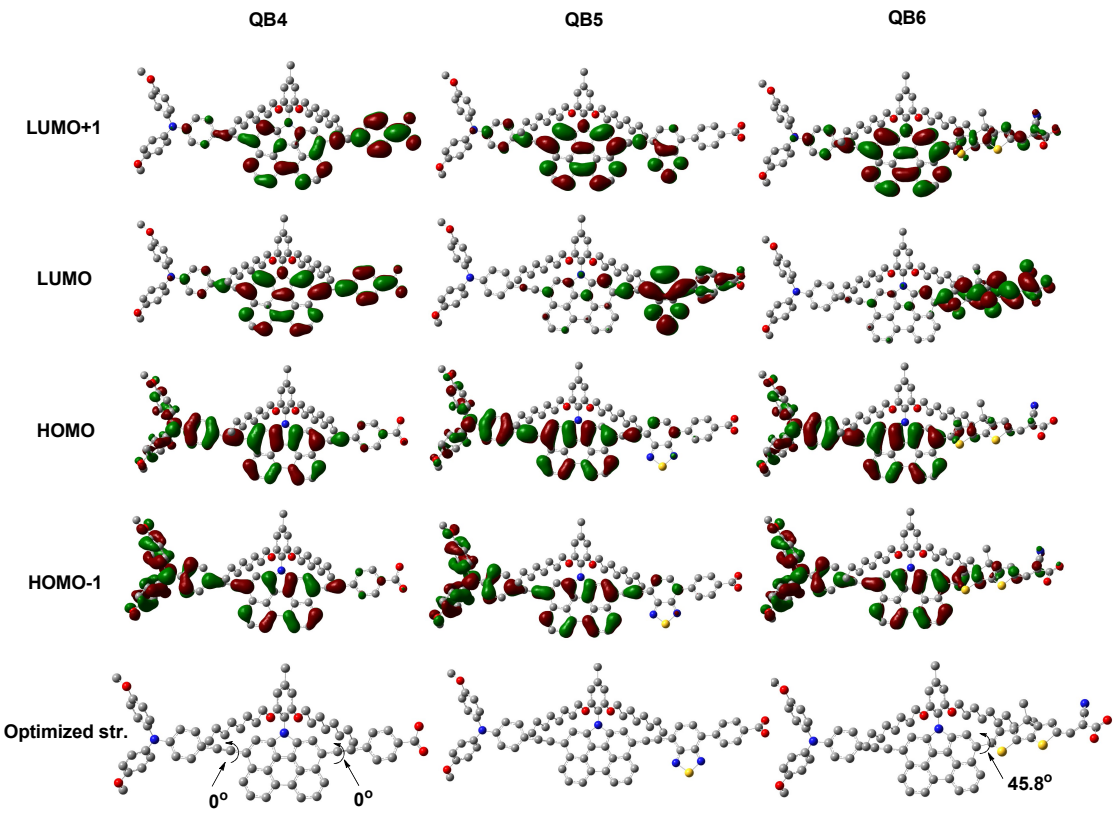

Figure 3.4 Calculated HOMO and LUMO profiles and energy levels of **QB4**, **QB5** and **QB6** (B3LYP/6-31G*).

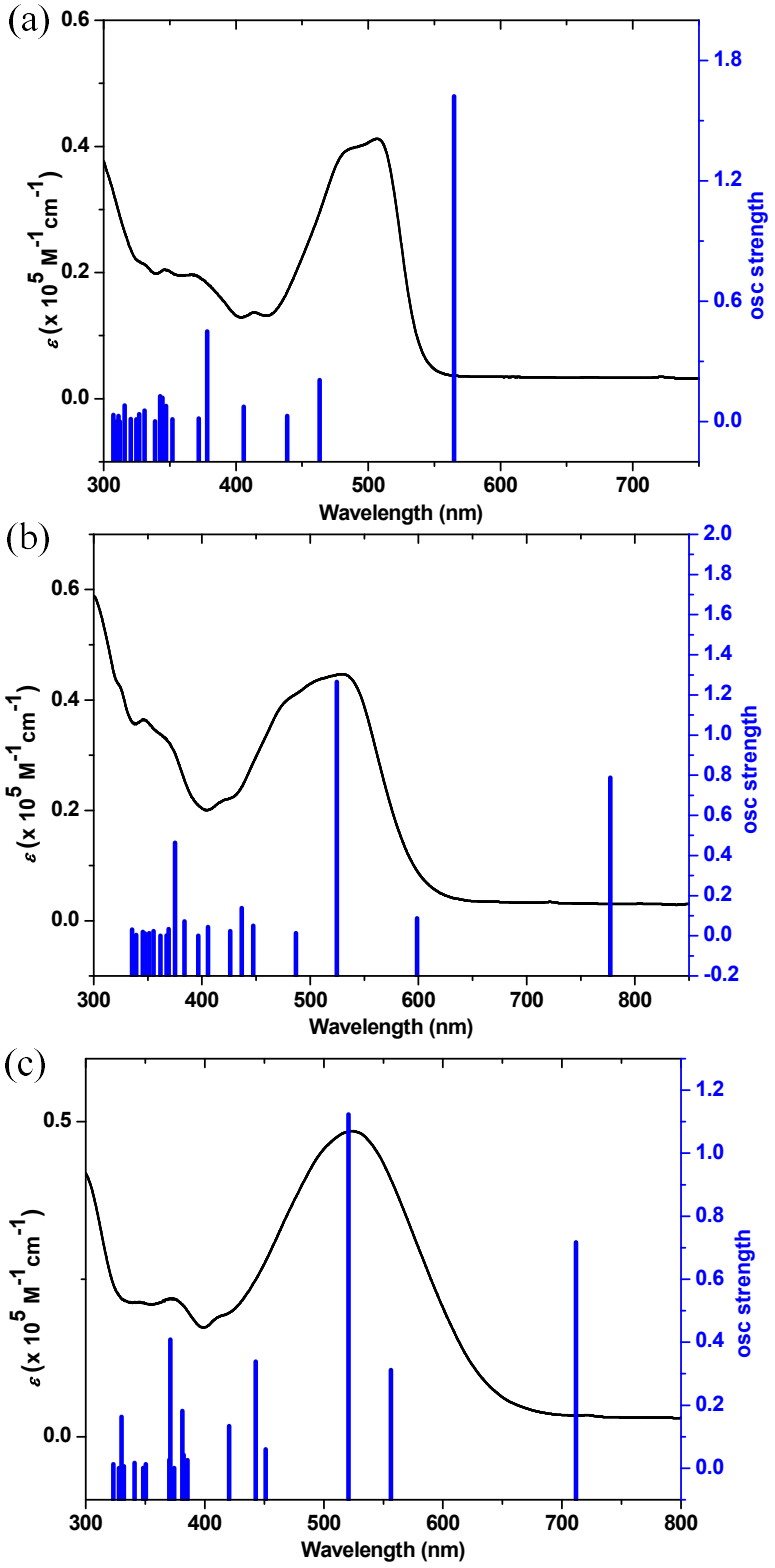

Figure 3.5 UV-Vis spectrum and calculated stick spectrum for (a) **QB4**, (b) **QB5** and (c) **QB6**.

Table 3.2 TD-DFT (B3LYP/6-31G*) calculated energies, oscillator strength (*f*) and compositions of major electronic transitions of **QB4**.

Energy (cm^{-1})	**Wavelength (nm)**	***f***	**Major contributions**
17703.18544	564.87	1.6204	HOMO→LUMO (99%)
21583.5456	463.32	0.2077	H-1→LUMO (98%)
22794.99872	438.69	0.0288	HOMO→L+1 (95%)
24639.60144	405.85	0.0744	H-2→LUMO (91%)
26442.26304	378.18	0.4494	HOMO→L+2 (91%)
26890.7104	371.88	0.0161	H-1→L+1 (91%)
28410.26944	351.99	0.012	H-1→L+3 (12%), HOMO→L+3 (84%)
28803.06416	347.18	0.0778	H-4→LUMO (28%), H-3→LUMO (57%)
29033.74032	344.42	0.119	H-5→LUMO (22%), H-4→LUMO (45%), H-3→LUMO (25%)
29182.14736	342.67	0.1264	H-5→LUMO (75%), H-4→LUMO (14%)

29506.38448	338.91	0.0016	HOMO→L+4 (82%)
30218.57696	330.92	0.0557	H-2→L+1 (61%), H-1→L+2 (15%)
30602.49952	326.77	0.0368	H-7→LUMO (24%), H-1→L+2 (48%)
30788.00832	324.80	0.0123	H-7→LUMO (55%), H-2→L+1 (22%), H-1 →L+2 (13%)
31211.45232	320.39	0.0127	H-1 → L+2 (13%), HOMO → L+5 (22%), HOMO→L+6 (36%)
31665.5456	315.80	0.0812	H-6 → LUMO (14%), H-1 → L+7 (10%), HOMO→L+7 (72%)
32037.36976	312.13	0.0008	HOMO→L+5 (61%), HOMO→L+6 (28%)
32125.2848	311.28	0.0285	H-6→LUMO (82%), HOMO→L+7 (12%)
32268.04592	309.90	0.0012	H-8→LUMO (40%), HOMO→L+6 (13%), HOMO→L+10 (19%)
32531.79104	307.39	0.0337	H-1 → L+3 (12%), HOMO → L+8 (20%), HOMO→L+9 (48%)

Table 3.3 TD-DFT (B3LYP/6-31G*) calculated energies, oscillator strength (*f*) and compositions of major electronic transitions of **QB5**.

Energy (cm^{-1})	**Wavelength**	***f***	**Major contributions**

	(nm)		
12867.05168	777.17	0.7871	HOMO→LUMO (99%)
16704.66416	598.63	0.0871	H-1→LUMO (98%)
19064.65872	524.53	1.2649	HOMO→L+1 (96%)
20543.0832	486.78	0.0127	H-2→LUMO (98%)
22358.64976	447.25	0.0505	H-3→LUMO (57%), HOMO→L+2 (34%)
22896.62528	436.75	0.1381	H-1→L+1 (69%), HOMO→L+2 (22%)
23470.08944	426.07	0.023	H-3→LUMO (26%), H-1→L+1 (25%), HOMO→L+2 (41%)
24656.5392	405.57	0.0431	H-4→LUMO (91%)
25218.71152	396.53	0.0002	H-5→LUMO (99%)
26059.9536	383.73	0.0718	H-2→L+1 (75%), HOMO→L+3 (15%)
26660.03424	375.09	0.463	H-2→L+1 (12%), HOMO→L+3 (72%)
27081.05856	369.26	0.0337	H-1→L+2 (92%)
27223.81968	367.32	0.0015	H-7→LUMO (94%)
27657.74896	361.56	0.0006	H-6→LUMO (100%)
28140.8784	355.35	0.0238	HOMO→L+4 (65%)
28469.14832	351.26	0.0135	H-1→L+5 (13%), HOMO→L+5 (83%)
28807.09696	347.14	0.0117	H-8→LUMO (71%), H-3→L+1 (17%)
28949.85808	345.42	0.0197	H-8→LUMO (15%), H-3→L+1 (62%)
29478.15488	339.23	0.0047	H-9→LUMO (46%), HOMO→L+7 (28%)
29816.10352	335.39	0.0305	H-9→LUMO (19%), HOMO→L+7 (55%)

Table 3.4 TD-DFT (B3LYP/6-31G*) calculated energies, oscillator strength (*f*) and compositions of major electronic transitions of **QB6**.

Energy (cm^{-1})	**Wavelength (nm)**	***f***	**Major contributions**
14048.66208	711.81	0.7166	HOMO→LUMO (99%)
17972.57648	556.40	0.3114	H-1→LUMO (97%)
19202.58048	520.76	1.1229	HOMO→L+1 (91%)
22163.46224	451.19	0.0601	H-3→LUMO (79%), H-2→LUMO (13%)
22583.68	442.79	0.3385	H-3→LUMO (19%), H-2→LUMO (38%), H-1 →L+1 (38%)
23790.29376	420.34	0.1337	H-2→LUMO (39%), H-1→L+1 (53%)
25943.80896	385.45	0.0257	H-4→LUMO (46%), H-2→L+1 (11%), HOMO →L+2 (23%), HOMO→L+3 (14%)
26164.8064	382.19	0.0423	H-4→LUMO (43%), HOMO→L+2 (37%)
26231.75088	381.21	0.1818	H-3→L+1 (38%), HOMO→L+3 (42%)
26712.46064	374.35	0.0003	H-5→LUMO (98%)
26946.36304	371.10	0.408	H-3 → L+1 (25%), HOMO → L+2 (26%), HOMO→L+3 (34%)
27014.92064	370.16	0.0266	H-3→L+1 (19%), H-2→L+1 (66%)
28530.44688	350.50	0.0126	H-1→L+4 (12%), HOMO→L+4 (83%)

28701.4376	348.41	0.0011	H-7→LUMO (93%)
28707.89008	348.34	0.001	H-6→LUMO (95%)
29328.13472	340.97	0.0168	HOMO→L+5 (81%)
30122.59632	331.98	0.0066	H-8→LUMO (50%), H-1→L+2 (23%)
30291.97392	330.12	0.163	H-4→L+1 (17%), H-1→L+3 (60%)
30499.25984	327.88	0.0006	H-9→LUMO (31%), H-4→L+1 (10%), H-1→L+2 (38%)
30950.93344	323.09	0.013	H-9→LUMO (26%), H-4→L+1 (30%), HOMO →L+7 (18%)

Although *N*-annulated perylene with bulky phenyl group as core is used, due to the high planarity of the sensitizers favored by the presence of the perylene spacer and triple bond linker, a fast intramolecular charge transfer should be expected as well as an unfavorable π–π stacking during the uptake process, which may lead to charge recombination. In this case, the addition of chenodeoxycholic acid (CDCA) to the dye solutions could be useful because the CDCA can insert itself between the sensitizers minimizing detrimental dye aggregation effects.[17] In addition, the use of a co-adsorbent such as CDCA ensures a uniform coverage of the inorganic semiconductor, thereby lowering the probability of recombination. Meanwhile, CDCA also could lower the amount of sensitizers loaded on the working electrode. On this basis, the use of CDCA as co-adsorbent has been evaluated: we prepared solutions of

the dyes with or without 30 mM CDCA and studied the influence of the amount of additive on photovoltaic parameters and on the dye loading, which are shown in Table 3.5. The efficiency of the **QB4**-**6** without the presence of CDCA was measured to be 4.71% (V_{oc} = 0.82V, J_{sc} = 7.96 mA•cm^{-2}, *ff* = 0.72), 5.65% (V_{oc} = 0.78V, J_{sc} = 10.24 mA•cm^{-2}, *ff* = 0.71) and 4.27% (V_{oc} = 0.75V, J_{sc} = 8.77 mA•cm^{-2}, *ff* = 0.65) (Figure 3.6). With the addition of 30 mM CDCA the performance of the **QB4**, **QB5** and **QB6** sensitized devices was significantly improved. In particular, the short-circuit photocurrent density (J_{SC}) augmented from 7.92 to 8.73, from 10.24 to 14.49, and from 8.77 to 13.30 mA/cm^2 for **QB4**, **QB5** and **QB6** based cells, respectively, resulting from large enhance of the light-harvesting ability, although the dye loading density (c_m) was decreased from 2.74 to 1.94, 3.78 to 2.61, 2.19 to 1.77, 10^{-8} mol cm^{-2} μm^{-1}, respectively. The V_{oc} of **QB4**-**QB6** was slightly changed from 0.82 to 0.76 V, 0.78 to 0.78 V and 0.75 to 0.79 V, respectively. On the whole, PCE of 5.14, 8.38, and 7.78% has been achieved with **QB4**, **QB5** and **QB6** sensitized devices. The action spectrum of incident photo-to-current conversion efficiency (IPCE) and the photocurrent density–voltage (*J*–V) curves based on the three sensitizers in the presence of 30 mM CDCA are illustrated in Figure 3.6. Remarkably broad and high IPCE covering most of the visible region were observed for all dyes, which is in consistence with their absorption spectra. The IPCE spectra of **QB4** dye showed a maximum of ~85% at 450 nm, slightly higher with respect to the ~80% obtained for the **QB5**-based device at 450 nm and to the plateau at 75%, ranging from 450 to 550 nm, observed for **QB6**. Meanwhile, the onset of IPCE was largely red-shifted from

650 nm for **QB4** to 770 nm for **QB5** and **QB6**. All these factors confirm the superior photovoltaic properties of the **QB4-QB6** dyes.

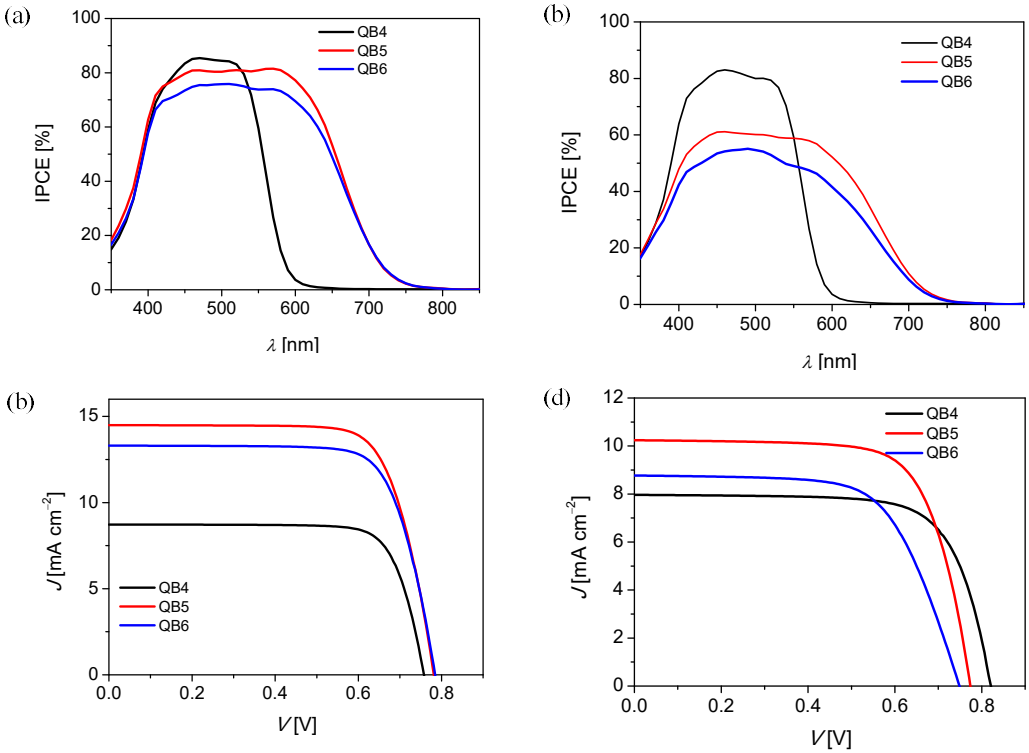

Figure 3.6 (a) IPCEs spectra and (b) Current-voltage characteristics recorded for DSCs devices fabricated with the three dyes in the presence of 30 mM CDCA and (c) IPCEs spectra and (d) Current-voltage characteristics recorded for DSCs devices fabricated with the three dyes without CDCA.

Table 3.5 Photovoltaic parameters of cells measured at various irradiances (G) of simulated AM 1.5 sunlight.

dye	CDCA (mM)	PCE (%)	$^{a}J_{EQE}$ [mA cm^{-2}]	J_{sc} [mA cm^{-2}]	V_{oc} [v]	FF (%)	c_m [10^{-8} Mμm^{-1}]
QB4	0	4.71	7.92	7.96	0.82	0.72	2.74
	30	5.14	8.32	8.73	0.76	0.78	1.94
QB5	0	5.65	10.35	10.24	0.78	0.71	3.78
	30	8.38	14.43	14.49	0.78	0.74	2.61
QB6	0	4.27	8.74	8.77	0.75	0.65	2.19
	30	7.78	13.06	13.30	0.79	0.74	1.77

[a] J_{EQE} was derived by wavelength integration of the product of the standard AM1.5 emission spectrum (ASTM G173-03) and the EQEs measured at the short circuit. The validity of measured photovoltaic parameters was evaluated by comparing the

calculated J_{EQE} value with the experimentally measured J_{sc} value.

To further understand the dye structure-device performance relationship, we conducted further physical measurements of **QB4**-**QB6** cells in their better testing condition. For a short-circuit DSC device, it is known that the J_{sc} is measured at the condition of a considerable low electron density in the nanocrystalline titania film and the charge recombination flux is significantly reduced. Thereby, the measured J_{sc} is roughly proportional to the photocarrier generation flux. The validity of this analysis motivated us to compare the dye structure correlated V_{oc} variation at a given J_{sc} by measuring *J*-*V* curves under various light intensities and plotting V_{oc} as a function of J_{sc} (Fig. 3.7a). It is noted that at a given J_{sc}, the **QB6** cell exhibits a higher V_{oc} than **QB5**, while **QB4** gives the lowest V_{oc} value.

It is widely recognized that for a fixed redox electrolyte in DSCs, the rise or fall of V_{oc} is determined by the titania electron quasi-Fermi-level ($E_{F,n}$), which intrinsically stems from a change of titania conduction band edge (E_c) and/or a variation of titania electron density.[18] At a given flux of photocarrier generation, the titania electron density is determined by the interfacial recombination rate of titania electrons with electron accepting species in electrolytes and/or dye cations. Thereby charge extraction (CE) and transient photovoltage decay (TPD) measurements[19] were further carried out to understand the electronic origins of the aforesaid V_{oc} fluctuation. As shown in Figure 3.7b, the cells made with **QB5** and **QB6** give a slightly similar extracted charge (Q) at the same potential bias V_{oc}, suggesting a fixed conduction-band edge of titania with respect to the electrolyte Fermi-level, whereas

the **QB4** cell exhibits a slightly larger Q value at the same V_{oc}, suggesting a downward shift of titania conduction band edge with respect to the electrolyte Femi level. This may give evidence for slightly lower V_{oc} of cell with **QB4**. Due to the slight difference, the V_{oc} values of **QB4-QB6** also show very small difference. As Figure 3.7c presents, the **QB5** and **QB6** cell displays much longer charge recombination lifetime (τ) than **QB4** cells at a given charge Q, accounting for the aforementioned superior photovoltage at a given J_{sc} for **QB5** and **QB6**.

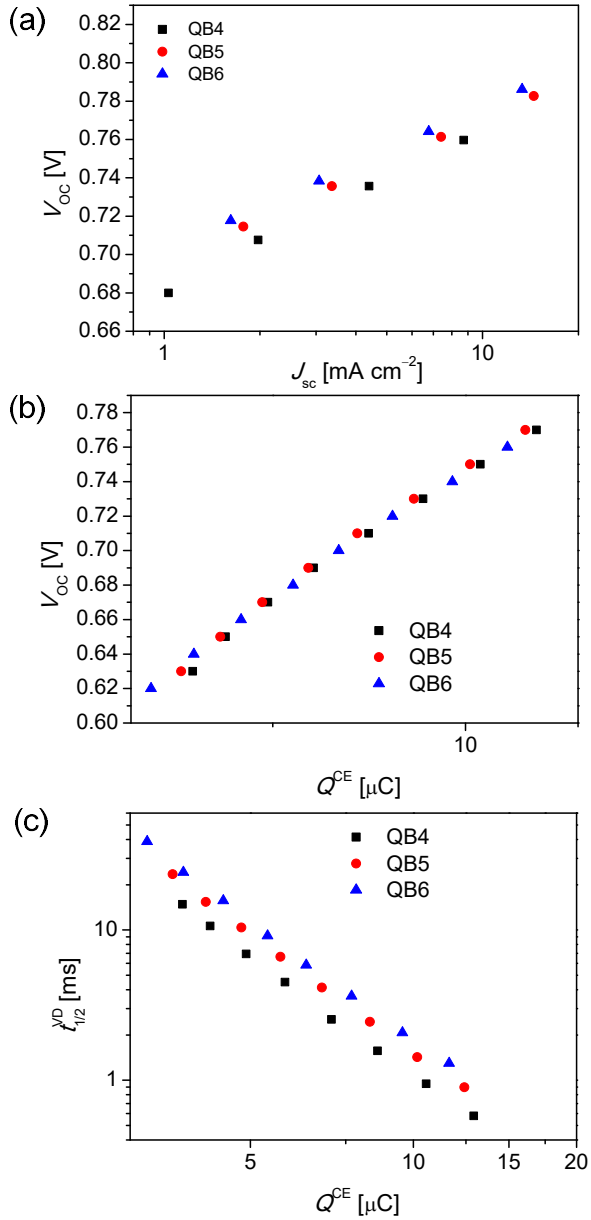

Figure 3.7 (a)open-circuit photovoltage plotted as a function of short-circuit photocurrent density. (b) Plots of open-circuit photovoltage versus extracted charge. (c) Plots of lifetime of photoinjected electrons in titania as a function extracted charge.

3.3 Conclusion

In summary, we have synthesized three new push-pull type dyes (**QB4-QB6**) by using the alkoxy-wrapped *N*-annulated perylene unit as the π-bridge and triple bond as π-spacer. Varying the acceptor unit in the general selected structure, all dyes exhibited remarkable solar-to-energy conversion efficiencies resulting from favourable

light-harvesting capacity and high absorptivity. Due to the high planarity of the structure, the addition of CDCA additive helps the efficiency of the final device by minimizing detrimental dye aggregation effects. In fact, all dyes show a better PCE value in the presence of CDCA co-adsorbent. In particular, **QB5** based device showed PCE as high as 8.38%, highlighting that the coplanar NP unit is a good building block for the design of sensitizers for high performance DSCs. New structures can be engineered by selecting different donor units and anchoring groups, as partners of the coplanar NP, in order to gain deeper insight into the potentialities of this new class.

3.4 Experimental section

3.4.1 General

Reagents and measurement methods were similar to those in Chapter 2.

3.4.2 Detailed synthetic procedures and characterization data

Compound 3-5

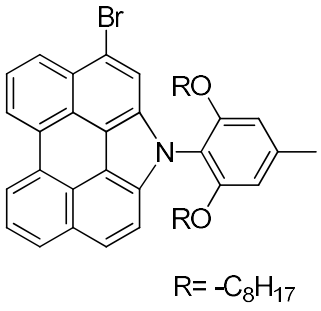

To the solution of compound **3-4** (892 mg, 1.46 mmol) in DCM (200 mL) was slowly added NBS (260 mg, 1.46 mmol) in portion over half an hour at 0^{o}C. The mixture was stirred at 0^{o}C for 30 min. The reaction mixture was quenched with water (50 mL). The organic layer was washed with water, and then washed with saturated brine and dried over anhydrous Na_2SO_4. The solvent was removed under reduced pressure and the

crude product was purified by column chromatography (silica gel, hexane : DCM = 6 : 1) to give compound **3-5** as a yellow solid (705mg, 70%). ^{1}H NMR ($CDCl_3$, 300 MHz): δ ppm = 8.65-8.70 (m, 2H), 8.34 (d, *J* = 8.4 Hz, 1H), 8.13 (d, *J*= 8.4 Hz, 1H), 7.80-7.91 (m, 4H), 7.56 (d, *J*= 8.7Hz, 1H), 6.63 (s, 2H), 3.91 (t, *J* = 6.3 Hz, 4H), 2.51 (s, 3H), 1.32-1.37 (m, 4H), 0.97-1.03 (m, 4H), 0.82-0.87 (m, 16H), 0.72 (t, *J* = 7.2 Hz, 6H). ^{13}C NMR ($CDCl_3$, 75 MHz): δ ppm = 155.77, 139.69, 133.43, 132.66, 130.74, 130.08, 129.06, 128.22, 125.32, 125.21, 124.75, 124.71, 124.59, 124.54, 123.59, 121.11, 120.77, 119.28, 117.46, 117.29, 116.99, 115.49, 113.73, 106.75, 69.04, 31.50, 28.97, 28.93, 28.89, 25.73, 22.45, 22.38, 13.93. HR-MS (APCI, *m*/*z*): calcd. for $C_{43}H_{49}BrNO_2$ ([M+1]), 690.2941; found, 690.2940 (error: -0.2 ppm).

Compound 3-6

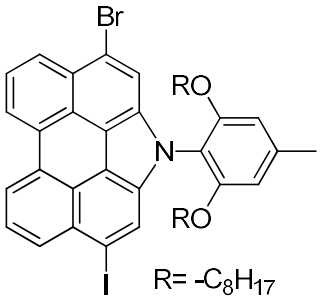

To a solution of **3-5** (69 mg, 0.1 mmol) in dicloromethane (10 mL) was added several drops of trifluoroacetic acid under argon atmosphere at room temperature. After the mixture was stirred for 10 minutes, N-Iodosuccinimide (22.4 mg, 0.1 mmol) was added into the mixture. After stirring for half an hour, the mixture was poured into water. The aqueous layer was extracted with dicloromethane, and the combined organic phase was washed with saturated brine and dried over anhydrous Na_2SO_4. The solvent was removed under reduced vacuum and the residue was purified by column

chromatography (silica gel, DCM: hexane = 1:6) to afford **3-6** as an yellow solid (49 mg, 60%). ^{1}H NMR ($CDCl_3$, 300 MHz): δ ppm = 8.67-8.71 (m, 2H), 8.36 (d, *J* = 8.4 Hz, 1H), 8.25 (d, *J* = 8.4 Hz, 1H), 8.15 (s, 1H), 7.85-7.92 (m, 3H), 6.63 (s, 2H), 3.95 (t, *J* = 6.3 Hz, 4H), 2.51 (s, 3H), 1.36-1.41 (m, 4H), 0.82-1.00 (m, 20H), 0.70 (t, *J* = 7.2 Hz, 6H). ^{13}C NMR ($CDCl_3$,75 MHz): δ ppm = 155.58, 140.03, 133.59, 132.76, 130.45, 130.25, 130.13, 129.36, 128.21, 126.17, 125.69, 125.44, 125.15, 124.34, 123.87, 121.61, 121.51, 119.32, 117.91, 117.75, 116.84, 113.04, 106.51, 92.09, 69.02, 31.51, 29.05, 28.97, 28.89, 25.81, 22.44, 22.42, 13.92. HR-MS (APCI, *m*/*z*): calcd. for $C_{43}H_{48}BrINO_2$ ([M+1]), 816.1908; found, 816.1891 (error: -2.0 ppm).

Compound 3-7

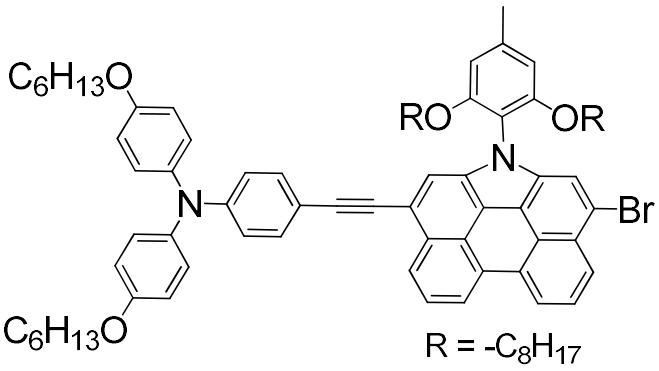

To a suspended solution of **3-6** (82 mg, 0.1 mmol), 4-ethylnyl-N,N-bis(4-(hexyloxy)phenyl)aniline (**3-2**, 37 mg, 0.08 mmol), and tetrakis(triphenylphosphine)palladium (5.5 mg, 0.005 mmol) in THF (10 mL) was added CuI (2 mg, 0.01 mmol), triethylamine (2 ml) under argon. The reaction mixture was stirred at 70^{o}C for 24 h. The crude compound was extracted into ethyl acetate, washed with brine and water, and dried over anhydrous sodium sulfate. After removing solvent under reduced pressure, the residue was purified by column chromatography (silica gel, DCM : hexanes = 1 : 4) to yield a dark yellow solid(52

mg, 45% yield). ^{1}H NMR ($CDCl_3$, 500 MHz): δ ppm = 8.69-8.72 (m, 2H), 8.56 (d, *J* = 8.0 Hz, 1H), 8.34 (d, *J* = 8.0 Hz, 1H), 7.88-7.92 (m, 3H), 7.80 (s, 1H), 7.45 (d, 1H), 7.46 (d, *J* = 8.5 Hz, 2H), 7.10 (d, *J* = 9.0 Hz, 4H), 6.92 (d, *J* = 8.5 Hz, 2H), 6.86 (d, *J* = 9.0 Hz, 4H), 6.63 (s, 2H), 3.96 (t, *J* = 6.5 Hz, 4H), 3.92 (t, *J* = 6.5 Hz, 4H), 2.50 (s, 3H), 1.75-1.82 (m, 4H), 1.45-1.49 (m, 4H), 1.35-1.38 (m, 12H), 0.95-1.00 (m, 4H), 0.81-0.94 (m, 22H), 0.66 (t, *J* = 6.5 Hz, 6H). ^{13}C NMR ($CDCl_3$,125 MHz): δ ppm = 155.82, 155.77, 148.59, 140.17, 139.91, 139.62, 133.62, 132.75, 132.28, 130.56, 130.16, 129.76, 128.24, 126.96, 125.39, 125.09, 124.89, 124.55, 124.49, 124.01, 121.39, 121.28, 119.46, 119.19, 119.15, 117.75, 117.56, 117.37, 117.20, 115.35, 114.78, 113.29, 106.63, 93.78, 86.41, 69.03, 68.28, 31.60, 31.52, 29,69, 29.32, 29,01, 28.93, 28.89, 25.79, 25.76, 22.61, 22.43, 22.39, 14.02, 13.94. HR-MS (APCI, *m*/*z*): calcd. for $C_{75}H_{86}BrN_2O_4$ ([M+1]), 1157.5765; found, 1157.5757 (error: -0.7 ppm).

Compound 3-10

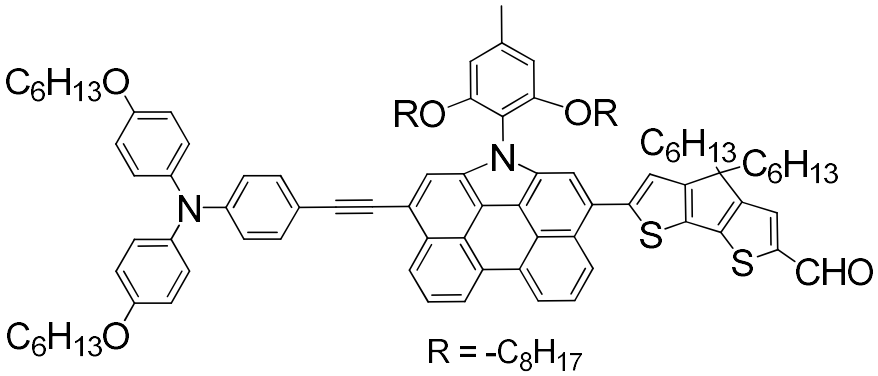

A 100 mL Schlenk flask was charged with **3-7** (115 mg, 0.1 mmol), pinacolborane (63 mg, 0.5 mmol), triethylamine (102 mg, 1.0 mmol), $PdCl_2(PPh_3)_2$ (4 mg, 0.005 mmol) and 1,2-dichloroethane (10 mL) under argon. The reaction mixture was stirred at 90 °C overnight. After removal of the solvent, the crude compound was extracted into ethyl acetate, washed with brine and water, and dried over anhydrous sodium sulfate.

The starting material **3-7** was almost gone, so the residue was used for next step without purification. To the suspension of the residue, **3-9** (58 mg, 0.12 mmol), and tetrakis(triphenylphosphine)palladium (11.6 mg, 0.01 mmol) in toluene (5 mL) was added potassium carbonate aqueous solution (2 M, 0.4 mL) under argon. The reaction mixture was refluxed for 24 h and then water (5 mL) added. The crude compound was extracted with ethyl acetate three times, followed by washing with brine and water, and dried over anhydrous sodium sulfate. After removing solvent under reduced pressure, the residue was purified by column chromatography (silica gel, ethyl acetate : hexanes = 1 : 50) to yield a viscous red oil (72 mg, 50% yield). ^{1}H NMR ($CDCl_3$, 300 MHz): δ ppm = 9.85 (s, 1H), 8.72-8.74 (m, 2H), 8.56 (d, *J* = 8.0 Hz, 1H), 8.46 (d, *J* = 8.0 Hz, 1H), 7.93(t, *J* = 8.0 Hz, 1H), 7.87(t, J = 8.0 Hz, 1H), 7.81 (s, 1H), 7.73 (s, 1H), 7.61 (s, 1H), 7.44 (d, *J* = 8.5 Hz, 2H), 7.32 (s, 1H), 7.09 (d, *J* = 9.0 Hz, 4H), 6.92 (d, *J* = 8.5 Hz, 2H), 6.86 (d, *J* = 9.0 Hz, 4H), 6.64 (s, 1H), 3.90-3.96 (m, 8H), 2.49 (s, 3H), 1.94-1.98 (m, 4H), 1.77-1.81 (m, 4H), 1.45-1.49 (m, 4H), 1.35-1.40 (m, 14H), 1.10-1.23 (m, 14H), 1.08-1.11 (m, 4H), 0.76-0.95 (m, 36H), 0.65 (t, *J* = 7.5 Hz, 6H). ^{13}C NMR ($CDCl_3$, 125 MHz): δ ppm = 182.47, 163.02, 157.40, 155.85, 155.82, 149.42, 148.62, 148.40, 142.86, 140.18, 139.87, 134.59, 133.56, 133.29, 132.31, 130.89, 130.57, 129.80, 128.95, 127.83, 127.06, 126.99, 125.13, 124.94, 124.47, 124.21, 123.78, 121.70, 121.25, 121.20, 119.47, 119.16, 118.15, 117.83, 117.56, 117.01, 115.37, 114.79, 113.44, 106.70, 93.96, 88.46, 69.06, 68.31, 54.22, 37.74, 31.63, 31.51, 29.71, 29.6, 29.33, 29.04, 29.00, 28.89, 25.81, 25.77, 24.71, 22.62, 22.59, 22.43, 22.41, 14.04, 13.94. HR-MS (APCI, *m*/*z*): calcd. for

$C_{97}H_{115}N_2O_5S_2$ ([M+1]), 1451.8242; found, 1451.8238 (error: -0.3 ppm).

QB4.

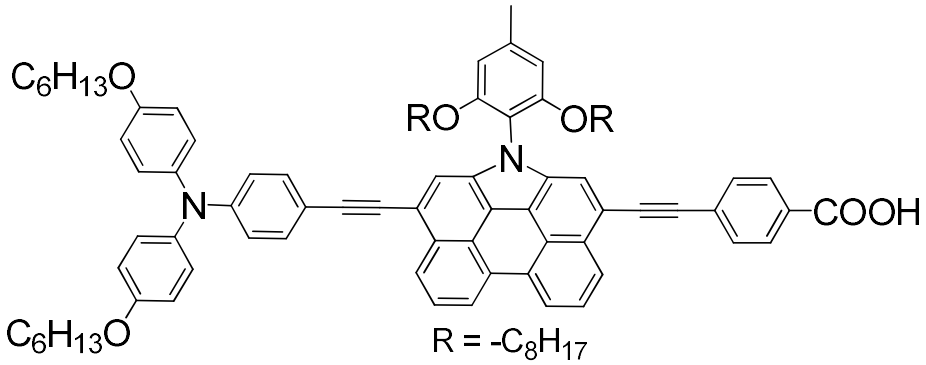

To a suspended solution of **3-1** (77 mg, 0.1 mmol), 4-ethylnyl-*N*,*N*-bis(4-(hexyloxy)phenyl)aniline (**3-2**, 56 mg, 0.12 mmol), 4-ethylnylbenzoic acid (**3-3**, 18 mg, 0.12mmol), triethylamine (2 ml) and tetrakis(triphenylphosphine)palladium (5.5 mg, 0.005 mmol) in THF (10 mL) was added CuI (2 mg, 0.01 mmol) under argon. The reaction mixture was stirred at 70 ^{o}C for 24 h. The crude compound was extracted into ethyl acetate, washed with brine and water, then acidified with 2 M hydrochloric acid aqueous solution (3 mL) and dried over anhydrous sodium sulfate. After removing solvent under reduced pressure, the residue was purified by flash chromatography with chloroform and methanol/chloroform (1/10, v/v) in turn as the eluent to yield a dark red powder (37 mg, 30%). ^{1}H NMR (THF-d_8, 500 MHz): δ ppm = 8.80 (d, *J* = 6.5Hz, 2H), 8.57 (t, *J* = 8.5 Hz, 2H), 8.08 (d, *J* = 7.5 Hz, 2H), 7.89-7.94 (m, 2H), 7.84 (s, 1H), 7.75 (m, 3H), 7.43 (d, *J* = 8.5 Hz, 2H), 7.07 (d, *J* = 9.0 Hz, 4H), 6.88 (m, 6H), 6.79 (s, 2H), 3.93-3.98 (m, 8H), 2.51 (s, 3H), 1.75-1.79 (m, 4H), 1.48-1.51 (m, 4H), 1.29-1.37 (m, 12H), 0.78-0.96 (m, 26H), 0.64 (t, *J* = 7.0 Hz, 6H). ^{13}C NMR ($CDCl_3$, 125 MHz): δ ppm = 163.51, 155.94, 155.83, 148.63, 140.12, 139.98, 134.02, 133.19, 132.30,

131.35, 130.16, 129.75, 129.64, 126.99, 125.38, 124.17, 123.89, 121.42, 121.26, 120.16, 119.40, 118.94, 118.85, 118.16, 117.73, 115.34, 114.64, 113.35, 106.75, 94.20, 88.42, 69.07, 68.28, 31.60, 31.53, 29.69, 29.00, 28.92, 25.81, 25.75, 22.61, 22.43, 22.41, 14.03, 13.93. HR-MS (APCI, *m*/*z*): calcd. for $C_{84}H_{91}N_2O_6$ ([M+1]), 1223.6872; found, 1223.6881 (error: +0.8 ppm).

QB5.

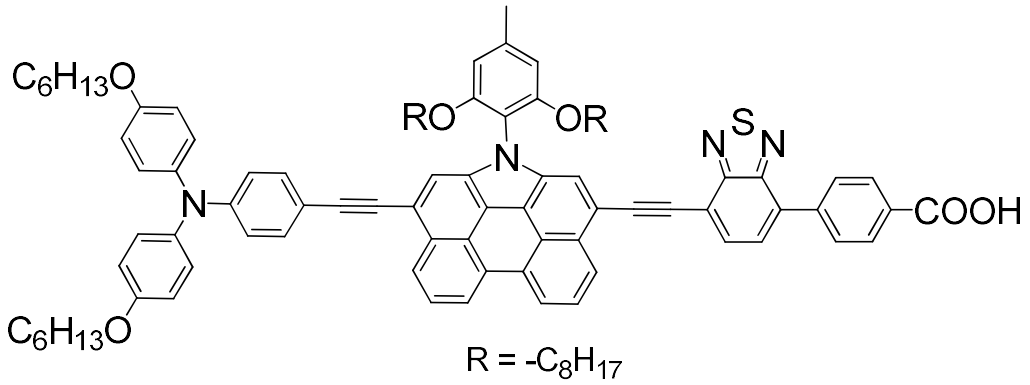

To a suspended solution of **3-7** (58 mg, 0.05 mmol), compound **3-8** (17mg, 0.06 mmol), triethylamine (2 ml) and tetrakis(triphenylphosphine)palladium (5.5 mg, 0.005 mmol) in THF (10 mL) was added CuI (2 mg, 0.01 mmol) under argon. The reaction mixture was stirred at 70^{o}C for 24 h. The crude compound was extracted into ethyl acetate, washed with brine and water, then acidified with 2 M hydrochloric acid aqueous solution (3 mL) and dried over anhydrous sodium sulfate. After removing solvent under reduced pressure, the residue was purified by flash chromatography with chloroform and methanol/chloroform (1/10, v/v) in turn as the eluent to yield a dark red powder (23.7 mg, 35%). ^{1}H NMR (THF-d8, 500 MHz): δ ppm = 8.94 (d, *J* = 8.0 Hz, 1H), 8.1-8.85 (m, 2H), 8.56 (d, *J* = 8.0 Hz, 1H), 8.17-8.23 (m, 4H), 7.92-8.06 (m, 5H), 7.76 (s, 1H), 7.17 (d, *J* = 8.5 Hz, 2H), 7.08 (d, *J* = 8.5 Hz, 4H), 6.88 (m, 6H),

6.81 (s, 2H), 3.94-4.00 (m, 8H), 2.53 (s, 3H), 1.75-1.79 (m, 4H), 1.43-1.51 (m, 4H), 1.36-1.38 (m, 12H), 0.91-0.94 (m, 18H), 0.79-0.81 (m, 8H), 0.56-0.61 (t, J = 7.5 Hz, 6H). ^{13}C NMR ($CDCl_3$, 125MHz): δ ppm = 169.02, 156.08, 155.88, 149.02, 140.16, 140.04, 134.24, 132.33, 131.65, 130.50, 129.28, 128.48, 127.01, 125.63, 127.01, 125.63, 125.21, 124.22, 121.46, 121.32, 120.24, 119.43, 119.14, 118.92, 117.83, 115.39, 114.46, 106.83, 94.32, 85.54, 69.14, 68.31, 31.93, 31.62, 31.54, 29.70, 29.36, 29.34, 29.01, 28.95, 28.93, 25.81, 25.77, 22.69, 22.62, 22.42, 14.10, 14.03, 13.92. HR-MS (APCI, m/z): calcd. for $C_{90}H_{93}N_4O_6S$ ([M+1]), 1357.6810; found, 1357.6818 (error: +0.6 ppm).

QB6.

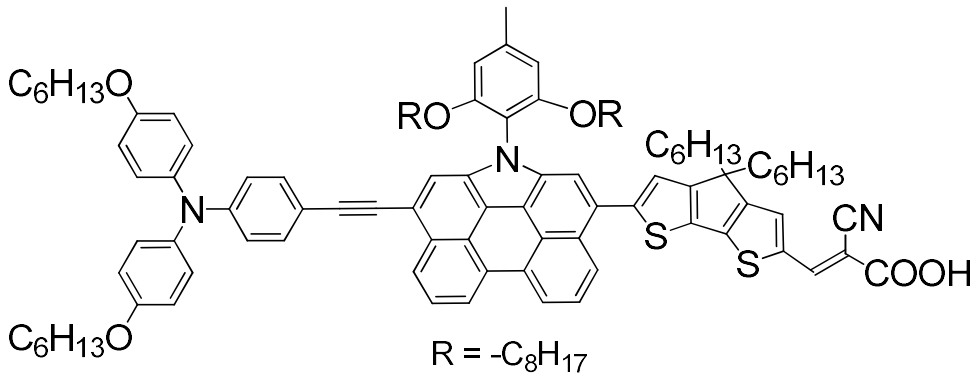

To a stirred solution of **3-11** (43 mg, 0.03 mmol) and cyanoacetic acid (10 mg, 0.12 mmol) in chloroform (5mL) was added piperidine (25 mg, 0.3 mmol). The reaction mixture was refluxed under argon for 18 h and then acidified with 2 M hydrochloric acid aqueous solution (5mL). The crude product was extracted by chloroform, washed with water, and dried over anhydrous sodium sulfate. After removing solvent under reduced pressure, the residue was purified by flash column chromatography with chloroform and methanol/chloroform (1/10, v/v) in turn as the eluent to yield a dark

red powder (40 mg, 87%). ^{1}H NMR (THF-d_8, 500 MHz): δ ppm= 8.79 (broad, 2H), 8.55 (m, 2H), 8.38 (s, 1H), 7.73-7.92 (m, 5H), 7.49 (s, 1H), 7.44 (d, *J* = 8.5 Hz, 2H), 7.07 (d, *J* = 9.0 Hz, 4H), 6.88 (m, 6H), 6.78 (s, 2H), 3.93-3.99 (m, 8H), 2.49 (s, 3H), 2.05-2.07 (m, 4H), 1.75-1.79 (m, 4H), 1.46-1.51 (m, 4H), 1.22-1.41(m, 14H), 1.20-1.24 (m, 14H), 1.09-1.11 (m, 4H), 0.79-0.86 (m, 36H), 0.64 (t, *J* = 7.5 Hz, 6H). ^{13}C NMR (THF-d_8, 75 MHz): δ ppm= 161.49, 156.21, 154.79, 154.38, 147.44, 138.60, 133.52, 132.13, 131.81, 130.63, 129.64, 129.38, 129.17, 128.26, 127.73, 126.31, 125.50, 123.63, 123.40, 122.66, 122.31, 120.45, 119.88, 117.55, 117.35, 116.43, 116.24, 116.08, 115.29, 113.69, 113.17, 111.52, 105.00, 92.37, 86.61, 67.23, 66.36, 52.68, 36.17, 30.18, 30.14, 30.14, 30.07, 28.19, 27.89, 27.62, 27.53, 27.49, 24.42, 24.33, 21.13, 21.07, 20.92, 19.97, 11.98, 11.93. HR-MS (APCI, *m*/*z*): calcd. for $C_{100}H_{116}N_3O_6S_2$ ([M+1]), 1518.8300; found, 1518.8295 (error: -0.4 ppm).

3.4.3 Device fabrication and characterization

A 4.5- μ m-thick, transparent layer of 25-nm-sized TiO_2 particles was first screen-printed on FTO glass (Nippon Sheet Glass, Solar, 4 mm thick) and further coated with a 5.0-μm-thick second layer of scattering titania particles (WER4-O, Dyesol) to produce a bilayer titania film, which was used later as the negative electrode of a DSC. The preparation procedures of TiO_2 nanocrystals and paste for screen-printing were reported in a previous paper.[16] The film thickness was monitored with a bench-top Ambios XP-1 stylus profilometer. After sintering at 500 oC and cooling to room temparature, a circular titania electrode (~0.28 cm^2) was stained by

immersing it overnight into a solution of 150 uM dye dissolved in a binary solvent of chloroform and ethanol (volume ratio, 1/4). The dye-coated titania electrode was then rinsed with acetonitrile and dried by air flow, and was further assembled with a thermally platinized FTO positive electrode by a 25-mm-thick Surlyn (DuPont) hot-melt gasket and sealed up by heating. The internal space was perfused with an electrolyte with the aid of a vacuum-back-filling system.

Transient photoelectrical experiments were measured with an Autolab-PGSTAT302N electrochemical workstation. The steady and perturbing lights on the photoanode side of a testing cell were supplied with white and red light-emitting diodes, respectively. We used the red light to generate a photovoltage perturbation near the open-circuit photovoltage of a testing cell under a certain white light and measured the voltage decay process thereafter. The modulated photovoltage by the red pulse of a testing cell was below 5 mV. The electron lifetime can be obtained by fitting a stretched exponential function to the photovoltage decay. The electron density was estimated by the charge extraction method. A testing cell was first kept at open circuit under white light and subsequently the white light was turned off upon switching the cell from open circuit to short circuit to record the resulting current transient, and the electron density was obtained by current integration.

3.5 References

1 (a) Oregan, B.; Grätzel, M. *Nature* **1991**, *353*, 737. (b) Imahori, H.; Umeyama, T.; Ito, S. *Acc. Chem. Res*. **2009**, *42*, 1809. (c) Hagfeldt, A.; Boschloo, G.; Sun, L.; Kloo, L.; Pettersson, H. *Chem. Rev*. **2010**, *110*, 6595. (d) Hardin, B. E.; Snaith, H. J.;

McGehee, M. D. *Nat. Photonics* **2012**, *6*, 162. (e) Ying, W.; Yang, J.; Wielopolski, M.; Moehl, T.; Moser, J.–E.; Comte, P.; Hua, J.; Zakeeruddin, S. M.; Tian, H.; Grätzel, M. *Chem. Sci.* **2014**, *5*, 206. (f) Huang, Z.; Feng, H.; Zang, X.; Iqbal, Z.; Zeng, H.; Kuang, D.; Wang, L.; Meierd, H.; Cao, D. *J. Mater. Chem. A* **2014**, *2*, 15365.

2 (a) Clifford, J. N.; Martínez-Ferrero, E.; Viterisi, A.; Palomares, E. *Chem. Soc. Rev.* **2011**, *40*, 1635. (b) Liang, M.; Chen, J. *Chem. Soc. Rev.* **2013**, *42*, 3453.

3 (a) Mishra, A.; Fischer, M. K. R.; Bäuerle, P. *Angew. Chem. Int. Ed.* **2009**, *48*, 2474. (b) Ooyama Y.; Inoue, S.; Nagano, T.; Kushimoto, K.; Ohshita, J.; Imae, I.; Komaguchi, K.; Harima, Y. *Angew. Chem. Int. Ed.* **2011**, 50, 7429. (c) Li, C.; Wonneberger, H. *Adv. Mater.* **2012**, 24, 613.

4 (a) Li, L.-L.; Diau, E. W.-G. *Chem. Soc. Rev.* **2013**, *42*, 291. (b) Yella, A.; Lee, H.-W.; Tsao, H. N.; Yi, C.; Chandiran, A. K.; Nazeeruddin, M. K.; Diau, E.W.-G.; Yeh, C.-Y.; Zakeeruddin, S. M.; Grätzel, M. *Science* **2011**, *334*, 629. (c) Mathew, S.; Yella, A.; Gao, P.; Humphry-Baker, R.; Curchod, B. F. E.; Ashari-Astani, N.; Tavernelli, I.; Rothlisberger, U.; Nazeeruddin, M. K.; Grätzel, M. *Nat. Chem.* **2014**, *6*, 242. (d) Yella, A.; Mai, C.-L.; Zakeeruddin, S. M.; Chang, S.-N.; Hsieh, C.-H.; Yeh, C.-Y.; Grätzel, M. *Angew. Chem. Int. Ed.* **2014**, *53*, 2973. (e) Higashino, T.; Imahori, H. *Dalton Trans*. **2015**, *44*,448. (f) Wang, Y. ; Chen, B.; Wu, W.; Li, X.; Zhu, W.; Tian, H.; Xie, Y. *Angew. Chem. Int. Ed.* **2014**, 53, 10779.

5 (a) Vercelli, B.; Zotti, G.; Berlin, A. *ACS Appl. Mater. Interfaces* **2012**, 4, 3233. (b) Wu, W. J.; Guo, F. L.; Li, J.; He, J. X.; Hua, J. L. S*ynth. Metal* **2010**, 160, 1008. (b) Karlsson, K. M.; Jiang, X; Eriksson, S. K.; Gabrielsson, E.; Rensmo, H.; Hagfeldt, A.;

Sun, L. C. *Chem.-Eur. J.* **2011**, 17, 6415. (c) Funabiki, K.; Mase, H.; Saito, Y.; Otsuka, A.; Hibino, A.; Tanaka, N.; Miura, H.; Himori, Y.; Yoshina, T.; Kubota, Y.; Matsui, M. *Org. Lett*. **2012**, 14, 1246.

6 (a) Chen, L.; Li, C.; Müllen, K. *J. Mater. Chem. C* **2014**, *2*, 1938. (b) Shibano, Y.; Umeyama, T.; Matano, Y. and Imahori, H. *Org. Lett*. **2007**, 9, 1971. (c) Edvinsson, T.; Li, C.; Pschirer, N.; Schöneboom, J.; Eickemeyer, F.; Sens, R.; Boschloo, G.; Herrmann, A.; Müllen, K. and Hagfeldt, A. *J. Phys. Chem. C* **2007**, 111, 15137. (d) Li, C.; Yum, J.-H.; Moon, S.-J.; Herrmann, A.; Eickemeyer, F.; Pschirer, N. G.; Erk, P.; Schöneboom, J.; Müllen, K.; Grätzel, M. and Nazeeruddin, M. K. *ChemSusChem* **2008**, 1, 615, (e) Jin, Y. H.; Hua, J. L.; Wu, W. J.; Ma, X. M. and Meng, F. S. *Synth. Met.* **2008**, 158, 64; (f) Planells, M.; Cespedes-Guirao, F. J.; Goncalves, L.; Sastre-Santos, A.; Fernandez-Lazaro, F. and Palomares, E. *J. Mater. Chem.* **2009**, 19, 5818; (g) Li, C.; Liu, Z. H.; Schoneboom, J.; Eickemeyer, F.; Pschirer, N. G.; Erk, P.; Herrmann, A. and Müllen, K. *J. Mater. Chem.* **2009**, 19, 5405; (h) Imahori, H. and Mathew, S. *J. Mater. Chem.* **2011**, 21, 7166; (i) Jiao, C.; Zu, N.; Huang, K.-W.; Wang, P. and Wu, J. *Org. Lett.* **2011**, 13, 3652. (j) Sharma, G. D.; Balraju, P.; Mikroyannidis, J. A. and Stylianakis, M. M. *Sol. Energy Mater. Sol. Cells* **2009**, 93, 2025; (k) Sharma, G. D.; Suresh, P. ; Mikroyannidis, J. A. and Stylianakis, M. M. *J. Mater. Chem.* **2010**, 20, 561.

7 (a) Luo, J.; Xu, M.; Li, R.; Huang, K.-W.; Jiang, C.; Qi, Q.; Zeng, W.; Zhang, J.; Chi, C.; Wang, P.; Wu, J. *J. Am. Chem. Soc.* **2014**, *136*, 265. (b) Luo, J.; Wang, X.; Fan, L.; Li, G.; Qi, Q.; Huang, K.-W. ; Tam, T. L. D.; Zhang, J.; Wang. Q.; Wu, J. *J. Mater.*

Chem. C. **2016**, 4, 3709.

8 (a) Yao, Z.; Yan, C.; Zhang, M.; Li, R.; Cai, Y. and Wang, P. *Adv. Energy Mater.* **2014**, 4, 1400244; (b) Zhang, M.; Yao, Z.; Yan, C.; Cai, Y.; Ren, Y.; Zhang, J. and Wang, P. *ACS Photonics* **2014**, 1, 710; (c) Yang, L.; Ren, Y.; Yao, Z.; Yan, C.; Ma, W. and Wang, P. *J. Phys. Chem. C* **2015**, 119, 980; (d) Yao, Z.; Wu, H.; Ren, Y.; Guo, Y. and Wang, P. *Energy Environ. Sci.* **2015**, 8, 1438; (e) Yao, Z.; Zhang, M.; Wu, H.; Yang, L.; Li, R. and Wang, P. *J. Am. Chem. Soc.* **2015**, 137, 3799. (f) Li, X.; Zheng, Z.; Jiang, W.; Wu, W.; Wang, Z.; and Tian, H. *Chem. Commun.* **2015**, 51, 3590; (g) Yang, L.; Zheng, Z.; Li, Y.; Wu, W.; Tian, H. and Wang, Z. *Chem. Commun,* **2015**, 51, 4842.

9 Qi, Q.; Wang, X.; Fan, L.; Zheng, B.; Zeng, W.; Luo, J.; Huang, K.-W.; Wang, Q.; Wu, J. *Org. Lett.* **2015**, 17, 724

10 Ripolles-Sanchis, T.; Guo, B. C.; Wu, H. P.; Pan, T. Y.; Lee, H. W.; Raga, S. R.; Fabregat-Santiago, F.; Bisquert, J.; Yeh, C. Y.; Diau, E. W.-G. *Chem. Commun*. **2012**, *48*, 4368.

11 Wang, X. Z.; Yang, J.; Yu, H.; Li, F.; Fan, L.; Sun, W.; Liu, Y.; Koh, Z. Y.; Pan, J. H.; Yim, W.-L.; Yan, L.; Wang, Q. *Chem. Commun.* **2014**, *50*, 3965.

12 Zhang, M.; Wang, Y.; Xu, M.; Ma, W.; Li, R. and Wang. P. *Energy Environ. Sci*. **2013**, 6, 2944.

13 Luo, J.; Zhang, J.; Huang, K.-W.; Qi, Q.; Dong, S.; Zhang, J.; Wang P. and Wu, J. *J. Mater. Chem. A* **2016**, 4, 8428.

14 Zhu, W.; Wu, Y.; Wang, S.; Li, W.; Li, X.; Chen, J.; Wang, Z.-S.and Tian, H. *Adv. Funct. Mater.* **2011**, 21, 756.

15 Lin, L.-Y.; Tsai, C.-H.; Wong, K.-T.; Huang, T.-W.; Hsieh, L.; Liu, S.-H.; Lin, H.-W.; Wu, C.-C.; Chou, S.-H.; Chen, S.-H. and Tsai, A.-I. *J. Org. Chem.* **2010**, 75, 4778.

16 Page, J. A.; Wilkinson, G. *J. Am. Chem. Soc.* **1952**, *74*, 6149.

17 (a) Wu, Y.; Marszalek, M.; Zakeeruddin, S. M.; Zhang, Q.; Tian, H.; Grätzel, M.; Zhu, W. *Energy Environ. Sci,* **2012**, 5, 8261. (b) Haid, S.; Marszalek, M.; Mishra, A.; Wielopolski, M.; Teuscher, J.; Moser, J.-E.; Humphry-Baker, R.; Zakeeruddin, S. M.; Grätzel, M.; Bäuerle. P. *Adv. Funct. Mater.* **2012**, 22, 1291.

18 (a) Wang, P.; Zakeeruddin, S. M.; Comte, P.; Charvet, R.; Humphry-Baker, R.; Grätzel, M. *J. Phys. Chem. B,* **2003**, 107, 14336. (b) Stergiopoulos, T.; Falaras, P. *Adv. Energy Mater* **2012**, 2, 616.

19 (a) O'Regan, B.; Bakker, K.; Kroeze, J.; Smit, H.; Sommeling, P.; Durrant, J. R. *J. Phys. Chem. B* **2006**, 110, 17155. (b) Duffy, N. W.; Peter, L. M.; Rajapakse, R. M. G.; Wijayant, K. G. U. *Electrochem. Commun.* **2000**, 2, 658.

Chapter 4 Methylthio-capped rylenes and their stableradical cations and dications

4.1 Introduction

Radical cations and dications of π-conjugated oligomers and polymers,[1-4] have attracted considerable attention, mainly owing to their vital role in charge-transporting in organic electronics, such as OFETs, organic solar cells and single-molecule wires.[5-7] Their structures, the distribution of charge and spin in a molecule as well as mechanism of charge transport are of great interest. Significant progress has been made in isolating and characterizing radical cations and dications of oligomers with well-defined structures to address these issues.[8] For example, Rathore and co-worker reported the isolation and characterization the radical cations of oligo(*para*-phenylene)s.[9] The alternation of the bond lengths and a decrease in the dihedral angle of the two nearly coplanar *para*-phenylene units in radical cation form indicated an increase of the quinoidal character. Very recently, the radical cations and dications of [*n*]CPPs (*n* = 5, 6, 8, 10, 12) were isolated and characterized.[10] The spin and charges in the oxidized species were fully delocalized over the entire phenylene rings. Moreover, the diradical character in the higher order dications was clarified. Although significant progress has been made in isolating and characterizing π-radical cations and dications, the majority of them are limited to π-conjugated oligomers. Isolation and characterization of radical cation and dication of wholly conjugatied π-system such as PAHs were rare due to their intrinsic high reactivity. Meanwhile, graphene nanoribbons (GNRs), in which the lateral quantum confinement opens an

electronic gap that is a function of the ribbon width, have opened the opportunities toward carbon-based nanoelectronics.[11] *N*-annulated rylenes can be regarded as perfect model compounds for the narrowst armchair GNRs (5-AGNR) with nitrogen atoms annulated to the armchair edges.[12] As introduced in chapter 1, recently, significant progress has been made in the synthesis of long rylene molecules by using *N*-annulated perylene (NP) as the building block.[13] Also, soluble and stable quinoidal perylene and even high order quinoidal rylenes ribbons with chain-length dependent ground state and properties have been successfully synthesized and characterized.[14] The redox properties of largely π-conjugated rylene molecules are among the most interesting characteristics of these compounds. However, very rare study has been done to investigate their radical cations and dications.

Herein, in this chapter we will report the synthesis and characterization of methylthio-capped rylenes, and the isolation and characterization of their corresponding radical cation and the dications. As shown in Figure 4.1, *ortho*-alkoxy substituted phenyl group was chosen to suppress the problematic aggregation as well as to ensure sufficient solubility. Moreover, the end-capping with methylthio groups are expected to be effective for stabilization of the oxidized species (*via* hyperconjugation and spin delocalization mechanism).[15] All these compounds showed unique size-dependence properties and the spin and charge were completely delocalized over all conjugation backbone in radical cations and dications forms, as assessed by UV-vis-NIR spectra, electron spin resonance (ESR) and NMR studies. of the unique diradical character is also clarified for the high order rylene dications.

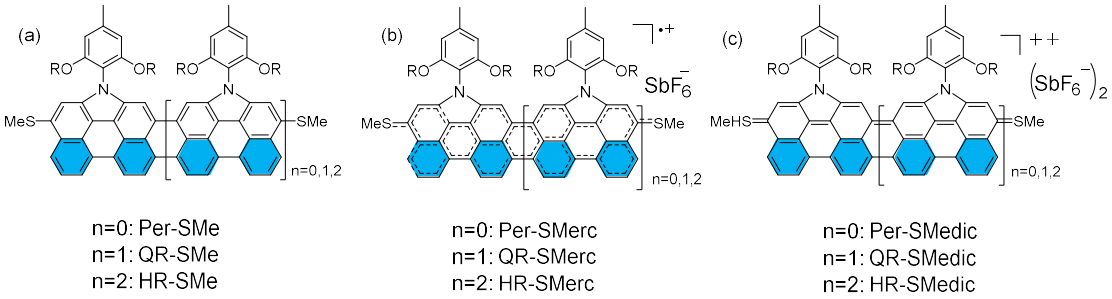

n=0: Per-SMe
n=1: QR-SMe
n=2: HR-SMe

n=0: Per-SMerc
n=1: QR-SMerc
n=2: HR-SMerc

n=0: Per-SMedic
n=1: QR-SMedic
n=2: HR-SMedic

Figure 4.1 Structures of (a) the neutral dimethyl-capped rylenes and the corresponding (b) radical caitons and (c) dications.

4.2 Results and discussion

The synthetic route for the methylthio-capped rylenes**Per-SMe**, **QR-SMe** and **HR-SMe** is outlined in Scheme 4.1. Alkoxyl chain wrapped NP **4-1** and dibromo-NP **4-2** were synthesized according to our previous report.[16] Selective bromination by NBS gave monobromo-NP **4-4** in 70% yields. Pd-catalysed borylation of **4-2** with pinacolborane afforded the compound **4-3** in 76% yields. The key intermediate **4-5** was then prepared by the monolithiation of **4-4** followed by reaction with anhydrous dimethyldisulfide and subsequent bromination. Compound **4-6** was obtained by oxidative coupling of **4-4** in the present of NBS and TFA in chloroform. Compound **4-7** and compound **Per-SMe** were prepared by the dilithiation of **4-6** and **4-2** followed by reaction with anhydrous dimethyldisulfide. Suzuki coupling of compound **4-3** and **4-5** generated the compound **4-8**. The final compound **QR-SMe** and **HR-SMe** were successfully prepared by oxidative cyclodehydrogenation of the corresponding precursors **4-7** and **4-8** with DDQ/$Sc(OTf)_3$. The absorption spectra of **QR-SMe** and **HR-SMe** are similar to those of the previously reported *N*-annulated quaterrylene and hexarylene, respectively.[17,13a] The longer fused rylenes (for example, octarylene) were not obtained under the same conditions because of the difficulty in purification and

instablility of the crude product. **Per-SMe** is yellow powder, **QR-SMe** and **HR-SMe** are dark green powder and soluble in normal organic solvents such as DCM, chloroform and tetrahydrofuran. For **Per-SMe** and **QR-SMe**, their structures were supported by clean ^{1}H NMR and high resolution mass spectra. For **HR-SMe**, the structure of the final product was confirmed by high resolution mass spectra and featured UV-vis-NIR spectra.

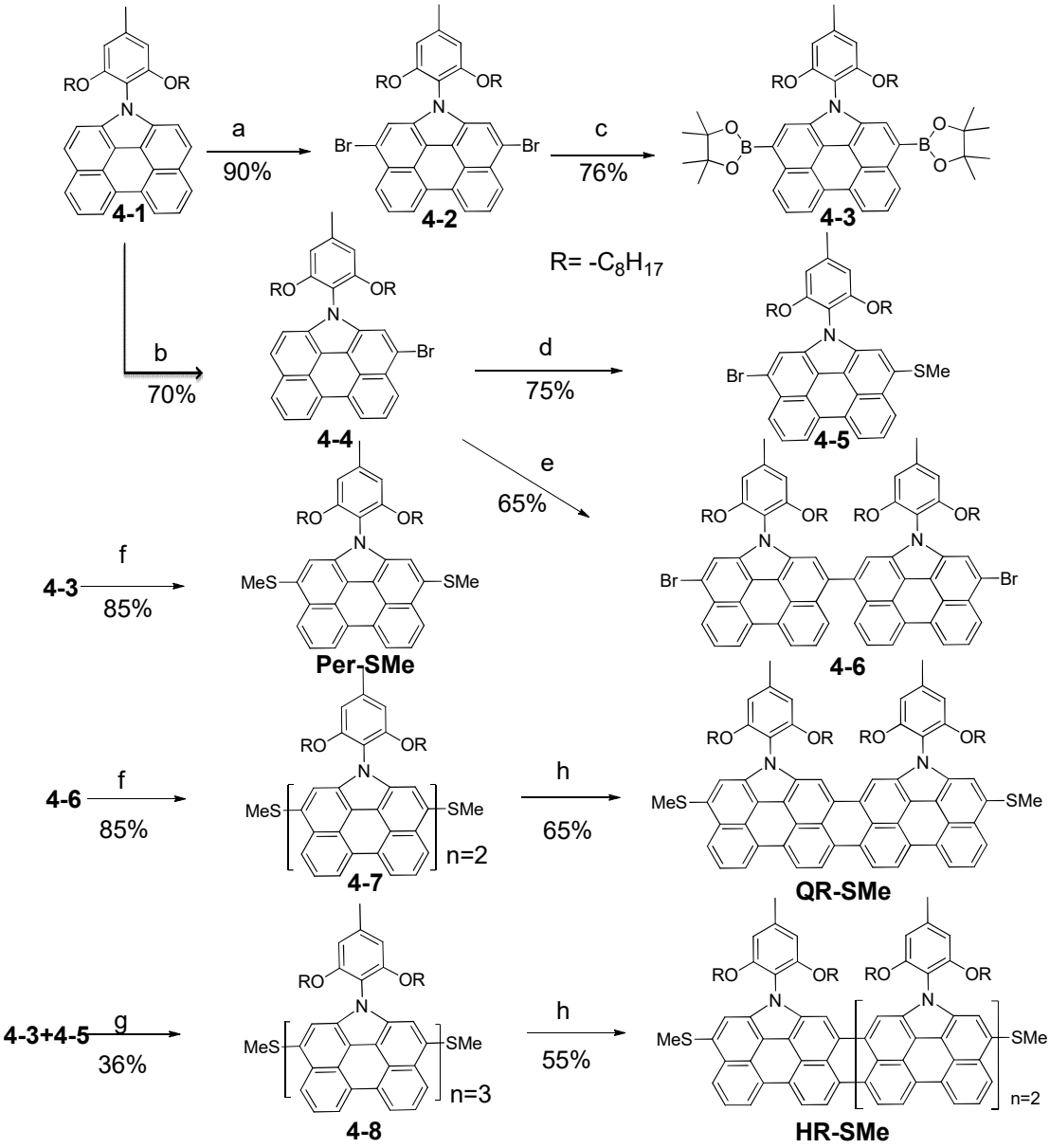

Scheme 4.1 Synthetic route of **Per-SMe**, **QR-SMe** and **HR-SMe**. Reagents and conditions: (a) NBS,$CHCl_3$,rt; (b) NBS, $CHCl_3$, 0 ^oC; (c) pinacolborane, $Pd(PPh_3)_2Cl_2/Et_3N$/1,2-dichloroethane, 90 ^oC; (d) i) *n*-BuLi/THF/-78 ^oC, dimethyldisulfide, RT; ii) NBS, THF, RT; (e) NIS/TFA, $CHCl_3$; (f) *n*-BuLi/THF/-78 ^oC, then dimethyldisulfide, RT; (g) $Pd(PPh_3)_4/K_2CO_3$, toluene, reflux; (h) DDQ/$Sc(OTf)_3$, toluene, relux; 24h for **QR-SMe**, 48h for **HR-SMe**.

The optical properties of neutral methylthio-capped rylenes were evaluated with the aid of UV-vis-NIR spectroscopy. The electronic absorption spectra of **Per-SMe**, **QR-SMe** and **HR-SMe**, in dichloromethane, were recorded under conditions of identical concentration (0.1 mM) at room temperature and are compiled in Figure 4.2 and the data is collected in Table 4.1. The rylene arrays showed broad absorption bands that shifted bathochromically upon the increasing of conjugation length of rylene backbone, which is consistent with previously reported *N*-annulated quaterrylene and hexarylene. As shown in Figure 4.2, the spectrum of **QR-SMe** and **HR-SMe** displays a drastical bathochromic shift (235 nm, 407 nm) compared with **Per-SMe**, respectively, which reflects that the ladder-type conjugated structure leads to a great degree of planarity and large delocalization of π-electrons.

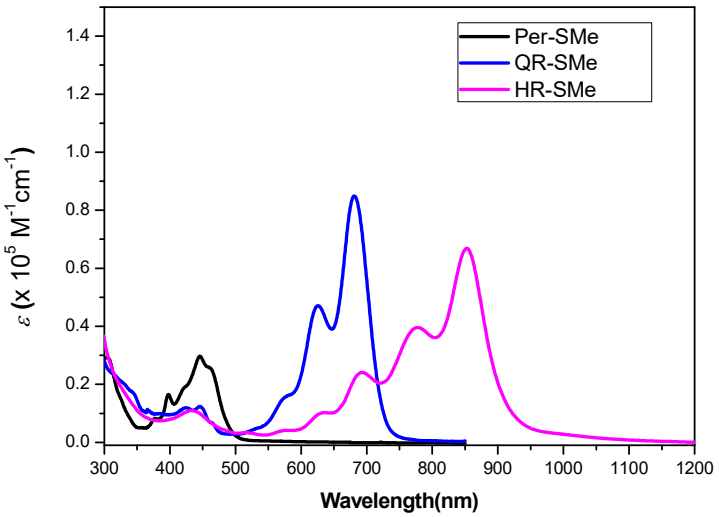

Figure 4.2 The UV-Vis-NIR absorption spectra of **Per-SMe** (black), **QR-SMe** (blue)

and **HR-SMe** (pink) in dichloromethane.

Next, the electrochemical properties of **Per-SMe**, **QR-SMe** and **HR-SMe** were investigated by cyclic voltammetry (CV) and differential pulse voltammetry (DPV) in deoxygenated DCM solution containing 0.1 M tetra-*n*-butylammonium hexafluorophosphate ($TBAPF_6$) as supporting electrolyte.

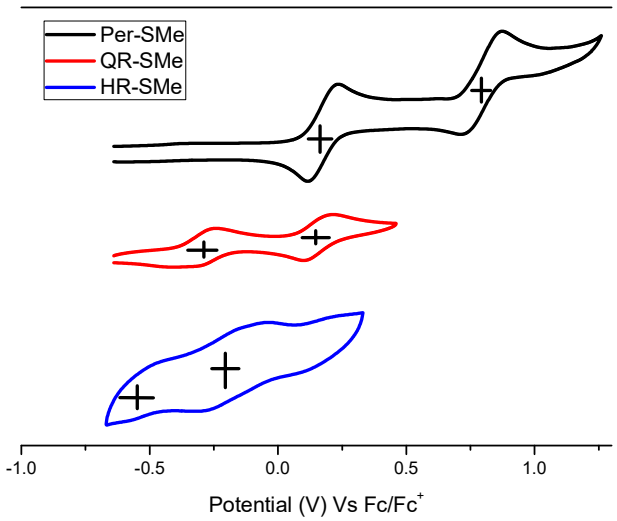

Figure 4.3 Cyclic voltammograms of **Per-SMe**, **QR-SMe** and **HR-SMe** in dry DCM.

Multiple reversible oxidative waves were observed for all three compounds (see the list of half-wave oxidation potentials $E_{1/2}^{ox}$ in Table 4.1). The $E_{1/2}^{ox}$ of **Per-SMe** externally calibrated by ferrocene was found to be 0.16 and 0.79 V, corresponding to the formation of a radical cation and dication, respectively. For **QR-SMe**, two well-separated reversible oxidation waves with $E_{1/2}^{ox}$ = -0.30, 0.16V (*vs* Fc/Fc^+) were also found. For **HR-SMe**, the first two oxidation reversible waves were found with $E_{1/2}^{ox}$ = -0.55 and -0.21V. From the oxidation potential, we can find that the longer the conjugation length, the easier to be oxidised. The HOMO and LUMO energy levels were then estimated according to equations: HOMO = -[4.8 + E_{ox}^{onset}] eV, and LUMO = -(E^{opt}-HOMO) eV, where E_{ox}^{onset} is the onset of the first oxidation (*vs* Fc^+/Fc) and

the E^{opt} is the optical energy gap estimated form the lowest energy absorption onset. The HOMO and LUMO energy levels of **Per-SMe**, **QR-SMe** and **HR-SMe** were determined to be -4.96, -4.50, -4.25 eV (HOMO) and -2.48, -2.86, -2.95 eV (LUMO), respectively (Table 4.1). The E^{opt} were measured to be 2.48, 1.64, and 1.30 eV, respectively. The reversible oxidation potentials make it possible to carefully study their redox properties. The electrochemical oxidation process of **Per-SMe** can be monitored by UV-vis-NIR absorption spectroscopy using a spectroelectrochemcial cell. Electrochemical oxidation was then carried out in a stepwise manner in dry DCM at suitable applied voltages (+0.5 and +1.2 V *vs* Fc/Fc^+), the final spectrum in the stationary state for the 1e (red line) and 2e (blue line) oxidation state are shown in Figure 4.4a. The UV-vis absorption spectrum of neutral **Per-SMe** in CH_2Cl_2 showed weak and broad absorption in the 300– 550 nm region. After1e oxidation, new absorption peaks at 555, 598, 744, 815 nm appeared. The new absorption peaks were ascribed to the generation of corresponding radical cation. For 2e oxidation, the strong absorption at 517.5 nm is due to the quinoidal structure in corresponding dication (Table 4.1). The electrochemical oxidation of **QR-SMe** was also carried out at suitable applied voltages (-0.05 and +0.45 V *vs* Fc/Fc^+) with the same procedure. The final stationary the 1e (red line) and 2e (blue line) oxidation spectrums of **QR-SMe** were shown in Figure 4.4b. In sharp contrast, the spectrum of **QR-SMe** displays a drastically bathochromic shift (222 nm) compared with **Per-SMe** due to extended electron delocalization. After 1e oxidation, new absorption peaks at 555, 598, 744, 815 nm were found. The generated spectrum after 2e oxidation displayed an intense

absorption band with maximum at 800 nm, along with a shoulder at 723 nm, which is similar to that of quinoidal closed-shell **QR-CN.**[14a] The spectrum showed approximately 283 nm red shift compared to that of the dication of **Per-SMe** with a drastic increase of the extinction coefficient (Table 4.1). These observations indicate that **QR-SMe** dication has a closed-shell quinoidal structure in the ground state. The electrochemical oxidation of **HR-SMe** was then carried out at suitable applied voltages (-0.35 and +0.05 V *vs* Fc/Fc+) in a same procedure. The final stationary 1e (red line) and 2e (blue line) oxidation spectrums of **QR-SMe** were shown in Figure 4.4c. For 1e oxidation, featured absorption peaks at 626, 690, 987, 1291 nm were found. Interestingly, the spectrum of **HR-SMe** dication after 2e oxidation showed quite different structure. OPA spectrum of **HR-SMe** dication displayed an intense band at 883 nm together with a shoulder at longer wavelength (981 nm). The characteristic structured long-wavelength absorption bands were quite similar to that of our previously reported open-shell singlet diradical HR-CN,[14a] indicating an open-shell singlet ground state of **HR-SMe** dication.

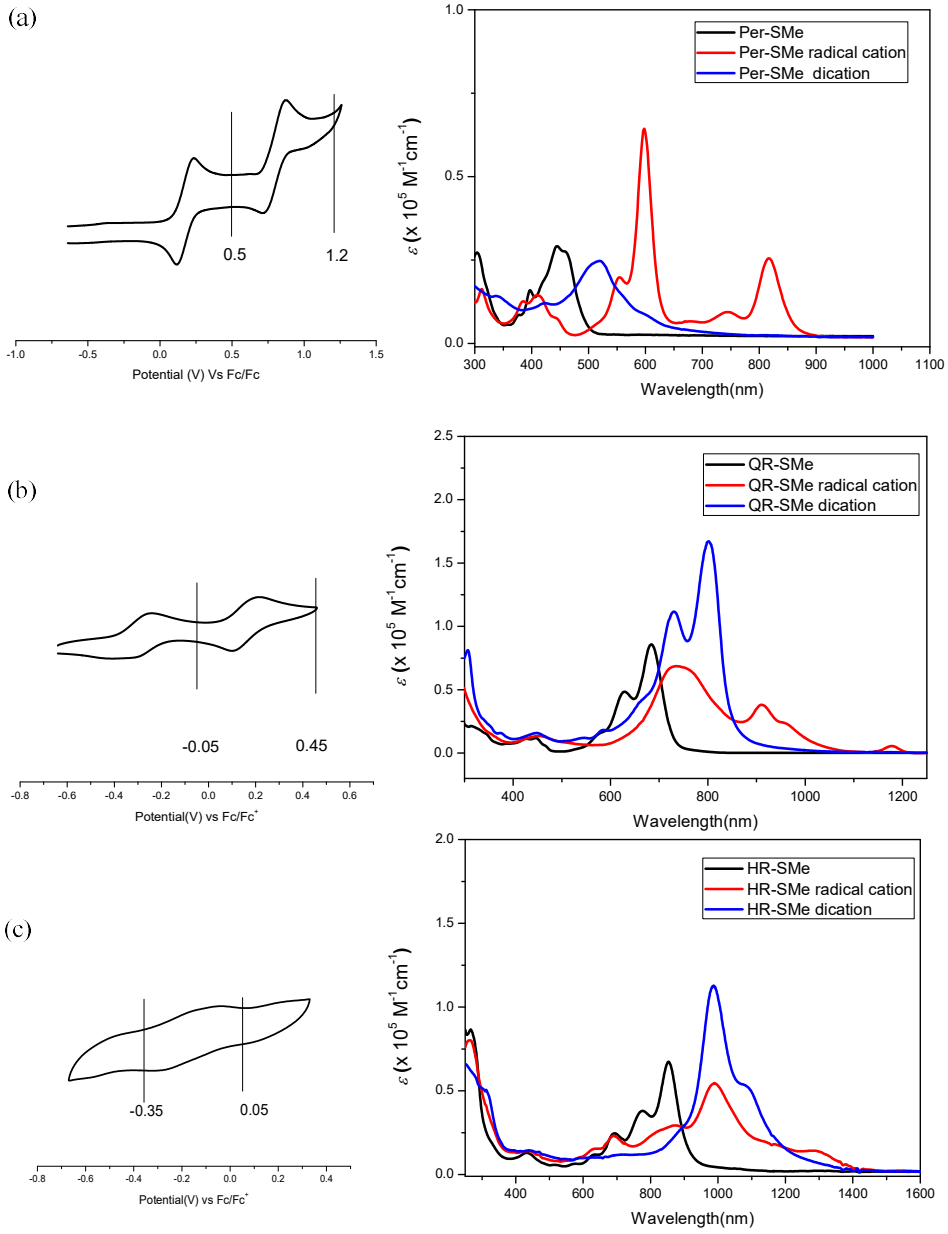

Figure 4.4 Electrochemical oxidation spectra of (a) **Per-SMe** (b) **QR-SMe** and (c) **HR-SMe** recorded in DCM.

In order to get stable materials, chemical titration with $NOSbF_6$ was then done to confirm the transformation from neutral species to radical cations and dications as well as the stability. As shown in Figure 4.5, continuous UV-vis-NIR changes were recorded upon chemical oxidation. The data was recorded in Table 4.1. The corresponding radical cations and dications were successfully generated and could be

reversibly reduced back to neutral compounds *via* addition of triethylamine, and all compounds showed consistent absorption with ectrochemically oxidatised species. However, it is worth to note that dication of **Per-SMe** cannot be obtained by chemical oxidation with even using large access $NOSbF_6$ or $SbCl_5$. This may due to its high second oxidation potential and strong repulsion of two positive charges in limited space. Although all maxima of absorption bands were same, the band shape of **QR-SMe** dication was slightly different in electrochemical oxidation and in chemical oxidation. This may due to the effect of generated salt specie in chemical oxidation. Interestingly, good stability was found for all compounds in each stage. All methylthio-capped rylene radical cations and dications exhibited a large bathochromic shift in the maximum absorption relative to those of the neutral species. Moreover, significant size dependence was observed for the radical cations and dications; larger π-extended rylene absorbed at longer wavelengths. It is also noteworthy that due to negligible absorption in the visible region (400–700 nm), **QR-SMerc** and **HR-SMedic** are almost colorless in solution, which can be used as transparent materials.

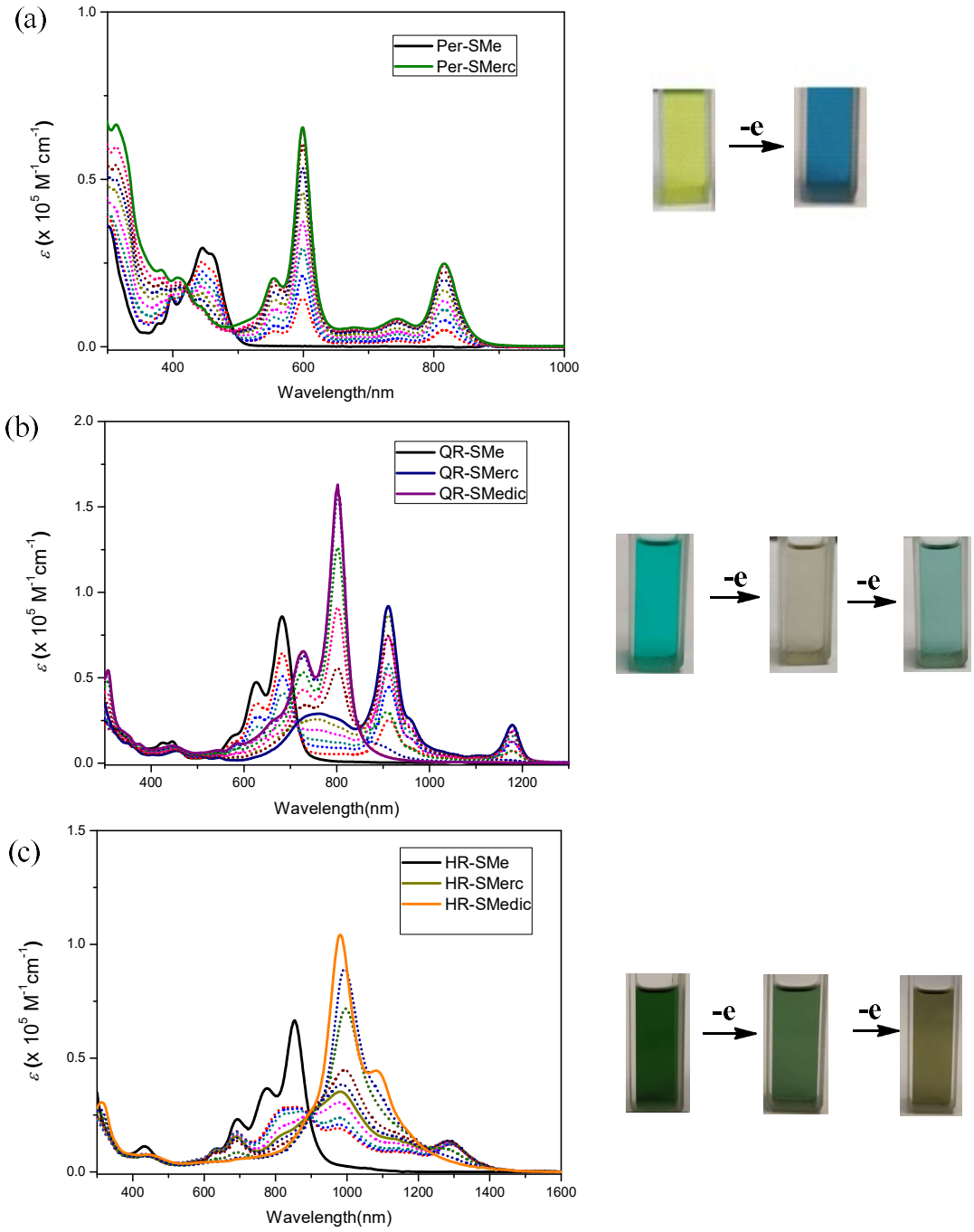

Figure 4.5 Chemical titration spectra by using $NOSbF_6$ of (a) **Per-SMe** (b) **QR-SMe** and (c) **HR-SMe** recorded in DCM.

Table 4.1 Summary of optical and electrochemical properties of **Per-SMe**, **QR-SMe** and **HR-SMe** and their corresponding radical cations and dications.

Molecules	[a]λ_{abs} (nm)	[b]λ_{abs} (nm)	[b]ε ($M^{-1}cm^{-1}$)	E_g^{opt} (eV)	$E_{1/2}^{ox}$ (V)	[c]HOMO (eV)	[opt]LUMO (eV)
Per-SMe	445 460	445 460	29000 27700	2.45	0.16 0.79	-4.96	-2.48
Per-SMerc	555 598 744 815	555 598.5 744 815	20600 65300 83400 24900				
Per-SMedic	517.5						
QR-SMe	573.5 625.5 682	573.5 625.5 682	16000 47800 86000	1.67	-0.30 0.16	-4.50	-2.86
QR-SMerc	756 911 1177	756 911.5 1176.5	29400 91400 23000				
QR-SMedic	723 800.5	723 800.5	64000 162000				-
HR-SMe	633.5 690.8 772	633.5 690.8 772	10100 23900 36100	1.31	-0.55 0.21	-4.25	-2.95

	853	853	67400				
HR-SMerc	626 690.5 987 1291	626 690.5 986 1290	9100 15400 35600 12800				
HR-SMedic	883 981.5 1089	883 981 1089	24900 104000 44000				

[a] electrochemical oxidation; [b] chemical oxidation with $NOSbF_6$; [c] HOMO = -(4.8+$E_{1/2}$ ^{ox}); ^{opt}LUMO = E_g^{opt} + HOMO; rc = radical cation; dic = dication.

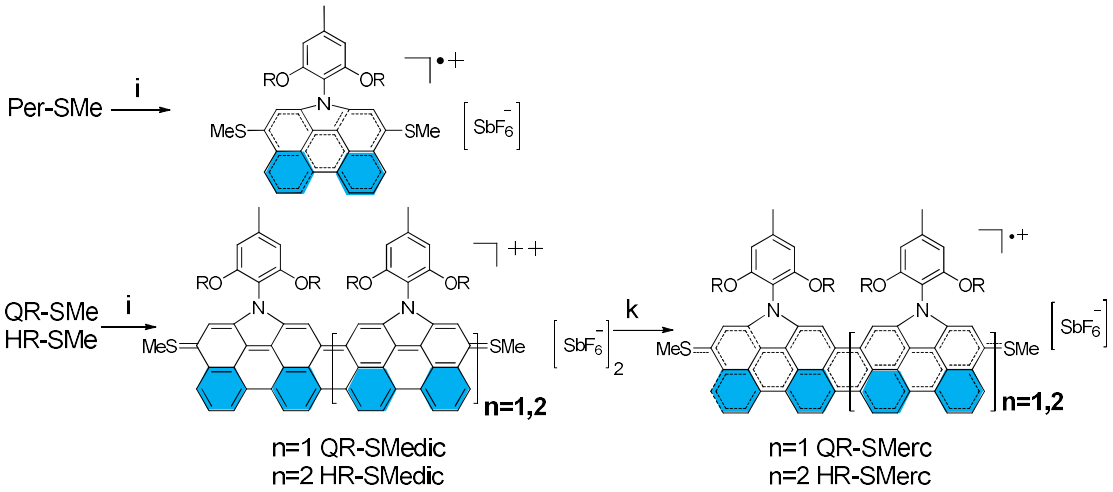

Scheme 4.2 Synthetic route of corresponding radical cations and dications. Reagents and conditions: (i) $NOSbF_6$/DCM, RT, 5 mins; (k) reaction of 1 equiv. neutral compound and 1 equiv. corresponding dication in dry in DCM, RT, 5mins.

The synthesis and isolation of corresponding radical cation and dication were then successfully carried out by using a nitrosonium hexafluoroantimonate ($NOSbF_6$) as an oxidant (Scheme 4.2). **Per-SMe** was fully converted to the corresponding radical cation as purple solid by employing 1.5 equiv of $NOSbF_6$ in CH_2Cl_2 at room temperature. For **QR-SMe** and **HR-SMe**, we first synthesized pure corresponding

dication by using 2.1 equiv $NOSbF_6$ followed by recrystallization in DCM/hexane, even though the selective single-electron oxidation of neutral **QR-SMe** and **HR-SMe** by $NOSbF_6$ was not very successful. Then the reaction of 1 equiv. neutral compound and 1 equiv. corresponding dication afforded radical cation **QR-SMerc** and **HR-SMerc** as dark solid quantitively. All the radical cations and dications showed very good stability in dicloromethane. For the radical cations, **Per-SMerc**, **QR-SMerc** and **HR-SMerc** were stable under nitrogen and were stored at −30 °C for more than 3 months. **Per-SMerc** can be easily converted to neutral **Per-SMe** within 12h at room temperature when exposed to air mainly because of moisture, while **QR-SMerc** and **HR-SMerc** was much more stable. On the other hand, all dications were remarkably stable under nitrogen and no apparent decomposition was observed at $-30^{o}C$ even after several months.

All radical cations were ESR active and ^{1}H NMR silent at room temperature, which was consistent with the formation of paramagnetic species. As shown in Figure 4.6, All radical cations showed intense one-line ESR spectra with g_e = 2.0047, 2.0032, and 2.0030, respectively. Calculations of charge and spin density of radical cations provided further evidence for the spin delocalization. The spin density of the radical cation was almost fully delocalized all over the backbone. It is noteworthy that the longer the length, the smaller the g_e value. This may result from the change of spin density distribution upon increasing of π-conjugation. With longer conjugation length, spin will mainly distributed over the backbone rather than terminal S atoms.

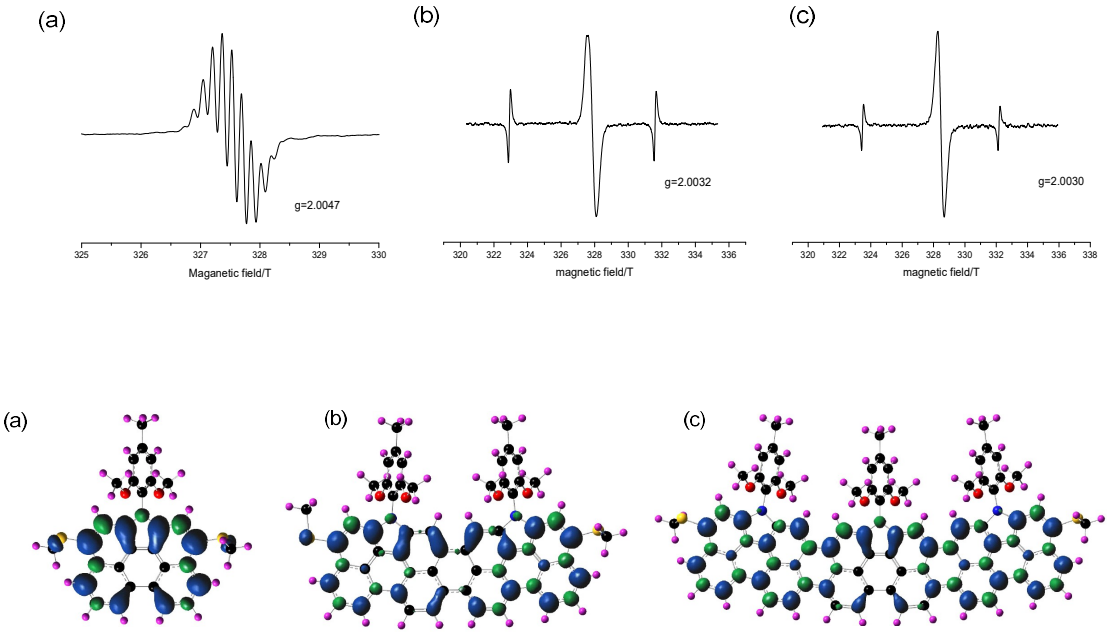

Figure 4.6 ESR spectra and corresponding spin density distribution of (a) **Per-SMerc**, (b) **QR-SMerc** and (c) **HR-SMerc** recorded in DCM at -80 ^{o}C. Spin density distribution at an iso value 0.002.

Fortunately, we were able to get the good quality single crystals of **Per-SMerc**, **QR-SMerc** for X-ray crystallographic analysis by solvent diffusion methods (Figure 4.7).

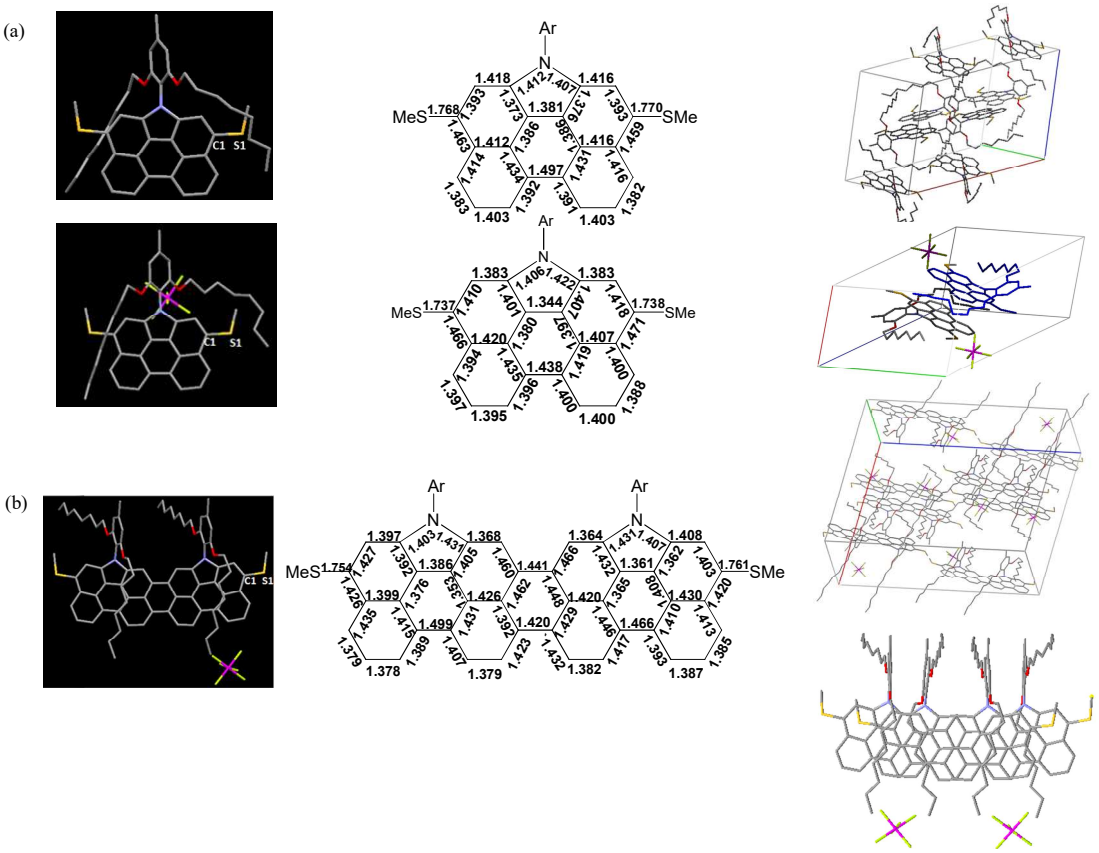

Figure 4.7 (a) X-ray crystallographic structure and selected bond lengths of **Per-SMe** and **Per-SMerc** (T= 100K). (b) X-ray crystallographic structure and selected bond lengths of the backbone of **QR-SMerc** (T= 100K).

For **Per-SMe**, twostructures with almost same bond lengths were found in X-ray crystallographic at T = 100 K mainly due to twisted *ortho*-alkoxy substituted phenyl group and flexibility of methylthio groups. The molecule showed a bent structure due to the fusion of five-membered ring at the bay region of perylene and owing to slight distortion, this molecule is not symmetric. Because of the presence of bulky substitution, no continuously stacked columnar superstructure was observed. The C1-S1 (average 1.769Å) bond showed typical C-S single bond character. In contrast, the C1-S1 bond in **Per-SMerc** form （average 1.738Å） became much shorter, which is consistent with the delocalization of spin and positive charge over all the backbone. Interestingly, the **Per-SMerc** adopted a slipped dimeric structure in an antiparallel

packing mode with a short packing distance of ca. 3.23 Å through both spin−spin and π−π interactions. Besides a dimer structure formed by the next two molecules (up and down) as stated, columnar superstructure was observed. For **QR-SMerc**, the structure was bent and unsymmetic. The C1-S1 (average 1.758 Å) was shorter than normal C-S single bond. The extension of π-conjugation length resulted in longer C1-S1 bond length than that of **Per-SMerc**. **QR-SMerc** adopted a dimeric structure in an parallel packing mode with a short packing distance of ca. 3.2 Å through both spin−spin and π−π interaction. From calculation (Figure 4.8), the dimer showed small singlet diradical character (y_0 = 1.8%), indicating a strong anti-ferromagnetic coupling between the two radical cations.

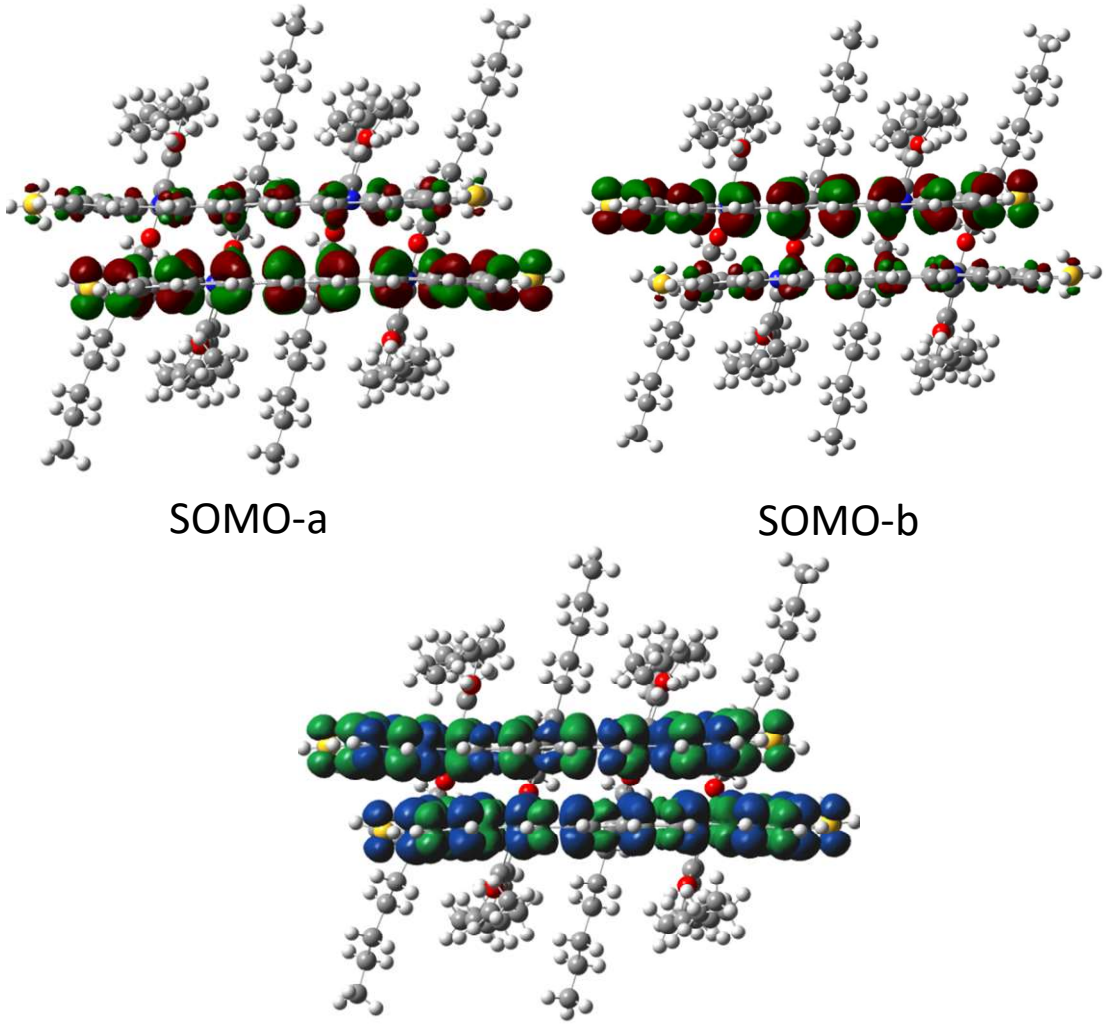

Figure 4.8 Calculated (UCAM-B3LYP) SOMO-α/β profile and spin density distribution of the singlet diradical form of the **QR-SMerc** dimer.

For the dications, **QR-SMedic** is ESR silent and display blue-shifted absorption compared to the respective radical cations, which is consistent with the closed-shell ground state. Clear ^{1}HNMR of **QR-SMedic** in CD_2Cl_2 and ^{1}HNMR of **QR-SMe** in C_6D_6 was recorded at room temperature (Figure 4.9). It is needed to claim that different deuterium reagents were used because of the different solubility of neutral form and dication form. As show in Figure 4.9a, clear ^{1}HNMR peaks were observed for **QR-SMe**. Upon transformation into **QR-SMedic**, for aromatic region of the

backbone, 7 sets of broad but clear peaks were found, indicating symmetric geometry. Furthermore, the chemical shift of H atoms at a, g, j, e sites in low field clearly claimed the formation of quinoidal structure in dication form, which is consistent with the UV-vis-NIR absorption spectra and silent ESR activity. All these factors further confirm the accuracy of the transformation from neutral species to radical cation and dication forms.

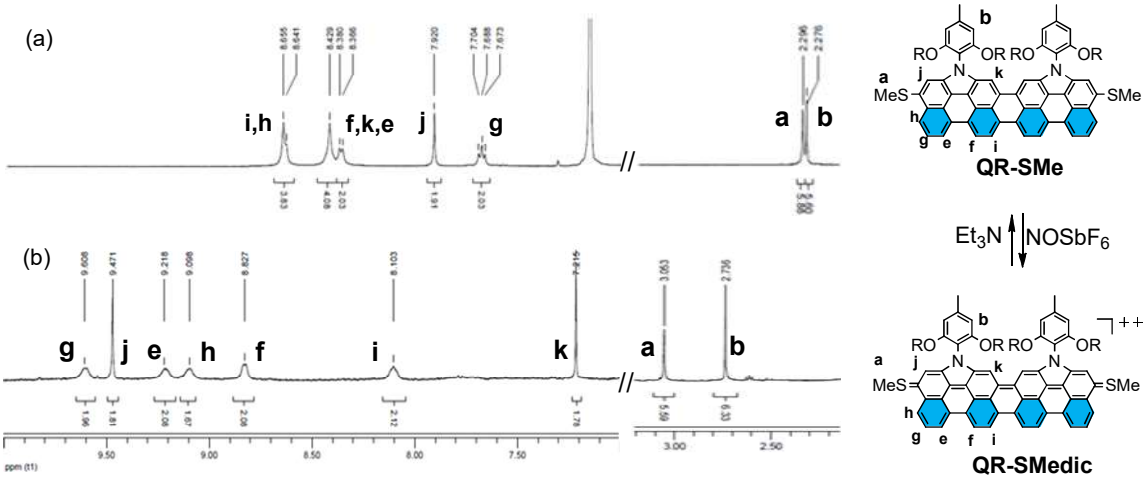

Figure 4.9 ^{1}H NMR spectra of a) **QR-SMe** in C_6D_6 and b) **QR-SMedic** in CD_2Cl_2.

HR-SMedic showed strong ESR in both solution and solid state (Figure 4.10). A broad ESR signal with *g* tensor of $g_e = 2.0029$ was observed for both a DCM solution and solid state of **HR-SMedic** (Figure 4.10), and the signal intensity decreased with a decrease in temperature, indicating a singlet diradical ground state for **HR-SMedic**, and this result was consistent with the observed UV-vis-NIR absorption spectrum. The singlet diradical ground state of **HR-SMedic** may due to the accumulated

resonance energy *via* formation of six aromatic naphthalene units in the diradical form.[18]

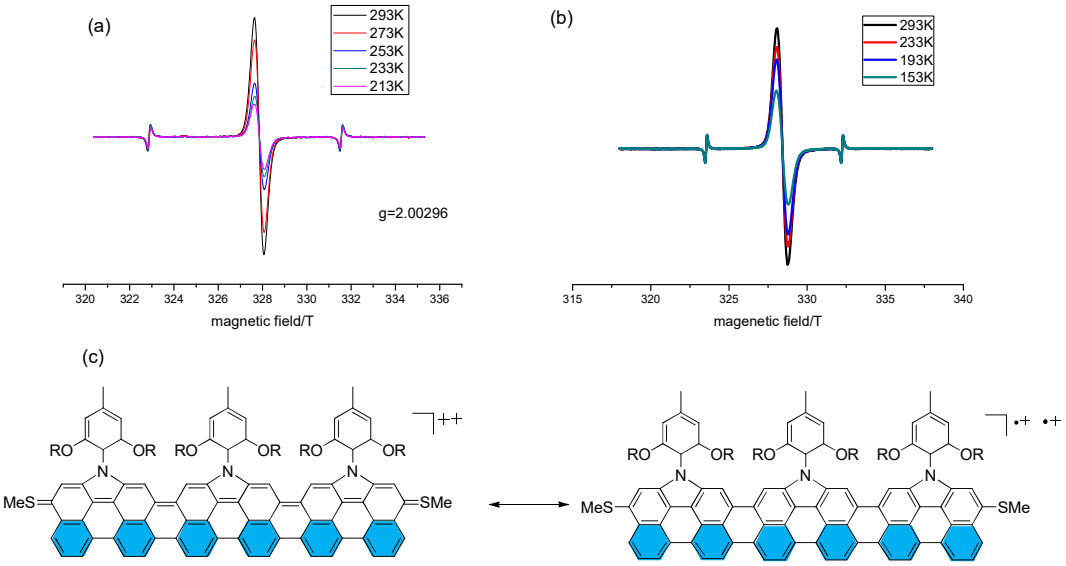

Figure 4.10 (a) VT- ESR spectra of **HR-SMedic** in DCM; (b) VT-ESR spectra of **HR-SMedic** in solid state; (c) two resonance forms of **HR-SMedic**.

To gain deeper insight into the ground-state geometry and electronic structure, DFT calculations were performed for all the compounds with the B3LYP/6-31G (d) level basis set (Figure 4.10). From the calculation, the featured S1-C1 bond lengths for **Per-SMe**, **QR-SMe** and **HR-SMe** were estimated to be 1.797, 1.796, and 1.796 Å respectively. Upon transformation into radical cations, the S1-C1 bond lengths all became samller than that of neutral forms, indicating delocalization of spin and charge. Interestingly, the length of the S1-C1 bond in radical cation form follows the sequence: **Per-SMerc** (1.778 Å) < **QR-SMerc** (1.786 Å) < **HR-SMerc** (1.787 Å), probably due to the extension of π-conjugation. For **Per-SMedic** and **QR-SMedic**, the S1-C1 bond length became smaller than that of corresponding radical cation, indicating closed-shell quinoidal structures. In contrast, the S1-C1 bond length in **HR-SMedic**

became longer than that of radical cation form, and the S1-C1 bond length followed the sequence as **HR-SMe** (1.796 Å) > **HR-SMedic** (1.791 Å) > **HR-SMerc** (1.787Å). Moreover, the bond lengths of C1-C3 and C1-C2 became similar both in **HR-SMe** and **HR-SMedic**. These features indicated the open-shell ground state of **HR-SMedic**.

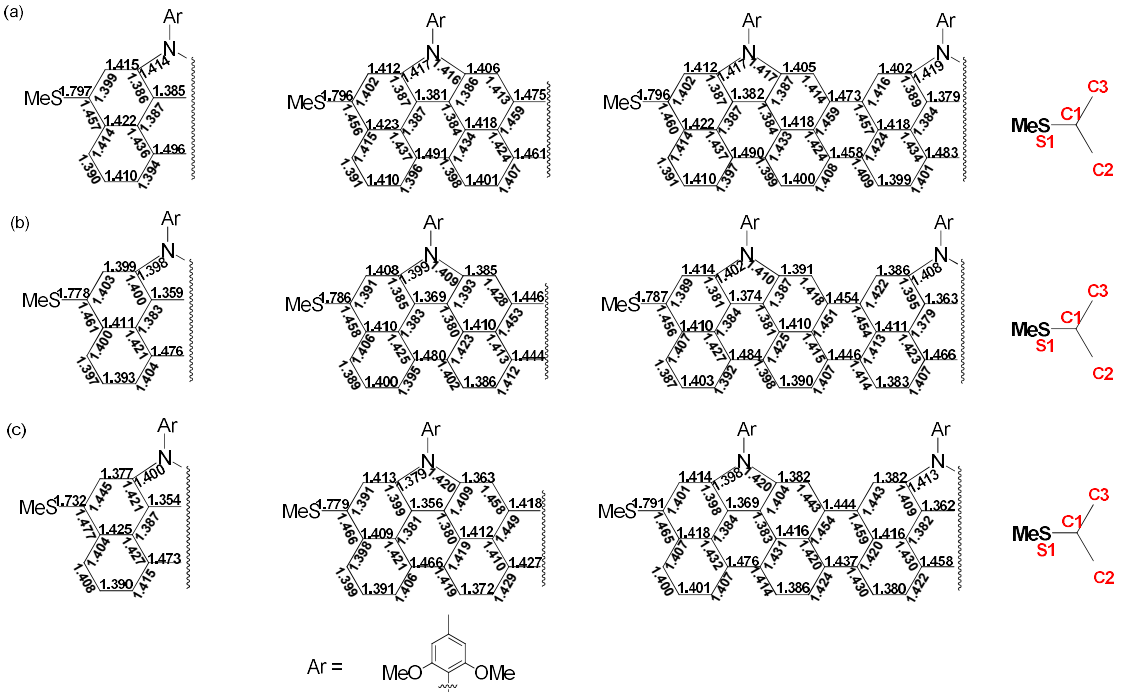

Figure 4.11 Calculated bond lengths of (a) **Per-SMe**, **QR-SMe** and **HR-SMe**; (b) **Per-SMerc**, **QR-SMerc** and **HR-SMerc**; (c) **Per-SMedic**, **QR-SMerdic** and **HR-SMedic** at B3LYP/6-31G(d.p) basis set. Long alkoxyl chain was replaced by methoxyl group in calculation.

Analyses on the calculated nucleus independent chemical shift (NICS) values (for example, NICS(1)) revealed that more aromatic benzenoid characters of the six-membered rings of the rylene moieties are seen (e.g. ring A) as prolonging the molecular lengths from **Per-SMedic**, **QR-SMedic** to **HR-SMerc** (Figure 4.12).This Calculations provided further evidence for diradical character in larger rylene dications, **HR-SMedic**.

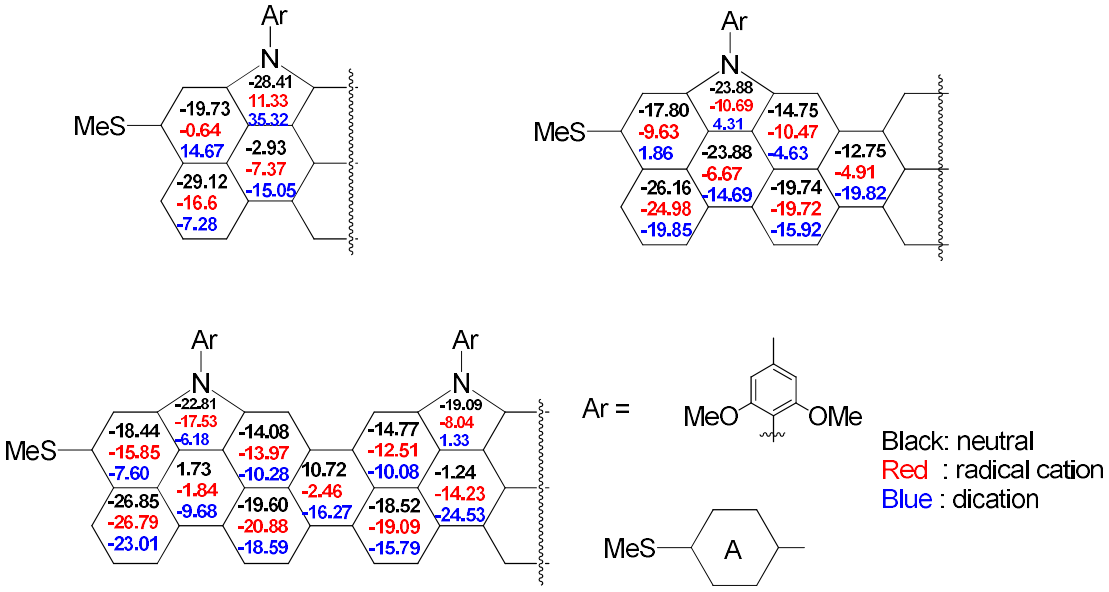

Figure 4.12 Calculated NICS (1) values of dimethylthio-capped rylenes at the B3LYP/6-31G level.

4.3 Conclusion

In summary, a series of radical cations and dications/diradical dications derived from methylthio-capped *N*-annulated rylenes were successfully synthesized by one- or two-electron chemical oxidation with $NOSbF_6$. Both oxidized species are stable and showed a large bathochromic shift into NIR region. The spin and charges in the oxidized species were delocalized over the backbone. Furthermore, the ground state electronic structures of dications are changed from a closed-shell for **Per-SMedic** and **QR-SMedic** to an open-shell singlet diradical for **HR-SMedic**. Although many radical cations and dications of π-conjugated oligomers have been isolated, stable charge species of wholly conjugated system were rare. These findings will aid in developing new NIR chromophores as well as understanding of charge and spin in the conjugated systems, and in the design of π-conjugated materials for molecular electronics.

4.4 Experimental section

4.4.1 General

All reagents and starting materials were obtained from commercial suppliers and used without further purification unless otherwise noted. Anhydrous toluene and THF were distilled from sodium-benzophenone immediately prior to use. The ^{1}H NMR and ^{13}C NMR spectra were recorded in solution of $CDCl_3$, C_6D_6, CD_2Cl_2 or THF-d_8 on Bruker DPX 300 or DRX 500 NMR spectrometers with tetramethylsilane (TMS) as the internal standard. The following abbreviations were used to explain the multiplicities: s = singlet, d = doublet, t = triplet, m = multiplet. MALDI-TOF or APCI mass spectrometry was used to confirm the mass of compound. The electrochemical measurements were carried out in anhydrous methylene chloride with 0.1 M $TBAPF_6$ as the supporting electrolyte at room temperature under the protection of nitrogen. A gold stick was used as working electrode, platinum wire was used as counting electrode, and Ag/AgCl (3M KCl solution) was used as reference electrode. The potential was externally calibrated against the ferrocene/ferrocenium couple. Steady-state UV-vis absorption were recorded on a Shimadzu UV-3600 plus spectrometer. The solvents used for UV-vis measurements are of HPLC grade (Merck). All reaction conditions dealing with air- and moisture sensitive compounds were carried out in a dry reaction vessel under an Argon atmosphere. ESR spectrum was measured for CH_2Cl_2 solution of a sample. Mn^{2+} in MnO was used as an external standard for calibration of the magnetic field.

4.4.2 Detailed synthetic procedures and characterization data

Compound 4-4

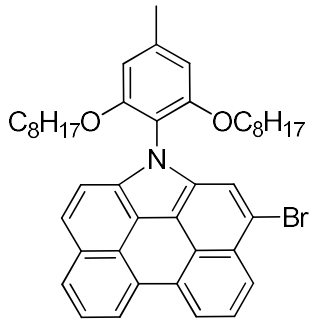

To the solution of compound **4-1** (892 mg, 1.46 mmol) in DCM (200 mL) was slowly added NBS (260 mg, 1.46 mmol) in portion over half an hour under 0°C. The mixture was then stirred for 30 min. The reaction mixture was quenched with water (50 mL). The organic layer was washed with water, and then washed with saturated brine and dried over anhydrous Na_2SO_4. The solvent was removed under reduced pressure and the crude product was purified by column chromatography (silica gel, hexane : DCM = 6 : 1) to give compound **4-4** as a yellow solid (0.7 g,70%).^{1}H NMR ($CDCl_3$, 300 MHz): δ ppm = 8.65-8.70 (m, 2H), 8.34 (d, *J* = 8.4 Hz, 1H), 8.13 (d, *J*= 8.4 Hz, 1H), 7.80-7.91 (m, 4H), 7.56 (d, *J*= 8.7Hz, 1H), 6.63 (s, 2H), 3.91 (t, *J* = 6.3 Hz, 4H), 2.51 (s, 3H), 1.32-1.37 (m, 4H), 0.97-1.03 (m, 4H), 0.82-0.87 (m, 16H), 0.72 (t, *J* = 7.2 Hz, 6H). ^{13}C NMR ($CDCl_3$, 75 MHz): δ ppm = 155.77, 139.69, 133.43, 132.66, 130.74, 130.08, 129.06, 128.22, 125.32, 125.21, 124.75, 124.71, 124.59, 124.54, 123.59, 121.11, 120.77, 119.28, 117.46, 117.29, 116.99, 115.49, 113.73, 106.75, 69.04, 31.50, 28.97, 28.93, 28.89, 25.73, 22.45, 22.38, 13.93. HR-MS (APCI, *m*/*z*): calcd. for $C_{43}H_{49}BrNO_2$ ([M+1]), 690.2941; found, 690.2940 (error: -0.2 ppm).

Compound 4-3

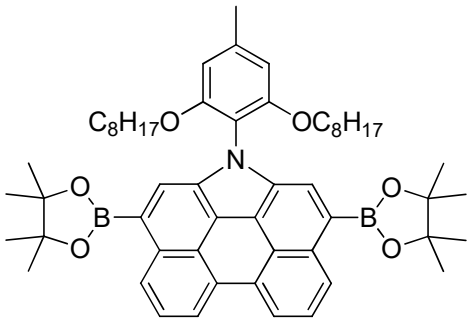

A 100 mL Schlenk flask was charged with **4-2** (76.9 mg, 0.1 mmol), pinacolborane (63.0 mg, 0.5 mmol), triethylamine (51.0 mg, 0.5 mmol), $PdCl_2(PPh_3)_2$ (4.0 mg, 0.005 mmol) and 1,2-dichloroethane (10 mL) under argon. The reaction mixture was stirred at 90 °C overnight. After removal of the solvent, the crude product was purified by column chromatography (silica gel, hexane : DCM = 5 : 1) to give compound **4-3** as a yellow solid (65.5 mg, 76%). ^{1}H NMR ($CDCl_3$, 500 MHz): δ ppm = 8.99 (d, *J* = 8.4 Hz, 2H), 8.69 (d, *J* = 7.5 Hz, 2H), 8.21 (s, 2H), 7.87 (t, *J* = 7.8 Hz, 2H), 6.64 (s, 2H), 3.90 (t, *J* = 6.3 Hz, 4H), 2.53 (s, 3H), 1.45 (s, 24H), 1.30-1.36 (m, 4H), 0.96-1.03 (m, 4H), 0.80-0.86 (m, 16H), 0.70 (t, *J* = 7.2 Hz, 6H). ^{13}C NMR ($CDCl_3$, 75 MHz): δ ppm = 155.99, 139.11, 133.55, 132.66, 130.80, 126.59, 124.95, 124.92, 124.67, 120.29, 120.13, 114.21, 106.64, 83.31, 68.92, 31.49, 29.01, 28.88, 28.87, 25.68, 25.01, 22.40, 13.90. HR-MS (APCI, *m*/*z*): calcd. for $C_{55}H_{72}B_2NO_6$ ([M+1]), 864.5557; found, 864.5584 (error: +3.0 ppm).

Compound 4-6

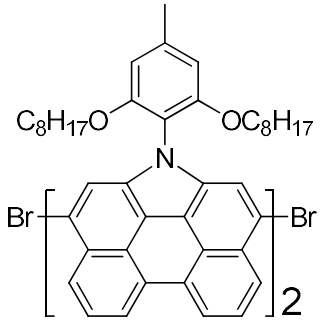

A 100 mL Schlenk flask was charged with **4-4** (69.0 mg, 0.1 mmol), *N*-iodosuccinimide (22.4 mg, 0.1 mmol), and dichloromethane (10 mL) under argon. Then 0.2ml trifluoroacetic acid (0.15ml, 2mmol) was added dropwisely. The reaction mixture was stirred for 30min. The reaction was quenched by adding water. Then the mixture was extracted with dichloromethane 3 times and the organic phase was dried with sodium sulfate. After removal of the solvent, the crude product was purified by column chromatography (silica gel, hexane : DCM = 4 : 1) to give compound **4-6** as a yellow solid (44.8 mg, 65%). ^{1}H NMR ($CDCl_3$, 500 MHz): δ ppm = 8.77 (d, *J* = 7.5 Hz, 2H), 8.71 (d, *J* = 7.5 Hz, 2H), 8.40 (d, *J* = 8.5Hz, 2H), 7.93-7.96 (m, 4H), 7.80 (d, *J* = 8.5Hz, 2H), 7.74 (s, 2H), 7.65 (t, *J* = 7.5 Hz, 2H), 6.60 (s, 2H), 6.56 (s, 2H), 3.82-3.96 (m, 8H), 2.44 (s, 6H), 1.37-1.42 (m, 8H), 0.81-0.99 (m, 40H), 0.64-0.70 (m, 12H). ^{13}C NMR ($CDCl_3$, 125 MHz): δ ppm = 155.67, 155.56, 139.55, 136.76, 133.33, 132.67, 130.93, 130.17, 129.51, 128.27, 125.51, 125.31, 124.70, 124.44, 124.37, 121.15, 120.84, 119.44, 117.45, 117.08, 116.91, 113.56, 106.58, 106.40, 69.03, 68.95, 31.52, 29.05, 29.04, 28.94, 28.87, 28.85, 25.80, 25.64, 22.45, 22.41, 22.31, 13.93, 13.90. HR-MS (APCI, *m*/*z*): calcd. for $C_{86}H_{95}Br_2N_2O_4$ ([M+1]), 1377.5653; found, 1377.5637 (error: -1.2 ppm).

Compound 4-5

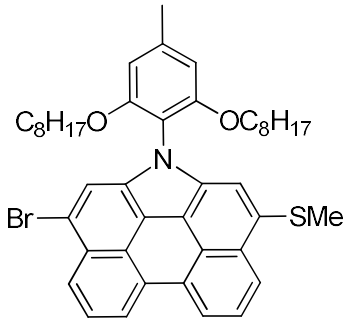

To a solution of **4-2** (689 mg, 1 mmol) in dry THF (25 mL) was added dropwise 2.5 M *n*-BuLi in hexane solution (0.4 mL, 1.1 mmol) at -78 ^{o}C under argon atmosphere. After the mixture was stirred at -78 ^{o}C for 1 h, anhydrous dimethyl disulfide (170 mg, 1.3 mmol) was added into the mixture. After slowly warming up to room temperature overnight, the mixture was poured into aqueous NH_4Cl solution. The aqueous layer was extracted with ethyl acetate, and the combined organic phase was washed with saturated brine and dried over anhydrous Na_2SO_4. The solvent was removed under reduced vacuum and the residue was dissolved in dichloromethane and *N*-bromosuccinimide(265.5mg, 1.5mmol) was added. The reaction mixture was stirred for 30 mins, The reaction mixture was quenched with water (10 mL). The organic layer was washed with water, and then washed with saturated brine and dried over anhydrous Na_2SO_4. The solvent was removed under reduced pressure and the crude product was purified by column chromatography (silica gel, hexane : DCM = 3 : 1) to give compound **4-5** as a yellow solid (551.3 mg, 75%). ^{1}H NMR ($CDCl_3$, 500 MHz): δ ppm = 8.69-8.72 (m, 2H), 8.54(d, *J* = 8.5Hz, 1H), 8.34 (d, *J*= 8.0Hz, 1H), 7.87-7.91 (m, 3H), 7.69 (s, 1H), 6.64 (s, 2H), 3.92(t, *J* = 6.5Hz, 4H), 2.60 (s, 3H), 2.51 (s, 3H), 1.33-1.39 (m, 4H), 0.96-1.01 (m, 4H), 0.80-0.89 (m, 16H), 0.69 (t, *J* = 7.5 Hz, 6H). ^{13}C NMR ($CDCl_3$,125 MHz): δ ppm = 155.87, 140.03, 133.26, 132.91,

131.29, 130.74, 130.67, 129.39, 128.38, 125.52, 125.08, 125.03, 124.66, 124.59, 123.79, 121.48, 121.41, 119.49, 117.81, 117.36, 117.06, 115.89, 113.59, 106.83, 69.24, 31.72, 29.24, 29.21, 29.09, 26.01, 22.65, 22.60, 19.11, 14.14. HR-MS (APCI, *m*/*z*): calcd. for $C_{44}H_{51}BrNO_2S$ ([M+1]), 736.2818; found, 736.2819 (error: +0.1 ppm).

Compound Per-SMe

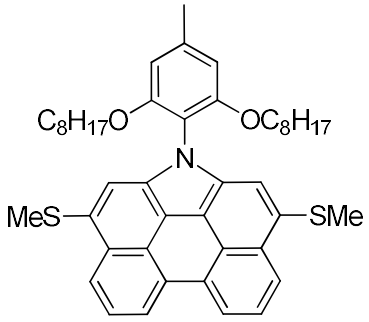

To a solution of **4-2** (769 mg, 1 mmol) in dry THF (25 mL) was added dropwise 2.5 M *n*-BuLi in hexane solution (0.9 mL, 2.2 mmol) at -78 ^{o}C under argon atmosphere. After the mixture was stirred at -78 ^{o}C for 1 h, anhydrous dimethyl disulfide (235.5 mg, 2.5 mmol) was added into the mixture. After slowly warming up to room temperature overnight, the mixture was poured into aqueous NH_4Cl solution. The aqueous layer was extracted with ethyl acetate, and the combined organic phase was washed with saturated brine and dried over anhydrous Na_2SO_4. The solvent was removed under reduced vacuum and the residue was purified by column chromatography (silica gel, DCM: hexane = 1:3) to afford **Per-SMe** as an orange solid (598.4 mg, 85%). ^{1}H NMR ($CDCl_3$, 500 MHz): δ ppm = 8.70 (d, *J* = 7.5Hz, 2H), 8.53(d, *J* = 8.0Hz, 2H), 7.89 (t, *J* = 8.0Hz, 2H), 7.71 (s, 2H), 6.66 (s, 2H), 3.91(t, *J* = 6.5Hz, 4H), 2.60 (s, 6H), 2.52 (s, 3H), 1.34-1.38 (m, 4H), 0.96-1.01 (m, 4H),

0.78-0.92 (m, 16H), 0.69 (t, J = 7.5 Hz, 6H). ^{13}C NMR ($CDCl_3$,125 MHz): δ ppm = 155.68 139.54 132.82 130.77 130.322 129.16 124.69 124.49 123.29 120.88 117.63 117.14 113.66 106.69 68.99 31.40 29.61 28.92 28.75 25.68 22.33 18.96 13.81. HR-MS (APCI, m/z): calcd. for C $_{45}$ H $_{54}$ N O $_2$ S $_2$ ([M+1]), 704.3590; found, 704.3596 (error: +0.8 ppm).

Compound 4-7

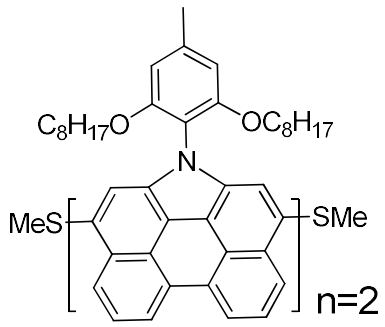

To a solution of **4-6** (137.7 mg, 0.1 mmol) in dry THF (10 mL) was added dropwise 2.5 M n-BuLi in hexane solution (0.1 mL, 0.25 mmol) at -78 ^{o}C under argon atmosphere. After the mixture was stirred at -78 ^{o}C for 1 h, anhydrous dimethyl disulfide (34 mg, 0.26 mmol) was added into the mixture. After slowly warming up to room temperature overnight, the mixture was poured into aqueous NH_4Cl solution. The aqueous layer was extracted with ethyl acetate, and the combined organic phase was washed with saturated brine and dried over anhydrous Na_2SO_4. The solvent was removed under reduced vacuum and the crude product was purified by column chromatography (silica gel, hexane : DCM = 3 : 1) to give compound **4-7** as a yellow solid (110.3 mg, 85%). ^{1}H NMR ($CDCl_3$, 500 MHz): δ ppm = 8.75 (d, J = 7.5Hz, 2H), 8.67 (d, J = 7.5Hz, 2H), 8.57 (d, J = 8.0Hz, 2H), 7.93 (t, J = 8.0Hz, 2H), 7.80 (s, 2H), 7.78 (d, J = 8.5Hz, 2H), 7.73 (s, 2H), 7.62 (t, J = 7.5Hz, 2H), 6.59 (s, 2H), 6.56 (s,

2H), 3.81-3.93(m, 8H), 2.65 (s, 6H), 2.43 (s, 6H), 1.34-1.39 (m, 8H), 0.79-1.01 (m, 40H), 0.63-0.69 (m, 12H). ^{13}C NMR ($CDCl_3$,125 MHz): δ ppm = 155.71 155.61 139.24 136.43 133.18 132.73 131.17 130.44 129.76 129.46 129.31 125.23 124.81 124.67 124.39 124.21 123.14 120.75 120.42 118.24 117.52 117.32 117.24 113.89 106.67 106.50 69.00 68.93 31.44 29.62 28.99 28.95 28.85 28.78 28.74 25.69 25.54 22.34 22.31 22.20 19.10 14.03 13.82. HR-MS (APCI, *m/z*): calcd. for $C_{88}H_{101}N_2O_4S_2$ ([M+1]), 1313.7197; found, 1313.7205 (error: +0.6 ppm).

Compound 4-8

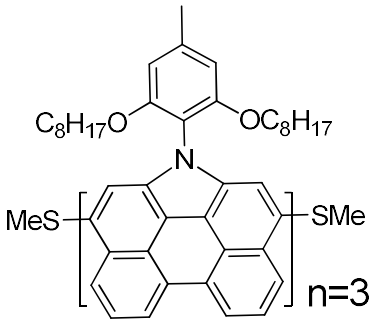

Compound **4-3** (86.4 mg, 0.1 mmol) and compound **4-5** (220.3 mg, 0.3 mmol), $Pd(PPh_3)_4$ (11.5 mg, 0.01 mmol) and Cs_2CO_3 (130.0 mg, 0.4 mmol) were added into three-neck bottle under argon. Then degassed toluene (15 mL) and DMF (0.6 mL) were added and the mixture was purged with argon. The mixture was stirred at 90 °C for 48 hours. After reaction completed and cooled to room temperature, water was added. The product was extracted with hexane (3 x 20 mL). The organic layer was washed with saturated brine and dried over anhydrous Na_2SO_4. The solvent was removed under vacuum and the residue was purified by column chromatography (silica gel, hexane : DCM = 2 : 1) to afford the pure product **4-8** as a yellow solid (69 mg, 36%). ^{1}H NMR ($CDCl_3$, 300 MHz): δ ppm = 8.66-8.76 (m, 6H), 8.57 (d, *J* =

8.1Hz, 2H), 7.94 (t, *J* = 8.1Hz, 2H), 7.72-7.81 (m, 10H), 7.58-7.64 (m, 4H), 6.46-6.40 (m, 6H), 3.80-3.88(m, 12H), 2.64 (s, 6H), 2.43 (s, 6H), 2.33 (s, 3H), 1.34-1.39 (m, 12H), 0.80-0.96 (m, 60H), 0.61-0.68 (m, 18H). ^{13}C NMR ($CDCl_3$,75 MHz): δ ppm = 155.77 155.69 155.59 139.24 136.69 135.98 133.26 133.17 132.70 131.19 130.80 130.44 130.41 129.66 129.53 129.33 125.34 124.99 124.82 124.71 124.66 124.41 124.22 124.16 123.12 120.73 120.70 120.67 120.43 120.39 120.27 118.33 118.30 117.59 117.55 117.52 117.41 117.21 115.89 114.03 113.91 106.74 106.63 106.46 106.42 106.40 69.00 68.90 31.53 31.44 31.36 29.60 29.03 28.96 28.85 28.79 28.73 25.71 25.66 25.57 25.54 25.47 22.32 22.30 22.21 19.12 13.99 13.82 HR-MS (APCI, *m*/*z*): calcd. for $C_{131}H_{148}N_3O_6S_2$ ([M+1]), 1923.0804; found, 1923.0797 (error: -0.4 ppm).

Compound QR-SMe

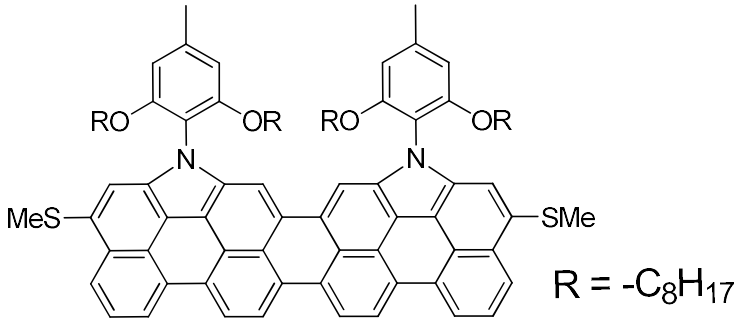

A mixture of compound **4-7** (19.2 mg, 0.01mmol), $Sc(OTf)_3$ (39.4 mg, 0.08 mmol), DDQ (17.9 mg, 0.08 mmol) in toluene (10 mL) was refluxed for 48 h under nitrogen atmosphere. After cooling to room temperature, $N_2H_4 \cdot H_2O$ (0.1 mL) was added. The reaction mixture was stirred for 1 h. The solvent was evaporated under reduced pressure, and the crude product was eluted from short silica gel column using THF. Precipitation from methanol, by redissolving in deacidifed dichloromethane,

precipitation from acetonitrile, and washing thoroughly with copious amount of methanol, hexane, and diethyl ether afforded the product as a green solid (12.5 mg, 65%). ^{1}H NMR (Benzene-d_6, 500 MHz): δ ppm = 8.67 (br, 4H), 8.43 (br, 4H), 8.38 (d, *J* = 7.0Hz, 2H), 7.92 (s, 2H), 7.70 (t, *J* = 8.0Hz, 2H), 6.40 (s, 4H), 3.55-3.62(m, 8H), 2.30 (s, 6H), 2.28 (s, 6H), 1.23-1.27 (m, 8H), 0.85-0.90 (m, 16H), 0.70-0.74 (m, 24H), 0.64 (t, J = 7.0Hz, 12H). ^{13}C NMR spectra cannot be obtained due to strong aggregation due to strong aggregation induced by π-π stacking between the quaterrylene units. HR-MS (APCI, m/z): calcd. for $C_{88}H_{99}N_2O_4S_2$ ([M+1]), 1311.7041; found, 1311.7043 (error: +0.1 ppm).

Compound HR-SMe

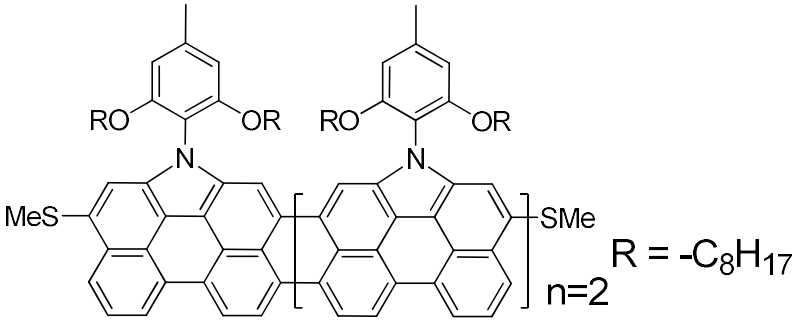

A mixture of compound **4-8** (19.2 mg, 0.01mmol), $Sc(OTf)_3$ (39.5 mg, 0.08 mmol), DDQ (18.2 mg, 0.08 mmol) in toluene (10 mL) was refluxed for 48 h under nitrogen atmosphere. After cooling to room temperature, $N_2H_4 \cdot H_2O$ (0.1 mL) was added. The reaction mixture was stirred for 1 h. The solvent was evaporated under reduced pressure, and the crude product was eluted from silica gel using THF. Precipitation from methanol, by redissolving in deacidifed dichloromethane, precipitation from acetonitrile, and washing thoroughly with copious amount of methanol, hexane, and diethyl ether afforded the product as a dark blue solid (10.2 mg, 55%). ^{13}C NMR

spectra and ^{1}HNMR cannot be obtained due to strong aggregation due to strong aggregation induced by π-π stacking between the hexarylene units.

Synthesis of Per-SMerc. In glovebox, to a suspension solution of **Per-SMe** (35.2 mg, 0.05 mol) in CH_2Cl_2 (2 mL) was slowly added a solution of $NOSbF_6$ (26.5 mg, 0.1 mol) in CH_2Cl_2/CH_3CN (4/0.1 mL) at room temperature. After stirring for 0.5 h at this temperature, the reaction mixture was passed through a pad of Celite with CH_2Cl_2 as eluent. Then the eluent was concentrated in vacuo to about 1 mL, and hexane (10 mL) was added. The resulting precipitate was collected by filtration and washed with 1:1 (v/v) CH_2Cl_2/hexane to give the title compound (42.2 mg, 90%) as a purple solid.

Synthesis of QR-SMedic. In glovebox, to a suspension solution of **QR-SMe** (13.1 mg, 0.01 mol) in CH_2Cl_2 (2 mL) was slowly added a solution of $NOSbF_6$ (8.0 mg, 0.03 mol) in CH_2Cl_2/CH_3CN (4/0.1 mL) at room temperature. After stirring for 0.5 h at this temperature, the reaction mixture was passed through a pad of Celite with CH_2Cl_2 as eluent. Then the eluent was concentrated in vacuo to about 1 mL, and hexane (10 mL) was added. The resulting precipitate was collected by filtration and washed with 1:1 (v/v) CH_2Cl_2/hexane to give the title compound (16.0 mg, 90%) as a dark green solid. ^{1}H NMR (CD_2Cl_2, 500 MHz): 9.57 (br, 2H), 9.43 (s, 2H), 9.18(br, 2H), 9.06 (br, 2H), 8.79 (br, 2H), 8.06 (br, 2H), 7.18 (s, 2H), 6.91 (s, 4H), 4.23 (br, 8H), 3.01 (s, 6H), 2.70 (s, 6H), 1.50-1.56 (m, 8H), 0.98 (br, 8H), 0.79-0.81(m, 8H), 0.50-0.61 (m, 24H), 0.40 (br, 12H).

Synthesis of QR-SMerc. In glovebox, to a suspension solution of **QR-SMedic** (8.9 mg, 0.005 mol) in CH_2Cl_2 (2 mL) was slowly added a solution of **QR-SMe** (6.6 mg, 0.005 mol) in CH_2Cl_2 (2 mL) at room temperature. After stirring for 0.5 h at this temperature, Then the solution was concentrated in vacuo to about 1 mL, and hexane (10 mL) was added. The resulting precipitate was collected by filtration and washed with 1:1 (v/v) CH_2Cl_2/hexane to give the title compound (11.6 mg, 75%) as a black solid.

Synthesis of HR-SMedic. In glovebox, to a suspension solution of **HR-SMe** (9.6 mg, 0.005 mol) in CH_2Cl_2 (2 mL) was slowly added a solution of $NOSbF_6$ (2.7 mg, 0.01 mol) in CH_2Cl_2/CH_3CN (2/0.05 mL) at room temperature. After stirring for 0.5 h at this temperature, the reaction mixture was passed through a pad of Celite with CH_2Cl_2 as eluent. Then the eluent was concentrated in vacuo to about 0.5 mL, and hexane (10 mL) was added. The resulting precipitate was collected by filtration and washed with 1:1 (v/v) CH_2Cl_2/hexane to give the title compound (10.7 mg, 90%) as a black solid.

Synthesis of HR-SMerc. In glovebox, to a suspension solution of **HR-SMedic** (11.9 mg, 0.005 mol) in CH_2Cl_2 (2 mL) was slowly added a solution of **HR-SMe** (9.6 mg, 0.005 mol) in CH_2Cl_2 (2 mL) at room temperature. After stirring for 0.5 h at this temperature, Then the solution was concentrated in vacuo to about 1 mL, and hexane (10 mL) was added. The resulting precipitate was collected by filtration and washed with 1:1 (v/v) CH_2Cl_2/hexane to give the title compound (15.1 mg, 70%) as a black solid.

4.5 References

(1) (a) Shirakawa, H.; Louis, E. J.; MacDiarmid, A. G.; Chiang, C. K.; Heeger, A. J. *Chem. Commun.* **1977**, *16*, 578. (b) MacDiarmid, A. G. *Angew. Chem., Int. Ed.* **2001**, *40*, 2581. (c) Wallow, T. I.; Novak, B. N. *J. Am. Chem. Soc.* **1991**, *113*, 7411. (d) Berresheim, A. J.; M üller, M.; M üllen, K. *Chem. Rev*. **1999**, *99*, 1747.

(2) (a) Roncali, J. *Chem. Rev*. **1992**, *92*, 711. (b) McCullough, R. D. *Adv. Mater.* **1998**, *10*, 93. (c) *Handbook of Oligo- and Polythiophenes*; Fichou, D., Ed.; Wiley-VCH: Weinheim, Germany, **1999**. (d) Bauerle, P.; Mitschke, U.; Gruner, G.; Rimmel, G. *Pure Appl. Chem.* **1999**, *71*, 2153.

(5) (a) Scherf, U.; List, E. J. W. *Adv. Mater.* **2002**, *14*, 477. (b) Li, J. Y.; Ziegler, A.; Wegner, G. *Chem. Eur. J.* **2005**, *11*, 4450. (c) Perepichka, I. I.; Perepichka, I. F.; Bryce, M. R.; Palsson, L.-O. *Chem. Commun.* **2005**, 3397-3399. (4) (a) Davis, W. B.; Svec, W. A.; Ratner, M. A.; Wasielewski, M. R. *Nature* **1998**, *396*, 60. (b) Kraft, A.; Grimsdale, A. C.; Holmes, A. B. *Angew. Chem., Int. Ed.* **1998**, *37*, 402. (c) Van Hutten, P. F.; Krasnikov, V. V.; Hadziioannou, G. *Acc. Chem. Res.* **1999**, *32*, 257.

(5) (a) Bredas, J. L.; Street, G. B. *Acc. Chem. Res*. **1985**, 18, 309. (b) Patil, A. O.; Heeger, A. J.; Wudl, F. *Chem. Rev*. **1988**, 88, 183. (c) Tolbert, L. M. *Acc. Chem. Res*. **1992**, 25, 561.

(6) (a)Watson, M. D.; Fechtenkötter, A.; Müllen, K. *Chem. Rev*. **2001**, 101, 1267. (b) Bendikov, M.; Wudl, F.; Perepichka, D. F. *Chem. Rev.* **2004**, 104, 4891.

(7) (a)Anthony, J. E. *Chem. Rev*. **2006**, 106, 5028. (b) Grimsdale, A. C.; Leok Chan, K.; Martin, R. E.; Jokisz, P. G.; Holmes, A. B. *Chem. Rev*. **2009**, 109, 897. (c) Heinze,

J.; Frontana-Uribe, B. A.; Ludwigs, S. *Chem. Rev*. **2010**, 110, 4724.

(8) (a) Nishinaga, T.; Wakamiya, A.; Yamazaki, D.; Komatsu, K. *J. Am. Chem. Soc*. **2004**, 126, 3163. (b) Yamazaki, D.; Nishinaga, T.; Tanino, N.; Komatsu, K. *J. Am. Chem. Soc.* **2006**, 128, 14470. (c) Marchetti, F.; Pinzino, C.; Zacchini, S.; Pampaloni, G. *Angew. Chem., Int. Ed.* **2010**, 49, 5268. (d) Chen, X.; Ma, B.; Chen, S.; Li, Y.; Huang, W.; Ma, J.; Wang, X. *Chem. - Asian J*. **2013**, 8, 238

(9) (a) Banerjee, M.; Lindeman, S. V.; Rathore, R. J. *Am. Chem. Soc*. **2007**, 129, 8070. (b) Banerjee, M.; Shukla R.; Rathore, R. *J. Am. Chem. Soc*. **2009**, 131, 1780.

(10) (a) Kayahara, E.; Kouyama, T.; Kato, T.; Takaya, H.; Yasuda, N.; Yamago, S. *Angew. Chem. Int. Ed.* **2013**, 52, 13722. (b) Toriumi, N.; Muranaka, A.; Kayahara, E.; Yamago, S.; Uchiyama, M. *J. Am. Chem. Soc.* **2015**, 137, 82. (c) Kayahara, E.; Kouyama, T.; Kato, T.; Yamago, S. *J. Am. Chem. Soc*. **2016**, 138, 338.

(11) (a) Novoselov, K. S.; Geim, A. K.; Morozov, S. V.; Jiang, D.; Zhang, Y.; Dubonos, S. V.; Grigorieva, I. V.; Firsov, A. A. *Science* **2004**, *306*, 666. (b) Geim, A. K.; Novoselov, K. S. *Nat. Mater.* **2007**, *6*, 183. (c) Li, X.; Wang, X.; Zhang, L.; Lee, S.; Dai, H. *Science* **2008**, *319*, 1229. (d) Wang, X.; Ouyang, Y.; Li, X.; Wang, H.; Guo, J.; Dai, H. *Phys. Rev. Lett.* **2008**, *100*, 206803

(12) (a) Qian, H.; Wang, Z.; Yue, W.; Zhu, D. *J. Am. Chem. Soc*. **2007**, 129, 10664. (b) Qian, H.; Negri, F.; Wang, C.; Wang, Z. *J. Am. Chem. Soc*. 2008, 130, 17970.

(13) (a) Li, Y.; Gao, J.; Motta, S. D.; Negri, F.; Wang, Z. *J. Am. Chem. Soc*. **2010**, 132, 4208.(b) Yuan, Z.; Lee, S.-L.; Chen, L.; Li, C.; Mali, K. S.; De Feyter, S.; Müllen, K. *Chem. Eur. J*. **2013**, 19, 11842.

(14) (a) Zeng, Z.; Lee, S.; Zafra, J. L.; Ishida, M.; Zhu, X.; Sun, Z.; Ni, Y.; Webster, R. D.; Li, R.-W.; López Navarrete, J. L.; Chi, C.; Ding, J.; Casado, J.; Kim, D.; Wu, J. *Angew. Chem. Int. Ed.* **2013**, *52*, 8561. (b) Zeng, Z.; Lee, S.; Zafra, J. L.; Ishida, M.; Bao, N.; Webster, R. D.; López Navarrete, J. T.; Ding, J.; Casado, J.; Kim, D.; Wu, J. *Chem. Sci.* **2014**, *5*, 3072. (c) Zeng, Z.; Lee, S.; Son, M.; Fukuda, K.; Burrezo, P. M.; Zhu, X.; Qi, Q.**;** Li, R.-W.; Lopez Navarrete, J. T.; Ding, J.; Casado, J.; Nakano, M.; Kim, D.; Wu, J. *J. Am. Chem. Soc.* **2015**, 137, 8572.

(15) Henderson, J. C.; Kiya, Y.; Hutchison, G. R.; Abruñ a, H. D. *J. Phys. Chem. C* **2008**, 112, 3989.

(16) Qi Q.; Wang X.; Fan L.; Zheng B.; Zeng W.; Luo J.; Huang, K.-W.;Wang Q.; Wu J.. *Org. Lett.* **2015**, 17, 724.

(17) (a) Li, Y.; Wang, Z. *Org. Lett*. **2009**, 11, 1385. (b) Jiao, C.; Huang, K.-W.; Luo, J.; Zhang, K.; Chi, C.; Wu, *J. Org. Lett.* **2009**, 11, 4508.

(18) (a) Ohashi, K.; Kubo, T.; Masui, T.; Yamamoto, K.; Nakasuji, K.; Takui, T.; Kai, Y.; Murata, I. *J. Am. Chem. Soc.* **1998**, *120*, 2018. (b) Shimizu, A.; Kubo, T.; Uruichi, M.; Yakushi, K.; Nakano, M.; Shiomi, D.; Sato, K.; Takui, T.; Hirao, Y.; Matsumoto, K.; Kurata, H.; Morita, Y.; Nakasuji, K. *J. Am. Chem. Soc.* **2010**, *132*, 14421. (c)Chase, D. T.; Rose, B. D.; McClintock, S. P., Zakharov, L. N.; Haley, M. M. *Angew. Chem. Int. Ed.* **2011**, *50*, 1127. (d)Shimizu, A.; Kishi, R.; Nakano, M.; Shiomi, D.; Sato, K.; Takui, T.; Hisaki, I.; Miyata, M.; Tobe, Y. *Angew. Chem. Int. Ed.* **2013**, *52*, 6076.（e）Sun, Z.; Wu, J. *J. Org. Chem.* **2013,** 78, 9032. (f) Sun, Z.; Huang, K.-W.; Wu, J. *J. Am. Chem. Soc*. **2011**, 133, 11896. (g) Li, Y.; Heng, W.-K.; Lee, B. S.;

Aratani, N.; Zafra, J. L.; Bao, N.; Lee, R.; Sung, Y. M.; Sun, Z.; Huang, K.-W.; Webster, R. D.; López Navarrete, J. T.; Kim, D.; Osuka, A.; Casado, J.; Ding, J.; Wu, J. *J. Am. Chem. Soc.* **2012**, 134, 14913. (h) Sun, Z.; Lee, S.; Park, K.; Zhu, X.; Zhang, W.; Zheng, B.; Hu, P.; Zeng, Z.; Das, S.; Li, Y.; Chi, C.; Li, R.; Huang, K.; Ding, J.; Kim, D.; Wu, J. *J. Am. Chem. Soc.* **2013**, 135, 18229. (i) Sun, Z.; Ye, Q.; Chi, C.; Wu, J. *Chem. Soc. Rev*. **2012**, 41, 7857. (j)Sun Z.; Zeng Z.; Wu, J. *Acc. Chem. Res*. **2014**, 47 (8), 2582. (k) Zeng Z.; Shi X.; Chi C.; López Navarrete, J. T.; Casado J.; Wu, J. *Chem. Soc. Rev*. **2015**,44, 6578.

Chapter 5 Synthesis of stable *N*-annulated rylenequinone

5.1 Introduction

Benzoquinones (BQs) are of great interest due to their important role in biologic process in organism associated with the proton-coupled electron transfer.[1] Among them, para-BQ has a un-ignorable diradical character in due to the recovery of aromaticity of the central benzenoid ring, and thus it is highly reactive.[2] A general design to enhance stability is usually achieved through effective steric protection and/or extensive spin delocalization.[3] For example, usually, for phenoxyl, the stability is guaranteed by the introduction of sterically bulky groups (e.g., *tert*-butyl) at the 2,6-positions. However, the bulky *tert*-butyl groups at the 2- and 6-positions can inhibit the interaction of the neiborhoods.[4] π-extended benzoquinones without bulky group is very rare due to the synthetic challenge and instability. Recently, our group demonstrated facile synthesis and characterization of a series of quinoidal rylene based stable diradicaloids with unique magnetic and electronic properties by using *N*-annulated perylene (NP) as the basic building block, which can be regarded as derivatives of π-extended *p*-quinodimethane (*p*-QDM).[5] In these structures, the *N*-site and *peri*-edges allows eay functionalization, opening opportunities to enhance solubility, stablility as well as preparation of π-extended analogues. Inspiring by these results, herein, we report the design and synthesis of a series of stable π-extended rylenequinones (Figure. 5.1). Limited by time, their properties and chemical reactivity will only be briefly discussed, further physical characterizations are underway.

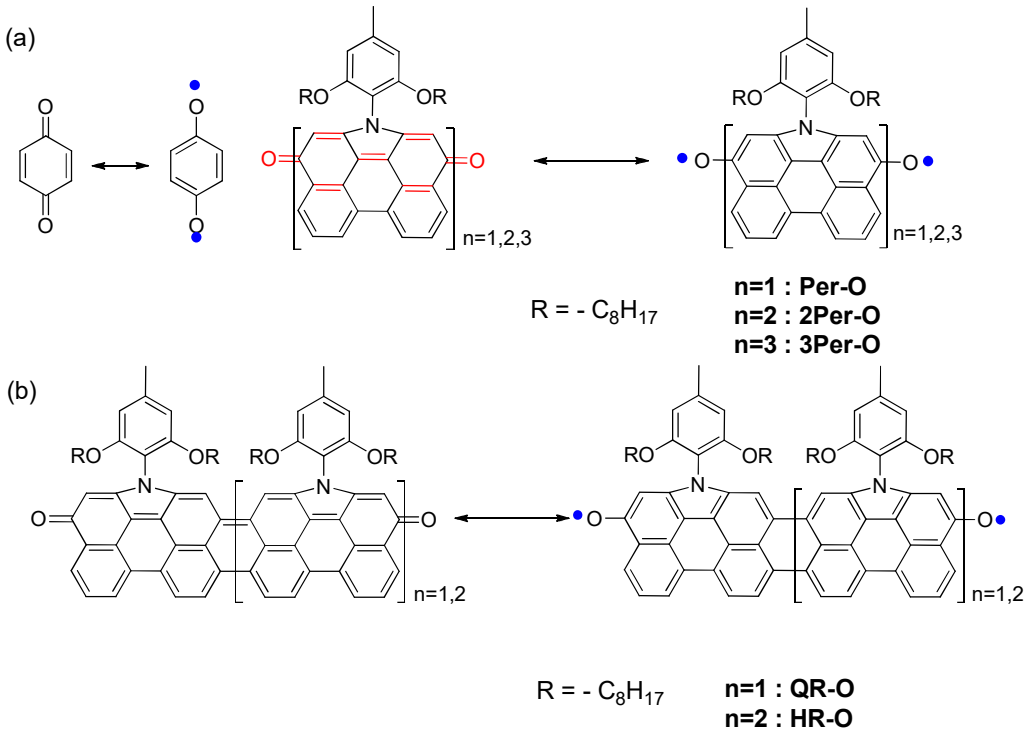

Figure 5.1 Structures and resonance forms of extended rylenequinones.

5.2 Results and discussion

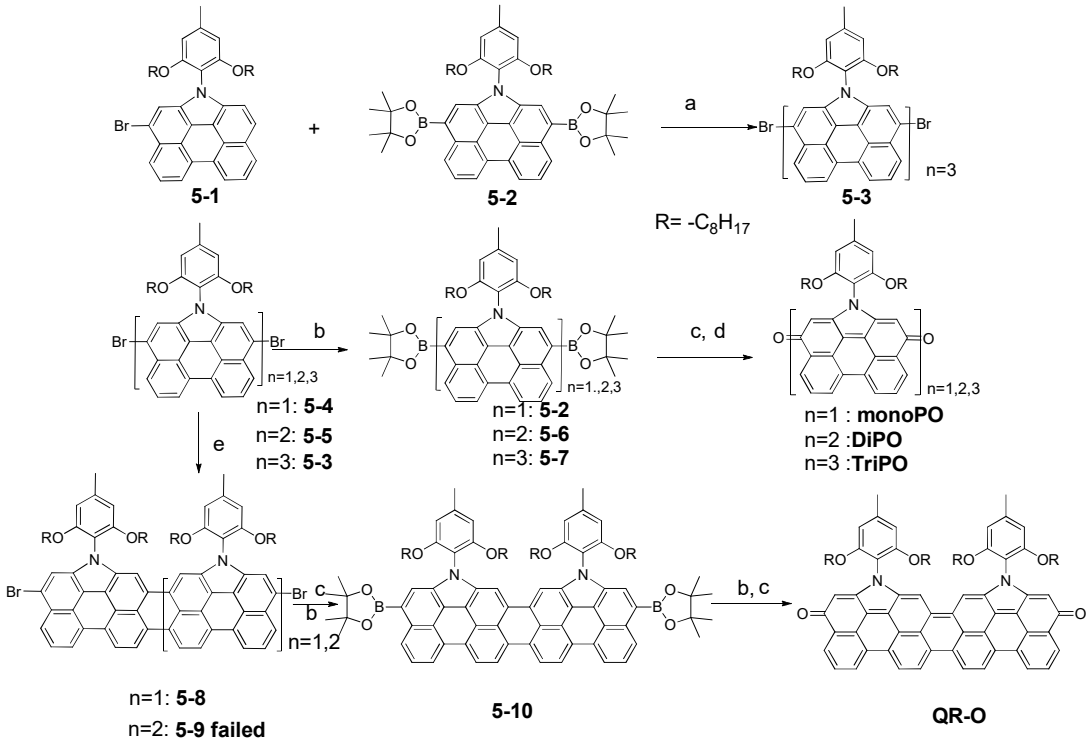

Sheme 5.1 Synthetic route of rylenequinones. Reagents and conditions: (a) $Pd(PPh_3)_4/K_2CO_3$/Toluene; (b) pinacolborane, 1,2-dichloroethane, Et_3N, $Pd(PPh_3)_2Cl_2$, 90^oC; (c) 35%H_2O_2, DMF, 24h; (d) PbO_2, DCM; (e) DDQ/$Sc(OTf)_3$, toluene, reflux.

The synthetic route for the rylenequinones was shown in Scheme 5.1. Compound **5-1**, **5-2**, **5-3**, **5-4** and **5-5** were reported in former chapters. **5-6** and **5-7** were synthesized by Pd-catalysed borylation of dibromo-precursors with pinacolborane in 66% and 55% yields, repectively. Compounds **5-8** and **5-9** successfully prepared by oxidative cyclodehydrogenation of the corresponding precursors **5-5** and **5-3** with DDQ/$Sc(OTf)_3$. The absorption spectra of **5-8** is similar to those of the previously reported *N*-annulated quaterrylene. However, due to unfused byproduct and purifuication problem, pure **5-9** cannot be obtained. **5-10** was also synthesized by Pd-catalysed borylation of dibromo-precursors with pinacolborane in 60%. Then treatment of **5-2**, **5-6**, **5-7** and **5-10** 35% H_2O_2 followed by further oxidation with PbO_2 afforded **Per-O**, **2Per-O**, **3Per-O** and **QR-O** in almost quantitative yields. New method is needed to synthesize **HR-O** in the future. For **Per-O**, the structure was confirmed by their ^{1}H NMR, high resolution mass spectra and X-ray crystallographic analysis. For **2Per-O**, **3Per-O** and **QR-O**, these products were carefully purified by column chromatography followed by preparative thin-layer chromatography and the purity of the final products was confirmed by high-resolution APCI mass spectrometry. Crystals of these compounds are still under growing. As **HR-O** is still under synthesis, so only oligomer arrary of rylenequinones (**Per-O**, **2Per-O**, **3Per-O**) was discussed.

The UV-vis-NIR absorption spectra are shown in Figure 5.2 and the data was summarized in Table 5.1. The monomer **Per-O** displayed an intense absorption band with maximum at 427 nm ($\varepsilon = 48700\ M^{-1}\ cm^{-1}$). The long tail indicated the possible aggregation. In contrast, the absorption spectrum of **2Per-O** displays an intense

absorption band with maxima at 1040 nm (ε = 14000 M^{-1} cm^{-1}). The characteristic structured long-wavelength absorption band was observed in the near IR region extending up to 1300 nm, with a very small optical energy gap of 0.95 eV. Such remarkable red-shift of the lowest excitation band and the band shape change as compared to **Per-O** imply a transformation of their electronic ground state. The trimer **3Per-O** also showed a very broad NIR band extending to 1300 nm as observed in **2Per-O** and relatively intense band with λ_{max} of 449 nm (ε = 43700 M^{-1} cm^{-1}) in the visible region. It was found that the wavelengths of lowest transition band are not further extended despite the extension of chain length, and the relative intensity of higher energy bands emerged around 420-500 nm are enhanced upon the number of rylene core increases in nPer-O. This characteristic band around 420-500 nm may originate from the absorption of aromatic NP cores, which indicates the recovery of the aromatic-like rylene cores by means of perturbation of the quinoidal electronic structures with terminal spin localization.[5]

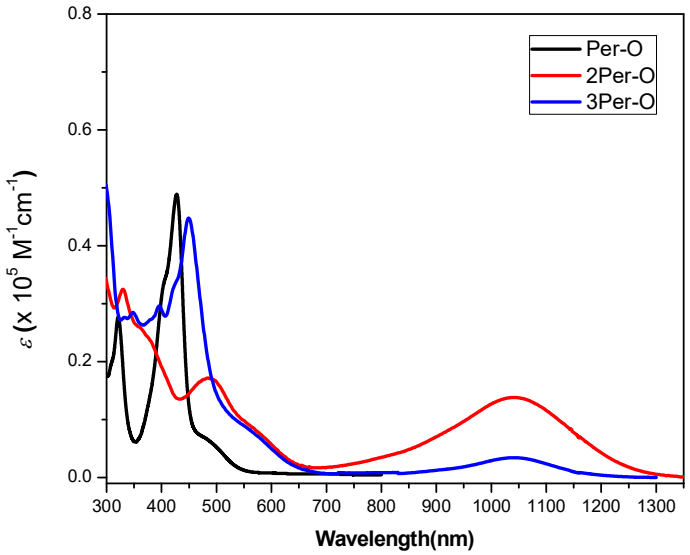

Figure 5.2 The UV-vis-NIR absorption spectra of rylene quinones in DCM.

Table 5.1 Summary of optical and electrochemical properties of **Per-O**, **2Per-O** and **3Per-O**.

	λ_{max}	ε (M^{-1} cm^{-1})	$E_{1/2}^{ox}$ (eV)	$E_{1/2}^{red}$ (eV)	HOMO(V)	LUMO(V)	E_g^{EC}(eV)	E_g^{opt}(ev)
Per-O	427	48700		-1.27 -1.48	-5.78[a]	-3.53		2.43
2Per-O	490 1045	17000 14000	-0.11 0.32 0.51	-0.97 -1.35	-4.69	-3.83	0.86	0.95
3Per-O	449 1045	43700 3820	-0.11 0.47	-1.05 -1.35	-4.69	-3.75	0.94	1.01

The HOMO and LUMO energy levels were estimated according to equations: HOMO = -(4.8 + $E_{1/2}^{ox}$) eV, and LUMO = -(4.8 + $E_{1/2}^{red}$); [a] HOMO = LUMO-E_g^{opt}.

The electrochemical properties of **Per-O**, **2Per-O** and **3Per-O** were investigated by cyclic voltammetry (CV) in deoxygenated DCM solution containing 0.1 M tetra-n-butylammonium hexafluorophosphate ($TBAPF_6$) as supporting electrolyte

(Figure 5.3). The HOMO and LUMO energy levels were estimated according to equations: HOMO = -[4.8 + E_{ox}^{onset}] eV, and LUMO = -[4.8 + E_{red}^{onset}] eV, where E_{ox}^{onset} and E_{red}^{onset} are the onset of the first oxidation and reduction wave respectively (*vs* Fc^{+}/Fc). The HOMO and LUMO energy levels of **Per-O**, **2Per-O** and **3Per-O** were determined to be -5.78, -4.69, -4.69 eV (HOMO) and -3.53, -3.83, -3.75 eV (LUMO), respectively (Table 5.1). The electrochemical energy gaps were calculated accordingly to be 0.86 and 0.94 eV for **2Per-O** and **3Per-O**. The trend is in agreement with the optical energy gaps. No oxidative wave was observed for neutral **Per-O**, and the chain-length dependence of electrochemical behavior must be correlated to the change of π-conjugation and electronic structure in these extensive homologues.

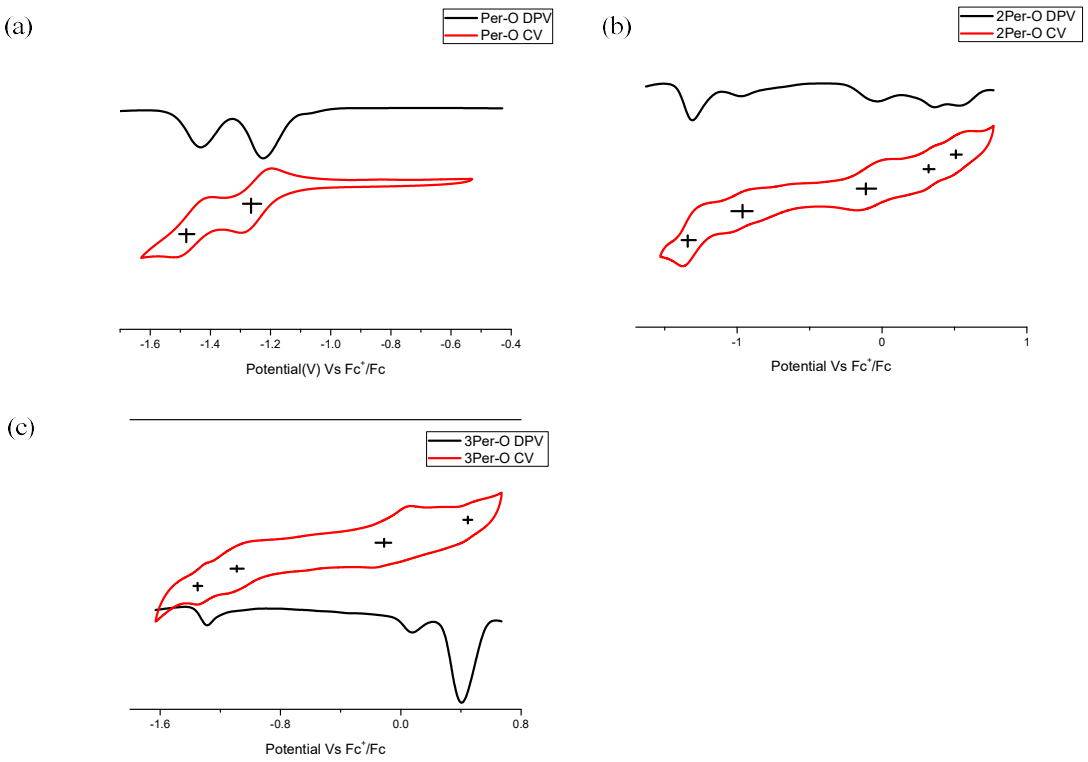

Figure 5.3 Cyclic voltammograms and differential pulse voltammograms of (a) **Per-O**; (b) **2Per-O**; (c) **3Per-O** in dry DCM with $TBAPF_6$ as supporting electrolyte,

Ag/AgCl as reference electrode, Au disk as working electrode, Pt wire as counter electrode.

Single crystal suitable for crystallographic analysis was obtained for **Per-O** a by solvent diffusion method and the structure was shown in Figure 5.4.

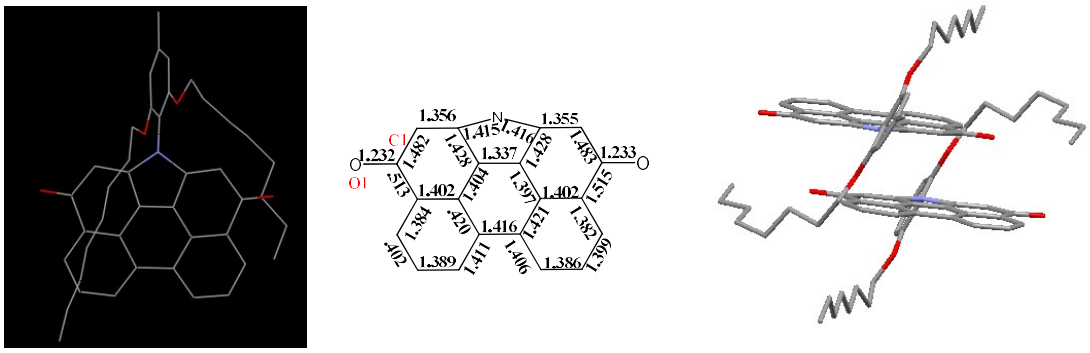

Figure 5.4 X-ray crystallographic structure of **Per-O**.

It adopted a slipped dimeric structure in an antiparallel packing mode with a short packing distance of ca. 3.33 Å through both dipole−dipole and π−π interactions. The featured bond length (O1-C1) is to be 1.23 Å in average, indicating closed-shell quinone structure.

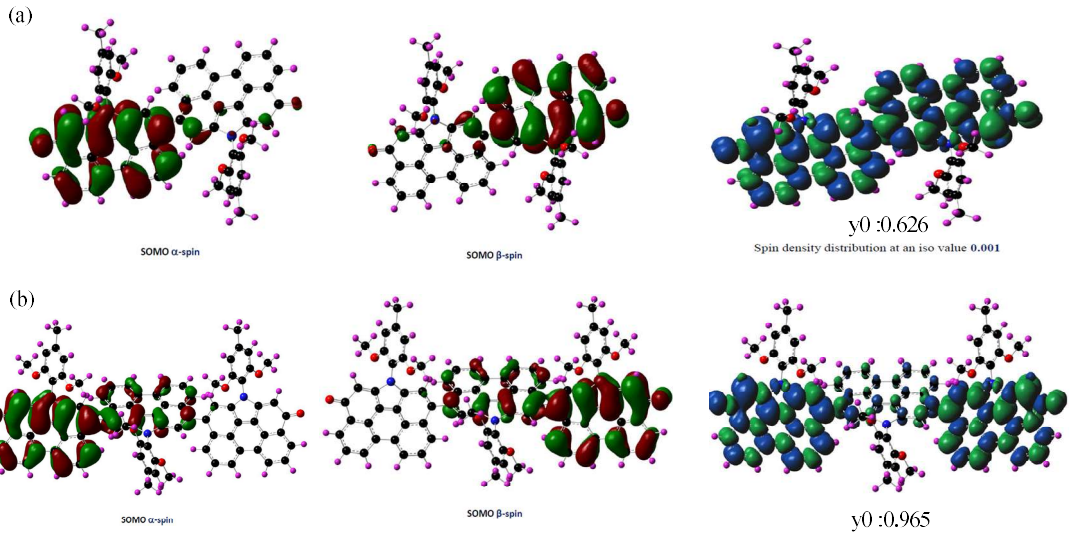

Figure 5.5 Calculated (CAM-B3LYP/6-31G(d,p)) spin density distribution of the singlet diradical form of (a) **2Per-O** and (b) **3Per-O**.

The spin-unrestricted DFT calculations were done to understand the ground state of the target compounds (Figure 5). A typical disjointed feature in the singly occupied molecular orbital (SOMO) profiles of the diradical species was found; the unpaired

electrons (α and β) were mainly delocalized at the backbone of terminal rylene units. Accordingly, large spin densities also mainly distributed on the terminal substituted rylene units.

The diradical character (y_0) of **2Per-O** and **3Per-O** was estimatedto be 0.626and 0.965, respectively. ESR measurement of the solution of **2Per-O** in DCM clearly displayed a weak single-line ESR spectrum with g_e = 2.00337 (Figure 5.5), indicating that the compound displays an open-shell singlet diradical ground state and the weak ESR signals come from the thermally excited triplet diradical. Furthure characterization of magnetic properties of **2Per-O**, **3Per-O** is still underway.

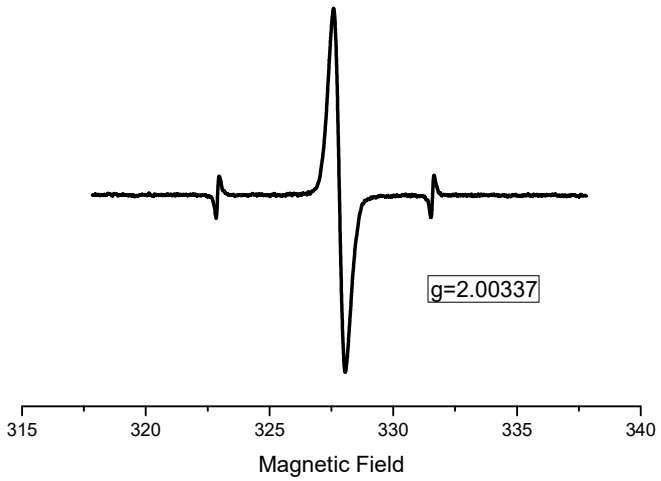

Figure 5.6 ESR spectra of the diradicals **2Per-O** in CH_2Cl_2 at room temperature.

5.3 Conclusion

In conclusion, a series of stable *N*-annulated rylenequinones chromophores were successfully synthesized. Our preliminary characterizations showed that the **nPer-O** (*n*= 1,2,3) displayed a clear chain-length dependence of the photophysical and electrochemical properties as well as magnetic properties. **Per-O** is typical

closed-shell π-extended quinone, while **2Per-O** and **3Per-O** have an open-shell diradical ground state. Further studies such as synthesis of fully fused π-extended rylenequinone (**HR-O**), crystallographic analysis, SQUID, transient absorption, TPA measurements and DFT calculations are underway to better understand this unique system.

5.4 Experimental section

5.4.1 General

All reagents and measurement methods were similar to those in Chapter 4. Continuous wave X-band ESR spectra were obtained with a Bruker ELEXSYS E500 spectrometer using a variable temperature Bruker liquid nitrogen cryostat.

5.4.2 Detailed synthetic procedures and characterization data

Compound 5-6

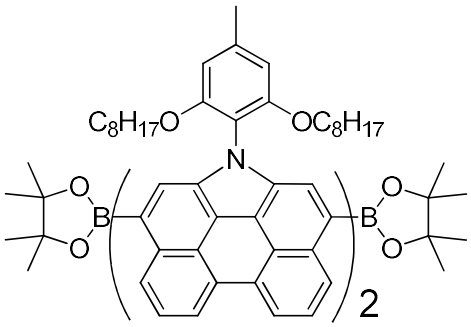

A 100 mL Schlenk flask was charged with **5-5** (137.6 mg, 0.1 mmol), pinacolborane (63.0 mg, 0.5 mmol), triethylamine (51.0 mg, 0.5 mmol), $PdCl_2(PPh_3)_2$ (4.0 mg, 0.005 mmol) and 1,2-dichloroethane (10 mL) under argon. The reaction mixture was stirred at 90 °C overnight. After removal of the solvent, the crude product was purified by column chromatography (silica gel, hexane : DCM = 5 : 1) to give compound **5-6** as a yellow solid (97 mg, 66%). ^{1}H NMR ($CDCl_3$, 500 MHz): δ ppm = 9.04 (d, J = 8.0 Hz,

2H), 8.71 (d, *J* = 7.5 Hz, 2H), 8.67 (d, *J* = 7.5 Hz,2H), 8.27 (s, 2H), 7.89 (t, *J* = 8.0 Hz, 2H),7.76(d, *J* = 8.0Hz, 2H), 7.71(s, 2H), 7.60 (t, *J* = 8.0 Hz，2H)， 6.57 (s, 2H), 6.53 （s, 2H）, 3.76 - 3.90 (m, 8H), 2.42 (s, 6H), 1.47 (s, 24H), 1.26-1.37 (m, 8H), 0.96-1.03 (m, 8H), 0.67-0.98 (m, 40H), 0.66 (t, *J* = 7.5 Hz, 12H). HR-MS (APCI, *m*/*z*): calcd. for $C_{98}H_{119}B_2N_2O_8$ ([M+1]), 1473.5437; found, 1473.5441.

Compound Per-O, 2Per-O and 3Per-O, QR-O

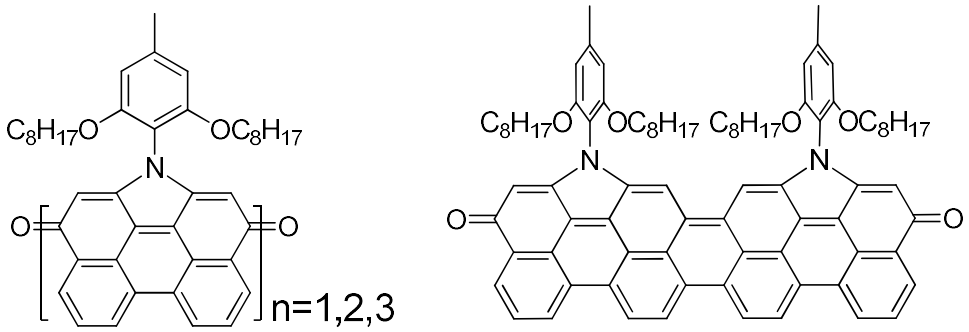

Similar procedure was used to synthesize the oligomers. A 25 mL Schlenk flask was charged with diboronic ester precursor **(**0.1 mmol), 35% H_2O_2 (2 mmol), dimethylformaide (10ml). The reaction mixture was stirred at room temperature overnight. This conversion was quantitative monitered by TLC. Then the solvent was removed and the solid was dried under vaccum. The residue was then loaded to 25 ml schlenk flask with 10 ml anhydrous DCM under argon. PbO_2 (10 mmol) was added. The mixture was stirred for 2h monitered by TLC. The solvent was removed under vacuum and the residue was purified by column chromatography (silica gel, DCM) followed by preparative thin-layer chromatography to afford the desired product. **2Per-O**: HR-MS (APCI, *m*/*z*): calcd. for $C_{86}H_{95}N_2O_6$ ([M+1]), 1251.7191; found,

1251.7185. **3Per-O:** HR-MS (APCI, *m*/*z*): calcd. for $C_{129}H_{142}N_3O_8$ ([M+1]), 1261.7231; found, 1261.7219. **QR-O:** HR-MS (APCI, *m*/*z*): calcd. for $C_{86}H_{93}N_2O_6$ ([M+1]), 1249.7134; found, 1251.7123. The crystal growing for **2Per-O**, **3Per-O** and **QR-O** are in progress.

5.5 References

(1) (a)Graige, M. S.; Paddock, M. L.; Bruce, J. M.; Feher, G.; Okamura, M. Y. *J. Am. Chem. Soc.* **1996**, 118, 9005. (b) Kurisu, G; Zhang, H.; Smith, J. L.; Cramer, W. A. *Science* **2003**, 302, 1009. (c) Seta, P.; Bienvenue, E.; Moore, A. L.; Mathis, P.; Bensasson, R. V.; Liddell, P.; Pessiki, P. J.; Joy, A.; Moore, T. A.; Gust, D. *Nature* **1985**, 316, 653. (d) Osycczka, A.; Moser, C. C.; Daldal, F.; Dutton, P. L. *Nature* **2004**, 427, 607.

(2) Fu, Q.; Yang, J.; Wang, X.-B. *J. Phys. Chem. A* **2011**, 115, 3201.

(3)(a) Sun, Z.; Ye, Q.; Chi, C.; Wu, J. *Chem. Soc. Rev.* **2012**, 41, 7857. (b)Sun Z.; Zeng Z.; Wu, J. *Acc Chem. Res.*, **2014**, 47 (8), 2582. (c) Zeng Z.; Shi X.; Chi C.; López Navarrete, J. T.; Casado J.; Wu, J. *Chem. Soc. Rev*. **2015**,44, 6578.

(4) (a) Müller E.; Schick A.; Scheffler K. *Chem. Ber.*, **1959**, 92, 474. (b) Altwicker E. R. *Chem. Rev.* **1967**, 67, 475. (c) Manner V. W.; Markle T. F.; Freudenthal J. H.; Roth J. P.; Mayer J. M. *Chem. Commun.*, **2008**, 256. (d) Wittman J. M.; Hayoun R.; Kaminsky W.; Coggins M. K.; Mayer J. M. J. *Am. Chem. Soc.* **2013**, 135, 12956. (a) Zhang K.; Huang K.; Li, J.; Chi C.; Wu, J. Org. Lett., 2009, 11, 4854.

(5)(a) Zeng, Z.; Lee, S.; Zafra, J. L.; Ishida, M.; Zhu, X.; Sun, Z.; Ni, Y.; Webster, R.

D.; Li, R.-W.; López Navarrete, J. L.; Chi, C.; Ding, J.; Casado, J.; Kim, D.; Wu, J. *Angew. Chem. Int. Ed.* **2013**, 52, 8561 (b) Zeng, Z.; Lee, S.; Zafra, J. L.; Ishida, M.; Bao, N.; Webster, R. D.; López Navarrete, J. T.; Ding, J.; Casado, J.; Kim, D.; Wu, J. *Chem. Sci.* **2014**, 5, 3072. (c) Zeng, Z.; Lee, S.; Son, M.; Fukuda, K.; Burrezo, P. M.; Zhu, X.; Qi, Q.; Li, R.-W.; Lopez Navarrete, J. T.; Ding, J.; Casado, J.; Nakano, M.; Kim, D.; Wu, J. *J. Am. Chem. Soc*. **2015**, 137, 8572.

Chapter 6 Conclusions and Future Research

The overall objective of this thesis was to develop functional *N*-annulated rylene based chromophores and investigate their possible application based on three strategies: (a) "push-pull" modification, (b) core extension and (c) quinoidization.

At the beginning, we adopted "push-pull" modification to firstly use alkoxy-wrapped *N*-annulated perylene as a rigid and coplanar π-spacer for the design of push-pull type sensitizers (Chapter 1). The obtained dyes **QB1**-**QB3** were then applied in DSCs device and showed good light harvesting ability and superior device performance compared to many known perylene-based sensitizers. Next, based on the preliminary results, **QB4-QB6** with modified structures were then designed and synthesized (Chapter 3). The device showed better results, indicaiting rational design of "push-pull" motif. All these results together with other work in our group highlight that the coplanar NP unit is a good building block for the design of sensitizers for high performance DSCs.

In Chapter 4, we adopted extension method to successfully design and synthesize a series of methylthio-capped *N*-annulated rylenes. Their interesting redox properties were carefully studied. Furthermore, we successfully prepared and isolated the remarkably stable radical cations and dications derived from methylthio-capped *N*-annulated rylenes by one- or two-electron chemical oxidation with $NOSbF_6$. Both oxidized species showed a large bathochromic shift into NIR region. We also clarified the open-shell singlet diradical ground state of **HR-SMedic**. These results will open

new opportunities in developing new NIR chromophores for π-electron materials for molecular electronics (eg. organic conductor).

In Chapter 5, we adopted quinoidization as well as extension in order to synthesize stable *N*-annulated rylenequinones chromophores. Although a lots of work needed for this part in the future, our preliminary characterizations showed that the remarkably stable **nPer-O** (n= 1,2,3) displayed a clear chain-length dependence of the photophysical and electrochemical properties as well as magnetic properties. **2Per-O** and **3Per-O** displayed singlet diradical ground state. More work is underway to understand the interesting properties and investigate the possible application of the rylenequinones.

Despite encouraging achievements in this thesis, preparation of functional rylene chromophores still suffers from limitations such as synthetic challenges to obtain higher homologues, insufficient solubility and stability. Synthesis in some cases is also restricted by the multiple steps and overall low yields, which limit their practical applications. Therefore, there is an urgent need to find more efficient strategy to attain stable functional rylene chromphore in relatively large scale. It is noteworthy that although several rylene-based chromophores show promising open-shell properties, the application is still limited. More work need to be done to exploit their applications in spin-based electronics and photonics in the future.

Appendix NMR of New Compounds

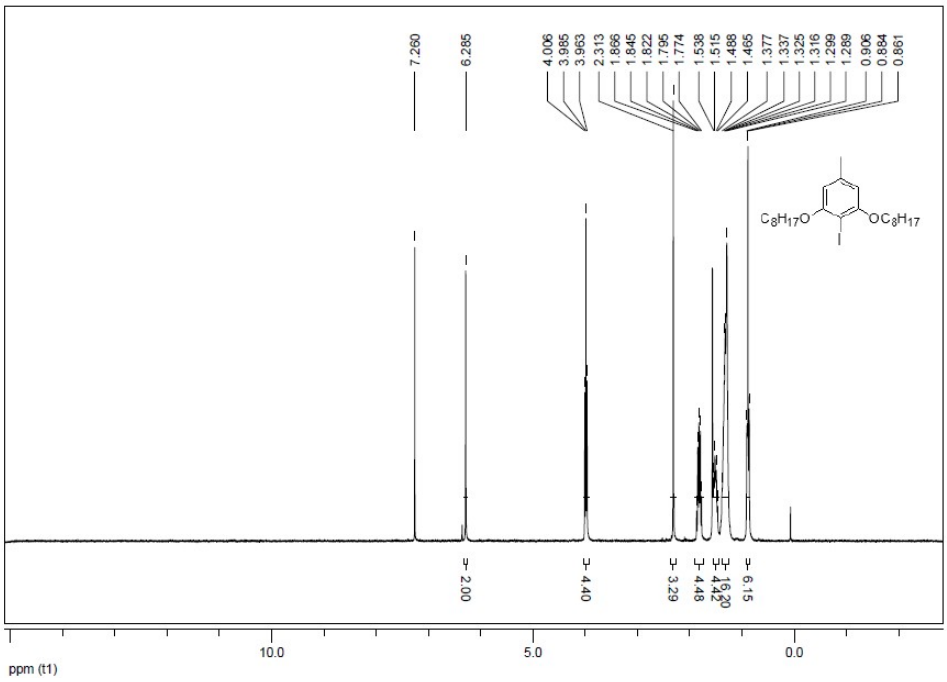

^{1}H NMR spectrum (300 MHz, $CDCl_3$) of **2-2**.

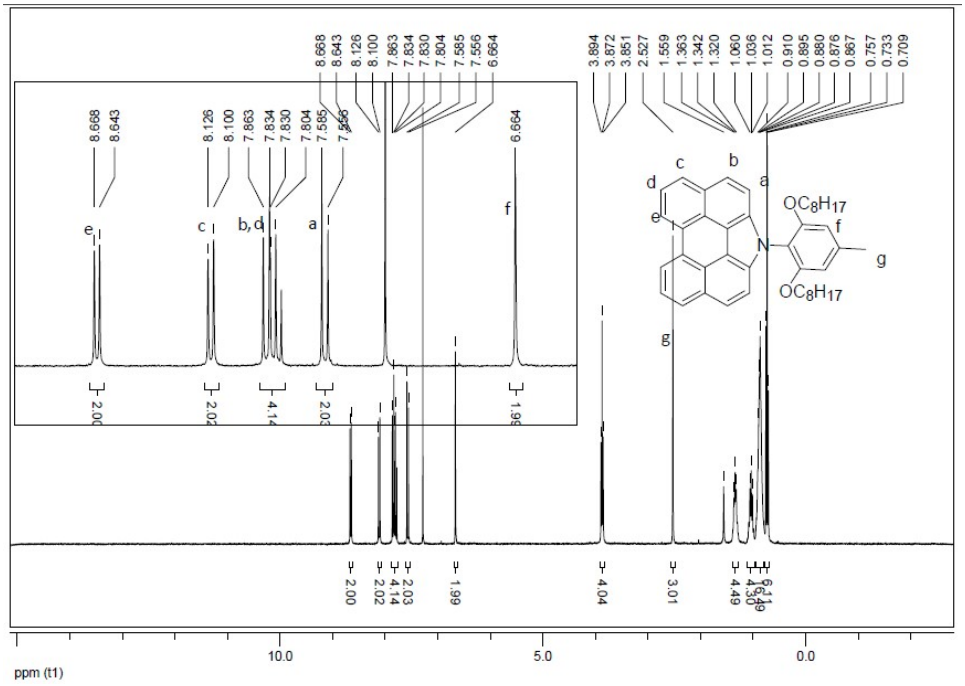

^{1}H NMR spectrum (300 MHz, $CDCl_3$) of **2-3**.

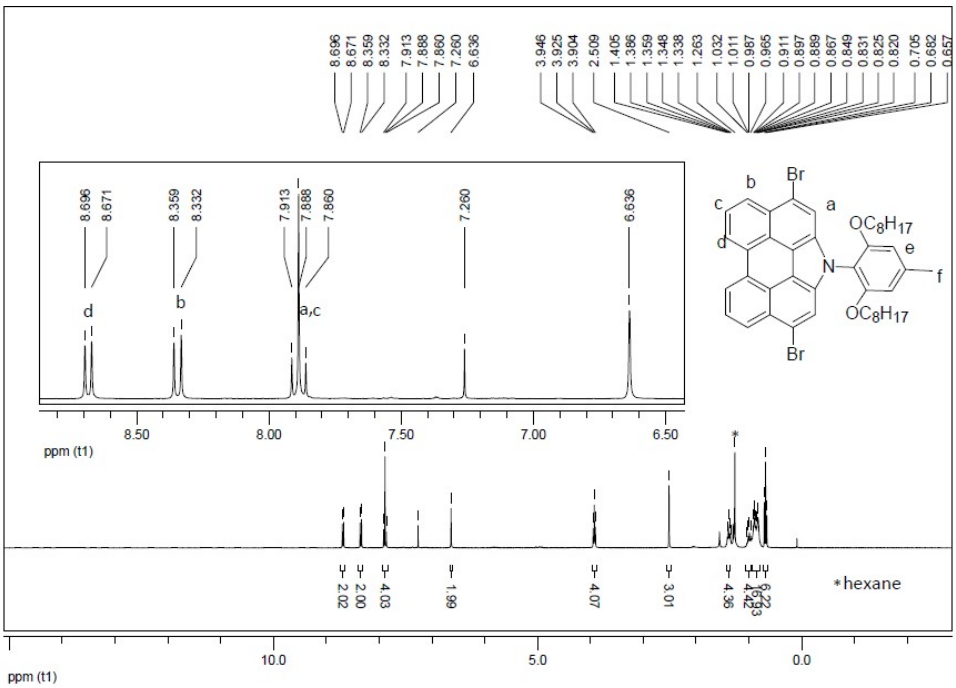

^{1}H NMR spectrum (300 MHz, $CDCl_3$) of **2-4**.

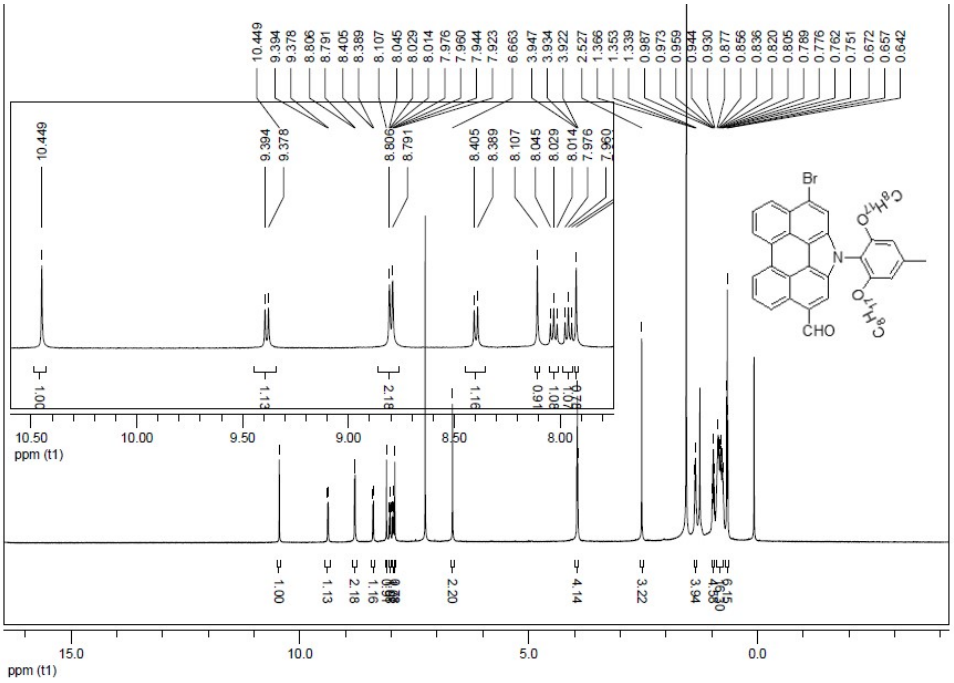

^{1}H NMR spectrum (500 MHz, $CDCl_3$) of **2-5**.

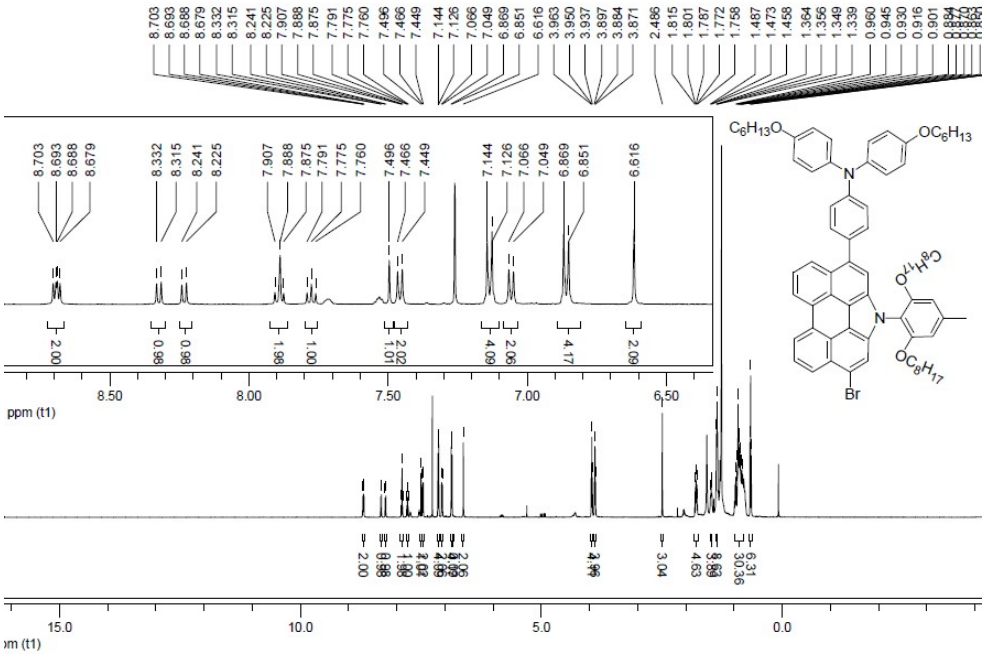

^{1}H NMR spectrum (500 MHz, $CDCl_3$) of **2-8**.

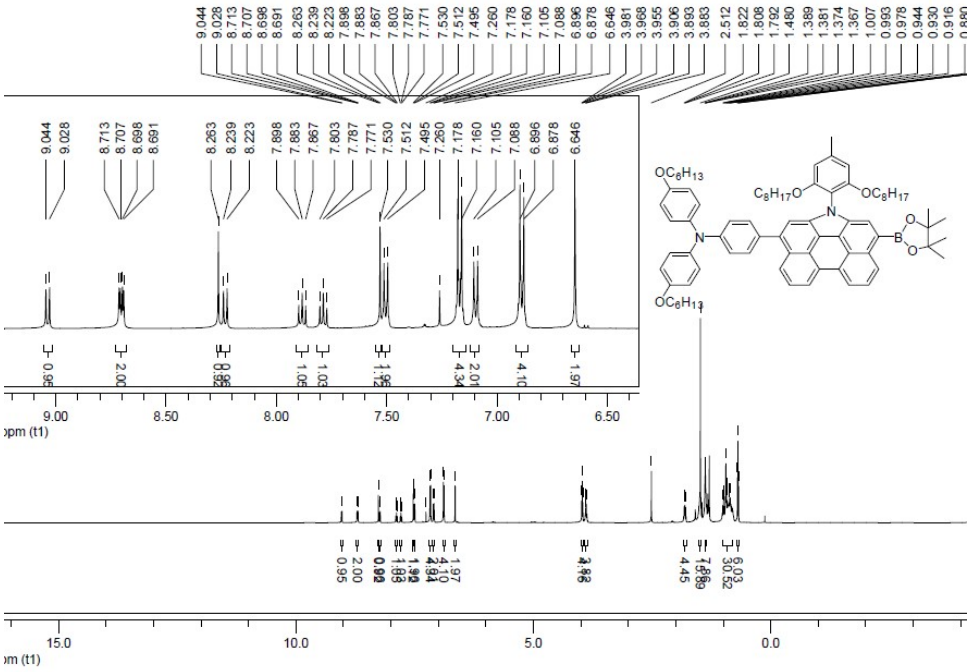

^{1}H NMR spectrum (500 MHz, $CDCl_3$) of **2-9**.

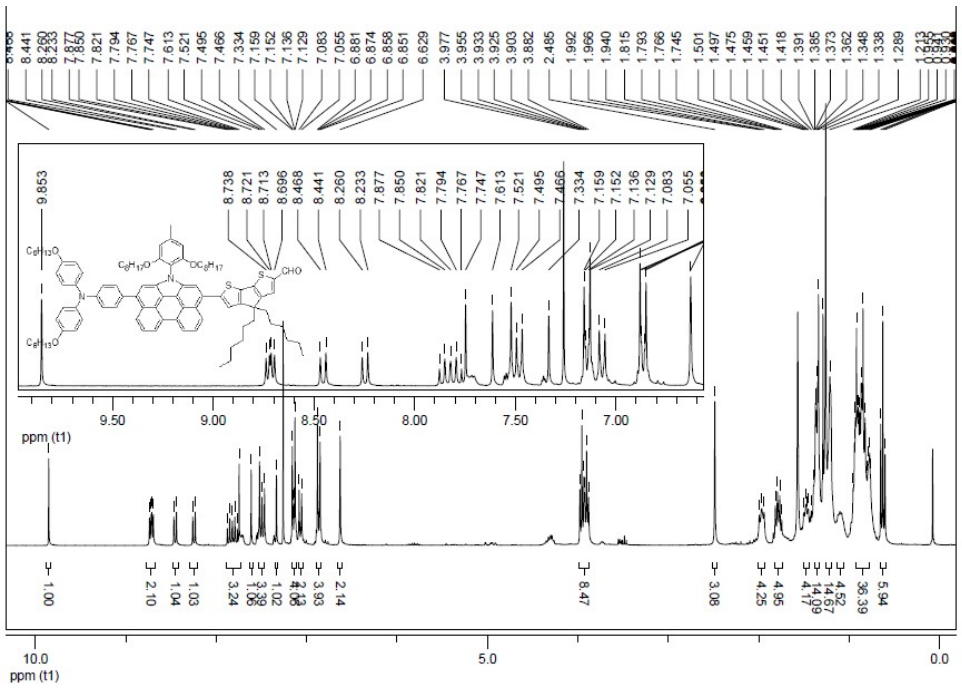

^{1}H NMR spectrum (300 MHz, $CDCl_3$) of **2-12**.

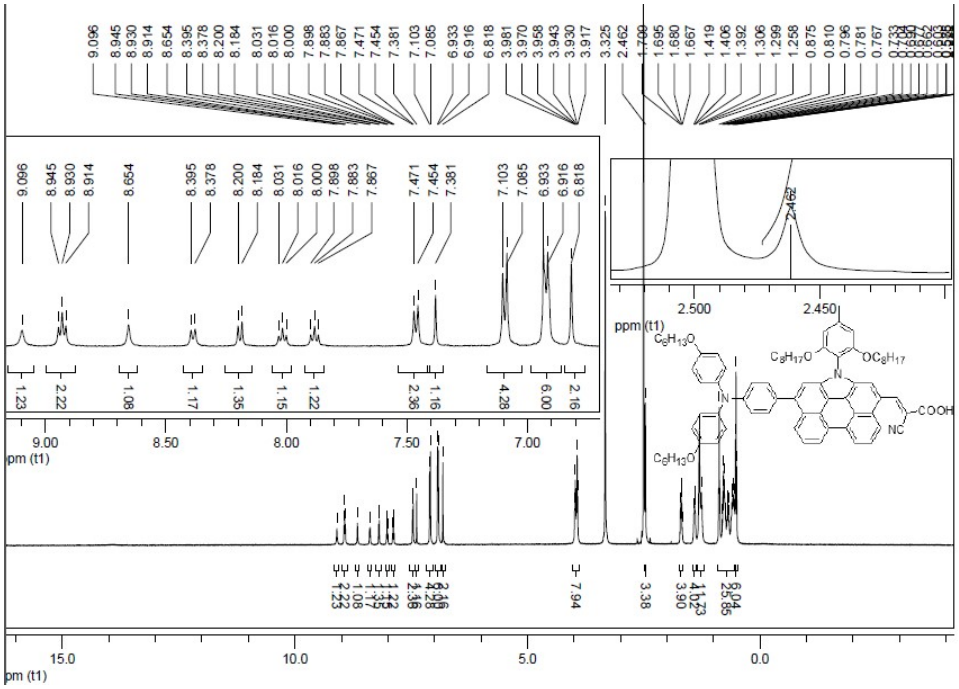

^{1}H NMR spectrum (500 MHz, THF-d_8) of **QB1**.

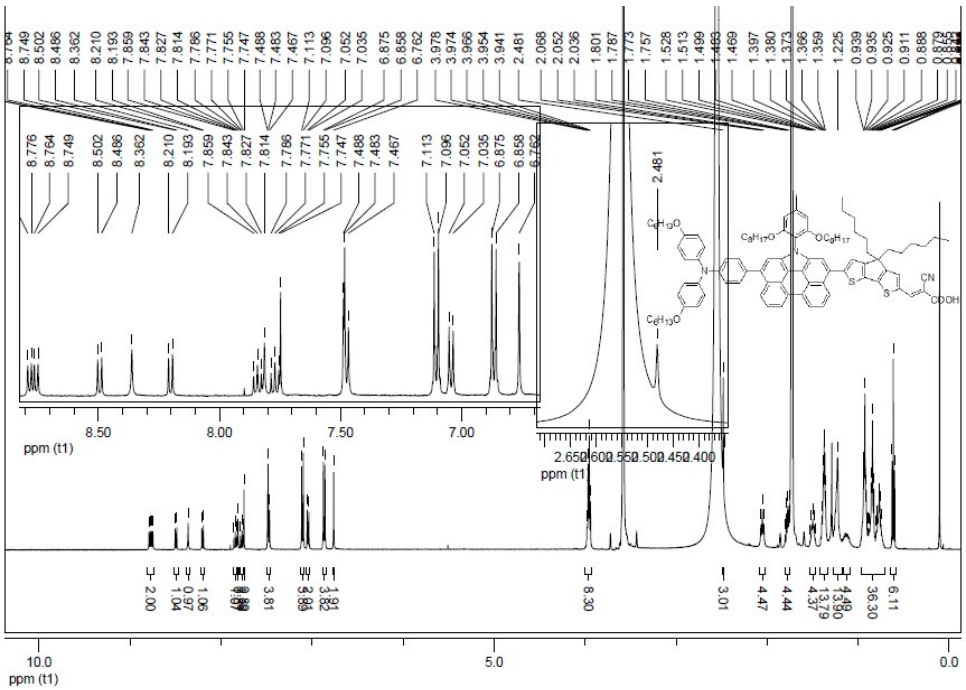

^{1}H NMR spectrum (500 MHz, THF-d_8) of **QB2**.

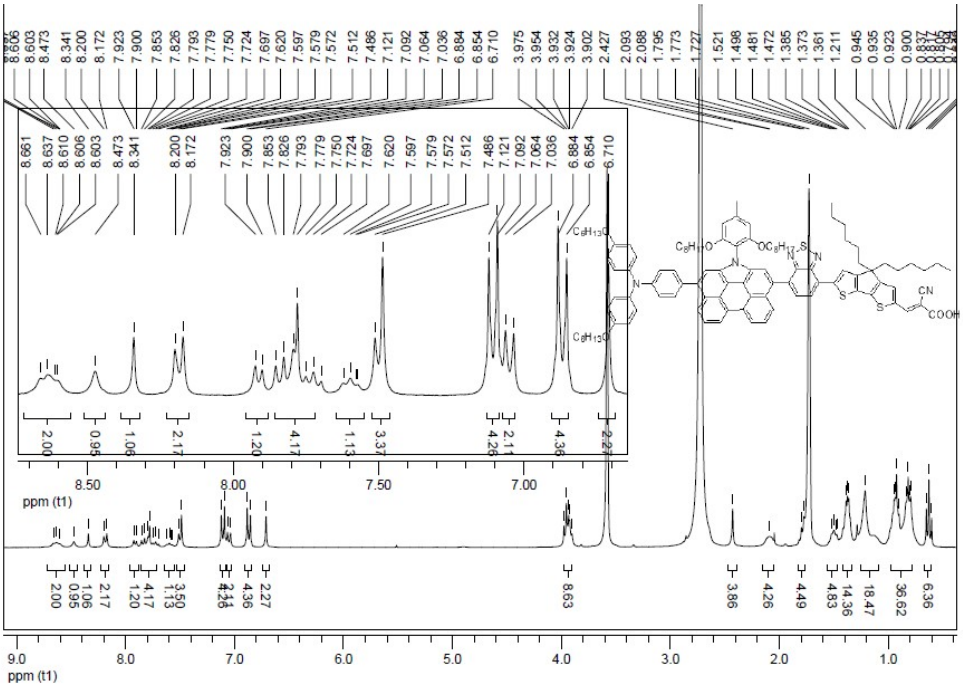

^{1}H NMR spectrum (300 MHz, THF-d_8) of **QB3**

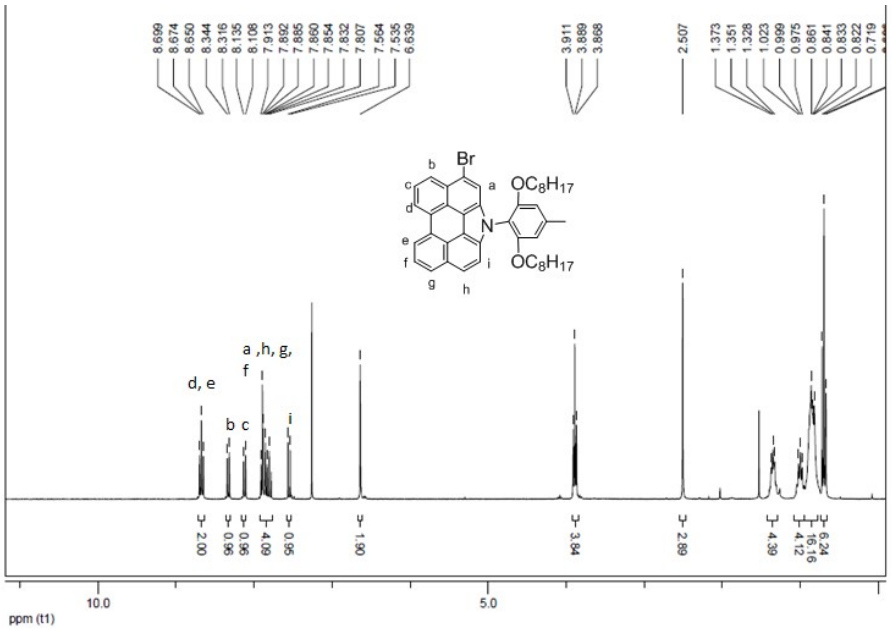

^{1}H NMR spectrum (300 MHz, $CDCl_3$) of **3-5**.

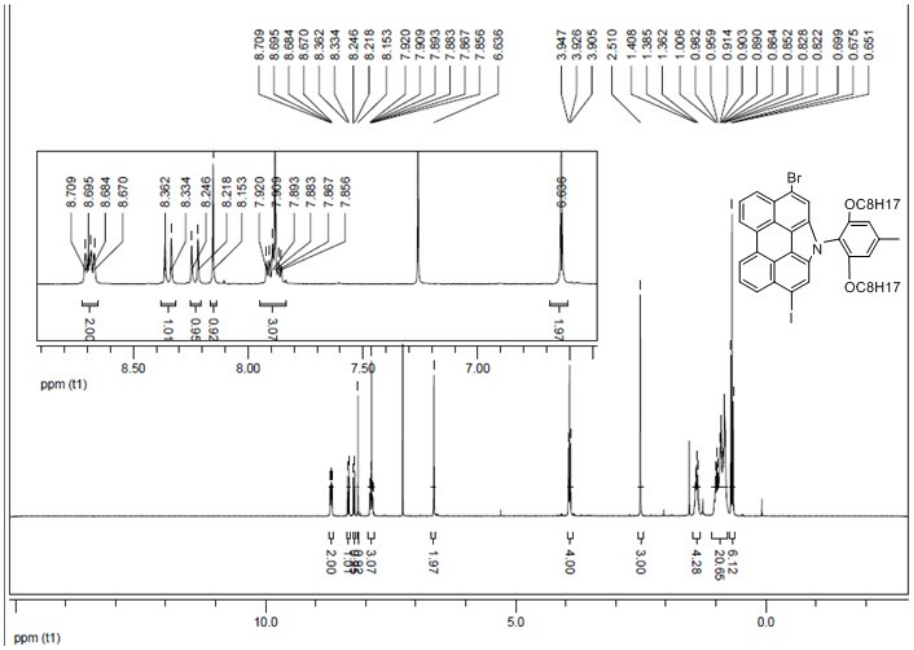

^{1}H NMR spectrum (300 MHz, $CDCl_3$) of **3-6**.

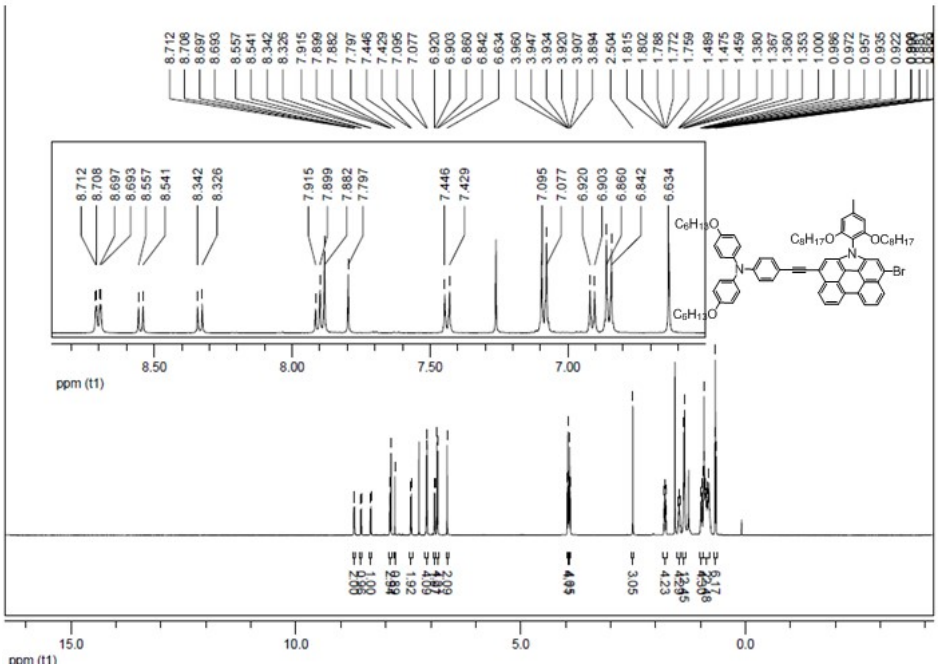

^{1}H NMR spectrum (500 MHz, $CDCl_3$) of 3-**7**.

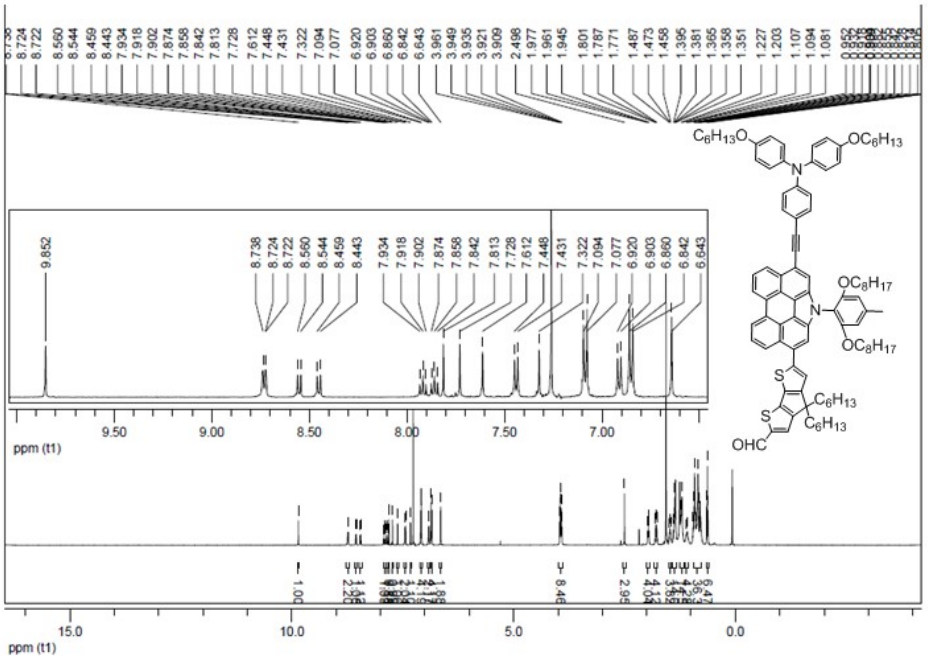

^{1}H NMR spectrum (500 MHz, $CDCl_3$) of **3-10**.

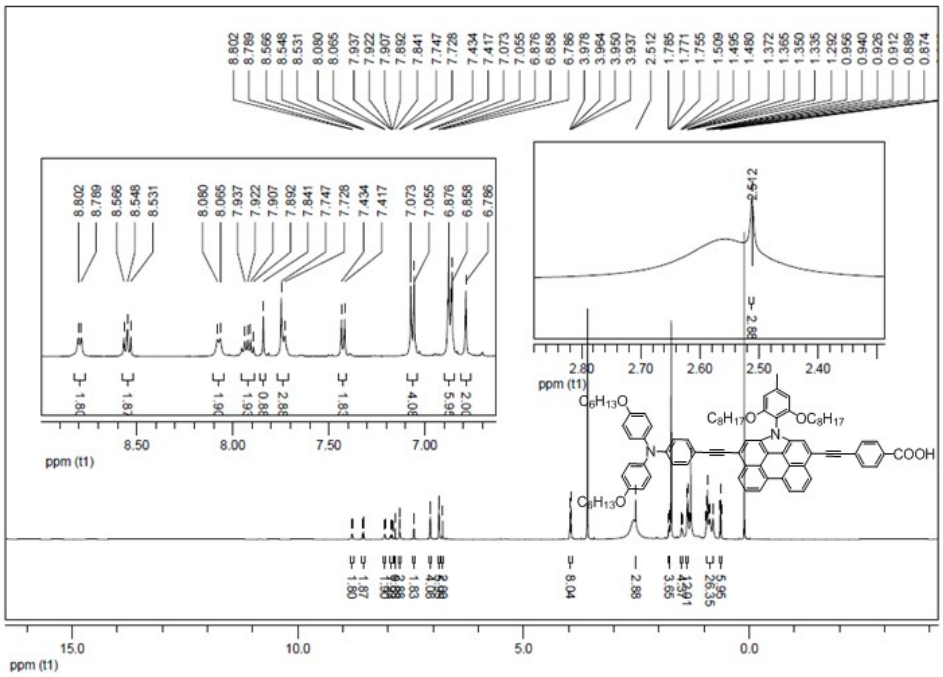

^{1}H NMR spectrum (500 MHz, THF-d_8) of **QB4**.

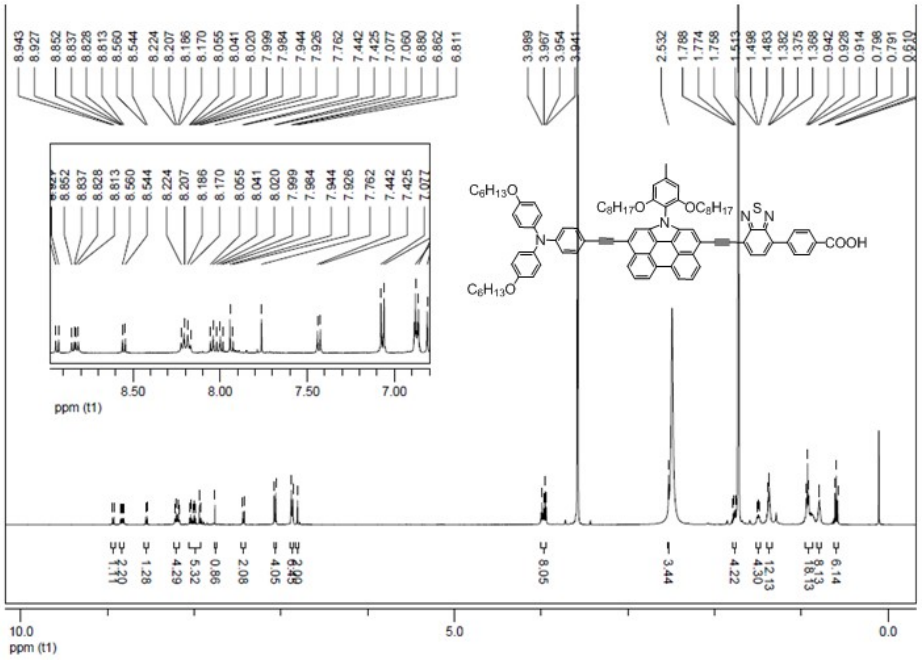

^{1}H NMR spectrum (500 MHz, THF-d_8) of **QB5**.

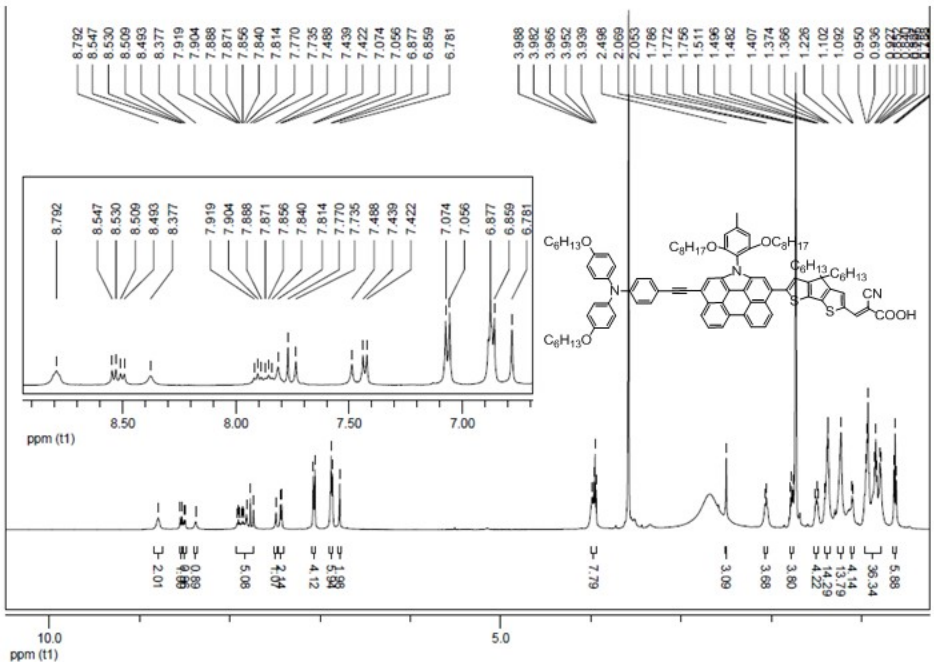

^{1}H NMR spectrum (500 MHz, THF-d_8) of **QB6**.

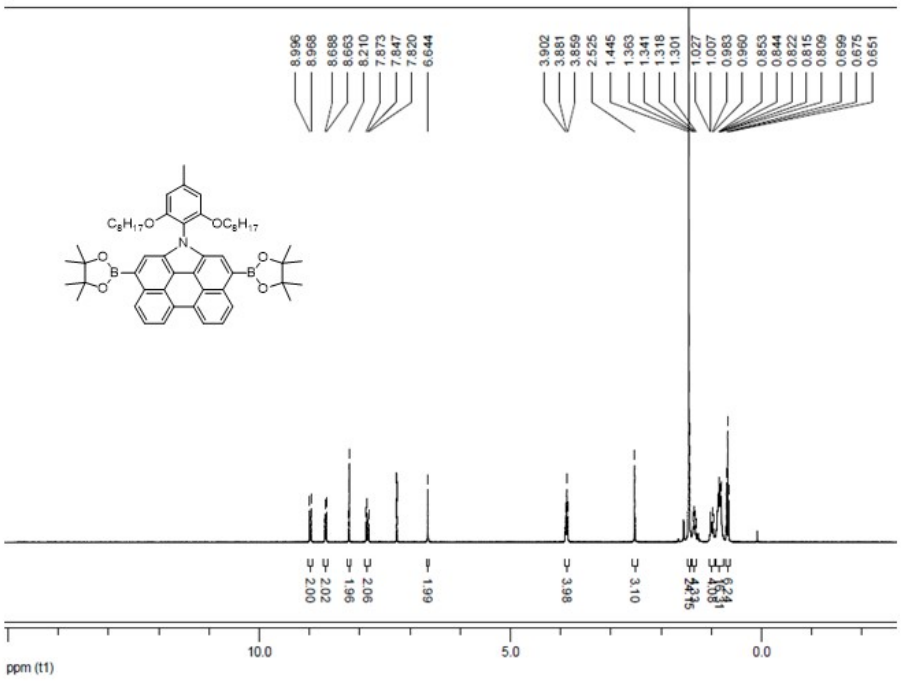

^{1}H NMR spectrum (500 MHz, $CDCl_3$) of **4-3**.

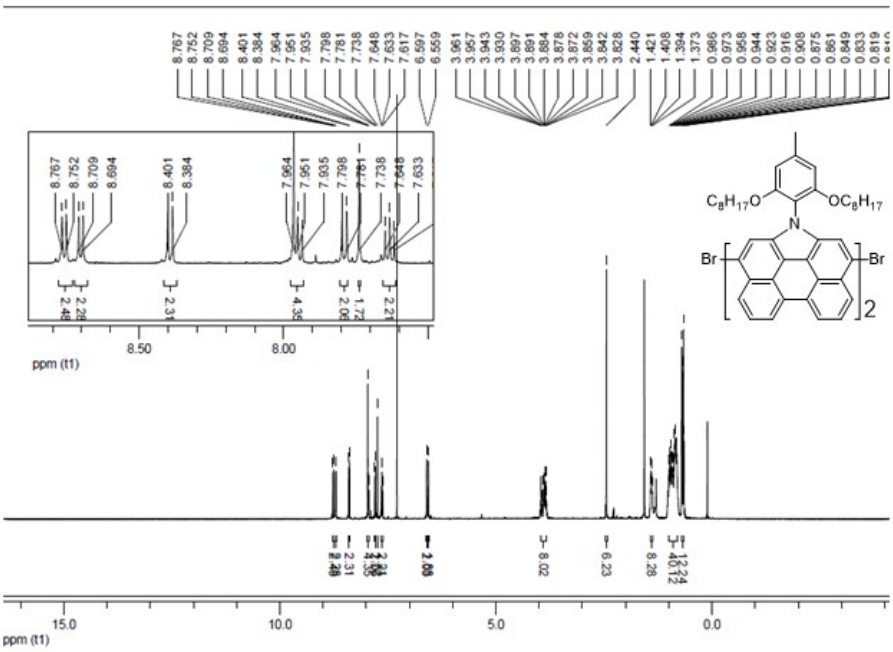

^{1}H NMR spectrum (500 MHz, $CDCl_3$) of **4-6**.

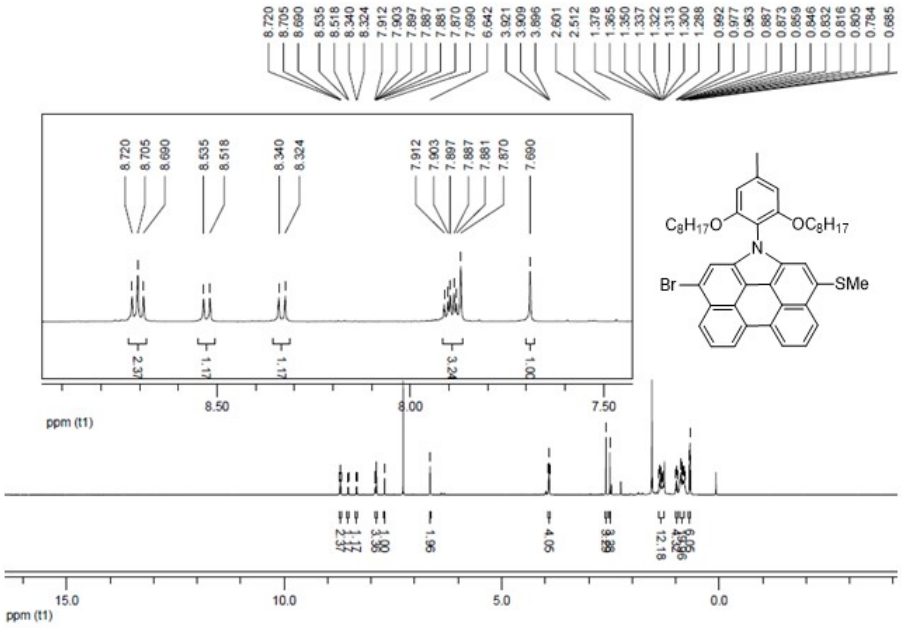

^{1}H NMR spectrum (500 MHz, $CDCl_3$) of **4-5**.

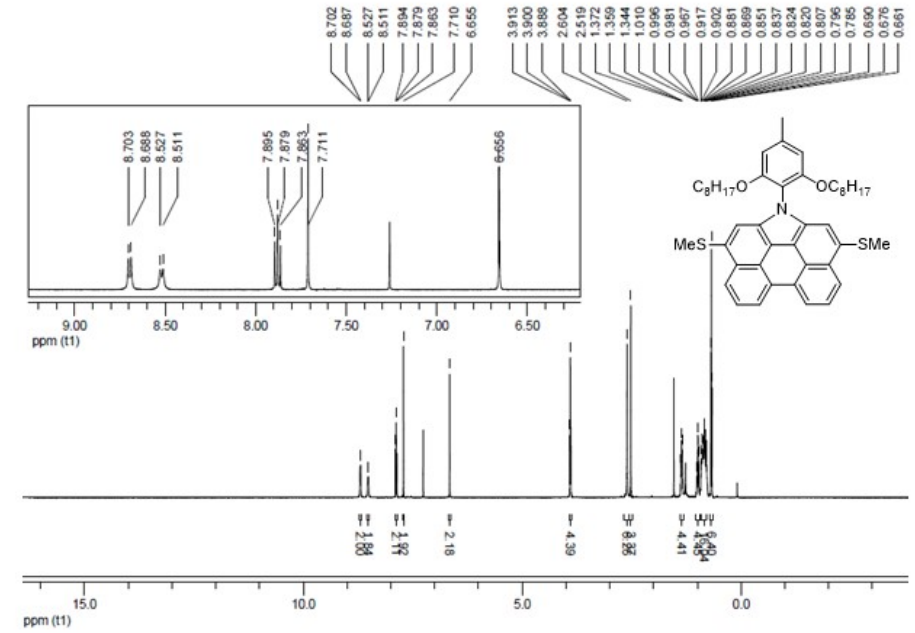

^{1}H NMR spectrum (500 MHz, $CDCl_3$) of **Per-SMe**.

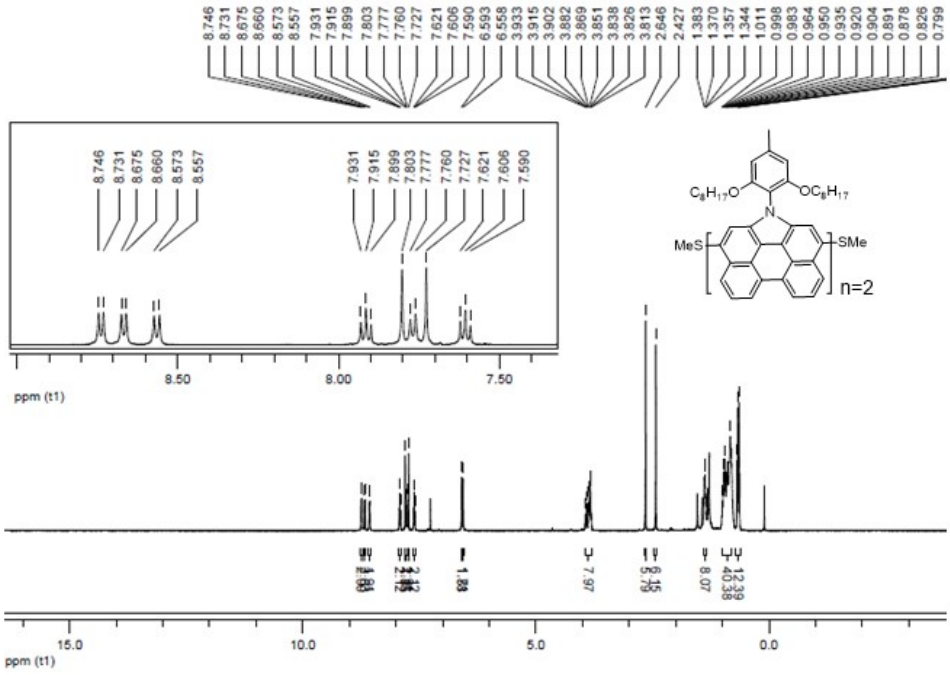

^{1}H NMR spectrum (500 MHz, $CDCl_3$) of **4-7**.

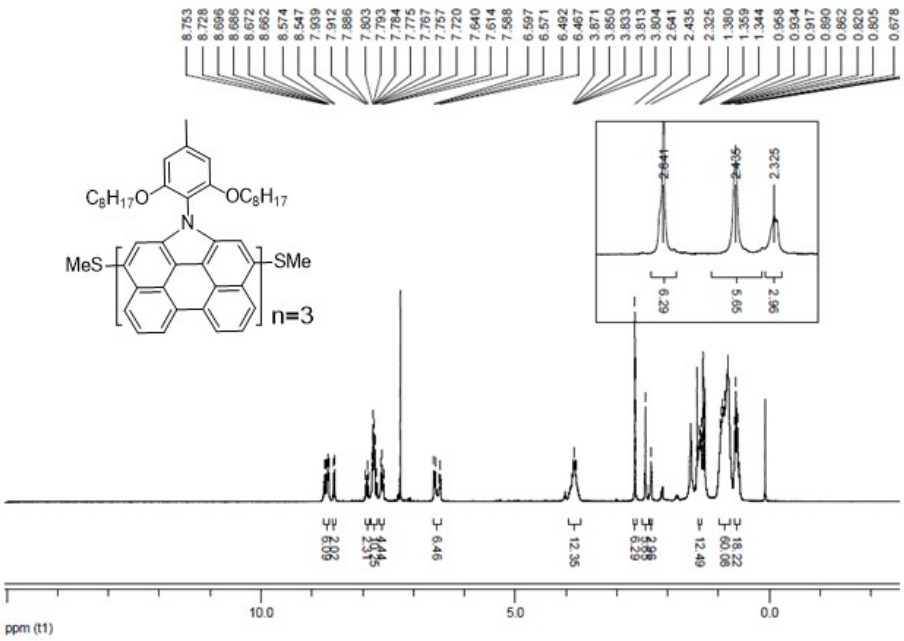

^{1}H NMR spectrum (300 MHz, $CDCl_3$) of **4-8**.

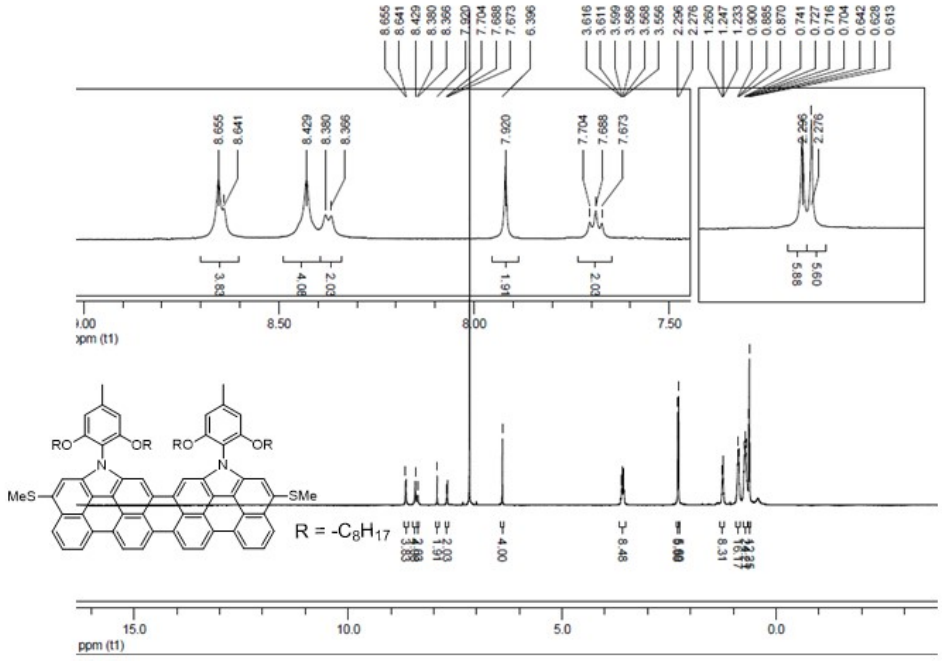

^{1}H NMR spectrum (500 MHz, C_6D_6) of **QR-SMe**.

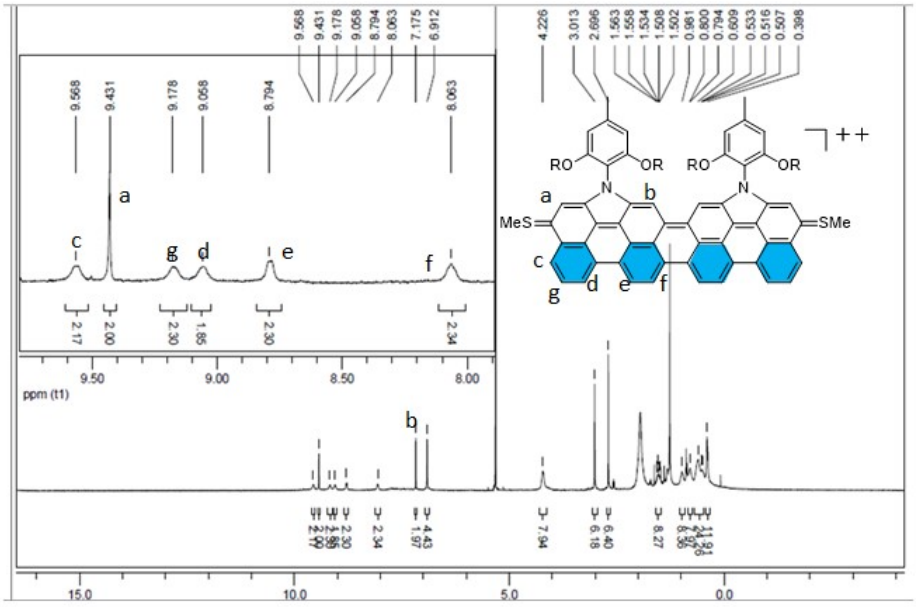

^{1}H NMR spectrum (500 MHz, CD_2Cl_2) of **QR-SMedic**.

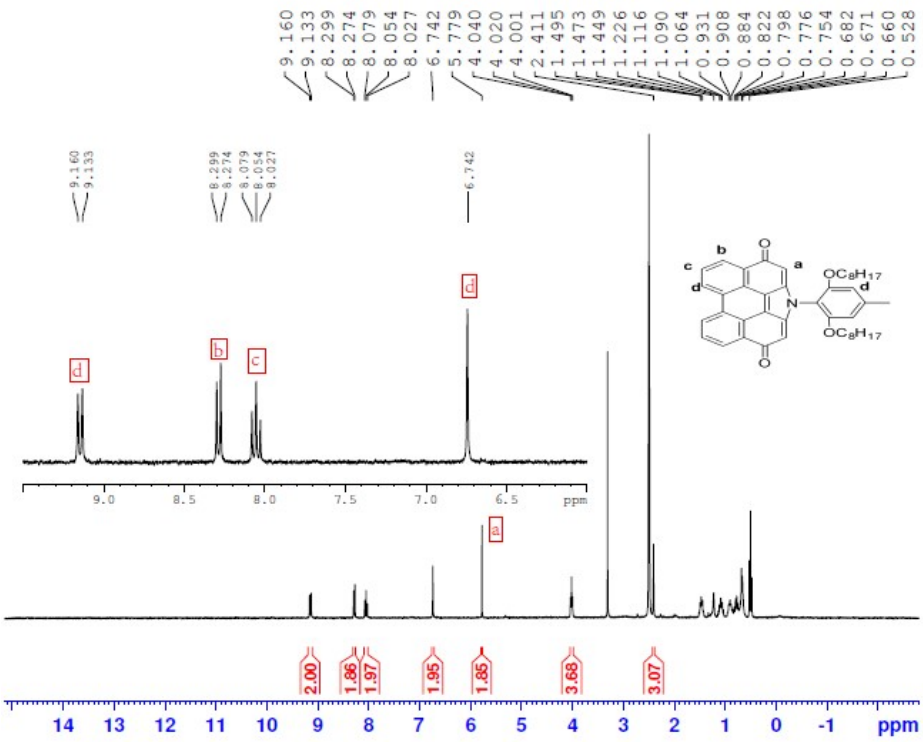

^{1}H NMR spectrum (500 MHz, DMSO-d_6) of **Per-O**.

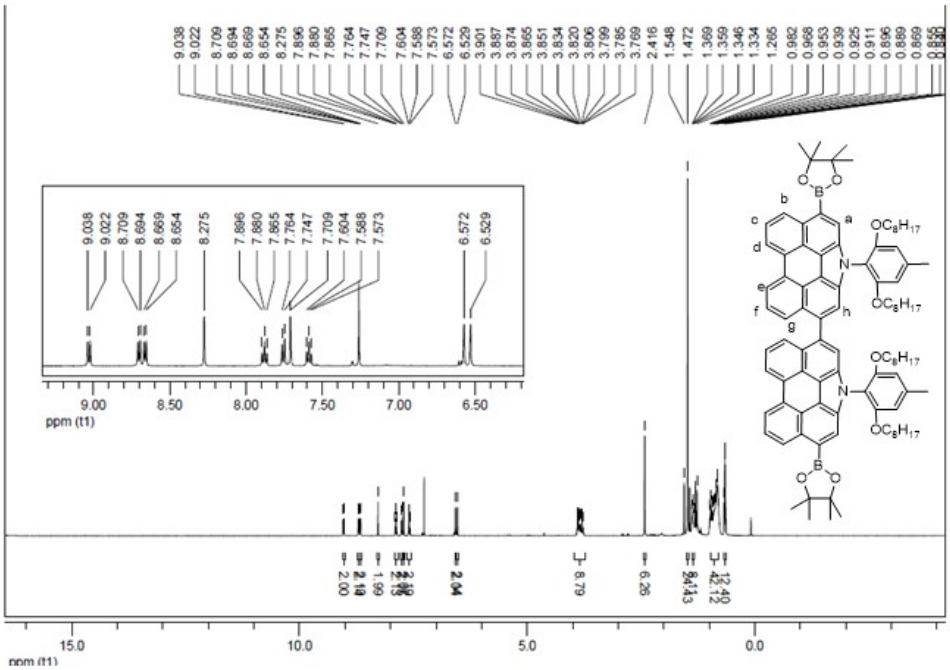

^{1}H NMR spectrum (500 MHz, $CDCl_3$) of **5-6**.

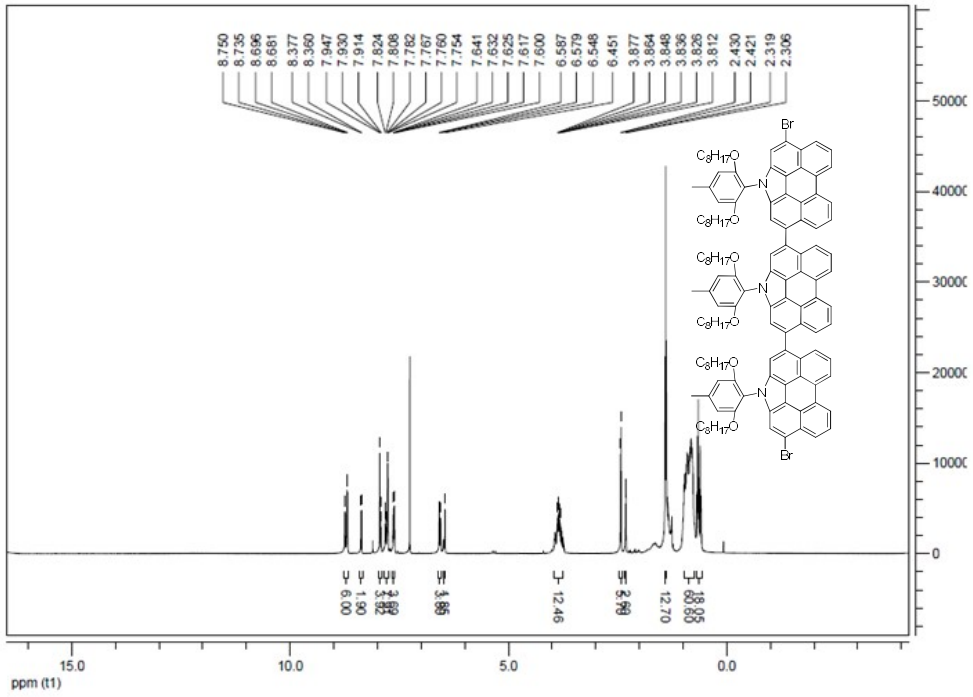

^{1}H NMR spectrum (500 MHz, $CDCl_3$) of **5-3**.